The novobiocin-induced turnover of fibronectin via low density lipoprotein receptor-related protein 1 alters matrix morphology with physiological consequences on cell growth and migration

A thesis submitted in the fulfilment of the requirements for the degree of

Doctor of Philosophy in Biochemistry

Of

Rhodes University

By

Natasha Marie-Eraine Boël

December 2018

ABSTRACT

Fibronectin (FN), an extracellular matrix protein, is secreted as a soluble dimer which is assembled into an insoluble extracellular matrix. The dynamics of FN matrix assembly and degradation play a large role in cell migration and invasion thereby contributing to the metastatic potential of cancer cells. Previous studies have shown the direct binding of Heat Shock Protein 90 kDa (Hsp90) and FN *in vitro*, and that inhibition of Hsp90 with novobiocin (NOV) caused internalisation of the FN matrix. Low density lipoprotein receptor-related protein 1 (LRP1) is a ubiquitous receptor known to bind both Hsp90 and FN. Using an LRP1 expressing Hs578T breast cancer cell line and an isogenic mouse embryonic fibroblast (MEF) model system of differential LRP1 expression we demonstrate that LRP1 is involved in turnover of FN in response to C-terminal Hsp90 inhibition. The first objective of this study was to identify the mechanism of NOV-induced LRP1-mediated FN turnover. Our data show that NOV-mediated FN turnover via LRP1 did not require the activity of matrix metalloproteinases (MMPs), which play an important role in processing and degradation of the extracellular matrix and FN. In addition, the levels of the main FN receptor responsible for its extracellular assembly, β1-integrin, did not change in response to NOV. LRP1 is known to undergo regulated intramembrane proteolysis (RIP) which generates smaller fragments that may translocate to the nucleus and modulate gene transcription. Using inhibitors of LRP1 cleavage and nuclear fractionation we determined that LRP1 processing was not required for the NOV-induced FN response suggesting that a mechanism unrelated to LRP1 RIP is involved. A possible mechanism may be in altered Hsp90-LRP1 cell signalling as we observed disruption of the FN-Hsp90-LRP1 complex at the cell surface in NOV treated cells. How this affects downstream eHsp90-LRP1 signalling is still to be determined but may be related to a significant increase in phospho-AKT and loss of phospho-ERK upon NOV-treatment; two key signalling proteins involved in FN matrix regulation and which are downstream of LRP1 signalling. The second objective of this study was to determine the physiological consequences associated with FN turnover in response to NOV treatment. Using migration assays we demonstrated that levels of insoluble matrix-associated FN and FN concentration are not solely responsible for migratory capacity of cells on decellularized extracellular matrices, but rather that structural composition and integrity of the matrix plays a bigger role. Using confocal and scanning electron microscopy, we identified NOV treated matrices to be flatter, less mature and contain thicker, rope-like FN fibrils to which cells adhered better but were generally less proliferative. Comparatively, cells adhered less to the more mature and 3-dimensional untreated matrices but exhibited increased spreading and cell growth, which may in part be due to the thinner fibrils and web-like matrix. In summary, this study substantiates the role of LRP1 in NOV-mediated FN turnover, and provides new insights into the possible mechanisms of the Hsp90-LRP1 mediated loss of FN matrix. This is the first study to demonstrate some of the functional consequences related to FN turnover by NOV at the ECM level.

DECLARATION

I declare that this thesis is my own, unaided work. It is being submitted for the degree of Doctor of Philosophy in Biochemistry of Rhodes University. It has not been submitted before for any degree or examination at any other university.

Some of the tables, figures and narrative of the literature review form part of a book chapter which I co-authored this year, the citation of which is: Boel N.ME., Edkins A.L. (2018). Regulation of the Extracellular Matrix by Heat Shock Proteins and Molecular Chaperones. In: Binder R., Srivastava P. (eds) Heat Shock Proteins in the Immune System. Springer, Cham. I confirm that I have received permission to reproduce the manuscript as part of my thesis from the publisher.

Some of the data in Chapter 3 form part of an original published manuscript the citation of which is: Boel, N.ME., Hunter, M.C. & Edkins, A.L. (2018). LRP1 is required for novobiocin-mediated fibronectin turnover. *Scientific Reports,* 8, 11438. For this manuscript, I am the first author and was directly responsible for collection and analysis of data and writing of the manuscript with input from my supervisor. This work is published under an open access Creative Commons license.

Ms Natasha Marie-Eraine Boël
March 2019
Grahamstown, South Africa

TABLE OF CONTENTS

LIST OF FIGURES

LIST OF SUPPLEMENTARY FIGURES

LIST OF TABLES

LIST OF ABBREVIATIONS

17-AAG	17-(Allylamino)-17-demethoxygeldanamycin
17-DMAG	17-(Dimethylaminoethylamino)-17-demethoxygeldanamycin
ADAMTs	A Disintegrin And Metalloproteinase with Thrombospondin Motifs
Akt	Protein kinase B
ANOVA	Analysis Of Variance
ATCC	American Type Culture Collection
ATP	Adenosine Triphosphate
ATPase	Adenosine 5` Triphosphatase
BACE-1	β-site of Amyloid precursor protein Cleavage Enzyme-1
BSA	Bovine Serum Albumin
CA1	Coumermycin A1
CDM	Cell-derived matrix
CL	Cleared lysate
CTD	C-terminal Domain
DMEM	Dulbecco's Modified Eagle Medium
DNA	Deoxyribonucleic Acid
DTSSP	3,3'-Dithiobis[sulfosuccinimidyl]propionate
DOC	Sodium deoxycholate
EC_{50}	Effective Concentration resulting in a 50% reduction in cell viability
ECM	Extracellular matrix
ECL	Enhanced chemiluminescence
EDTA	Ethylenediaminetetraacetic Acid
EGFR	Epidermal Growth Factor Receptor
ERK	Extracellular signal-regulated kinase
ET	Endotoxin
FCS	Fetal Calf Serum
FN	Fibronectin
GA	Geldanamycin
HCl	Hydrochloric acid
HER-2	Human Epidermal growth factor Receptor 2
Hop	Hsp70/Hsp90 organizing protein
HSF	Heat Shock Factor
Hsp	Heat Shock Protein
HSR	Heat Shock Response
HRP	Horseradish Peroxidase
IB	Immunoblot
ICD	Intracellular domain
Ig	Immunoglobulin
IP	Immunoprecipitation
IPTG	Isopropyl β-D-1-thiogalactopyranoside
kDa	Kilodalton
LDL	Low-density lipoprotein
LPS	Lipopolysaccharide
LRP1	Low density lipoprotein Receptor-related Protein-1
LRP1-58	58 kDa fragment of LRP1

LRP1-85	85 kDa fragment of LRP1
LRP1-ICD	LRP1 intracellular domain
LRPab	LRP1 blocking antibody
LSM	Laser Scanning Microscope
MAPK	Mitogen Activated Protein Kinase
MEF-1	Murine Embryonic Fibroblast-1
MMP	Matrix Metalloproteinase
mRNA	Messenger RNA
MW	Molecular Weight
NHS	N-Hydroxysuccinimide
NOV	Novobiocin
NFkB	Nuclear Factor kappa B
NP40	Nonidet-P-40
NTD	N-terminal Domain
PBS	Phosphate Buffered Saline
PCR	Polymerase Chain Reaction
PMSF	Phenylmethanesulfonylfluoride
q-RT-PCR	Quantitative Reverse Transcriptase-Polymerase Chain Reaction
RAP1	Receptor Associated Protein 1
RGD	Arginine-Glycine-Aspartic acid tripeptide
RIP	Regulated Intramembrane Proteolysis
RIPA	Radio-immunoprecipitation assay
RTK	Receptor Tyrosine Kinase
SDS	Sodium-Dodecyl-Sulphate
SDS-PAGE	Sodium-Dodecyl-Sulphate Polyacrylamide Gel Electrophoresis
SN	Supernatant
SMC	Smooth Muscle Cell
TBS	Tris-Buffered Saline
TBST	Tris-Buffered Saline with Tween-20
TGF	Transforming Growth Factor
TIMPs	Tissue Inhibitors of Metalloproteinases
tPA	Tissue-type Plasminogen Activator
TRAP1	Tumour necrosis factor type 1 Receptor Associated Protein
UNT	Untreated
uPA	Urokinase-type Plasminogen Activator
uPAR	Urokinase-type Plasminogen Activator Receptor
UK	United Kingdom
USA	United States of America
UV	Ultra-violet
WB	Western Blot
WCL	Whole Cell Lysate

LIST OF SYMBOLS

α	Alpha
β	Beta
°C	Degree Celsius
m	Metres
µm	Micrometres
M	Molar
mM	Millimolar
µM	Micromolar
nM	Nanomolar
g	Grams
mg	Milligrams
µg	Micrograms
L	Litres
ml	Millilitres
µl	Microlitres
kDa	Kilodaltons
Da	Daltons
min	Minutes
hrs	Hours
%	Percent or g/100 ml
U	Units
x *g*	Relative centrifugal force to gravity
rpm	Revolutions per minute
v/v	Volume per volume
w/v	Weight per volume
V	Volts
pH	Negative log of hydrogen ion concentration

ACKNOWLEDGEMENTS

To the ultimate supervisor of all time, Prof Adrienne Edkins: No words can describe how grateful I am to have had your support and guidance over these past 6 years. Thank you for your endless enthusiasm and encouragement, and for sharing your wisdom and passion with me throughout my postgraduate career. Thank you for the numerous opportunities you have given me during my time in BioBRU. You have been, and will continue to be, an inspiration to me.

To Rhodes University and the National Research Foundation: This work would not have been possible without your financial support. Thank you for affording me this opportunity to pursue my dreams.

To my awesome lab, BioBRU: What an incredible team we make! Thank you all for your support and input into my work and for making our lab such a fantastic work environment. A special thank you to Dr JoAnne de la Mare and Dr Stacey Mattison for your friendship, advice (on just about everything) and support during my time at Rhodes. I will treasure all the memories we have made together!

To my bestie, Dr Jason Sterrenberg: Words cannot express how big a part you have played in my life. Thank you for your guidance in my work (and life in general) and for being my most fierce and loyal friend! You always managed to put a smile on my face on those tough days and made me realize that I'm still somewhat smart. Thank you for the endless laughter, advice and support that you have given me over these past 6 years.

To my boyfriend, Jason Spencer: Thank you for coming into my life when you did. Even though it's been a short period of time, I feel like you have been there with me through it all. Thank you for your support, for keeping me well fed, constantly entertained and simply happy. I appreciate you.

To my incredible parents, Henny and Tina Boel: Thank you for loving me, supporting me on all levels and always believing that I can achieve my highest goals. You can look forward to one final graduation ceremony (hopefully) in the back row of the Monument with your binoculars!

Chapter 1: **LITERATURE REVIEW**

1.1 Molecular chaperones and Heat shock proteins (Hsps)

Molecular chaperones are ubiquitous proteins involved in maintaining proteostasis by functionally assisting nascent peptide folding or refolding of denatured or misfolded proteins (Hendrick & Hartl, 1993). Chaperones act at the level of protein folding to maintain correctly folded and active states of intracellular proteins, assembly of complexes and protein transport (Kim et al., 2013). The same is true for proteins requiring export from the cell, including cytokines, extracellular matrix (ECM) proteins and receptors. Of the molecular chaperones, the heat shock protein (Hsp) family is the largest and most extensively studied, comprising several subfamilies (Hsp100, Hsp70, Hsp90, Hsp60, Hsp40 and small Hsps [Hsp10, Hsp27]), which have traditionally been classified according to their approximate molecular size (Hartl & Hayer-Hartl, 2002). Hsps are ubiquitous, highly conserved proteins which play similar roles in both eukaryotes and prokaryotes. Hsps are constitutively expressed in cells or accumulate when subjected to stresses such as heat, hypoxia, nutrient deprivation and carcinogens (Chaudhuri & Paul, 2006; Hartl & Hayer-Hartl, 2002). Hsps are also responsible for stabilising misfolded and/or aggregated proteins extracellularly due to the high degree of stress, and interactions of extracellular proteins which might occur in the extracellular environment (Hartl et al., 2011; Röhl, Rohrberg, & Buchner, 2013). Most Hsps require the free energy of ATP to assist in protein folding, whilst some, such as the smaller Hsps, have the ability to function independently of ATP (Chaudhuri & Paul, 2006; Jakob et al., 1993; Obermann et al., 1998). Hsps were first identified in the early 1970s in *Drosophila* cells upon exposure to heat, which caused the overexpression of this group of proteins (Ritossa, 1962; Tissières, Mitchell, & Tracy, 1974). It is now appreciated that when cells are exposed to stress conditions, members of the heat shock transcription factors (HSFs) are activated which induces a heat shock response (HSR) consequently triggering heat shock proteins (Hsps) to become overexpressed (Akerfelt, Morimoto, & Sistonen, 2010; Fulda, Gorman, Hori, & Samali, 2010). HSF-1 is one of the main regulators of this HSR (Anckar & Sistonen, 2011; Ruckova, Muller, & Nenutil, 2012).

1.2 Hsp90

Hsp90 is a one of the most abundant molecular chaperones in eukaryotes that facilitates client protein maturation, stabilization of aggregation-prone proteins, quality control of misfolded proteins and maintenance of proteins in their active conformations. Hsp90 is also responsible for the proteolytic turnover of over 300 intracellular proteins termed 'clients', many of which are involved in various signal transduction pathways (Khalil et al., 2011). In general, Hsps are part of the wider cellular proteostasis network that functions in normal and disease states to maintain protein homeostasis. Hsp90 is constitutively and abundantly expressed in eukaryotic cells under normal conditions, constituting 1-2% of total cellular protein, and functions in facilitating the later stages of protein folding and maintaining clients in easily activated states (Garrido, Gurbuxani, Ravagnan, & Kroemer, 2001). However, upon exposure to stress, cells begin to overexpress Hsp90 to levels comprising 4-6% of total cellular protein (Li, Sahu, & Tsen, 2011; Solit & Chiosis, 2008). A comprehensive and frequently updated list of *bona fide* Hsp90 interacting proteins can be found on the Picard laboratory web page (http://www.picard.ch/downloads/Hsp90interactors). Hsp90 exists as a homodimer with each monomer having three highly conserved domains; a 25 kDa ATP binding N-terminus which is connected via a charged linker region to the 35 kDa middle domain, and the 12 kDa C-terminal dimerization domain which has an alternative ATP binding site (Figure 1) (Nemoto & Sato, 1998). There is also an extension at the extreme end of the C-terminus containing a conserved MEEVD amino acid motif to which co-chaperones containing the tetratricopeptide (TPR) repeat (such as Hop, CHIP and DNAJC7) bind (Hartl *et al.,* 2011).

Two cytosolic Hsp90 isoforms have been identified; the inducible Hsp90α and constitutive Hsp90β, which are encoded for by separate genes and have high sequence similarity (Pepin, Momose, Ishida, & Nagata, 2000; Sreedhar & Csermely, 2004). In knockout studies, Hsp90β, but not Hsp90α was shown to be essential for placental development in mice and is embryonic lethal (Grad et al., 2010; Voss, Thomas, & Gruss, 2000). Hsp90 isoforms have also been found in the endoplasmic reticulum termed glucose regulated protein 94 (Grp94 or Gp96) and in the mitochondrial matrix termed tumour necrosis factor receptor-associated protein 1 (TRAP1 or Hsp75). TRAP1 is unique in its LxCxE motif, which binds the SV40 T-antigen binding domain of retinoblastoma protein (Chen et al., 1996), and absence of the highly charged linker region (Felts et al., 2000). A fifth isoform still under debate is Hsp90N, which

has been proposed to be distinct from cytosolic Hsp90 by having a unique 30 amino acid hydrophobic sequence at the N-terminus (which replaces the 25 kDa ATP binding site) (Grammatikakis et al., 2002). It has been suggested that this form of Hsp90 is found on the plasma membrane of cancer cells (Sreedhar & Csermely, 2004). Since the Hsp90N lacks the highly conserved N-terminal ATP binding pocket (which is necessary for most chaperone functions) it suggests then that Hsp90N would in fact be non-functional from the traditional perspective of Hsp90 chaperone activity (Schweinfest et al., 1998). However, studies by Grammatikakis et al (2002) have shown that Hsp90N can carry out functions previously thought to be solely dependent on the N-terminus, such as binding and activating oncogenes independently of co-chaperones. Conversely, it has been argued that Hsp90N is in fact not an additional Hsp90 isoform but rather a chromosomal rearrangement which occurred in a single cell line (Zurawska, Urbanski, & Bieganowski, 2008). Thus, there is still controversy as to whether Hsp90N should be classified as a distinct gene or whether the isoform arises from processing of one of the other Hsp90 transcripts only in specific contexts.

Hsp90 is a central component of the network of molecular chaperones in the cell which cooperate with Hsp70 and other co-chaperones and cofactors to regulate the folding, activity and stability of client proteins (Mayer & Bukau, 2005; Pratt, 1998; Taipale et al., 2012). This multi-chaperone complex was reported in the late 1970s for the canonical client protein group of steroid hormone receptors (Chang, Nathan, & Lindquist, 1997). More than 20 co-chaperones have been identified to regulate the function of Hsp90, (Li & Buchner, 2013) the protein Hop (Hsp70-Hsp90 organising protein, also known as stress induced phosphoprotein 1/STIP1) being one of the central co-chaperones in the Hsp90 cycle (Chang et al., 1997). Two monomers of Hsp90 associate in an open, inactive form with the C-termini constitutively dimerized and the N-termini separate (Csermely et al., 1998; Wandinger, Richter, & Buchner, 2008). Hsp70 binds the client protein in an ATP-dependent manner assisted by the chaperone activity of Hsp40 co-chaperones. This complex then delivers the client protein to Hsp90 via Hop which stabilizes the Hsp90 dimer and inhibits the ATPase activity (Chang et al., 1997; Wegele, Müller, & Buchner, 2004). The Hsp70-Hop complex consequently dissociates and is replaced by p23 and immunophilins to generate a closed complex, whereby the N-termini of Hsp90 dimerises and clamps the client protein (Pratt, 1998). Upon ATP hydrolysis which can be stimulated by the co-chaperone Aha1 (Mayer, Nikolay, & Bukau, 2002; Panaretou et al.,

2002), the client protein is released and the Hsp90 dimer adopts an open conformation again to accept another substrate (Hendrick & Hartl, 1993; Richter & Buchner, 2011).

1.3 Extracellular Hsp90 (eHsp90)

Numerous studies have focused on identifying the roles of intracellular Hsp90, but much less is known about the extracellular pool of Hsp90 (eHsp90). In 1986, Ullrich and colleagues identified Hsp90 on the surface of mouse cells (Ullrich et al., 1986). Since then Hsp90 has been detected by several groups in the extracellular space and on the surface of various cell types including fibrosarcoma, neuronal and breast cancer cells (Eustace et al., 2004; Hunter et al., 2014; Sidera, Samiotaki, Yfanti, Panayotou, & Patsavoudi, 2004; Sims, McCready, & Jay, 2011) . The term 'extracellular' is often used interchangeably to describe both membrane-bound and extracellular soluble forms of Hsp90. It is not known by what mechanism Hsp90 localizes to the extracellular space, but since these proteins lack a secretory signal sequence it must follow an alternative pathway to that of the canonical Golgi transport secretory pathway (McCready, Sims, Chan, & Jay, 2010). Thus, McCready and colleagues (2010) suggested that extracellular Hsp90 (eHsp90) is secreted via exosomes or more recently that Hsp90 binds to and disrupts plasma membranes followed by fusion with multivesicular bodies and exosomal release (Lauwers et al., 2018). Alternatively, cell lysis or proteolytic cleavage from the cell surface may release soluble Hsp90 into the extracellular space (Althoff et al., 2001; Calderwood et al., 2006). eHsp90 is thought to derive from the cytosolic Hsp90α and Hsp90β isoforms (Eustace et al., 2004). Some groups have reported the presence of both isoforms in the extracellular space (Hegmans *et al.,* 2004; Hunter *et al*., 2014) whilst others have suggested that only Hsp90α, and not Hsp90β, exists on the cell surface (Li *et al.,* 2007; Wang *et al.,* 2009). In a study by Eustace *et al.* (2004) it was found that Hsp90α, but not Hsp90β, was secreted to the extracellular space and was able to degrade the matrix by activation of MMP2 (which digests components of the ECM allowing for access to the vasculature system and metastasis). They also showed that Hsp90 inhibition resulted in decreased MMP2 activity which resulted in a loss of cancer invasiveness. Song and colleagues also reported that eHsp90 activates MMP2 and also serves as a substrate for proteolytic cleavage by MMP2 (Song et al., 2010). The predominant function of eHsp90 is suggested to be in the promotion of cell motility and tissue repair, as in the case of wound healing. eHsp90 is thought to chaperone a small group of extracellular client proteins relative to intracellular Hsp90 (McCready *et al.,*

2010; Hunter *et al.,* 2014) (Table 1). Sidera and colleagues reported eHsp90 binding of HER-2 to increase cell invasion and migration (Sidera et al., 2008). eHsp90 is also known to bind low density lipoprotein receptor-related protein-1 (LRP1) (Basu *et al.,* 2001; Gopal *et al.,* 2011) on subdomain II of LRP1. Several groups reported that eHsp90α was able to induce cell migration via its interaction with LRP1 (Chen *et al.,* 2010a; Cheng *et al.,* 2008). It was reported that these pro-motility effects were induced by the binding of a 115 amino acid fragment (termed F-5) located at the boundary between the middle domain and linker region on eHsp90 to LRP1 to activate the various downstream signalling pathways required to initiate cell motility, rather than via a chaperone-based mechanism (Cheng *et al.,* 2008; Chen *et al.,* 2010a; Li & Reynolds, 2012). A novel eHsp90 cross-membrane signalling pathway involving the extracellular and intracellular domains of LRP1 has been established to activate Akt kinases stimulating cell migration (Tsen et al., 2013). Some authors have argued that eHsp90 functions in a cytokine-like fashion via receptor-mediated induction of signalling pathways, distinct from the chaperoning function of intracellular Hsp90 (Hance et al., 2014). Although mechanistic reports of eHsp90 functions are scarce and not yet fully elucidated, eHsp90 has been of much interest due to its role in cancer invasiveness. Patsavoudi and colleagues have showed that a cell-impermeable monoclonal antibody, 4C5, was able to reduce breast cancer cell invasion *in vitro* and *in vivo* by selectively binding eHsp90 at the surface of tumour cells (Sidera *et al.,* 2011). Furthermore, the presence of eHsp90 is not specific to tumours since Hsp90α and Hsp90β isoforms have been shown to be localized on the cell surface of neural cells (Sidera et al., 2004) and in the conditioned medium of human dermal fibroblasts (Li et al., 2007). Additional roles for eHsp90 have also been demonstrated in the pathogenicity of viral and bacterial infections (Zügel & Kaufmann, 1999; Triantafilou & Triantafilou, 2004). This highlights important functional roles for eHsp90 in both normal and diseased states (Eustace & Jay, 2004). However, considering certain tumour cells constitutively express eHsp90 to achieve cell invasion, targeting eHsp90 could prove to be a potential therapeutic strategy for cancer (McCready *et al.,* 2010; Li *et al.,* 2011).

Table 1: Examples of Intracellular and Extracellular Hsp90 interacting proteins

Protein	Location	Function	Reference
Annexin	Extracellular	Indirectly increases plasmin activity in diabetic patients	(Lei et al., 2004; McCready et al., 2010)
MMP9		Stability of MMPs; promotes matrix catabolism and invasion of cancer cells	(Stellas et al., 2010)
MMP2			(Eustace et al., 2004; Tukaj et al., 2015)
MMP3			(Correia et al, 2013)
Hsp70		Creates receptor complex for Dengue virus entry in monocytes/macrophages	(Calderwood et al., 2016; Reyes-del Valle et al., 2005)
HER2-Erb2		Promotes cancer cell invasion	(Sidera et al., 2008)
LAP		Inactivation of TGF-β1 signaling pathway in cancer	(Suzuki & Kulkarni, 2010)
tPA		Promotes cancer cell motility	(McCready et al., 2010)
Cdc37		Responsible for kinase stability and maturation by Hsp90 chaperone complex	(El Hamidieh et al., 2012)
LRP1		Promotes invasion of glioblastoma cells via Akt-EphA2 signaling	(Gopal et al., 2011)
FN		Stabilisation of the ECM	(Hunter et al., 2014)
LOXL2		Regulates cell polarity and cancer cell metastasis	(McCready et al., 2014)
HSF1	Intracellular	Activates the RalGTP signal transduction pathway to regulate transcription of heat shock genes	(Hu & Mivechi, 2003; Kijima et al., 2018)
Stat3		Stabilizes STAT3 and promotes interleukin-6 (IL-6)- mediated signaling	(Sato et al., 2003; Setati et al., 2010)
Akt		Maintains Akt kinase activity through preventing dephosphorylation by PP2A	(Sato, Fujita, & Tsuruo, 2000)
HER2		Modulates the stability and trafficking of nascent ErbB2	(Xu et al., 2002)
Hop		TPR co-chaperone mediates transfer of clients from Hsp70 to Hsp90 complex	(Li et al., 2012; Perdew & Whitelaw, 1991)
EphA1		Responsible for EphA2 receptor stability and signaling	(Annamalai et al., 2009)
p53		Stabilizes the mutated p53 conformation	(Blagosklonny et al., 1996; Li et al., 2012)

1.4 Inhibition of Hsp90

Due to the role of Hsp90 as a chaperone of oncogenes and/or tumour suppressors (Table 1), Hsp90 has become an attractive drug target which has fueled the development of numerous Hsp90 inhibitors for cancer treatment. Hsp90 is in an activated complexed form upon binding of co-chaperones and client proteins. Kamal and colleagues showed that Hsp90 in tumours consists largely of this activated form and that Hsp90 inhibitors selectively accumulate in tumours at least in part due to the high affinity, activated form of Hsp90 in tumour cells versus low affinity, inactive forms in normal cells (Kamal et al., 2003). Inhibition of Hsp90 also renders tumour cells susceptible to treatment by chemotherapy and radiation. The motivation behind targeting Hsp90 inhibition for cancer therapy thus lies in its advantage in both depleting oncogenic proteins and interrupting multiple oncogenic pathways, and the increased ATPase activity in cancer cells (Piper & Millson, 2011; Trepel, Mollapour, Giaccone, & Neckers, 2010). The development of selective anti-cancer drug targets, such as trastuzumab, has had significant success, although the need to target multiple oncogenic proteins and pathways has led to the increased research into Hsp90 inhibitor drugs, since Hsp90 is considered a central node in signalling pathways. Consequently, Hsp90 inhibitors are being tested for their anti-cancer efficacy in combination with these other treatments to achieve better outcomes (Sidera & Patsavoudi, 2014). A novel mechanism of tumour regulation has been proposed which involves targeting of a modified chaperome network, termed the 'epichaperome', which consists of a highly integrated network of co-chaperones, isomerases and scaffold proteins with Hsp90 and Hsp70 (Rodina et al., 2016). This chaperome complex is present in over half of all tumours and was demonstrated to be more sensitive to inhibitors and thus a better chemotherapeutic target (Rodina et al., 2016).

1.4.1 N-terminal Hsp90 inhibition

There are effectively two groups of Hsp90 inhibitors which target either the C-terminus or N-terminus of Hsp90 (Figure 1). Hsp90 N-terminal inhibitors impair Hsp90 molecular chaperone function by competing with ATP at the ATPase domain on the N-terminus (Prodromou et al., 1997). Geldanamycin (GA) is a benzoquinone ansamycin antibiotic isolated from the fermentation broth of *Streptomyces hygroscopicus* and one of the first natural Hsp90 inhibitors discovered in 1970 (Deboer et al., 1970). GA functions by mimicking ATP structure

and preventing ATP binding at the N-terminus resulting in client degradation (Grammatikakis et al., 2002; Grenert et al., 1997; Prodromou et al., 1997). Since then, various synthetic GA derivatives have been developed, including radicicol, 17-(Allylamino)-17-demethoxygeldanamycin (17-AAG), which was the first Hsp90 inhibitor to enter into clinical trials, 17-(Dimethylaminoethylamino)-17-demethoxygeldanamycin (17-DMAG), IPI-504 and retaspamycin (Chiosis et al., 2002). Radicicol, another natural product Hsp90 inhibitor, was found to compete with GA for the Hsp90 ATP binding site (Roe et al., 1999). Utilizing knowledge of the natural product inhibitors' scaffold and interactions with the Hsp90 ATP binding pocket resulted in the development of second generation inhibitors of Hsp90 through chemical synthesis which exhibit increased potency and reduced toxicity. These second generation Hsp90 inhibitor compounds were designed to mimic the folded structure adopted by GA and radicicol when bound to Hsp90 and are divided into three major classes according to their core structures: purine, resorcinol, and benzamide. One of the first inhibitors created in the purine class was PU3 (Chiosis et al., 2001, 2002). A modified version of this, PU-H71, showed increased activity in tumours and better Hsp90 inhibitory activity (Caldas-lopes et al., 2009). Other purine-based inhibitors include BIIB02 (Lundgren et al., 2009) and CUDC-305 (Bao et al., 2009) as well as CNF2024/BIIB021 and Debio 0932 both of which are in clinical trials (Binder & Srivastava, 2018). The resorcinol class of inhibitors include AT13387 (formerly known as onalespib) (Woodhead et al., 2010), ganetespib (formerly known as STA-9090) (Shimamura et al., 2012), and NVP-AUY922 (Eccles et al., 2008). The third class are the benzamide-based scaffolds which include TAS-116 (Ohkubo et al., 2015), XL888 (Bussenius et al., 2012), and SNX-5422 (Infante et al., 2014).

One of the major problems associated with Hsp90 inhibition has been in the generation of a HSR brought about by specific binding to the N-terminal ATP-binding site of Hsp90 (Haggerty et al., 2014; Whitesell & Lindquist, 2005). Additionally, many of the N-terminal inhibitors have poor solubility, hepatotoxicity and/or lack of activity in animal studies. All clinical trial drugs of this group of Hsp90 inhibitors have been unsuccessful, which has been proposed to be in part due to their reported non-specificity for proteins other than Hsp90 thereby producing off-target effects (Wang, Koay, & McAlpine, 2017).

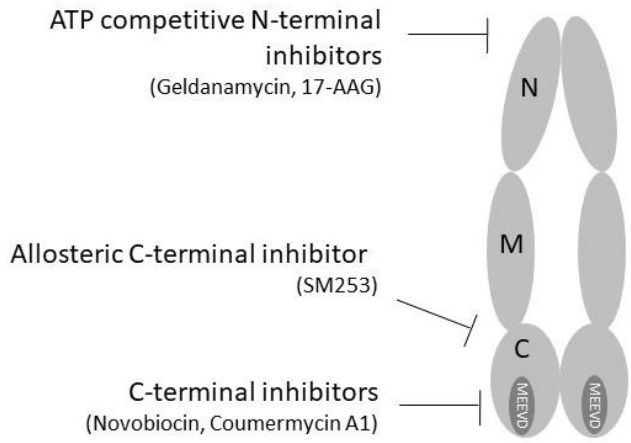

Figure 1: Domain structure of Hsp90 and the target domains of the main classes of Hsp90 inhibitors

Hsp90 consists of the 25 kDa N-terminal ATPase domain responsible for the ATP-dependent clamping mechanism associated with substrate binding, the 35 kDa middle (M) domain responsible for binding Hsp90 client proteins and the 12 kDa C-terminal domain responsible for Hsp90 dimerization and co-chaperone interactions via the conserved MEEVD motif.

1.4.2 C-terminal Hsp90 inhibition

C-terminal Hsp90 inhibitors, in contrast to N-terminal inhibitors, do not induce the HSR (Burlison, Neckers, Smith, Maxwell, & Blagg, 2006; Eskew et al., 2011) and are increasingly being pursued due to their better solubility and decreased hepatotoxicity in clinical trials. This type of inhibitor functions by an alternative mechanism, that is, by disrupting the dimerisation of Hsp90, as well as interfering with Hsp90 interaction with co-chaperones and some clients that bind the C-terminus such as HER2, p53 and Raf-1 (Trepel et al., 2010). The coumarin-containing antibiotic, novobiocin (NOV), was found to bind at a second ATP binding site at the C-terminus of Hsp90 (Marcu, Schulte, & Neckers, 2000). This C-terminal nucleotide pocket does not interact with GA or radicicol. NOV was originally used to treat bacterial infections by inhibiting bacterial DNA gyrase B (Burlison et al., 2006) and also inhibits mammalian DNA polymerase α and topoisomerases I and II (Edenberg, 1980; Hussy, Maass, Tummler, Grosse, & Schomburg, 1986). NOV was initially hypothesized to bind the N-terminal domain (NTD) of Hsp90 due to similarities with ATP, but was later shown to bind within the C-terminal domain (CTD) localized to residues 538-728 (Allan et al., 2006; Kamal et al., 2003). NOV is composed of three distinct parts upon which modifications can be made: the benzamide side chain, the

coumarin core and the noviose sugar. Utilizing the coumarin-ring structure of NOV, several analogues have since been developed to improve upon its' poor Hsp90 inhibitory activity including compound A4, DHN1 and DHN2 (Burlison et al., 2008). While no co-crystal structure of a C-terminal inhibitor such as NOV bound to Hsp90 exists, significant advances have been made toward elucidation of structure-activity relationships for NOV. One of the more potent novobiocin analogs created is KU-174 by the Blagg group (Donnelly et al., 2008). Coumermycin A1 is a coumarin antibiotic similar to NOV which functions to inhibit Hsp90 by disrupting the formation of the Hsp90 dimer which subsequently prevents binding between Hsp90 and several C-terminal co-chaperones (Allan et al., 2006; McConnell, Alexander, & Mcalpine, 2015). Another C-terminal inhibitor is the green tea extract, Epigallocatechin-3-Gallate (EGCG); this compound has reported anti-cancer activity and was found to interact within the same region of Hsp90 as NOV (Yin, Henry, & Gasiewicz, 2009). Other less-specific C-terminal inhibitors include the platinum-containing chemotherapeutic agent, cisplatin, and the microtubule stabilizer, Taxol (Donnelly & Blagg, 2008). One C-terminal inhibitor, RTA901 based on the novobiocin analog KU-32 (Reata Pharmaceuticals) is currently in a phase 1 clinical trial (Neckers et al., 2018).

1.4.3 Inhibition of Hsp90/co-chaperone interactions

Hsp90 requires a series of co-chaperones to assemble a chaperone complex in order to exert its functions. By targeting different Hsp90/co-chaperone interactions the chaperone cycle can be arrested and similar consequences to that of the direct inhibition of Hsp90 can be achieved (Sidera & Patsavoudi, 2014). Some of the co-chaperones targeted for disruption are Aha-1, Cdc37, Hop and p23 (Edkins, 2016). KU-135 and KU-174 are novobiocin-based C-terminal Hsp90 inhibitors containing a biaryl side chain that effectively disrupted the Hsp90α/Aha1 complex (Ghosh et al., 2015). Cdc37 acts as an adaptor, responsible for loading kinase clients onto the Hsp90 complex and facilitating kinase maturation (Pearl, 2005; Silverstein et al., 1998). Celastrol is a natural quinone methide triterpene isolated from the bark of *Tripterygium* species (Zhang et al., 2008). The action of this compound is predicted to occur by blocking the interaction site between Hsp90 and Cdc37 and preventing Hsp90 ATPase activity without inhibiting ATP binding (Zhang et al., 2009). Recently it has been shown that celastrol reacts with cysteine residues of Cdc37 (Sreeramulu et al., 2009) and directly interacts

with the co-chaperone p23 (Chadli et al., 2010). Another inhibitor of the interaction of Hsp90 with both Cdc37 and p23 is the natural compound Curcurbitacin D. Whilst this compound shares some structural similarity with celastrol, unlike celastrol it does not induce a HSR (Hall et al., 2015). Gedunin, another structurally similar natural compound directly binds p23 and induces degradation of Hsp90 client proteins (Patwardhan et al., 2013). Hop, is a major TPR containing co-chaperone responsible for client transfer from Hsp70 to the Hsp90 chaperone complex. Horibe and colleagues designed a TPR hybrid peptide based on the binding interface of the TPR2A domain to block the main interaction site between Hop and Hsp90 (Horibe et al., 2011). According to Horibe, this peptide has selective cytotoxic activity which allows it to discriminate between cancer and normal cell lines (Horibe et al., 2011). Pimienta and colleagues reported a small molecule, which they termed C9, to bind the TPR2A domain of Hop and thereby disrupt the Hsp90/Hop interaction (Pimienta, Herbert, & Regan, 2011). Another class of inhibitors which disrupt the binding of co-chaperones to Hsp90 include the Sansalvamide A compounds (a natural product isolated from a marine fungus) (Belofsky, Jensen, & Fenical, 1999). In contrast to the compounds described by Horibe and Pimienta which bind directly to Hop (Horibe et al., 2011; Pimienta et al., 2011), the Salsalvamide A compounds are allosteric inhibitors that bind to the middle domain of Hsp90 and disrupt the binding of co-chaperones to the C-terminus of Hsp90 such as that of FKBP38, FKBP52 and Hop (Alexander et al., 2009; Vasko et al., 2010). Several sansalvamide A derivatives including SM122, SM145 and SM253 (Koay et al., 2014) have demonstrated the ability to block binding of TPR containing co-chaperones at the Hsp90 C-terminus. These SM derivatives from the McAlpine group are significantly more potent inhibitors compared to novobiocin or other coumarin derivatives and have demonstrated improved solubility and cytotoxicity (McConnell et al., 2015). In particular, the SM compounds have demonstrated rapid induction of apoptosis, and do not induce the HSR. In contrast, compounds that target the N-terminus of Hsp90, specifically 17-AAG, do not induce apoptosis immediately, but rather trigger a rescue mechanism by producing large quantities of Hsp70, Hsp27 and HSF1 (McConnell et al., 2015; Wang & McAlpine, 2015).

1.4.4 Other forms of Hsp90 inhibition

Targeted inhibition of Hsp90-client interactions have also been developed although lack of knowledge regarding the molecular basis of these interactions has halted further development of these types of inhibitors. Altieri and colleagues disclosed a series of compounds that inhibit Hsp90 interactions with various Inhibitors of Apoptosis (IAPs), including survivin, XIAP, cIAPI/2 (Altieri, 2006). An example of such an inhibitor is shepherdin which is a peptidomimetic compound that inhibits Hsp90 interaction with survivin (Altieri, 2006). Several cell-impermeable Hsp90 inhibitors have been described which target extracellular Hsp90 including DMAG-N-oxide (Tsutsumi et al., 2008), non-cell permeable monoclonal antibody, 4C5 (Sidera et al., 2004), STA-12-7191 a biotinylated analogue of ganetespib (McCready et al., 2014), and fluorophore-tethered HS-27 and HS-131 (Barrott et al., 2013; Crowe et al., 2017). Issues surrounding the use of DMAG-N-oxide has been in that it generates metabolic byproducts which cause retinal damage, whilst the large size of the 4C5 monoclonal antibody may limit its ability to penetrate tumours (Kummar et al., 2011; McCready et al., 2014). More recently, the targeted inhibition of Hsp90α and Hsp90β specific isoforms has been explored. However, Hsp90α and Hsp90β share ~95% identity in their N-terminal ATP binding site (only two amino acids differ between these isoforms), making the development of Hsp90α- or Hsp90β-selective inhibitors extremely challenging. Wei Li's group have developed a monoclonal antibody, 1G6-D7, which binds to the F-5 region within the linker region and middle domain of Hsp90α and neutralizes the function of secreted Hsp90α (Zou et al., 2016). Data from the Blagg group have demonstrated the first N-terminal isoform selective inhibitor of Hsp90β, KUNB31. This compound exhibits 50-fold selectivity for Hsp90β, and selective activity towards cancer cells. Importantly, KUNB31 induced the degradation of selected Hsp90β-dependent clients without concomitant induction of Hsp90 levels (Khandelwal et al., 2018). A total of 17 small molecule inhibitors of Hsp90 have entered clinical trials since 1999 and although some Hsp90 inhibitors have shown clinical activity, none have been approved for clinical application in cancer treatments (Khandelwal et al., 2018; Wong & Jay, 2016). The research in the field of effective Hsp90 inhibition is still ongoing and hopes of Hsp90 inhibitors as part of a combinatorial therapy approach are largely being investigated (Sidera & Patsavoudi, 2014).

1.5 The Extracellular Matrix

The extracellular matrix (ECM) is a three-dimensional non-cellular component of tissues and organs, which exists to provide essential physical and biochemical cues for the cell. The ECM plays important roles in structural support and cell signalling, and contains proteins involved in regulating cell proliferation, migration, polarity and survival (Lin & Bissell, 1993; Hynes, 2009). The interaction of cells with the ECM is equally important for regulating these processes. Furthermore, the bidirectional communication between the ECM and the actin cytoskeleton, mediated largely by transmembrane integrin receptors, is important for cell adhesion and migratory functions (Bridgewater et al., 2012; Frantz et al., 2010). The importance of the ECM is made evident by the large array of diseases that may arise from abnormalities in the ECM including autoimmune and inflammatory diseases, cancer, fibrosis and atherosclerosis (Bonnans, Chou, & Werb, 2014; Cox & Erler, 2011). The ECM is composed of approximately 300 proteins, encompassing structural proteins, glycoproteins, growth factors and matricellular proteins (a partial list is presented in Table 2). The matricellular proteins are non-structural modulators of extracellular signals and are presumed to assist in providing a linkage between the ECM and cell surface receptors. These include thrombospondins, SPARC (Secreted Protein Acidic and Rich in Cysteine), osteopontins and tenascin-C (Bornstein & Sage, 2002). The ECM molecules are divided into two subgroups: the basement membrane (BM) which underlies epithelial cells and interstitial/stromal ECM which constitutes the intercellular spaces. The BM is composed largely of laminins, type IV collagen and proteoglycans (Frantz et al., 2010), whilst the stromal ECM includes collagens type I, II and III, fibronectin (FN), vitronectin (VN) and elastin (Huang & Greenspan, 2012). Each tissue in animals has a specific type of ECM; the ECM of bone tissue is comprised of collagen fibres and bone minerals, whilst blood plasma constitutes the ECM of blood. Fibroblasts are the major cells responsible for synthesising and maintaining the ECM in connective tissue, whilst chondrocytes and osteoblasts are responsible for cartilage and bone ECM formation, respectively (Huang & Greenspan, 2012). Many of these ECM proteins contain multiple domains with specific binding sites for macromolecules or receptors (Hynes, 2009). The ECM is highly dynamic and is constantly being remodelled to accommodate its variety of functions. ECM remodelling occurs in both physiological and pathological cases (Bonnans *et al.,* 2014; Daley *et al.,* 2008). Tissue homeostasis requires a balance between ECM synthesis and degradation. Perturbing homeostasis by loss of function mutations or modifications of ECM

molecules, and excessive deposition or removal of ECM components, results in progression of various disease states including fibrosis, cancer and other developmental abnormalities (Frantz et al., 2010; Lu et al., 2011a). The recognised importance of the ECM in mediating disease has increased targeted therapies of the ECM (Theocharis *et al.,* 2015). ECM proteins contain secretory signal peptides and enter the secretory pathway co-translationally via the translocon of the rough endoplasmic reticulum (rER). Within the ER lumen, protein folding proceeds with the assistance of chaperones (Hellewell & Adams, 2015). Because a major role of ECM proteins is to form extracellular structural networks and fibrils, an important aspect of transit through the secretory pathway is the shielding of matrix assembly sites that would otherwise promote intermolecular interactions. For other ECM proteins, associated ER-resident chaperones may contribute to blockade of matrix assembly sites (Hellewell & Adams, 2015).

1.5.1 ECM and cancer

Cancer metastases are defined by the movement of tumour cells from the primary location to distant sites in the body where secondary tumours form (Steeg, 2006). This process requires several steps including degradation of the ECM, tumour cell detachment from primary tumour and migration of cells in the blood stream, adhesion to tissues at a distant site and growth of secondary tumours (Lu, Weaver, & Werb, 2012; Steeg, 2006). Although matrix degradation is required for cancer cell metastasis, controlled matrix degradation is also required for normal cellular processes including cell adhesion, differentiation and proliferation where there is a continuous turnover of matrix molecules (Sottile & Chandler, 2005). ECM remodelling can occur either through extracellular proteases, including serine proteases, urokinase plasminogen activator (uPA), tissue-type plasminogen activator (tPA), and matrix metalloproteinases (MMPs), or by endocytosis and intracellular degradation (Sottile & Chandler, 2005). However, it is thought that these two mechanisms are not mutually exclusive. Loss of the matrix has been implicated in metastasis of tumours, in particular, the abnormal removal of ECM proteins has been shown to contribute to the onset or development of diseases including cancer (Galante & Schwarzbauer, 2007; Lu et al., 2012; Shi & Sottile, 2008). Tissue ECM homeostasis is mediated by the secretion of MMPs, uPA and tPA which in turn are regulated by their corresponding inhibitor proteins, tissue inhibitors of

metalloproteinases (TIMPs) and plasminogen activator inhibitors (Egeblad & Werb, 2002; Zhang et al., 2013). Similarly, focal adhesions are the point of cell-ECM matrix interaction and are comprised of integrins that cluster together and bind the ECM, thus triggering downstream pathways mediated through Focal Adhesion Kinase (FAK). These downstream signaling pathways are able to modulate MMP and TIMP levels to adjust ECM synthesis and degradation (Caccavari et al., 2010).

Table 2: Some molecules constituting the extracellular matrix (ECM)

ECM protein	Function	Link with disease	References
Fibronectin	Structural glycoprotein. Roles in cell migration, growth, differentiation.	Fibrosis, tumour progression.	(Fonović & Turk, 2014; Schwarzbauer & DeSimone, 2011; Theocharis et al., 2015)
Collagen	Structural glycoprotein. Cell-ECM links, tissue rigidity and strength. Several types exist with distinct functions.	Fibrosis, tumour progression, cardiovascular disease	(Egeblad, Rasch, & Weaver, 2010; Fonović & Turk, 2014; Frantz et al., 2010; Lu et al., 2011; Mouw, Ou, & Weaver, 2014)
Laminin	Structural glycoprotein. Cell adhesion, migration, differentiation.	Fibrosis, tumour progression	(Domogatskaya et al., 2012; Fonović & Turk, 2014)
Vitronectin	Glycoprotein associated with loose connective tissue and involved in wound healing and blood coagulation	Fibrosis, tumour progression.	(Leavesley et al., 2013; Zhu, Xiong, Trinkle, & Xu, 2014; Preissner & Reuning, 2011)
Elastin	Provides structural integrity mainly in connective tissues and arteries	Cardiovascular disease, cancer.	(Halper & Kjaer, 2014; Theocharis et al., 2015)
Dentin Matrix Protein 1	Regulates nucleation of hydroxyapatite in bone ECM	Osteoporosis	(Bellahcène et al., 2008; Narayanan et al., 2003)
SPARC/ osteonectin	Non-structural. Mediates cell-matrix interactions and collagen biosynthesis	Arthritis, cancer, diabetes, osteoporosis	(Bradshaw, 2012; Brekken & Sage, 2000; Chlenski et al., 2011)
Thrombospondin	Non Structural. Cell-matrix interactions	Angiogenesis	(Adams & Lawler, 2011; Halper & Kjaer, 2014)
Osteopontin	Non-structural. Ca-binding glycoprotein involved in attachment of cells in mineralized bone matrix	Osteoporosis	(Bellahcène et al., 2008; Sodek et al., 2000)
Tenascin	Non-structural. Mediates inflammatory processes mainly in connective tissues.	Tumour progression, inflammation	(Halper & Kjaer, 2014; Oskarsson et al., 2011)

Matrix degradation is important for the spread of cancer cells through the body; this degradation event is thought to promote invasion by triggering the activation and recruitment of certain proteases (MMPs, serine proteases, plasmin and cathepsin), all of which degrade the ECM and allow for cancer cells to migrate easily into the bloodstream and colonize tissue at distant sites (Stellas et al., 2010; Zhang et al., 2013). Certain growth factors are also liberated by cells during ECM degradation which further aids in the survival of these tumour cells (Steeg, 2006). The tumour stroma has been shown to exhibit some of the characteristics of a wound such as stiffening induced by ECM deposition and remodelling by fibroblasts (Pickup, Mouw, & Weaver, 2014). The ECM plays dynamic and opposing roles in regulating cell migration. A dense fibrillar network has been shown to serve as a barrier to migrating cells, and that degradation of the ECM is required to allow for paths in which cells can freely migrate (Condeelis & Segall, 2003; Egeblad et al., 2010; Friedl & Gilmour, 2009). Others demonstrate that the ECM network provides a scaffold on which cells can attach and subsequently migrate and that removal of this network renders cells more immobile (Lu et al., 2011; McCarthy & Furcht, 1984; Rozario & DeSimone, 2010).

1.6 Fibronectin structure

Of the proteins that constitute the ECM, fibronectin (FN) is one of the most abundant ECM proteins along with collagen. FN is a dimeric glycoprotein consisting of two subunits of between 200-250 kDa held together by disulphide bonds. This glycoprotein plays important roles in cell adhesion, motility, proliferation, differentiation, cytoskeletal organisation and oncogenic transformation amongst others (Schwarzbauer, 1991; To & Midwood, 2011). FN can be categorized as either plasma FN or cellular FN. Although there is only one gene in humans for FN, this can give rise to 20 potential FN isoforms through alternative splicing (Kumazaki et al., 1999). The different isoforms generated by alternative splicing are indicated as A, B and V in Figure 2. Plasma FN is produced by hepatocytes to circulate in the bloodstream as soluble FN, and cellular FN is produced by fibroblasts, endothelial cells, and many others (Lemmon, Ohashi, & Erickson, 2011). Due to its conformational flexibility in both plasma and fibrillar forms, FN is a mechanoregulator of the ECM. FN is made up of tandem repeats of three domain modules: Types I, II, and III. FN is versatile in its functions because it has co-existing binding sites present at its N-terminal domain for various molecules including heparin, actin, DNA and collagen, as well as cell surface proteins (Gutman, Yamada, &

Kornblihtt, 1986). The RGD (Arg-Gly-Asp) sequence is a ubiquitous cell binding region as it is recognized by a wide range of integrins and is also found in other proteins such as vitronectin, laminin, and thrombospondin (Wang, Seo, Fischbach, & Gourdon, 2016). Another important region on FN essential to mechanoregulation is the domain type $III_{12–14}$ sequence, which binds various growth factors important in cell signalling. Cysteines (indicated by "-S" in Figure 2) present in the C-terminal domain are responsible for joining FN monomers via disulphide bonds (Schwarzbauer, 1991). The 70 kDa N-terminal domain is essential for fibril formation; FN lacking this domain is incapable of assembly (Lemmon et al., 2011; Schwarzbauer, 1991). In particular, the domain type I_{1-5} repeats is considered crucial for FN matrix assembly (Lemmon et al., 2011).

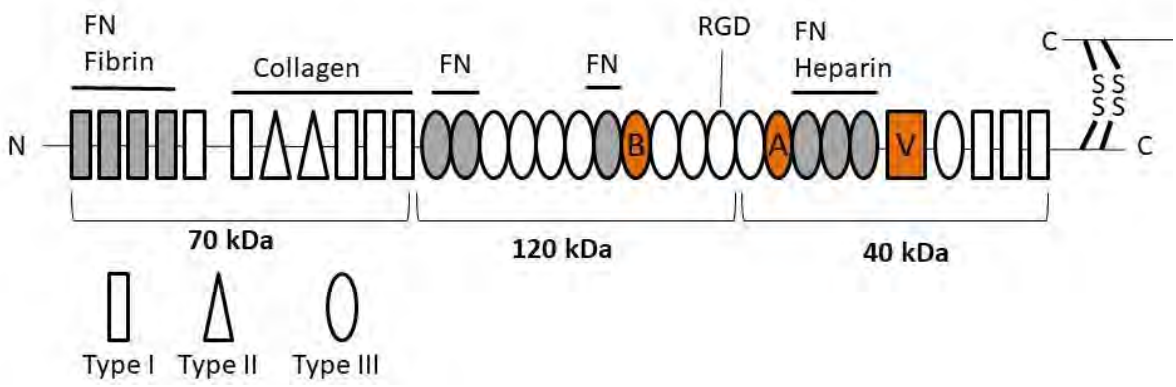

Figure 2: Domain structure of fibronectin (FN)

FN consists of 12 type I (rectangles), 2 type II (triangles) and 17 type III (ovals) repeats. Sets of repeats constitute binding domains for fibrin, FN, collagen and heparin, as indicated. The three alternatively spliced regions, EIIIA, EIIIB and V are in orange. The assembly domain and FN-binding sites are in grey. The FN glycoprotein is organised into functional domains: 70 kDa N-terminal domain, 120 kDa central binding domain (CBD) and 40 kDa heparin binding domain, as indicated. Two FN monomers bind by disulphide bonds, S-S, at the C-terminus to form a dimer. (Adapted from Wierzbicka-Patynowski & Schwarzbauer, 2003).

1.7 Fibronectin turnover

1.7.1 FN synthesis

The exact mechanism of fibronectin fibril formation is still unknown, but it is thought that fibronectin is produced as a soluble protein which is polymerized into insoluble fibrillar structures that form the bulk of the ECM and that this process may take as little as 20 minutes (To & Midwood, 2011). The process of fibrillogenesis is initiated by the binding of 70 kDa FN

domain to integrins, including α5β1, α3β1, and α4β1 (KcKeown-Longo & Mosher, 1985; Takada, Ye, & Simon, 2007). Integrins are the principal transmembrane protein receptors which provide a linkage between the ECM outside the cell and the cytoskeleton inside (To & Midwood, 2011). The binding of FN to integrins induces conformational changes in the actin cytoskeleton which causes receptor clustering. Binding of the RGD and synergy motifs on FN to α5β1 integrin transmits tension to the fibronectin molecules and stretches them, thereby exposing other FN-association binding sites in the molecule (Mosher, Fogerty, Chernousov, & Barry, 1991; Theocharis et al., 2015). This allows for nascent deoxycholate-soluble FN molecules to bind directly to one another, and recruit additional FN molecules to form ultrathin fibrils which polymerize upon addition of FN dimers to form mature, thick deoxycholate-insoluble FN fibrils and a complex network (Erickson, 2002). The exact process of conversion from soluble to insoluble FN and the proteins involved in crosslinking of FN fibrils is still under investigation (Ohashi & Erickson, 2009; Wierzbicka-Patynowski & Schwarzbauer, 2003). FN networks may also be initiated via self-assembly. FN contains conformational-dependent binding sites for itself located on domain types $I_{1–5}$, $III_{1–2}$, $III_{4–5}$, and $III_{12–14}$ (Wang et al., 2016). Multiple conformations of FN exist in the matrix (and in individual fibrils) however during ECM the conformation evolves from a compact form in early fibrils to an extended/unfolded form in mature fibrils and matrices (Wang et al., 2016). The deposition of ECM molecules including collagen and thrombospondin have been shown to be dependent upon the presence of fibronectin fibrils (Sottile & Hocking, 2002). Actin cytoskeleton rearrangements have also been shown to play a role in FN assembly (Daley et al., 2008). Activation of Rho GTPases induces changes in actin organisation and enhances FN assembly whilst the inhibition of actin organisation has been shown to promote endocytosis of FN and its subsequent degradation (Wierzbicka-Patynowski & Schwarzbauer, 2003).

1.7.2 FN degradation

Treatment of cells with a polyclonal antibody to fibronectin inhibited polymerization of fibronectin into matrix, and FN was found to be endocytosed and localized with lysosomes (McKeown-Longo & Mosher, 1985; Sottile & Hocking, 2002; Villiger et al., 1981). Since FN binds integrins, particularly the α5β1 integrin, during fibril formation, it is possible that FN

becomes internalised with the constitutive endocytosis-recycling pathway of integrins (Bretscher, 1989; Shi & Sottile, 2008; Sottile & Chandler, 2005).

Since ECM FN consists of large fibrils of high molecular weight multimers, these require initial proteolysis into smaller sized FN fragments (120 kDa, 70 kDa and 40 kDa) before endocytosis (Kenny *et al., 2*008; To & Midwood, 2011). Studies by Salicioni *et al.,* (2002) have shown that FN accumulates in the extracellular space in low density lipoprotein receptor-related protein 1 (LRP1)-deficient Chinese Hamster Ovary (CHO) cells. Thus, an alternative or additional pathway to the integrin-mediated pathway which regulates FN internalisation, may involve LRP1. Also, LRP1 mediates catabolism of FN and thus LRP1 serves as a potential regulator of FN turnover (Salicioni et al., 2002). However, LRP1 may not be the only receptor for FN uptake, as Gaultier *et al.,* (2010) showed that, in LRP1-deficient fibroblasts, the increased remodelling of FN was dependent on presence of uPA and the urokinase type plasminogen activator receptor (uPAR).

1.7.3 Regulation of the FN matrix by Hsp90

Regulation of the ECM by Hsps occurs at various levels within the cell both intracellularly and extracellularly (Figure 3). Various Hsps as well as co-chaperones such as Hop and p23 have been found on the plasma membrane and in the extracellular space (Eustace & Jay, 2004; Hegmans et al., 2004; Shin et al., 2003). An array of Hsps and some additional molecular chaperones involved in ECM regulation at various stages are listed in Table 3. FN has been reported as a novel interacting protein of extracellular Hsp90 and a direct role for Hsp90 in FN matrix stability and remodelling has been suggested (Figure 3) (Hunter et al., 2014). Surface associated Hsp90 and extracellular soluble Hsp90β were identified in breast cancer cell lines including Hs578T, MDA-231 and MCF-7 cells, and a complex containing Hsp90 and FN was identified by immunoprecipitation and tandem mass spectrometry. The direct binding of FN and Hsp90 *in vitro* and colocalisation of these proteins in breast cancer cell lines has been demonstrated (Hunter et al., 2014). Addition of exogenous Hsp90β in Hs578T cells increased the formation of extracellular FN matrix, while knockdown of Hsp90α or Hsp90β decreased the proportion of extracellular FN matrix, suggesting a role for extracellular Hsp90 in FN fibril formation. Upon inhibition of Hsp90 by novobiocin, the FN matrix was observed to

become unstable and degraded by a receptor-mediated endocytic mechanism (Figure 3) (Hunter et al., 2014).

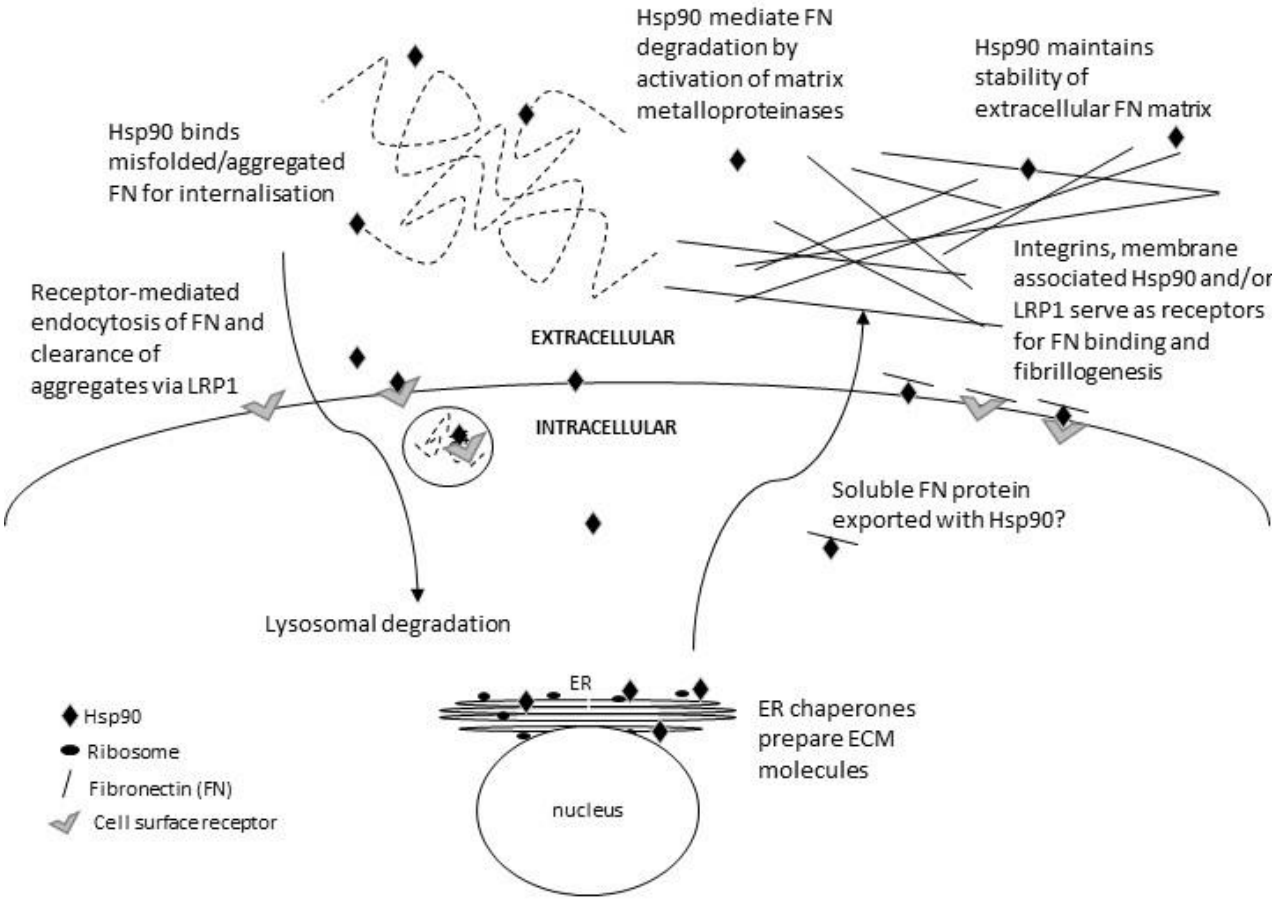

Figure 3: Proposed role of integrins, LRP1 and Hsp90 in FN turnover

Schematic illustration of intracellular and extracellular regulation of the ECM by Hsp90. Soluble FN molecules are modified and processed in the ER by ER molecular chaperones and enzymes and subsequently transported to the cell surface presumably bound to chaperones for secretion. Integrins bind the RGD motifs on FN and together with actin filaments cause the stretching of fibronectin which exposes its self-association sites to allow for addition of FN dimers to form an insoluble matrix. Extracellularly, ECM molecules assemble into polymeric complexes to form a structural scaffold or associate with the ECM assisted in part by extracellular Hsps or LRP1 which may serve as receptors to mediate this cell-ECM association. Proteases (MMP2 and uPA amongst others) activated by Hsps cleave the FN matrix into smaller fragments (120, 70, 40 kDa) in response to normal tissue turnover or wound healing. Misfolded and/or aggregated matrix molecules are bound by extracellular Hsps for clearance from the ECM and subsequent intracellular degradation. Upon binding LRP1, FN is internalised and delivered to lysosomes for degradation (Adapted from Boel & Edkins, 2018).

The exact mechanism by which Hsp90 influenced the FN matrix is presently unknown. It is not clear whether extracellular Hsp90 acts as a chaperone, cytokine or receptor for FN during internalisation, or whether this Hsp90-mediated turnover of FN requires an additional

receptor. A putative extracellular complex that exists between FN, Hsp90 and low density lipoprotein receptor related protein 1 (LRP1) on the surface of Hs578T cells has been shown (Boel, Hunter, & Edkins, 2018) and that internalisation of FN upon inhibition of Hsp90 by NOV requires the presence of LRP1. Given that both FN and Hsp90 interact with LRP1, it may be that NOV mediated its effects on FN either by modulating the Hsp90-FN-LRP1 complex to promote LRP1-mediated endocytic clearance of extracellular FN, or by activation of a signalling pathway due to a change in the Hsp90-LRP1 interaction or indeed a combination of both mechanisms. Armstrong and colleagues have also demonstrated a role for Hsp90 in FN regulation by showing that an N-terminal Hsp90 inhibitor, AUY922, increased expression of total FN and FN in the cytosol of prostate cancer cell lines and reduce secretion of FN which caused a marked reduction in cell invasion (Armstrong et al., 2018).

Table 3: Overview of some chaperones involved in ECM regulation

Chaperone	Location	Function in ECM	Reference
Hsp90	Intra- and Extracellular	Regulates turnover of FN	(Hunter et al., 2014)
	Intra- and Extracellular	Regulation of proteases (MMP) for degradation of ECM	(Sims et al., 2011)
Grp94	ER, extracellular	Regulates processing of integrins Mediates cell signalling at the cell surface to promote cell motility	(Arap et al., 2004; Liu et al., 2003)
Hop, Hsp70, p23	Intra- and Extracellular	Forms a complex with Hsp90 to assist in activation of proteases	(Sims et al., 2011)
Hsp70	Intra- and Extracellular	Activates cytokines contributing to accumulation of ECM proteins	(González-Ramos et al., 2013)
Hsp47	ER, extracellular	Procollagen maturation and collagen fibril processing in ECM	(Nagai et al., 2000; Taguchi & Razzaque, 2007; Jieqing Zhu et al., 2015)
Grp78/Bip	ER, extracellular	Endocytoses DMP1 in bone matrix. Binds cell surface receptors mediating ECM degradation. Regulates transport of ECM proteins in ER	(Lee et al., 2014; Li et al., 2013; Ravindran et al., 2011)
Hsp25/Hsp27	Cytoplasm, ER	Trafficking of mature, active aggrecan to the cell surface	(Zheng, Luo, & Tanzer, 1998)
MRJ/DNAJB6	Cytoplasm	Regulates uPAR-dependent cell adhesion to VN	(de Bock et al., 2010; Lin et al., 2014)
Clusterin	Extracellular	Clearing aggregates associated with protein deposition disorders	(Bartl et al., 2001; Zlokovic et al., 1996)
SPARC	Extracellular	Stabilizes procollagen Binds various ECM proteins Regulates levels of matrix metalloproteinases	(Lane & Sage, 1994; Martinek, Shahab, Sodek, & Ringuette, 2007)

Hsp90 has also been shown to regulate the function of FN-binding integrins in the ECM. Inhibition of cell surface Hsp90, with the small molecule, cell-impermeable N-terminal inhibitor DMAG-N-oxide, suppressed β1 integrin-mediated cell invasion in Matrigel invasion assays in T24 human bladder cancer, PC3M prostate cancer and B16 murine melanoma cancer cell lines (Tsutsumi et al., 2008). FN induces the association of integrins and c-Src at focal adhesion points, a key component in the cell migration process (Wozniak, Modzelewska, Kwong, & Keely, 2004). Tsutsumi and colleagues analysed focal adhesion assembly by immunoprecipitation of β1-integrin on FN coated and uncoated surfaces to determine that DMAG-N-oxide reduced c-Src binding to integrins. Disrupting the FN-stimulated interaction of β1-integrin with c-Src by the extracellular Hsp90 inhibitor reduced cell adhesion to the ECM and decreased cell motility (Tsutsumi et al., 2008). Again, the mechanism by which Hsp90 reduced integrin – c-Src binding remains undefined.

Extracellular Hsp90 appears also to participate in the remodelling of the extracellular matrix (ECM) through its interaction with MMPs. MMP2 and MMP9 are central players in cell migration and invasion due to their ability to digest ECM components and cleave cell adhesive contacts (Haas, 2005) and in the invasion of surrounding tissues and metastasis by tumour cells (Hance et al., 2012). Binding of Hsp90 appears to activate the pro-forms of these enzymes through their proteolytic cleavage, release active MMPs and thus permit ECM remodelling and enhanced invasion (Sims et al., 2011; Song et al., 2010).

Co-immunoprecipitation revealed a complex of Hsp90 and co-chaperones including Hsp70, Hsp40, Hop and p23, which assisted Hsp90α in activating MMP2 extracellularly in MDA-MB-231 breast cancer cells (Sims et al., 2011). Using zymography, the authors showed that in the presence of this complex, MMP2 activation was enhanced by 33 % in an ATP-independent manner, and was able to promote cell migration (Eustace et al., 2004; Sims et al., 2011). However, the mechanism of activation by this extracellular complex is still unclear and it is unknown whether extracellular Hsp90α acts as a chaperone or cytokine in its role in activating MMP2. In HT-1080 fibrosarcoma cells, plasmin activation assays demonstrated the ability of extracellular Hsp90α to activate a second extracellular protease, plasmin, by converting it from its precursor, plasminogen, to the active plasmin in much the same way as that of MMP2 (McCready et al., 2010). In the presence of DMAG-N-oxide, there was a 32% decrease in activated plasmin. Using transwell migration assays, inhibition of extracellular Hsp90α

decreased tumour cell migration compared to control treated cells. Cell migration is dependent in part on proteolysis of the ECM and these data suggest that plasmin may be contributing to cell migration via remodelling of the ECM and highlights the important regulatory role for Hsp90 in this process (McCready et al., 2010). McCready and colleagues identified a cohort of extracellular Hsp90α interacting proteins by mass spectrometry, most of which were in their inactive, precursor forms, and which they propose are activated by extracellular Hsp90α. They suggest that the potential role for extracellular Hsp90α may be through the appropriate activation of these proteins which then contribute to cell migration and invasion by enhancing remodelling of the ECM (Figure 3) (McCready et al., 2010). However, the mechanism by which Hsp90 activates these extracellular proteases remains undefined, although McCready and colleagues speculate that it may involve the proteolytic processing of inactive, precursor forms of these pro-invasive proteins (McCready et al., 2014; Sims et al., 2011).

1.8 Fibronectin in disease

FN plays important roles in tumour cell biology (Akiyama, Olden, & Yamada, 1995; Labat-Robert, 2002) and in the progression of fibrosis (Rukosuev, Nanaev, & Milovanov, 1990), synovial related diseases (Kimura et al., 2014) and Alzheimer's disease (Lemańska-Perek et al., 2009). Fibrosis is characterized by an excessive deposition of connective tissue that leads to the impairment of organ structure or function and is considered a chronic inflammatory tissue-repair response. In fibrosis and inflammation related diseases, the increased deposition of ECM components including FN is known to be a causative factor in the development of pathological conditions such as cirrhosis of the liver and Crohn's disease (Altrock et al., 2014). Rheumatoid arthritis (RA) is an autoimmune disease characterized by the chronic inflammation of synovial tissue, resulting in bone and joint erosion. The presence of cellular FN in rheumatoid synovial tissues has implicated FN in the pathogenesis of RA (Kimura et al., 2014). Alzheimer's disease is a neurodegenerative disease characterized by progressive loss in memory caused by the accumulation of amyloid plaques and tau aggregation in some regions of the brain. These amyloid plaques were shown to be correlated with high expression levels of FN, and that plasma FN could serve as a diagnostic biomarker for Alzheimer's dementia risk (Lemańska-Perek et al., 2009; Lepelletier et al, 2017). Several studies have shown that synthesis of extracellular matrix protein components such as

fibronectin is upregulated in patients with diabetes, and that these changes are associated with the development of basement membrane thickening, which is common in diabetic retinopathy and nephropathy (Das et al., 2014; Kim et al., 2007; Zhang et al., 2013).

Angiogenesis, the growth of new blood vessels in the vicinity of the tumour tissue is necessary for metastasis. Interestingly, FN has been reported to both promote and inhibit angiogenesis (Lochter & Bissell, 1995). The presence of FN has also been correlated with an enhanced ability of tumour cells to adhere and migrate (Lochter & Bissell, 1995). Increased turnover of the extracellular FN matrix in particular, has been correlated with enhanced metastatic capacity of tumour cells (Akiyama et al., 1995; Labat-Robert, 2002; To & Midwood, 2011). High FN levels are associated with increased invasion and metastatic capability in cancers such as lung and hepatic cancers (Akiyama et al., 1995; Ioachim et al., 2002; Zheng, Ritzenthaler, Roman, & Han, 2007) however in some cancer types, high levels of FN expression have been found to correlate with reduced cell proliferation, migratory capacity, and associated with a more favorable prognosis in breast cancer patients (Bae et al., 2013; Lochter & Bissell, 1995; Swiatoniowski et al., 2005). Studies have shown that FN also promotes cell invasion and migration via upregulating MMP2 and MMP9 levels in cancer (Egeblad & Werb, 2002; Lu et al., 2011). Also, FN fragments generated from MMP cleavage have been shown to have pro-migratory functions and stimulate FN matrix remodelling by activating the p38 MAPK pathway (Bourdoulous et al., 1998; Forsyth, Pulai, & Loeser, 2002).

1.9 Low density lipoprotein receptor-related protein 1 (LRP1)

The low density lipoprotein receptor-related protein 1 (LRP1), also termed CD91, is a member of the LDL receptor family. The LDL receptor was one of the first members to be identified as part of this receptor family and is responsible for cholesterol homeostasis (Brown, 1986). Other members of the LDL receptor family have more diverse functions. LRP1 is one such example, with roles in lipoprotein metabolism, signal transduction, entry of viruses and toxins, homeostasis of proteinases and their inhibitors, and in pathology of Alzheimer's disease (Kounnas et al., 1995; Rozanov, Hahn-Dantona, Strickland, & Strongin, 2004; Strickland et al., 1990). LRP1 is one of the largest endocytic receptors and is considered a scavenger receptor due to the large array of ligands (>30) which it binds. How LRP1 recognises so many structurally different and distinct molecules has raised questions regarding the

mechanisms by which ligands interact with this receptor. Targeted disruption of the LRP1 gene in mice results in embryonic lethality due to extensive hemorrhaging caused by failure to recruit and maintain cells in the vasculature thereby suggesting a biologically important role for this receptor in early development (Au, Arai, Fondrie, Muratoglu, & Strickland, 2018; Herz, Goldstein, Stricklandn, & Brown, 1991; Nakajima et al., 2014). Furthermore, selective LRP1 deletion in neurons, macrophages, smooth muscle cells and hepatocytes all lead to significant phenotypic changes suggesting key roles for LRP1 in various physiological processes (Basford, Moore, Zhou, Herz, & Hui, 2010; Ding, Xian, Holland, Tsai, & Herz, 2016; May et al., 2004).

1.9.1 LRP1 structure

LRP1 is synthesized as a 600 kDa transmembrane protein which is subsequently cleaved in the Golgi Apparatus by furin within the β-propeller domain producing a 515 kDa α-chain and 85 kDa β-chain. These two subunits associate non-covalently during transport to the cell surface and internalisation (Herz et al., 1991). The LRP1 structure illustrated in Figure 4 displays its five composing units. The N-terminal 515 kDa α-subunit contains the four ligand binding domains (I-IV) and is completely extracellular. The C-terminal 85 kDa β-subunit contains an extracellular part, a transmembrane spanning domain and a cytoplasmic intracellular domain containing 1 to 3 NPxY motifs that serve as endocytosis signals which target the receptor to clathrin coated pits (Strickland et al., 1995). Ligand binding is regulated, primarily during export of LRP1 to the cell surface, by the receptor-associated protein (RAP) which has a high binding affinity (K_d = 1-10 nM) for LRP1 (Iadonato *et al.*, 1993; Bu & Marzolo, 2001). RAP was identified when co-purified with LRP1 in human placenta (Herz *et al., 1*991). The major function of RAP is to serve as a chaperone by transiently binding newly synthesized LRP1 to assist in its transport from the ER to the Golgi without interference from other ligands, thereby enabling LRP1 to be successfully delivered to the plasma membrane (Lillis et al., 2008). Tissue transglutaminase (tTG) interacts directly with LRP1 and promotes association with β1 integrins and the ECM (Zemskov, Mikhailenko, Strickland, & Belkin, 2007).

The extracellular α-chain of LRP1 contains four ligand-binding domains (clusters I-IV on Figure 4). Most ligands bind clusters II and IV, which are flanked by epidermal growth factor homology domains (Figure 4) (Obermoeller-McCormick et al., 2000). Interestingly, the

cytoplasmic β-chain has been shown to bind adaptor and scaffold proteins via its NPxY motifs and serine/tyrosine residues which links the receptor to other membrane proteins or initiates signalling cascades within the cell (Boucher & Herz, 2011; Guttman et al., 2009). Phosphorylation of the serine and/or tyrosine residues, in particular Tyr4507, allows for interaction of the cytoplasmic domain with adaptor proteins such as FE65 for cell signalling (van der Geer, 1999; Li & Bu, 2001). Thus, LRP1 is implicated in two major physiological processes, namely endocytosis and regulation of signalling pathways.

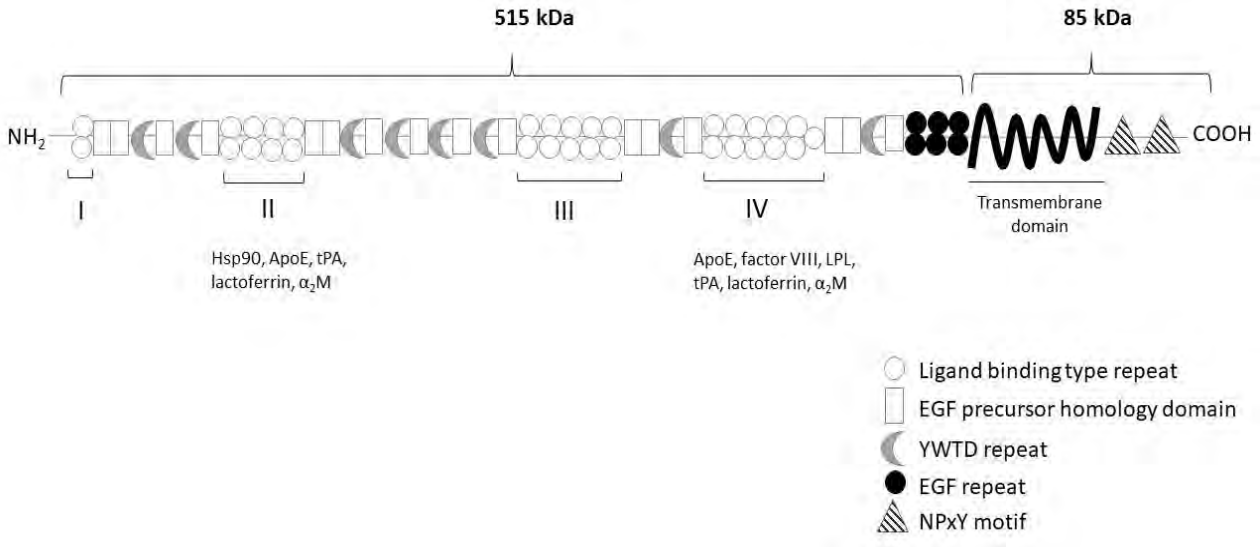

Figure 4: Structure of the 600 kDa low density lipoprotein receptor related protein (LRP1).

Cysteine rich ligand-binding type repeats (white circles) are arranged in four clusters (I-IV) along the extracellular 515 kDa domain to which distinct ligands bind as indicated. Each cluster is followed by 1-4 EGF homology domains (white rectangle and black circles) and an YWTD repeat (grey half-moon). The transmembrane domain spans the membrane bilayer and is followed by the 85 kDa intracellular domain containing the NPxY motifs (striped triangles). [Adapted from Herz & Strickland, 2001].

1.9.2 Regulated intramembrane proteolysis (RIP) of LRP1

LRP1 cell-surface levels are regulated by a process known as RIP (regulated intramembrane proteolysis) involving shedding, and proteolytic cleavage that releases the extracellular ectodomain (Quinn et al., 1999). Quinn and colleagues were one of the first to demonstrate that LRP1 can be shed by cleavage of the receptor at the membrane proximal region of the β-chain in human BeWo trophoblast cells. A number of other transmembrane receptors are

known to undergo regulated intramembrane proteolysis (RIP) including Notch, APP, ErbB4, CD44 and syndecan-3 amongst others (Liu et al., 2007). In addition to LRP1, other members of the LDL receptor family including LRP1B, LRP2 and LRP8 have been shown to undergo RIP (May, Reddy, & Herz, 2002).

The general mechanism of RIP is illustrated in Figure 5 whereby various proteinases act on LRP1 to cleave this receptor into smaller fragments. Following LRP1 cleavage by furin in the trans-Golgi, the mature form of LRP1 consists of two non-covalently associated subunits (Cam, Zerbinatti, Li, & Bu, 2005). The fate of the shed LRP1 515 kDa fragment of the ectodomain is not known but is thought to be able to still bind ligands, thereby reducing their interaction with the cell and regulating their endocytosis (Gaultier et al., 2008; Gorovoy, Gaultier, Campana, & Firestein, 2010). Cleavage of the 85 kDa membrane bound receptor fragment close to the membrane is facilitated by various MMPs including β-amyloid precursor protein-cleaving enzyme (BACE), MT1-MMP, and ADAMs 10/12/17 (a disintegrin and metalloproteinase) (Liu, Ranganathan, Robinson, & Strickland, 2007; Von Arnim et al., 2005) to release the extracellular receptor portion (Figure 5). Subsequent cleavage of the remaining transmembrane β-chain by the presenilin (PS)/ γ-secretase complex yields additional smaller fragments termed the LRP1 intracellular domain (LRP1-ICD) (Spuch, Ortolano, & Navarro, 2012). The shed LRP1-ICD has been shown to translocate to the nucleus where it interacts with various proteins and transcriptional modulators to regulate cell signalling and gene transcription (Kinoshita, Shah, Tangredi, Strickland, & Hyman, 2003; Zurhove et al., 2008). In the case of Notch, RIP is initiated upon ligand binding, and the released ICD acts as a transcription co-activator (Hu et al., 2003) whilst that of APP acts as a transcription co-repressor (Cao & Sudhof, 2001). In other RIP cases, ICD translocated fragments may serve to promote the degradation of transcription factors or modulate cell-cell interaction complexes (Marambaud et al., 2002, 2003). RIP of LRP1 currently has 2 major consequences, the first being the ability of the LRP1-ICD to translocate to the nucleus and suppress inflammation by reducing the transcription of lipopolysaccharide inducible genes by promoting the nuclear export of interferon regulatory factor 3 (Zurhove et al., 2008). The second is the ability of LRP1 to regulate hypoxia mediated angiogenesis by interacting with PARP1 and activating Cdk2 (Mao et al., 2015). Interestingly, LRP1 shedding has been shown to be increased in malignant cells (Selvais et al., 2011).

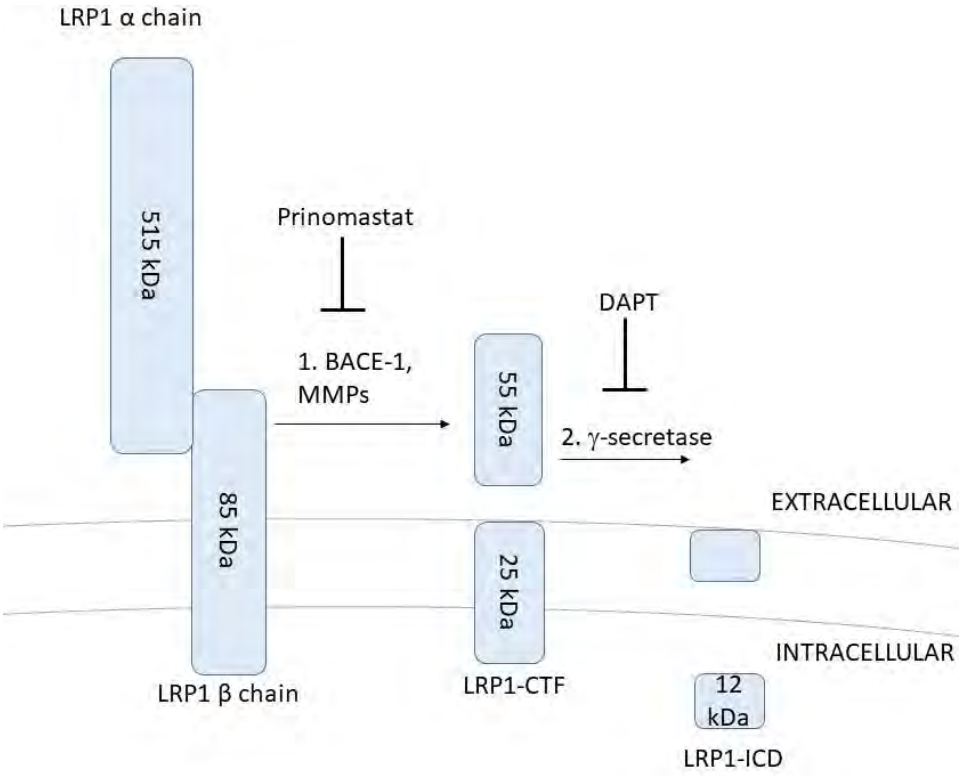

Figure 5: Regulated Intramembrane Proteolysis (RIP) of LRP1

After furin cleavage in the trans-Golgi, mature LRP1 consists of two non-covalently associated α and β subunits of 515 kDa and 85 kDa in size respectively. The 85 kDa membrane spanning subunit is cleaved by 1) BACE-1 and various MMPs at a region close to the membrane to yield fragments (55 kDa and 25 kDa). 2) The remaining 25 kDa fragment is further cleaved by gamma secretases to release the LRP1-ICD which is able to translocate to the nucleus. Inhibitors at each of the steps are indicated.

1.9.3 LRP1-Hsp90 cell signalling

Tsen and colleagues reported a role for eHsp90-LRP1 cross-membrane signalling, whereby binding of eHsp90 to LRP1 induced the activation of downstream signalling pathways involving Akt and mTOR to promote migration (Tsen et al., 2013). Several other groups have also suggested a role for eHsp90 in LRP1-mediated signalling by activation of various pathways including ERK1/2 and MMP2/9 (Hance et al., 2014; Sims et al., 2011; Song, Li, Lee, Schwartz, & Bu, 2009) some of which are essential to wound healing (Cheng et al., 2008; Tsen et al., 2013). The eHsp90-LRP1 interaction takes place on the extracellular subdomain II of the LRP1 α-chain (Figure 4) (Tsen et al., 2013). Cytoplasmic Hsp90β has been shown to stabilize the intracellular LRP1 β-chain (Jayaprakash et al., 2015). eHsp90 has also been shown to interact with other cell surface proteins including HER-2 which activates downstream pro-growth ERK and pro-survival PI3K pathways mediating increased cell invasion in breast cancer

(Calderwood et al., 2006). eHsp90-LRP1 interaction may also promote EMT (endothelial-mesenchymal transition) as has been shown in colorectal cancer cells via the activation the NFkB pathway (Nagaraju et al., 2014). In studies by Salicioni et al., (2002), FN was shown to be endocytosed by LRP1 highlighting a potential role for LRP1 as a catabolic receptor for FN. However, to date FN has not been demonstrated to directly bind LRP1, unlike eHsp90 (Basu et al., 2001). Given this, and the multiple eHsp90-LRP1 induced downstream targets, it seems plausible that several of these signalling pathways might converge to regulate FN matrix dynamics. Chen and colleagues reported that the activation of NFkB pathway by eHsp90-LRP1 signalling induces FN expression (Chen et al., 2013) and that activation of the Akt pathway is also important for the expression of FN (Qin, Zhang, Xu, & Wang, 2015). Somanath and colleagues showed that Akt was involved in regulating integrin activation and FN matrix assembly (Somanath, Kandel, Hay, & Byzova, 2007). It is possible then that anything which might disrupt eHsp90 binding to LRP1, or deactivation of Akt and NFkB pathways might lead to reduced FN expression or deregulated FN matrix remodelling which will have impacts on cell migration and metastasis.

1.10 Hypothesis

The NOV-induced turnover of FN is regulated by LRP1 and has physiological consequences on the FN extracellular matrix

1.11 Objectives

1. Investigate the mechanisms involved in NOV-induced turnover of FN in LRP1-expressing cells
2. To analyse the biological consequences associated with NOV-induced FN turnover

Chapter 2: **MATERIALS & METHODS**

2.1 Materials

All general reagents were purchased from Sigma-Aldrich (USA) and Merck Millipore (USA) . Tissue culture media and reagents, including fetal bovine serum [FBS], Dulbecco's Modified Eagle Medium [DMEM] with GlutaMAX™-I, 10 X Trypsin- Ethylenediaminetetraacetic acid (EDTA) and Penicillin/Streptomycin/Amphotericin [PSA] were from Thermo Fisher Scientific (USA) and Biowhittaker (Switzerland). Insulin was from Novorapid. Tissue Culture plasticware was from Corning Incorporated (USA) or Nest Biotechnology (China). Hybond nitrocellulose membrane, western blotting power pack and Chemidoc™ XRS were from Bio-Rad (USA). Chemical inhibitors were purchased from Sigma-Aldrich unless otherwise stated. 3,3'-dithiobis[sulfosuccinimidyl] propionate [DTSSP] (cat no.: 21578) were from Thermo Fisher Scientific (USA). MagReSyn™ Protein A and MagReSyn™ NTA were from ReSyn Biosciences (South Africa). Suppliers of other specialized reagents are referenced in text. Alexa Fluor-647 conjugated mouse anti-LAMP1 (E-5) antibody (sc-17768) and purified human fibronectin (sc-29011) was from Santa Cruz (USA). Human recombinant endotoxin free Hsp90β full length protein (SPR-102) was from StressMarq Biosciences (Canada). HRP conjugated donkey anti-rabbit secondary antibody (ab16284) (dilution 1:10 000), HRP conjugated goat anti-mouse secondary antibody (ab97110) (dilution 1:5000) and Alexa Fluor-488 conjugated donkey anti-rabbit antibody (ab150073) were from Abcam (UK). Alexa Fluor-488 conjugated donkey anti-mouse antibody (cat no.: A21202), Alexa Fluor-546 conjugated donkey anti-rabbit antibody (cat no.: A10040) were from Invitrogen (USA) used at a dilution of 1:1000. Details of primary antibodies used are listed in Table 4.

Table 4: Details of primary antibodies used in this research project

Primary antibody	Species	Dilution used in western blotting	Catalogue number	Vendor
Hsp90α/β	Mouse	1:1000	sc-13119	Santa Cruz
FN		1:1000 1:100 (Immunofluorescence)	F3648	Sigma
Tubulin		1:5000	ab7291	Abcam
GAPDH		1:5000	G8795	Sigma
β1 integrin		1:1000	610467	BD Biosciences
FN	Rabbit	1:1000 1: 100 (Immunofluorescence)	F0916	Sigma
Actin		1:1000	A2103	Sigma
LRP1		1:10 000 1:100 (Immunofluorescence) 1:100 (Immunoprecipitation)	ab92544	Abcam
Histone H3		1:10 000	ab1791	Abcam
Phospho-Akt (Ser473)		1:2000	CST4060	Cell Signalling Technologies
P44/P42 MAPK (Phospho-Erk1/2)		1:2000	CST4695	
Collagen 1		1:1000 1:100 (Immunofluorescence)	NB600-408	Novus Biologicals

2.2 Methods

2.2.1 Routine maintenance of cell lines

Hs578T (ATCC: HTB-126) breast cancer cell line and mouse embryonic fibroblasts (MEF) (i.e. LRP1 wild type MEF-1 [ATCC: CRL-2214], LRP1 deficient PEA-13 [ATCC: CRL-2216]) were purchased from the American Type Culture Collection (ATCC). Hs578T breast cancer cells were maintained in Dulbecco's Modified Eagle's Medium (DMEM) supplemented with 10% [v/v] fetal calf serum (FCS), 2 mM GlutaMAX™, 100 U/ml Penicillin/Streptomycin/Amphotericin (PSA) and 2 mM insulin (Novorapid, Canada). MEF lines were maintained in DMEM supplemented with 10% [v/v] FCS, 2 mM GlutaMAX™ and 100 U/ml PSA. All cell lines were maintained at 37 °C in a humidified atmosphere with 9% CO2.

2.2.2 Sodium Dodecyl Sulfate-Polyacrylamide Gel Electrophoresis (SDS-PAGE)

Proteins were separated by discontinuous SDS-PAGE according to the standard modifications of the established method (Laemmli, 1970). Proteins were resolved using a 4% [v/v] stacking gel (0.5 M Tris-Cl, pH 6.8) and 10% [v/v] resolving gel (1.5 M Tris-Cl, pH 8.8) at 120 V for 90 minutes in SDS-PAGE running buffer (0.25 mM Tris, 192 mM glycine, 1% [w/v] SDS). Samples were mixed with 5x SDS sample buffer (0.05 M Tris-Cl, 10% [v/v] glycerol, 2% SDS, 1% [w/v] bromophenol blue, 5% [v/v] β-mercaptoethanol) and boiled for 5 minutes before being loaded onto the gel. Blue prestained protein standard (New England BioLabs) or prestained protein marker (Thermo Scientific) were used for estimating molecular weights of proteins.

2.2.3 Immunoblotting and chemiluminescence-based detection

Resolved proteins were transferred on to nitrocellulose membrane in transfer buffer (25 mM Tris-Cl, 192 mM glycine, 20% [v/v] methanol) using a semi-dry blotting system (SD20 Semi Dry Blotter Maxi) for 50 minutes at 0.4 A. Transfer efficiency and protein levels were observed on the nitrocellulose membrane using Ponceau S stain (0.5% [w/v] Ponceau S, 1% [v/v] glacial acetic acid). Membranes were blocked for at least 1 hour at room temperature in 5% BLOTTO (5% [w/v] non-fat milk powder in Tris buffered saline [TBS: 50 mM Tris, 150 mM NaCl pH 7.5]). Membranes were incubated with primary antibody in 1% [w/v] BLOTTO at the recommended dilution overnight at 4˚C with gentle shaking. Membranes were washed thrice in TBST (TBS with 0.1% [v/v] Tween-20) for 5 minutes each time. Species matched secondary antibody conjugated to HRP was incubated with the membrane in 1% [w/v] BLOTTO for 45 minutes at

room temperature. Membranes were washed in TBST four times for 5 minutes each time. Detection of proteins was carried out using ECL Advanced western blotting detection kit in the Chemidoc™ XRS system (BioRad)

2.2.4 Cell cytotoxicity assay for Hsp90 inhibitors

The toxicity of Hsp90 inhibitors was assessed in Hs578T, MEF-1 and PEA-13 cell lines using methylthiazolyldiphenyl-tetrazolium bromide (MTT) (Sigma). MTT is a yellowish solution and is converted to water-insoluble MTT formazan of dark blue color by mitochondrial dehydrogenases of living cells. Cells of equal density (2 x 10^3 cells/well) were seeded in a 96 well plate and treated the following day with a range of Hsp90 inhibitor concentrations. After 3 days, all liquid was removed from wells and 50 µl of a 5 mg/ml MTT reagent was added to each of the wells and incubated for 4 hours at 37 °C. Solubilisation solution (10 % SDS in 0.01 M HCl) was added to the cells overnight at 37 °C and the following day, absorbances were read at 550 nm. This viability assay was carried out quintuplicate and the dose response and half maximal effective concentrations (EC50) determined using GraphPad Prism 4. In all instances, the term EC50 refers to cell toxicity.

2.2.5 Gelatin zymography assay

Equal cell numbers (6 x 10^5 cells/well) were allowed to adhere overnight in a 6 well plate and left untreated or treated with various inhibitors as described in figure legends for 16 hours in serum-free DMEM. Supernatants were harvested and centrifuged at 400 x*g* for 5 min at 4 ˚C to remove cell debris. Samples were resolved on a 10% (v/v) SDS-PAGE gel containing 0.1% (w/v) gelatin and run at 125 V for 90 minutes in chilled SDS running buffer. Gels were incubated 2x 30 min in 100 ml renaturing buffer (2.5% Triton-X-100 in dH2O) at room temperature with gentle shaking. Gels were incubated in 100 ml developing buffer (50 mM Tris-Cl pH 7.4, 10 mM $CaCl_2$, 0.02% NaN_3) in a closed tray for 16 hours at 37 ˚C. Gels were incubated in Coomassie stain (0.5 % [w/v] Coomassie Brilliant Blue R250 in destain Solution) for 1 hour and destained with destain Solution (40 % [v/v] methanol, 10 % [w/v] glacial acetic acid) until bands of clearance were observed. White bands of clearance against dark blue background indicated enzymatic activity. Parallel SDS-PAGE gels lacking gelatin which had not been renatured or developed were incubated directly in Coomassie stain to serve as a protein loading control.

2.2.6 Biochemical fractionation of insoluble and soluble fibronectin using a deoxycholate (DOC) assay

This assay was adapted from that published by Brenner and colleagues (Brenner, Corbett, & Schwarzbauer, 2000). MEF-1, PEA-13 and Hs578T cells were seeded in a 6-well plate (6 x 10^5 cells/well) and allowed to adhere overnight. Cells were treated as indicated in figure legends for 16 hours and scraped into DOC buffer (2% [w/v] deoxycholate, 20 mM Tris-HCl, pH 8.8, 2 mM phenylmethanesulfonylflouride [PMSF], 2 mM EDTA and 0.05% [v/v] protease inhibitor cocktail). Samples were vortexed for 2 minutes and centrifuged at 13000 rpm in a microfuge for 20 minutes at 4 ˚C. A volume of 200 µl of the supernatant containing soluble fibronectin was mixed with 80 µl of SDS sample buffer and the pellet containing insoluble fibronectin was resuspended in 80 µl SDS sample buffer. Samples were boiled and resolved by SDS-PAGE and/or immunoblotting.

2.2.7 Nuclear and cytosolic fractionation (REAP assay)

Equal cell numbers were allowed to adhere overnight in a 100 mm culture dish. The following day, cells were left untreated or treated with varying concentrations of NOV as indicated in figure legends for 16 hours prior to REAP subcellular fractionation using an adapted protocol from Suzuki and colleagues (Suzuki et al., 2010). The cell monolayer was washed twice with ice-cold PBS and cells were scraped with PBS using a plastic cell scraper. Cells were briefly centrifuged (400 x*g*, 10 seconds at room temperature) to collect cells and the cell pellet was triturated 5 times with ice-cold 0.1% (v/v) NP40-PBS. An aliquot was reserved for the whole cell lysate (WCL) and the remaining suspension briefly centrifuged (as done previously) to separate the supernatant containing cytosolic fraction (C). The remaining pellet was resuspended in cold 0.1% (v/v) NP40-PBS and centrifuged again as before. The resulting pellet containing the nuclear fraction (N), as well as the whole cell lysate (WCL) and cytosolic fractions, were mixed in a 1:1 (v/v) ratio with SDS sample buffer and sonicated at level 2 twice for 5 sec each time. Samples were boiled and stored at -20 ˚C until further analysis.

2.2.8 DTSSP cell surface crosslinking

Adherent cells from a T-75 cell culture flask were left untreated or treated as indicated in figure legends. Cells were washed twice in PBS and incubated with DTSSP (3 mg/ml) at 4˚C for 2 hours to allow for crosslinking of protein interactions. The DTSSP crosslinker contains NHS

moeities on both ends which are able to interact with lysine residues on proteins that are within interacting range (12Å) (Thermo Scientific). DTSSP was quenched with 1 M Tris-Cl (pH 7.5) at 4˚C for 15 minutes.

2.2.9 Immunoprecipitation of crosslinked complexes

Cells were washed with PBS before 1 ml of CellLytic M Cell Lysis Reagent (containing 0.05% [v/v] protease inhibitor cocktail) was added to the cells, incubated for 15 min with shaking and lysed with a cell scraper. Cell lysates were either centrifuged at 13000 rpm in a microfuge tube for 20 minutes at 4 ˚C and the supernatants harvested to generate cleared lysates (CL) or remained uncentrifuged as whole cell lysates (WCL). For Hsp90 IPs: WCL and CL were quantified by absorbance at 280 nm using the NanoDrop 2000 spectrophotometer (ThermoScientific, USA) and 500 µg of cell lysate was added to 5 µg of mouse anti-Hsp90 antibody (Catalog number: SMC-107) or isotype-control antibody overnight at 4 °C with end-over-end mixing. The next day, 20 µl of Protein A/G Plus Agarose beads (cat no: sc2003) was added to the lysate for 4 hours at 4 °C with end-over-end mixing. Beads were centrifuged at 3000 rpm for 1 min in a microfuge and the supernatant discarded. Beads were washed in PBS and centrifuged as before. Supernatants were again discarded, and beads washed an additional two times. After the final wash, beads were resuspended in 60 µl of 5x SDS-PAGE sample buffer (containing β-mercaptoethanol to cleave DTSSP bound proteins) and boiled for 5 min. Samples were centrifuged at 3000 rpm for 1 min and the supernatants retained for SDS-PAGE analysis and immunoblotting as described previously.

For LRP1 IPs, WCL and CL samples were split in half and incubated overnight at 4 °C with a volume of 10 µl of magnetic MagReSyn™ Protein A, which had been pre-equilibrated according to manufacturer's instructions and bound to 5 µg rabbit LRP1 or isotype control capture antibodies. Beads in suspension were collected using a magnet and washed three times in wash buffer (50 mM Tris, pH 7, 150 mM NaCl, 1% [v/v] Tween 20) followed by a final wash in dH_2O. LRP1 complexes were eluted from the beads by boiling in 5x SDS-PAGE sample buffer containing β-mercaptoethanol. Samples were resolved by SDS-PAGE and analysed by SDS-PAGE and immunoblotting as described previously.

2.2.10 4-well migration chamber assay

Hs578T cells were seeded (1 x 10^5 cells/ml) into an ibidi 4-well micro-Insert (Cat number: 80409) (10 µl/well) and allowed to reach confluency. Inserts were left untreated or treated with NOV for 16 hours at 37 °C. Inserts were removed and cell monolayers were rinsed in spent media. Images of cells were taken before (t=0 hrs) and after migration (t=20 hours) using the Zeiss Primovert Inverted light microscope with the 4x and 20x objectives. Migration was assessed by the degree of cell migration outward from the cell monolayer.

2.2.11 Scratch Assay to measure cell migration

Hs578T, MEF-1 and PEA-13 cells were seeded into wells of a 24-well culture dish and grown overnight or until confluent. To create wounds, a scratch was made down the centre of the well using a toothpick. Wells were washed with spent media and returned to incubate at 37 ˚C in fresh media containing either NOV, GA or eHsp90β as indicated in the figure legends for 12 hours. Photographs were taken immediately after wound initiation (t=0 hrs) and after cell migration (t= 12 hours) using a Zeiss Primovert inverted light microscope. For migration on FN, wells of a 24 well were coated with increasing concentrations of purified FN (Catalog number: sc-29011) by incubation at RT for 1 hour. FN was removed, and wells washed once with dH_2O. Cells were seeded into coated wells and migration measured as described. Marks were made on the bottom surface of wells to ensure identical fields of view were captured each time. For each image, distances between the two opposing lead edges were measured at least three times at different points across the length of the wound. Distances migrated were calculated by subtracting the distance measured at 12 hrs from the distance at 0 hrs.

2.2.12 Cell-derived matrix production

ECM production and harvesting protocols were adapted from published protocols (Castelló-Cros et al., 2009). Ethanol sterilized coverslips in a 6-well plate were incubated with 0.2% [w/v] sterile gelatin for 1 hour at 37 °C. Gelatin was crosslinked with 1% [v/v] sterile glutaraldehyde in PBS for 30 minutes at room temperature. Wells were washed thrice with PBS, 5 minutes each time. Crosslinker was quenched with 1 M sterile ethanolamine for 30 minutes at room temperature. Wells were washed thrice with PBS, 5 minutes each time. Cells were seeded into prepared 6-well plates (at a density of 6 x 10^5 cells/well or such that the

next day 100% confluency was observed). If coverslips were not used, then the above crosslinking and quenching steps were omitted, and cells seeded directly into wells. Upon confluency, the media was replaced with 50 µg/ml ascorbic acid containing media and was changed every second day thereafter. After 6 days of culture, wells were treated for 24 hours with NOV or Hsp90β as described in figure legends. The following day, cells were washed with PBS and incubated with 50 mM EDTA for 10 minutes at 37 °C. Cells were washed twice with PBS and then incubated with 37 °C preheated extraction buffer (20 mM NH_4OH, 0.5% [v/v] Triton-X in PBS) until complete cell lysis (as observed by assessing whether all cells had lifted using an inverted light microscope). This usually happened virtually instantaneously upon addition of extraction buffer. Without removing extraction buffer, PBS was added to each of the wells and placed at 4 °C overnight to improve the stability of the newly extracted matrices. To prevent any unwanted DNA, wells were incubated with 10 µg/ml DNAseI (Roche) for 30 minutes at 37 °C. Wells were washed three times with PBS. Cell-derived matrices were used immediately or stored in PBS containing PSA for up to 1 month at 4 °C covered in parafilm.

2.2.13 Indirect Immunofluorescence and Fluorescence microscopy

Coverslips to be visualized were flash-treated (<1 min) with ice-cold methanol and blocked with 1 % [w/v] BSA/TBS for 45 minutes at room temperature. Coverslips were incubated with appropriate primary antibodies in 1 % [w/v] BSA/TBS for 2 hours at room temperature and washed twice with PBS before incubating with the appropriate species-specific fluorophore conjugated secondary antibodies at room temperature for 1 hour in the dark. Coverslips were washed twice with PBS and rinsed briefly with Hoechst-33342 dye (Invitrogen) (1 µg/ml in distilled water) to stain nuclei blue. Coverslips were mounted onto glass slides using DAKO mounting medium. Immunofluorescence was detected using the Zeiss LSM780 Meta laser scanning confocal microscope and images analysed using Zen Blue Software and ImageJ. In cases where CDMs were processed for immunofluorescence of 3D projections, coverslips were fixed in 4% (v/v) formaldehyde for 15 min at RT and washed twice with 1x PBS. Coverslips were processed as described above but mounted using VECTASHIELD Antifade Mounting Medium which is glycerol based and does not solidify therefore allowing for accurate 3D quantifications of CDMs.

2.2.14 Scanning electron microscopy

The cell derived matrices harvested as described above were fixed in cold buffered fixative solution (2.5% [v/v] glutaraldehyde in 0.1 M sodium phosphate buffer) overnight at 4 °C. Coverslips were washed with cold 0.1 M sodium phosphate buffer twice 10 min each time. The CDM was dehydrated through a graded series of 30% [v/v] ethanol to 100% ethanol and subjected to critical point drying (Polaron Critical Point Drier) in liquid CO_2. Coverslips were attached to aluminium stubs via double sided carbon sticky tabs and coated with gold using a Quorum Q150RS coater. Stubs were viewed, and digital images captured on a Tescan VEGA TS 5136LM Scanning Electron Microscope operating at 1 kV.

2.2.15 Measuring ECM fibre thickness and orientation

To quantify the effects of various treatments on fibronectin topography we quantified the average thickness of ECM and fibronectin fibres observed in immunofluorescence or SEM images using the BoneJ plugin for ImageJ (Doube et al., 2010). Binary images of CDMs were run through the plugin using the thickness command which calculates the thickness and spacing of and between fibres generating numerical values assigned to average thickness and a colour coded image where white/yellow regions are thicker than purple/blue regions (see heat map scale bar in Figures). Pseudo-coloured spheres are fitted along fibres to represent intensity of thickness along fibres. Values obtained from triplicate images were analysed in GraphPad Prism 4.

To estimate the local orientation of the ECM and fibronectin fibres from immunofluorescence or SEM images, we used the ImageJ OrientationJ plugin, which evaluates the local orientation and isotropic properties (coherency and energy) of every pixel in an image (Rezakhaniha et al., 2012). Monochromatic SEM images or fibronectin channel confocal microscopy images were analyzed (http://bigwww.epfl.ch/demo/orientation/) as described in (Franco-Barraza et al., 2017). The plugin generated an HSB (hue-saturation-brightness) color coded image overlaid onto the original image. Graphical gaussian distribution curves represent the orientation distributions of fibres in an image.

2.2.16 Cell adhesion on CDMs

Cells seeded (5 x 10^4 cells/ml) into wells of a 24-well plate containing CDMs were allowed to adhere and spread over 4 hours under tissue culture conditions. After 4 hours, liquid was removed from wells and washed three times with PBS to remove any non-adherent cells. Cells were then fixed in 4% (v/v) formaldehyde for 15 min at RT. Fixative was removed and wells were rinsed with dH_20 and blotted dry. Cells were stained by incubating with 10% (w/v) crystal violet for 20 min at RT. Crystal violet stain was discarded and wells washed three times with dH_20 and blotted dry until stained cells could be visualised at the bottom of wells. Images of cells were taken using the Zeiss Primovert inverted light microscope. In ImageJ, the overall shape of cells was determined using a cell axial ratio defined by the ratio of the "length" (long axis) divided by the "breath" (short axis) of the cell; round objects present a ratio close to 1 while spindle-shaped morphologies have a ratio > 1. Crystal violet stain was solubilized in methanol for 10 min at RT with shaking and the absorbance measured at 570 nm.

2.2.17 Cell proliferation on CDMs

Cells were seeded (5 x 10^4 cells/ml) into wells of a 24 well plate containing prepared CDMs and incubated under tissue culture conditions for 48, 72 and 96 hours. At each time point, the plate was processed for cell growth using the MTT assay as described previously.

2.2.18 Hanging drop spheroid cell migration assay

Cells were suspended in complete medium (15 x 10^5 cells/ml) and 10 µl drops suspended on the underside of a sterile 100 mm cell culture dish to fit as many drops as was comfortably possible without touching. The bottom of the culture dish was filled with 5 ml PBS and the lid was inverted to close the dish so that cells were held in suspension in complete medium in the hanging drops. Drops were incubated under tissue culture conditions for 2-3 days allowing gravity in the pipetted droplets to concentrate cells at the liquid-air interface to generate spheroids. On the day of the assay, drops containing spheroid aggregates were gently sucked up using a 20 µl pipette tip and placed into media filled experimental wells and placed back into the incubator. Generally, two drops were placed per well of a 24 well. After spheroids had visibly adhered (~ 4 hours) images were taken using the Zeiss Primovert inverted light microscope. The time at which images were taken was recorded as t= 0 hours. Cells were allowed to migrate, and images were taken again after 20 hours. Migration was measured

using the ImageJ Analyse spheroid cell invasion 3D matrix macro plugin. The distance migrated was calculated by the formula: Distance migrated = area measured after migration (i.e. t= 20 hours) – area measured at start (i.e. t= 0 hours).

2.2.19 Solid-phase binding assay

CDMs were prepared in a 6-well cell culture plate as described previously. Solubilisation buffer (5 M guanidine with 10 mM dithiothreitol) was added to each of the CDM-containing wells (300 µl/well) for 5 min on ice. Dishes were scraped with a cell scraper and solubilised protein mixtures placed into microfuge tubes. An additional 200 µl of solubilisation buffer was added to each tube and mixed by end-over-end rotation at 4°C for 1 hour. Samples were centrifuged at 12000 *xg* for 15 min at 4°C. The supernatant was transferred to a new microfuge tube and protein concentrations were measured using absorbance at 280 nm on the NanoDrop2000 spectrophotometer. Solubilised protein mixtures were precoated onto the surfaces (50 µl/well) of a high binding 96-well ELISA plate for 5 hours at 22 °C. Liquid was removed and non-specific binding sites were blocked with 300 µl 3% (w/v) BSA in buffer A (20 mM Tris-HCl, 150 mM NaCl, 5 mM $CaCl_2$ [pH 7.4], 0.05 % [v/v] Tween-20) for 1 hour at 22°C. Wells were washed three times with 1% (w/v) BSA in buffer A and incubated with primary antibodies (as indicated in figure legends) in buffer A overnight at 4 °C. Wells were washed three times with 1% (w/v) BSA in buffer A and incubated with species specific HRP-conjugated secondary antibodies in buffer A for 1 hour at 22 °C. Wells were washed again three times with 1% (w/v) BSA in buffer A. To each well, 100 µl of HRP buffer substrate (25.7 mM citric acid, 48.6 mM Na_2HPO_4, 1 mg/mL 3,3'5,5'- Tetramethylbenzidine (TMB), 0.015 % (v/v) H_2O_2) was added for 20 minutes at RT. The reaction was stopped upon addition of 1 M sulfuric acid. Absorbances were measured at 450 nm.

2.2.20 Statistical Analyses

All assays were performed as independent experiments at least three times unless otherwise stated. Statistical significance was performed using either a one-way or two-way ANOVA with Bonferroni's Multiple Comparison Tests or unpaired two-tailed Students t-tests unless otherwise stated. Significant p-values in all figures were denoted by asterisks as follows: ***p<0.001, **p< 0.01, *p<0.5. All graphs were generated using GraphPad Prism Version 4 software for Windows (GraphPad Software, USA).

Chapter 3: **TOWARDS THE MECHANISM OF NOV-INDUCED FN TURNOVER VIA LRP1**

3.1 Introduction

We previously identified FN as a client of Hsp90 as it interacts directly with Hsp90 and is dependent on Hsp90 for stability and conformational regulation (Hunter et al., 2014). Inhibition of Hsp90 with NOV led to a destabilisation of the FN matrix resulting in FN internalisation via a receptor mediated process. LRP1 is a ubiquitous receptor responsible for the internalisation of numerous ligands and is known to function as a receptor for extracellular Hsp90 (Basu et al., 2001). It has also previously been reported that LRP1 is able to mediate FN internalisation and degradation (Salicioni et al., 2002). Together with our previous studies showing that NOV causes instability of the FN matrix and its subsequent internalisation (Hunter et al., 2014), we further showed that this internalisation was dependent on LRP1 by showing that loss of LRP1 renders cells less sensitive to FN turnover and degradation in response to NOV (Boel et al., 2018). In this study, we made use of the Hs578T breast cancer cell line, as well as an isogenic mouse embryonic fibroblast (MEF) model system of differential LRP1 expression. The MEF-1 cell line is derived from wild type mice, while the PEA-13 cell line are isogenic lines from LRP1 knockout mice. All of these cell lines express high levels of FN making this an ideal system to test the FN response to Hsp90 inhibition in both a normal and cancer cell model. We investigated the mechanism of NOV-induced FN turnover and proposed a role for LRP1 in mediating this process. We hypothesized that NOV-induced FN turnover may involve one or more of the following mechanisms:

1. Direct FN clearance by increased activity of MMPs and/or decreased levels of integrins;
2. Proteolytic processing of LRP1 to generate fragments which might affect FN turnover;
3. Changes in cell surface protein complexes by NOV treatment which may activate/deactivate downstream signalling cascades.

3.1.1 C-terminal Hsp90 inhibitors induce FN turnover in LRP1 expressing cells

We previously tested the effects of C-terminal Hsp90 inhibition on FN using novobiocin (NOV) (Boel et al., 2018). We subsequently sought to determine whether the effects observed with treatment of NOV was characteristic of C-terminal Hsp90 inhibition, or whether the same effect could be observed for N-terminal Hsp90 inhibition using geldanamycin (GA). In contrast to NOV, GA binds the amino-terminal nucleotide binding pocket of Hsp90 and disrupts its chaperoning function (Grenert et al., 1997). Although both NOV and GA can bind to the ATP binding site on the C-terminus of Hsp90, GA is unable to disrupt client interactions (Marcu et al., 2000). Using an MTT assay (which produced similar results to a WST1 assay) we compared the cytotoxicity of various C- and N-terminal inhibitors and determined working concentrations of these inhibitors in each of the Hs578T breast cancer, MEF-1 [$LRP1^{+/+}$] and PEA-13 [$LRP1^{-/-}$] cell lines (Table 5). The half maximal effective concentrations (EC50) was determined using a non-linear regression equation in GraphPad Prism 4. An interesting observation which emerged from this comparative analysis was that Hsp90 inhibitors such as 17-DMAG and Coumermycin A1 had enhanced toxicities relative to GA and NOV respectively. Another observation was that each of the inhibitors tested here (with the exception of 17-DMAG) were significantly more toxic to MEF-1 cells compared to Hs578T cells. Whether this response is due to a normal versus cancer cell type effect is unclear. On the other hand, LRP1-deficient MEFs (PEA-13) (Table 5) had an EC50 of 11.61 nM to GA, which was three-fold more sensitive than its wild-type LRP1-expressing counterpart (MEF-1 EC50: 34.92 nM). Conversely, LRP1-deficient PEA-13 cells appeared less sensitive to NOV (EC50: 130.4 µM) and SM253 (EC50: 10.87 µM) in comparison to the wild type cells (EC50: 45.63 µM and EC50: 6.56 µM respectively). It is unclear as to what caused this difference in sensitivity response of these Hsp90 inhibitors, but it may be related, to some extent, to C-and N-terminal alternate mechanisms of action. The SM253 inhibitor (Koay et al., 2014) appeared to have lower EC50 values in cell lines compared to NOV and GA, highlighting the improved cytotoxicity of these compounds. Considering both NOV and SM253 induced significant turnover of FN in MEF-1 cells it is possible that this is what is responsible for the lower EC50 values and increased sensitivity of this cell line.

MEF-1, PEA-13 and Hs578T cells were treated with increasing concentrations of GA and NOV for 16 hours, and the levels of FN compared (Figure 6). NOV initially increased levels of FN in MEF-1 cells followed by a dose dependent decrease (Figure 6A) whilst levels of FN in PEA-13 cells were unperturbed by NOV treatment (Figure 6B). GA treatment did not produce any significant changes in levels of FN in either MEF-1 or PEA-13 cell lines. The Hs578T breast cancer cell line, appeared to mimic the response observed in the MEF-1 cell line, that is, GA caused no change in FN levels whilst NOV caused a significant increase in FN followed by a dose dependent loss (Figure 6C). The differential response of FN to NOV between the LRP1-containing (Figure 6A,C) and LRP1-deficient (Figure 6B) cells supported a role for LRP1 in FN turnover, and suggested that N-terminal Hsp90 inhibition does not have the same effect on FN as C-terminal Hsp90 inhibition in MEFs.

It is unclear whether the effects observed on FN in response to NOV are as a result of Hsp90 inhibition or another effect related to treatment with NOV. To further investigate this, we compared the FN response using an alternative C-terminal Hsp90 inhibitor, coumermycin (CA1), as well as an alternative N-terminal inhibitor, 7-dimethylamino-ethylamino-17-demethoxydeldanamycin (17-DMAG), which are derivatives of NOV and GA, respectively. EC50 values for these compounds were determined in LRP1-containing cell lines (Table 5). Increasing CA1 treatment in MEF-1 cells caused a significant increase in FN at low concentrations followed by a dose dependent loss, whilst 17-DMAG showed no significant change in FN (Figure 7A). These results were similar to the FN response observed for NOV and GA treatments, respectively, in this cell line. In Hs578T cells, CA1 did not cause an increase in FN levels but there was a noticeable dose dependent loss which was not observed in 17-DMAG treatments (Figure 7B).

Furthermore, we obtained an allosteric C-terminal Hsp90 inhibitor (SM253) from Shelli McAlpine (University of New South Wales, AU) to test the effects on FN turnover by this alternative C-terminal Hsp90 inhibitor. SM253 binds Hsp90 at the N-middle domain and impacts the conformation of Hsp90 such that TPR containing cochaperones can no longer bind the C-terminus (Koay et al., 2014; Wang & McAlpine, 2015). Following an MTT assay to determine the cytotoxicity of this compound (Table 5), we treated cell lines with increasing concentrations of the inhibitor and probed for levels of FN (Figure 8). SM253 treatment caused significant dose dependent losses of FN in both LRP1-expressing cell lines but not in

LRP1-deficient cells (Figure 8A and B). Taken together, these data demonstrate that the effect of NOV is specific to LRP1-expressing cells and could be recapitulated by another C-terminal inhibitor, CA1, and an allosteric C-terminal inhibitor, SM253, but not by N-terminal inhibitors GA, or 17-DMAG.

Table 5: The cytotoxicity of Hsp90 inhibitors in murine embryonic fibroblasts and Hs578T cells measured using an MTT assay represented as the half maximal effective concentration (EC50)

	N-Terminal Inhibitors		C-Terminal Inhibitors		
	GELDANAMYCIN (GA)	17-DMAG	NOVOBIOCIN (NOV)	COUMERMYCIN (CA1)	SM253
MEF-1	34.92 nM	105.5 nM	45.63 µM	3.7 µM	6.56 µM
PEA-13	11.61 nM		130.4 µM		10.87 µM
Hs578T	350.25 nM	66.2 nM	214.9 µM	5.8 µM	11.01 µM
CHEMICAL STRUCTURE	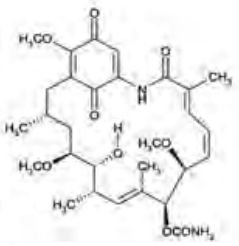	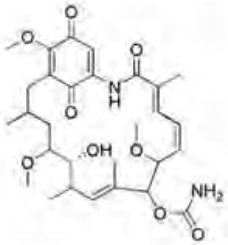	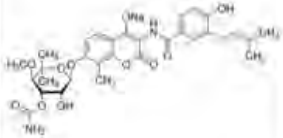	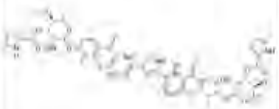	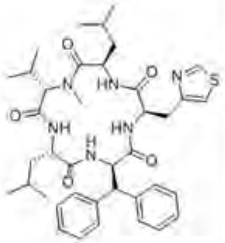
MODE OF ACTION	Binds Hsp90 N-terminus at ATP binding site	Binds Hsp90 N-terminus at ATP binding site. Less toxic GA derivative.	Binds Hsp90 C-terminus. Disrupts binding of TPR cochaperones (CYP40, PP5, FKBP51/52)	Binds Hsp90 C-terminus and prevents dimerisation. Disrupts binding of TPR cochaperones (CHIP, CYP40)	Binds Hsp90 Middle domain. Allosteric inhibition of TPR co-chaperones binding C-terminus

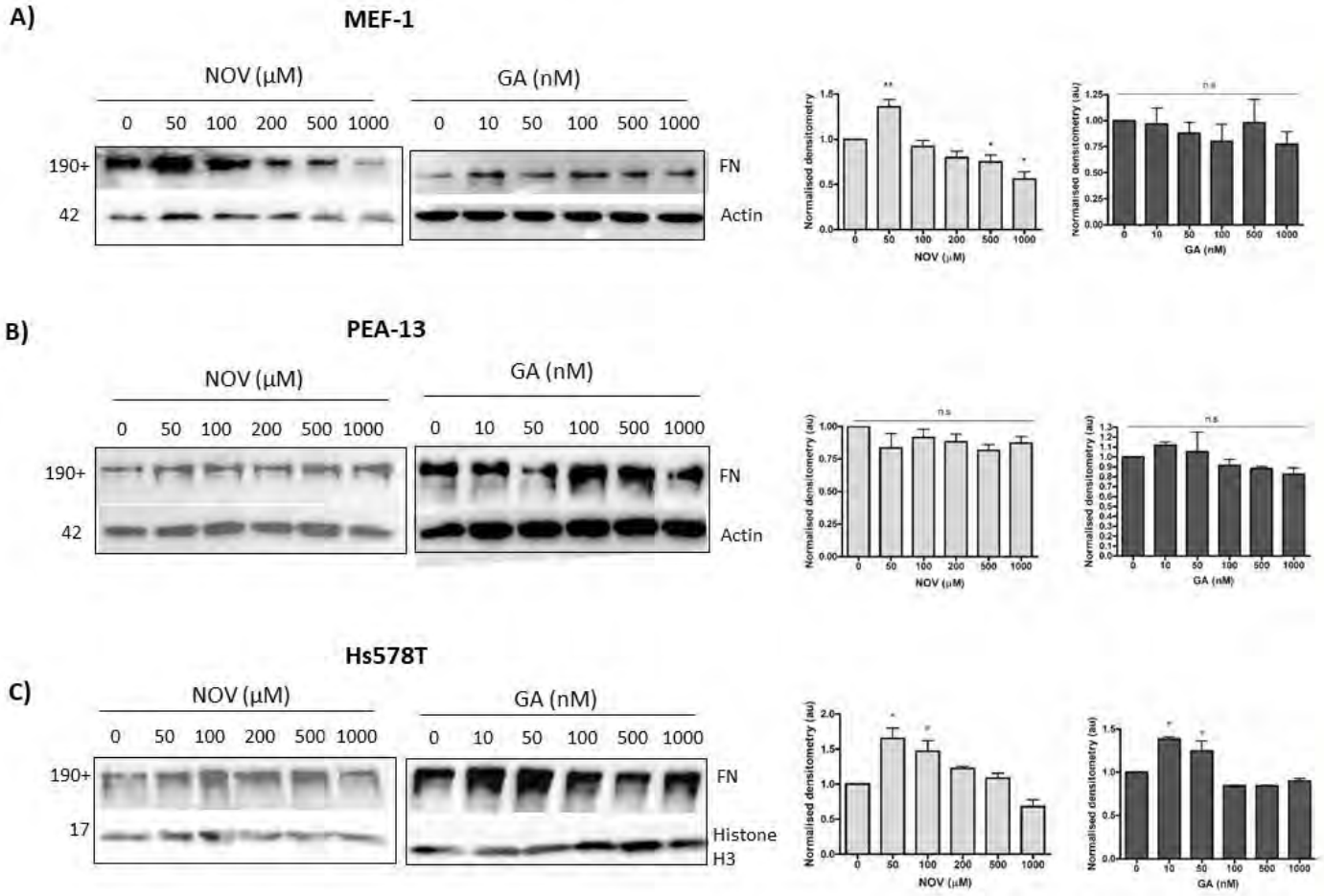

Figure 6: C-terminal Hsp90 inhibitors are more effective at reducing levels of the client protein, FN, in LRP1-expressing cells

Adherent cells were treated with increasing concentrations of the Hsp90 inhibitors, GA or NOV, for 16 hours at 37˚C, 9% CO_2 before being lysed and protein expression analysed by Western blot. **A)** MEF-1, **B),** PEA-13 **C)** and Hs578T cell lysates were probed for levels of FN using rabbit anti-FN primary antibodies. Actin or Histone H3 (H3) was used as the loading control. The densitometry represented alongside each of the immunoblots A)-C) was determined using ImageJ and statistical significance was determined using a one-way ANOVA and Bonferroni's post-tests in GraphPad Prism 4 (*= $p<0.05$, **= $p<0.01$, ***=$p<0.001$, ns= not significant). Images are representative or averages (±SD) of triplicate independent experiments.

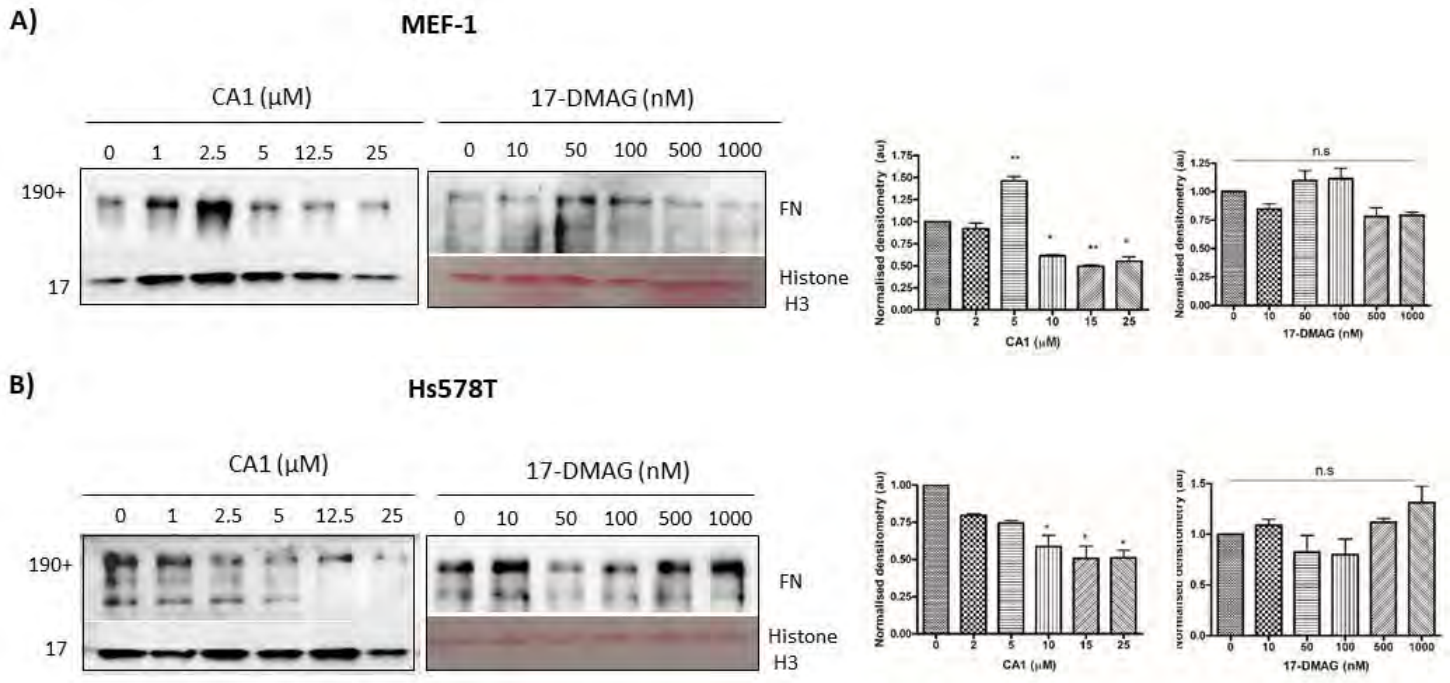

Figure 7: Alternative C- and N- terminal Hsp90 inhibitors produce similar FN responses to NOV and GA

Adherent **A)** MEF-1 and **B)** Hs578T cells were treated with increasing concentrations of the Hsp90 inhibitor coumermycin (CA1) or 7-dimethylamino-ethylamino-17-demethoxydeldanamycin (17-DMAG) for 16 hours at 37˚C, 9% CO_2 before being lysed and protein expression analysed by Western blot. Cell lysates were probed for levels of FN using rabbit anti-FN primary antibodies. Histone H3 was used as a loading control for CA1 treatments and the Ponceau stained membrane was used as a loading control for 17-DMAG treatments. The densitometry represented alongside was determined using ImageJ. Images are representative of triplicate experiments. Statistical significance was determined using a one-way ANOVA and Bonferroni's post-tests in GraphPad Prism 4 (*= $p<0.05$, **= $p<0.01$, ns= not significant). Images are representative or averages (±SD) of triplicate independent experiments.

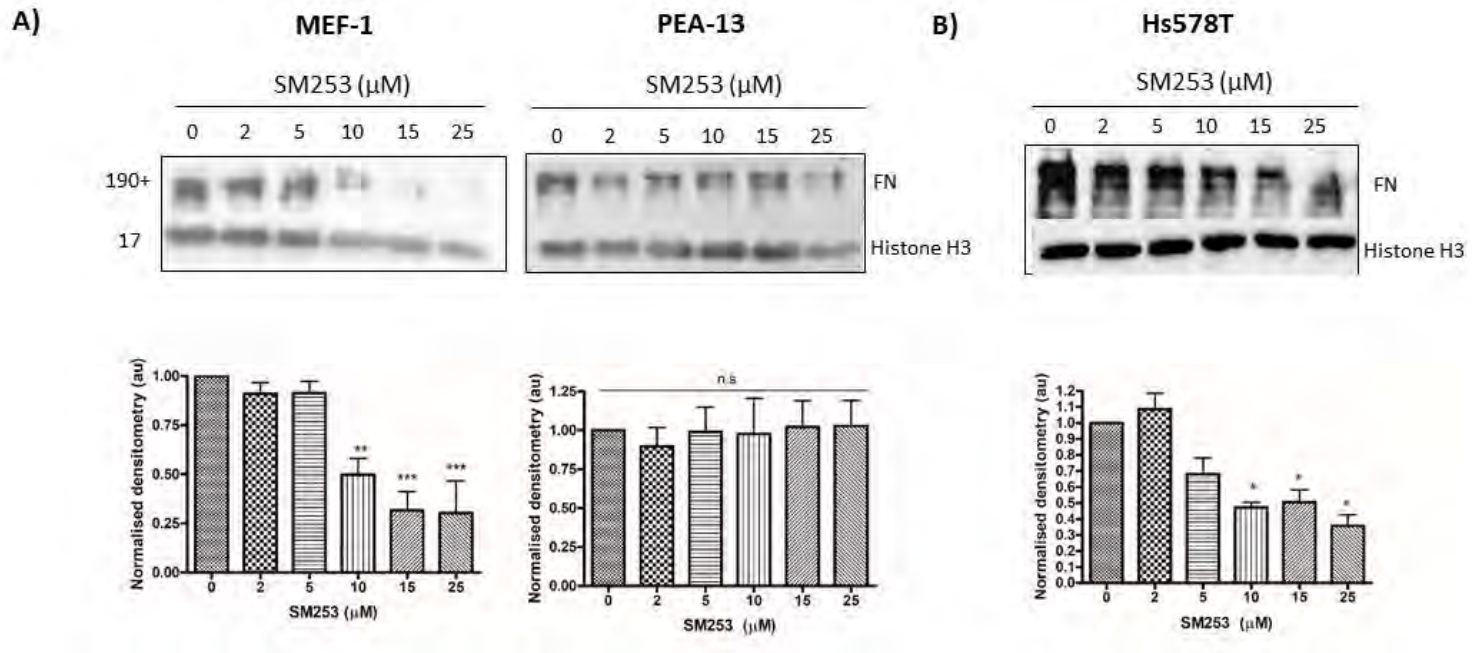

Figure 8: FN levels decrease in response to an allosteric C-terminal Hsp90 inhibitor in LRP1-expressing cells

Adherent cells were treated with increasing concentrations of SM253 for 16 hours at 37˚C, 9% CO_2 before being lysed and protein expression analysed by Western blot. **A)** MEF-1, PEA-13 and **B)** Hs578T cell lysates were probed for levels of FN using rabbit anti-FN primary antibodies. Histone H3 was used as a loading control. Densitometry was determined using ImageJ and statistical significance was determined using a one-way ANOVA in GraphPad Prism 4 (*= $p<0.05$, **= $p<0.01$, ***=$p<0.001$, ns= not significant). Images are representative or averages (±SD) of triplicate independent experiments.

3.1.2 Analysis of the effect of NOV on β1 integrin levels

At the cell surface, integrins bind and mediate the assembly of soluble FN (derived from intracellular FN) which induces the formation of short detergent soluble fibrils. These fibrils propagate to form a dense matrix of detergent insoluble fibrils, which are largely extracellular (Schwarzbauer & Sechler, 1999). An alternative way to induce FN turnover is to block assembly of FN. The main receptor responsible for FN synthesis and assembly are β1 integrins, in particular the α5β1 isoform (Schwarzbauer & Sechler, 1999). Here we investigated whether NOV was affecting the levels of the β1 integrin subunit, part of the main FN receptor responsible for its synthesis and fibrillogenesis. Immunoblotting for β1 integrin levels showed no significant differences in either of the NOV treated cell lines (Figure 9). PEA-13 cells showed significantly lower β1 integrin levels at the highest concentration of NOV but this is likely due to reduced levels of protein in this treatment as is evidenced by the loading control. However, even if this loss in β1 levels was true, it would still indicate that this was not the mechanism, as PEA-13 cells did not show NOV turnover in response to NOV.

3.1.3 NOV treatment causes internalisation of FN and LRP1

Hsp90 and FN are both able to interact with LRP1 (Basu et al., 2001; Boel et al., 2018; Salicioni et al., 2002). We showed previously that NOV treatment causes internalisation of FN by a receptor-mediated process. Treatment of Hs578T cells with methyl-b-cyclodextrin, an inhibitor of receptor mediated endocytosis, led to a dose-dependent and statistically significant reversal of the FN matrix phenotype in the presence of NOV (Hunter et al., 2014). FN in NOV treated cells was internalised into vesicles that were positive for the presence of endocytic markers including Rab5 and LAMP-1 (Hunter et al., 2014). We further demonstrated that NOV treatment increased the intensity of intracellular LRP1 staining and colocalisation with the endocytic marker, LAMP-1, in both MEF-1 and Hs578T cell lines (Figure 10). The fact that NOV induces FN internalisation and colocalisation with lysosomes, and LRP1 internalisation and colocalisation with lysosomes suggests that LRP1 may be mediating the internalisation and targeted degradation of FN in response to NOV treatment. Taken together, these data support a role for LRP1 in directly mediating the endocytosis of FN by NOV, which is consistent with previous reports of LRP1 as an endocytic receptor.

3.1.4 Analysis of MMPs in mediating FN turnover

MMPs play a large role in the degradation of ECM proteins prior to their internalisation in the cell (Etique, Verzeaux, Dedieu, & Emonard, 2013; Hynes & Naba, 2012). It would seem likely then that increased FN turnover in response to NOV may be mediated by an increase in the presence and activity of MMPs. To test this, we employed gelatin zymography assays to determine the activity of MMPs in MEF-1, PEA-13 and Hs578T cell lines upon inhibitor treatment (Figure 11). We measured the degree of gelatin degradation as an indication of activity which is also associated with the invasive potential of cells (Waas, Lomme, DeGroot, Wobbes, & Hendriks, 2002). We observed a significant dose dependent loss in MMP activity (Figure 11A) in response to NOV in the MEF-1 cells, whilst MMP activity in GA treated cells was unchanged, mimicking the response to that observed for total FN levels (Figure 6A). NOV also decreased MMP activity in PEA-13 cells but to a lesser extent than the LRP1 expressing lines (Figure 11B), whilst GA treatment did not cause any significant change. Hs578T MMP levels decreased dose dependently with NOV and were unchanged in GA treatments. These data suggest that MMP activities are attenuated upon C-terminal Hsp90 inhibition in both LRP1 expressing and deficient cell lines, and although the loss of MMP and FN are correlated, it is not immediately clear how reductions in MMP activity would explain the NOV-induced loss in FN protein levels.

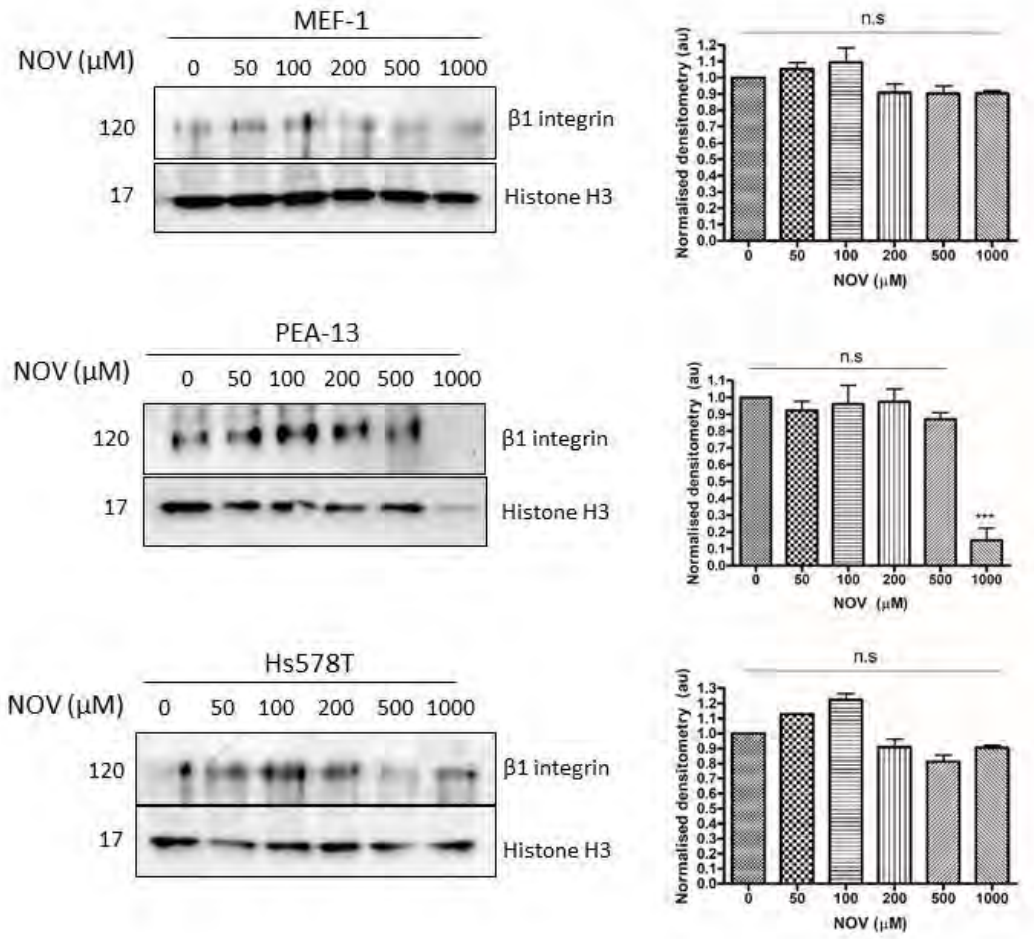

Figure 9: Levels of β1 integrin are not affected by NOV

Adherent cells were treated with increasing doses of NOV for 16 hours at 37 °C. Cells were lysed and equal amounts of total protein (50 μg) were loaded and resolved on a 10% SDS gel. Levels of β1 integrin were determined using rabbit anti-β1 integrin antibodies. Histone H3 was used as a loading control. Graphs alongside represent densitometry of immunoblots determined using ImageJ. Statistical significance was determined in GraphPad Prism 4 using a One-way ANOVA and Bonferroni's post-tests (***p<0.001, ns= not significant). Images are representative or averages (±SD) of triplicate independent experiments.

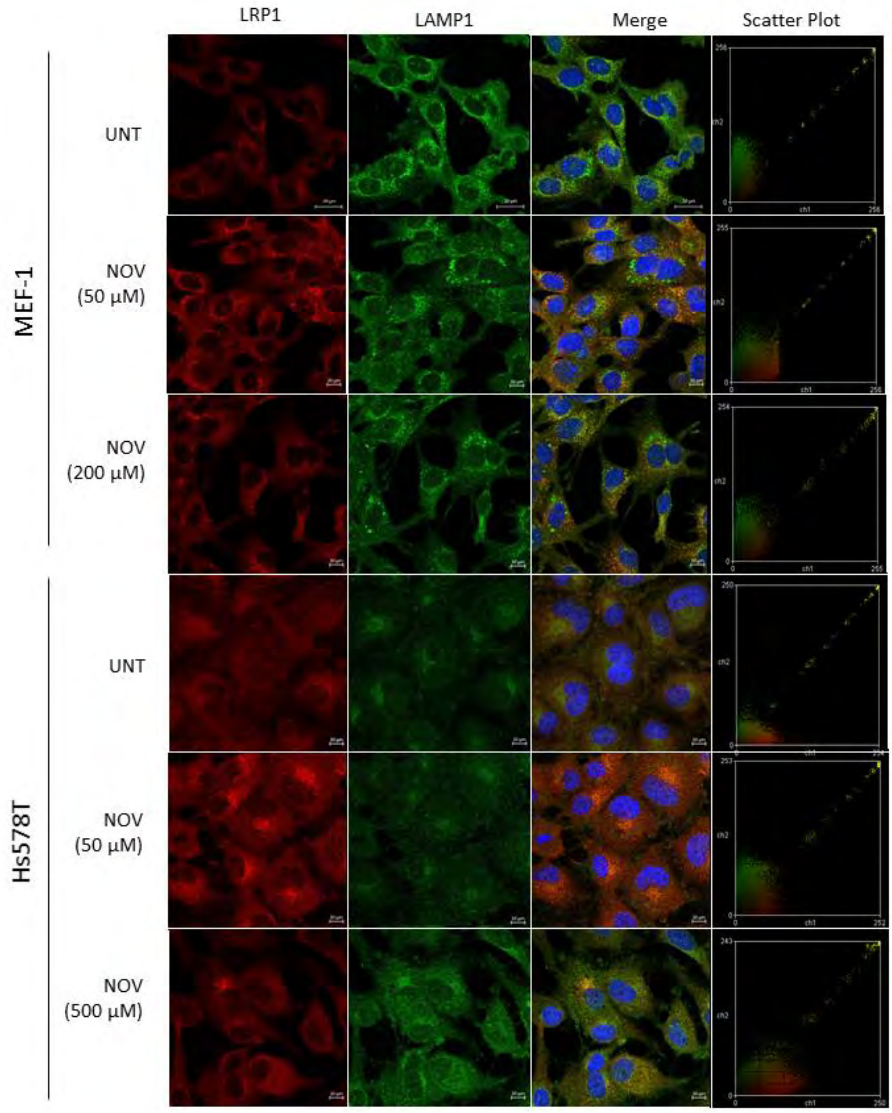

Figure 10: NOV treatment increased LRP1 and LAMP1 colocalisation in MEF-1 and Hs578T cells

Cells were treated with increasing concentrations of novobiocin (NOV) for 16 hours. Cells were fixed and incubated with rabbit anti-LRP1 (red) primary antibody followed by donkey anti-rabbit Alexa-fluor-488 and mouse anti-LAMP1 conjugated Alexa Fluor-647 (green). Nuclei were stained with (1 µg/ml) Hoechst-33342 (blue). Images were captured using the 63x objective on the Zeiss LSM 780 Meta laser scanning confocal microscope and analyzed using Zen Blue soſtware (Zeiss, Germany). Scatter plots were generated using Intensity Correlation Analysis plugin in ImageJ. Data are representative of images obtained from triplicate independent experiments with similar results. Scale bars represent 20 µm.

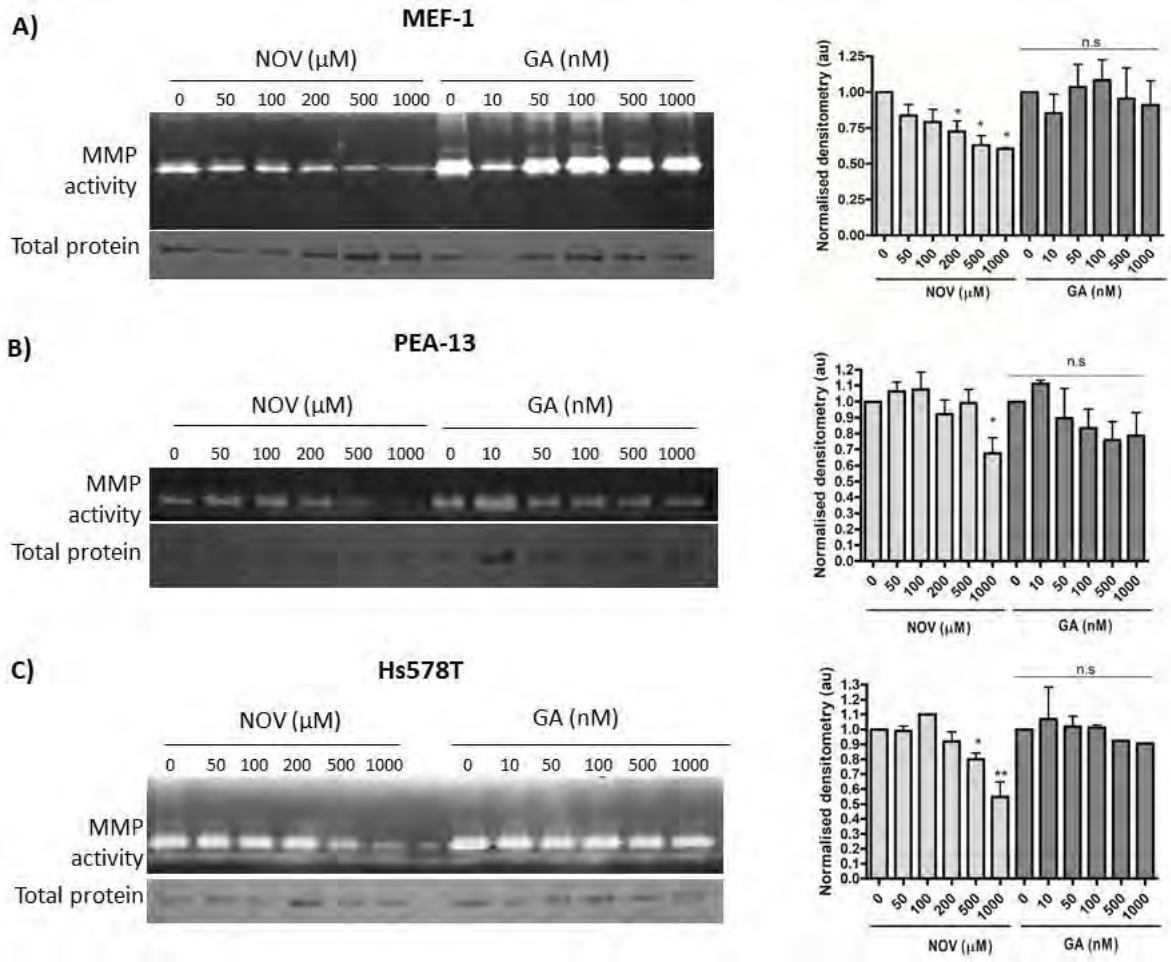

Figure 11: Activity of MMPs in response to Hsp90 inhibition

A) MEF-1, **B)** PEA-13 and **C)** Hs578T cells were treated with increasing concentrations of NOV or GA for 16 hours and the supernatants containing secreted MMPs were harvested and processed for gelatin zymography. Total protein in all cases is indicated by a Coomassie stained gel which serves as a loading control. Densitometry of MMP levels normalised to total protein is indicated alongside each of the zymograms. Statistical significance was determined in GraphPad Prism 4 using a One-way ANOVA and Bonferroni's Multiple comparisons post-tests (*p<0.5, **p<0.01, ns = not significant). Data are representative or averages (±SD) of triplicate independent experiments.

3.1.5 Investigating MMP-induced RIP of LRP1 in FN turnover

LRP1 is known to undergo RIP involving cleavage of the 85 kDa transmembrane subunit by MMPs and gamma-secretase to yield smaller LRP1 fragments of ~55 kDa, ~25 kDa and ~12 kDa (Derocq et al., 2012; May et al., 2002). Here, we observed no change on LRP1-85 levels in response to NOV however there was increase in an LRP1-58 fragment (Figure 12A). Evidence of LRP1 shedding and translocation of LRP1 fragments to the nucleus and other intracellular compartments where they may modulate transcriptional regulation has been demonstrated. The proteolytic processing of LRP1, in particular shedding of the LRP1-ICD (12 kDa fragment) has been shown to translocate to the nucleus where it interacts with various transcription modulators (Kinoshita et al., 2003; Zurhove et al., 2008). Considering NOV induced a markable increase in the LRP1-58 kDa fragment (Figure 12A) we sought to determine whether the increased generation of this fragment might generate LRP1-ICD fragments capable of localizing to the nucleus to indirectly modulate FN turnover by interacting with genes or transcription regulators responsible for FN synthesis or degradation. For this, we performed a fractionation assay to isolate the nuclear and cytosolic compartments of NOV treated cells in order to assess whether the LRP1-ICD may be present in the nucleus. Western analysis revealed increased levels of FN at low NOV concentrations in the cytosolic fractions compared to those isolated from untreated MEF-1 cells (Figure 12B), which is consistent with our data showing FN internalization upon NOV treatment. Interestingly, FN was also detected in the nuclear fractions (N), where we observed increased smearing of the FN signal with increasing NOV concentrations in nuclear fractions up to 200 µM NOV compared to the untreated nuclear fraction. This could indicate possible proteolysis of FN into several smaller bands in response to NOV, or it might be as a result of the insoluble nature of FN fractionating together with the insoluble nuclear fractions in this assay. Probing for LRP1 revealed that the LRP1-85 localised solely to the cytosolic fractions, with increased levels in the NOV treated samples up to 200 µM. These data also support the data in Figure 10 showing internalization of FN and LRP1 upon NOV treatment. The LRP1-58 fragment was detected in the higher NOV treated cytosolic fractions (200 µM and 500 µM) (Figure 12B), which might support a role for NOV-induced proteolytic processing of LRP1. No smaller LRP1 fragments, including the LRP1-ICD at 12 kDa, were observed in either of these treatments or fractions. Together, these data suggest that proteolytic processing of the ECM and RIP of LRP1

are not likely the only mechanisms involved in FN turnover, or that their involvement in this process is unclear.

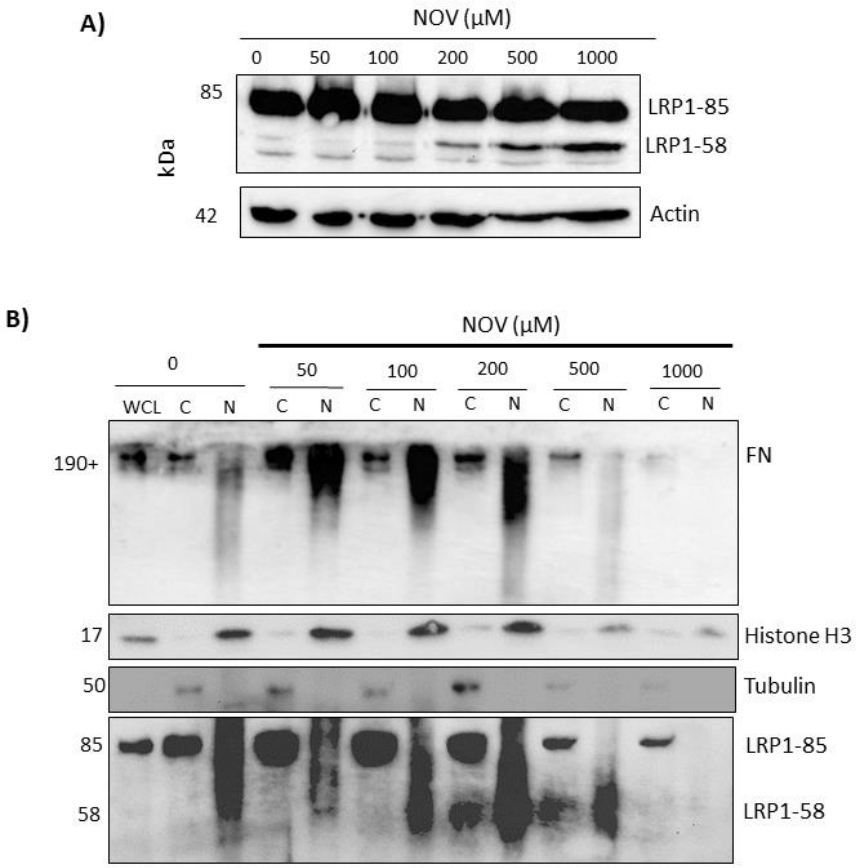

Figure 12: Fractionation assay of NOV treated MEF-1 cells

Adherent MEF-1 cells were treated with increasing concentrations of NOV for 16 hours and either **A)** lysed for western analysis and probed for LRP1 using anti-LRP1 antibodies or **B)** processed for REAP nuclear-cytosolic fractionation assay. Nuclear (N) and Cytosolic (C) fractions of each treatment were isolated and equal amounts of each fraction were loaded onto a 10% SDS gel. Cell lysates were probed for FN and LRP1 using rabbit anti-FN and rabbit anti-LRP1 antibodies respectively. Histone H3 was used as a loading control and fractionation marker for nuclear fractions and tubulin was used as a loading control and fractionation marker for cytosolic fractions.

Considering NOV induced the proteolytic processing of LRP1 evident by the generation of the LRP-58 kDa fragment (Figure 12A) we sought to determine whether this might be due to proteases responsible for LRP1 cleavage, which in turn might be responsible for degrading the ECM contributing to FN turnover. We used two specific inhibitors, Prinomastat and 3,5-Difluorophenacetyl-L-alanyl-S-phenylglycine t-butyl ester (DAPT) which block the activity of specific enzymes along the LRP1 proteolytic pathway (Figure 5) to determine whether inhibiting these enzymes might prevent LRP1 cleavage, and thereby prevent or reduce FN turnover in the presence of NOV.

Prinomastat, is a broad MMP inhibitor (Butler & Overall, 2007) with selectivity for MMPs 2, 3, 9, 13 and 14 (Sigma-Aldrich). We treated adherent MEF-1 and PEA-13 cells with increasing concentrations of Prinomastat (0 - 100 nM) for 16 hours (Figure 13) and observed a dose-dependent increase in levels of FN in MEF-1 cells, whilst LRP1 levels were unchanged (Figure 13A). At first, this response would seem to support the notion that inhibition of LRP1 processing early in the RIP pathway by MMPs prevents the ability of LRP1 to facilitate FN turnover, and thus we observe an accumulation of FN. However, since Prinomastat is a potent inhibitor of MMPs, and these are required for ECM turnover (Stellas et al., 2010; Zhang et al., 2013), the effect we are observing upon treatment is possibly due to inhibition of FN degradation/clearance and as a result we observe cumulative levels of this protein. This however, does not correlate with our zymography data in which we observe loss of MMP activity and reduced FN levels in NOV-treated cells. We then combined treatment of Prinomastat and NOV to determine if Prinomastat could inhibit the effects of NOV (Figure 13B). A working concentration of Prinomastat for effectively inhibiting MMP activity first needed to be determined. For this, we performed a zymography assay of Prinomastat and determined an effective concentration for MMP inhibition to be 1 nM (Supplementary Figure 1). We treated cells for 2 hours with 1 nM Prinomastat followed by treatment with increasing NOV for 16 hours. Prinomastat treatment coupled with increasing NOV concentrations caused a drastic loss in total FN, whilst LRP1 levels were unchanged and the 58 kDa LRP1 band was not detected (Figure 13B). These data appeared to suggest that NOV somehow induces proteolytic processing of LRP1 (seen with NOV alone, Figure 12A) and that inclusion of Prinomastat blocks this proteolysis and therefore stabilizes LRP1 levels. Interestingly, both NOV and Prinomastat decrease MMP activity; therefore, alone, the effect of NOV and

Prinomastat on FN and LRP1 is opposing even though the effect on MMP activity is the same. However, when combined they appear to have a synergistic effect on FN turnover. Also, the stabilization of LRP1 levels by Prinomastat in the presence of NOV (Figure 13B) is seen in spite of the fact that there is more turnover of FN suggesting that LRP1 processing and FN turnover are not mutually exclusive. Increasing Prinomastat treatment in PEA-13 cells, showed no significant change in FN levels, which in part supports a role for LRP1 in the FN loss observed in the MEF-1 line (Figure 13C).

DAPT, is an inhibitor of gamma secretase, which acts downstream of the RIP pathway (Figure 5) and is responsible for generation of the LRP1-ICD. DAPT is frequently used at a concentration of 10 μM (Gaultier, Salicioni, Arandjelovic, & Gonias, 2006; Zurhove et al., 2008). Increasing concentrations of DAPT in MEF-1 cells revealed an initial increase in FN followed by a loss (Figure 13D), similar to what was observed for FN levels in NOV treated cells, and was accompanied by a concomitant increase in LRP1 levels. The increased LRP1 levels are likely due to accumulation of and prevention of LRP1 proteolysis. When combined with NOV treatment (Figure 13E), levels of FN appeared to decrease whilst LRP1 levels increased in a dose dependent manner, but were generally reduced compared to treatment with DAPT alone which perhaps suggests that DAPT may be blocking NOV-mediated loss of LRP1. In PEA-13 cells, increasing DAPT concentrations caused a dose dependent loss in FN, suggesting that the FN turnover observed in response to DAPT in MEF-1 cells is independent of LRP1 (Figure13F).

These data do not convincingly demonstrate whether LRP1 processing is required for FN turnover, although taken together they suggest that inhibition of LRP1 and/or ECM degrading proteases is not sufficient to inhibit NOV-mediated FN turnover. Additional experiments, including combining treatments of DAPT and Prinomastat, would need to be done to explore this further. We may also need to take into consideration any other targets of these inhibitors which may be causing the observed effects.

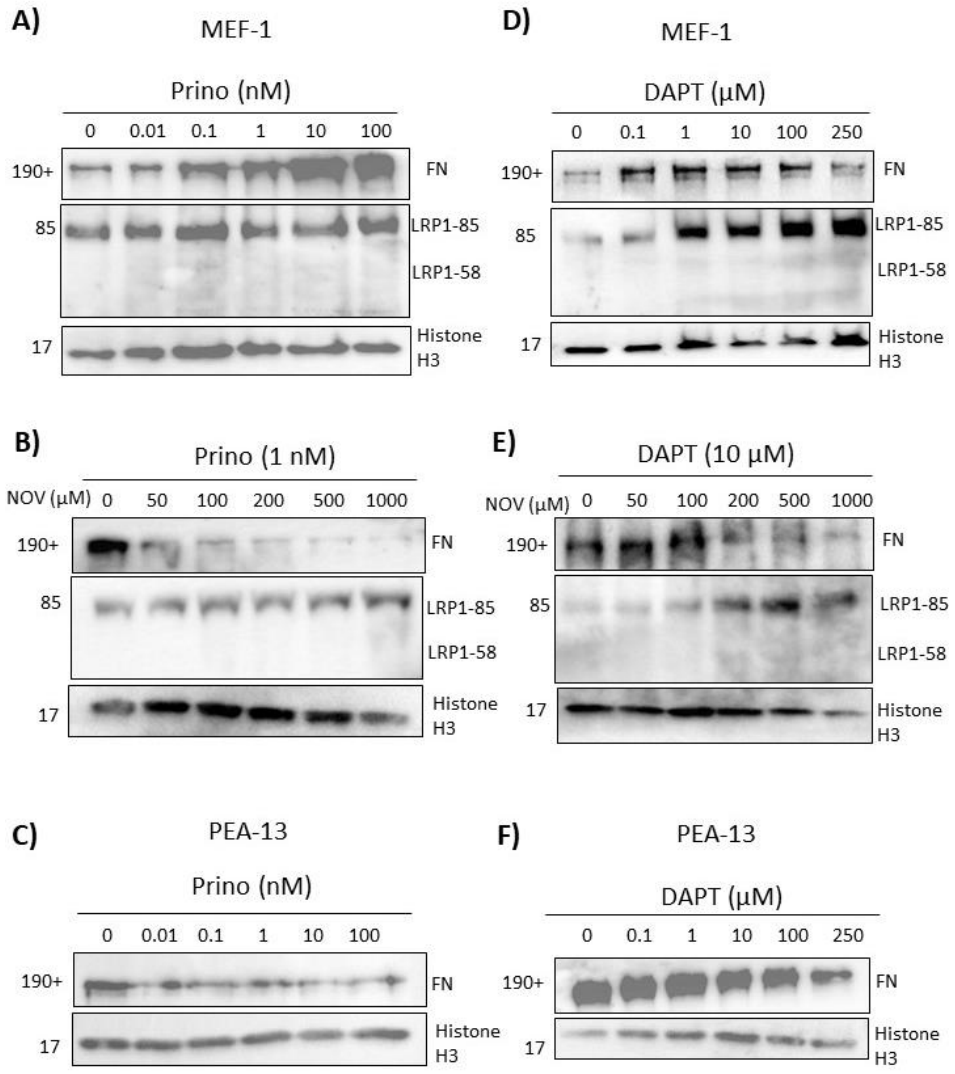

Figure 13: Inhibition of proteases related to LRP1 processing does not affect FN turnover.

Adherent MEF-1 cells were treated with increasing concentrations of **A)** Prinomastat (Prino) or **B)** 1 nM Prino for 2 hours following by varying concentrations of NOV for 16 hours. Cell lysates were probed for FN and LRP1 using rabbit anti-FN and rabbit anti-LRP1 antibodies respectively. **C)** PEA-13 cells were treated with increasing concentrations of Prino for 16 hours and lysates probed for FN. **D)** Adherent cells were treated with increasing concentrations of DAPT or **E)** 10 μM DAPT for 2 hours followed by increasing concentrations of NOV for 16 hours and probed for FN and LRP1 as described previously. **F)** PEA-13 cells were treated with increasing concentrations of DAPT and probed for FN. Histone H3 was used as a loading control in each of the treatments. Images are representative of triplicate experiments with similar results.

3.1.6 Analysis of signalling proteins downstream of the eHsp90-LRP1 interaction in NOV-mediated FN turnover response

Extracellular Hsp90 is known to use LRP1 as a cross-membrane signalling molecule. To determine whether LRP1-related downstream signalling pathways may be induced in response to NOV treatment we probed for two key signalling proteins, phospho-AKT and phospho-ERK which have previously been shown to be downstream of eHsp90-LRP1 to induce cell proliferation and migration (Gopal et al., 2011; Hance et al., 2012). Western analysis revealed opposing responses of these two proteins to NOV treatment (Figure 14). Levels of p-AKT were increased only at the highest concentration of NOV (i.e. 1000 μM) in both MEF-1 and PEA-13 cells, whereas p-AKT in Hs578T cells was increased at the lowest concentration of NOV (i.e. 50 μM) and thereafter dose-dependently decreased (Figure 14). Levels of p-ERK dose dependently decreased in MEF-1, PEA-13 and Hs578T cells. Also, of interest, levels of p-ERK were significantly lower in PEA-13 cells compared to its LRP1-expressing counterparts. Due to the sensitivity of phosphorylated proteins in BLOTTO it was challenging to get good signals of housekeeping proteins and thus here we made use of Ponceau stains as a loading control where the lowest bands typically indicative of histone were used as a marker of equal total protein. Taken together, the responses to NOV were conserved in LRP1 expressing or null cells and therefore this does not indicate that differential signalling via Akt or ERK may account for the difference in response of FN to NOV via LRP1.

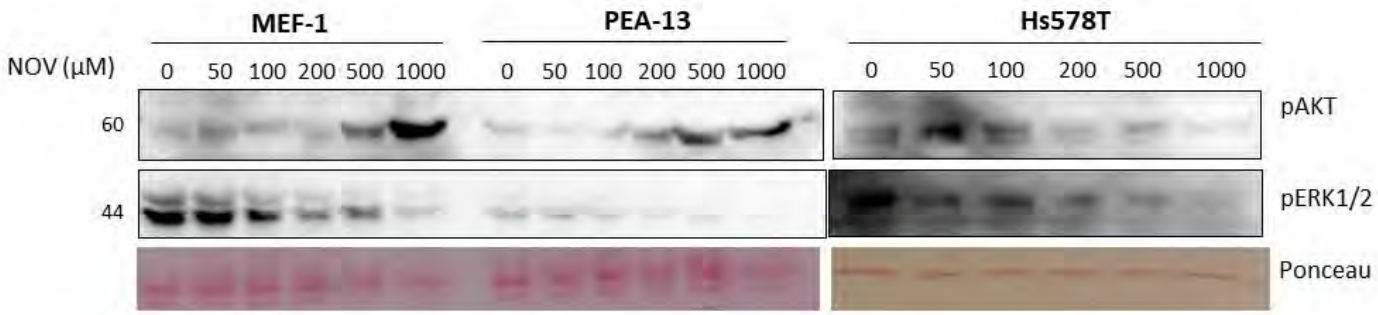

Figure 14: NOV has opposing effects on two key signalling proteins downstream of LRP1

Adherent cells were treated with increasing doses of NOV for 16 hours at 37 °C. Cells were lysed and equal amounts of total protein (50 μg) were resolved on a 10% SDS gel and probed for levels of phospho-AKT (pAKT) and phospho-ERK (pERK1/2) using rabbit anti-pAKT and rabbit anti-pERK antibodies respectively. Ponceau stain was used as a loading control. Images are representative of triplicate experiments.

3.1.7 Analysis of Hsp90-LRP1-FN complexes in response to NOV treatment

To determine whether extracellular Hsp90 was present in a complex with LRP1 and FN, cell surface proteins of Hs578T cells were crosslinked using the cell-impermeable, cleavable crosslinker DTSSP and probed for levels of Hsp90α/β, LRP1 and FN (Figure 15). We showed that treatment of cells with DTSSP led to the presence of higher molecular weight species (+190 kDa) of Hsp90 compared to the uncrosslinked cell lysate (-DTSSP). Levels of these high molecular weight FN complexes were decreased in NOV treated cell lysates. Cell lysates treated with the reducing agent, β-mercaptoethanol (βMer) lost these higher molecular weight complexes at 190+ kDa and produced increased levels of the reduced 135 kDa FN form. Uncomplexed FN was still present in each of the samples at ~135 kDa.

Hsp90 was also detected in higher molecular weight complexes at +190 kDa which upon cleavage were reduced to the 90 kDa form. Hsp90 complexes were reduced in NOV treated lysates compared to untreated lysates. LRP1 was also observed to be present in high molecular weight at +190 kDa in DTSSP treated cell lysates. Interestingly, LRP1 complexes appeared slightly increased in crosslinked NOV-treated cell lysates. As a control, trypsin, which should digest most extracellular protein complexes showed significantly reduced levels of all proteins (Figure 15), suggesting we were observing cell surface complexes.

We developed an immunoprecipitation technique to isolate the above crosslinked complexes. We have showed previously that cleared lysate Hsp90 IP fractions contained a common complex of FN, LRP1 and Hsp90 in both MEF-1 and Hs578T cells which was unperturbed by NOV treatment (Boel et al., 2018). Here we modified this immunoprecipitation protocol to isolate fractions which would represent soluble and insoluble fractions of these crosslinked complexes. Insoluble complexes may represent matrix or membrane associated complexes. Hs578T crosslinked whole cell lysates (WCL) or cleared lysates (CL) were immunoprecipitated with either Hsp90 (IP: Hsp90) (Figure 16A and B) or LRP1 antibodies (IP: LRP1) (Figure 16C and D). We assume the (WCL) immunoprecipitated fractions to be representative of an entire population of both soluble and insoluble crosslinked complexes, whilst (CL) fractions are first centrifuged at 13200 *xg* to remove insoluble material and should therefore theoretically only contain soluble Hsp90-containing complexes. In all cases, WCL fractions serve as a loading control and represent equal levels of proteins confirming that changes observed in IP fractions are not as a result of different starting concentrations of proteins in the samples (Figure 16).

We successfully isolated Hsp90-LRP1-FN complexes in an immunoprecipitation (IP) with either Hsp90α/β (Figure 16A) or LRP1 antibodies (Figure 16C) which were enriched compared to immunoprecipitations with an IgG isotype control antibody. In Hsp90 IPs, we isolated similar levels of FN and LRP1 in the soluble (CL) fractions of both untreated (U) and NOV treated (N) fractions. This is in agreement with LRP1 IPs performed in both MEF-1 and Hs578T cells (Boel et al., 2018). In WCL fractions, however, reduced levels of FN and LRP1 were observed in NOV treated samples compared to untreated samples in Hsp90 IPs (Figure 16B). We performed this IP using an LRP1 antibody, and similar to that for the Hsp90 IP, we observed unchanged levels of FN and Hsp90 in CL fractions of both untreated and NOV treated IPs (Figure 16D). However, in the WCL IPs, we observed increased levels of FN in NOV treated IP fractions compared to untreated fractions whilst levels of Hsp90 decreased. These data tentatively suggest that NOV treatment alters the complexes of LRP1, Hsp90 and FN in matrix or membrane fractions.

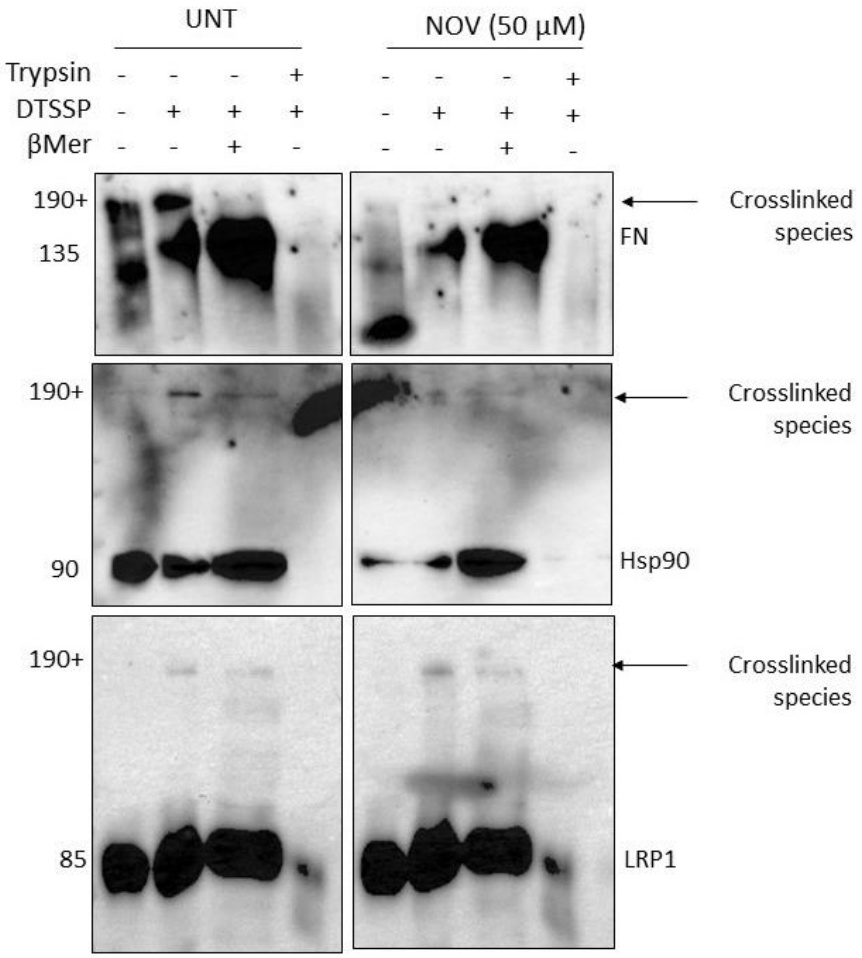

Figure 15: DTSSP crosslinking reveals Hsp90, LRP1 and FN in extracellular complexes

Adherent Hs578T cells were left untreated (UNT) or treated for 16 hours with 50 µM NOV. Surface proteins of Hs578T cells were chemically crosslinked with the thiol-cleavable DTSSP reagent either alone, or with the reducing agent β-mercaptoethanol (βMer) or trypsin. Equal amounts of protein samples were resolved on a 10% SDS gel and probed for FN, Hsp90α/β and LRP1 using rabbit anti-FN, mouse anti-Hsp90α/β and rabbit anti-LRP1 primary antibodies respectively. Arrows show proteins at higher molecular weights indicative of crosslinked species. The data shown are representative of a study performed in duplicate with similar results.

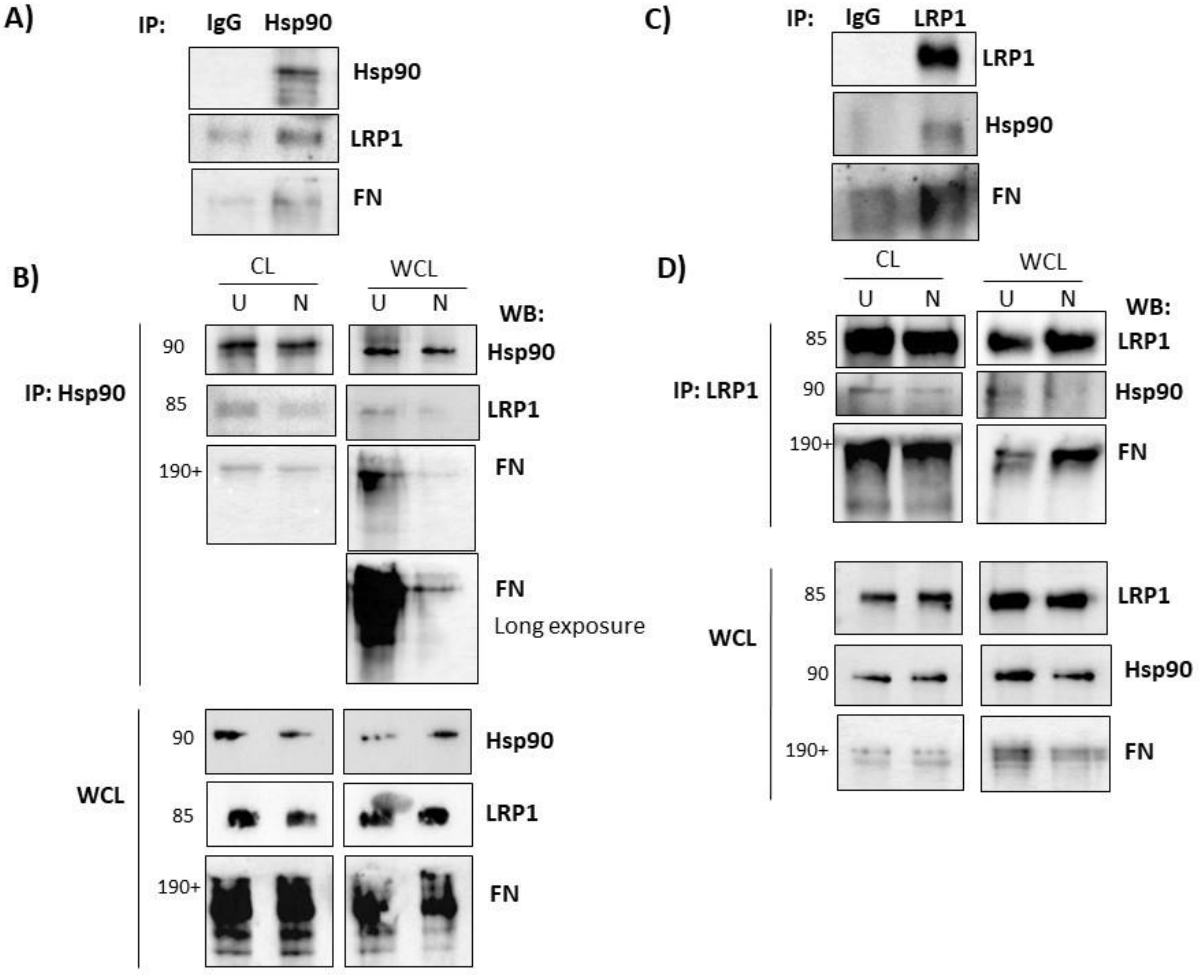

Figure 16: Immunoprecipitation of Hsp90 and LRP1 containing complexes from Hs578T cells

Adherent Hs578T cells were treated with or without NOV at 200 µM for 16 hours. Extracellular proteins were crosslinked with the cell-impermeable crosslinker, DTSSP (3 mg/ml), for 2 hours at 4 ˚C. The reaction was terminated by quenching in 1 M Tris-Cl (pH 7.5). Cells were scraped in lysis buffer and **A)** immunoprecipitated (IP) with either Hsp90 or isotype control IgG antibody coupled agarose beads. IP fractions were probed for FN, LRP1 and Hsp90. **B)** Cleared cell lysates (CL) which had been centrifuged at 13 200 *xg* for 20 min at 4°C or whole cell lysates (WCL) were immunoprecipitated (IP) with Hsp90 coupled agarose beads. Elution fractions were resolved and probed (WB) for FN, LRP1 and Hsp90. WCL fractions are shown below IP blots demonstrating equal levels of starting protein in each sample. Data shown are representative of triplicate experiments with similar results. **C)** Crosslinked Hs578T cell lysates were immunoprecipitated by MagReSyn™ Protein A coupled to either LRP1 or isotype control IgG antibodies. IP samples were probed for FN, Hsp90 and LRP1. **D)** Cleared cell lysates (CL) or whole cell lysates (WCL) were immunoprecipitated (IP) with LRP1 and elution fractions resolved and probed (WB) for FN, LRP1 and Hsp90. WCL fractions are shown below IP blots demonstrating equal levels of starting protein in each sample. Data shown are representative of triplicate experiments with similar results

3.2 Discussion

Studies within our group have shown the presence of Hsp90 in the extracellular space and identified FN as a client of Hsp90 as it directly binds to and is dependent on Hsp90 for stability and conformational regulation (Hunter et al., 2014). In Hs578T cells, inhibition of Hsp90 with NOV led to destabilisation of the FN matrix resulting in FN internalisation via a receptor mediated process (Hunter et al., 2014). We showed that the LRP1 receptor is required for the NOV-mediated turnover of extracellular FN (Boel et al., 2018). Here we demonstrate that FN turnover is specific to C-terminal Hsp90 inhibition and that this does not appear to involve significant changes in MMPs or FN assembly via integrins, but is more likely related to turnover and internalisation which may be the result of changes in complex formation between Hsp90, LRP1 and FN.

3.2.1 Loss of FN is specific to C-terminal Hsp90 inhibition

We showed here that turnover of FN was specific to C-terminal Hsp90 inhibition by demonstrating that NOV and CA1 (both C-terminal Hsp90 inhibitors) as well as an allosteric C-terminal inhibitor, SM253, caused a dose-dependent loss of FN. In each case, the loss of FN was specific to LRP1-expressing cells. In stark contrast, N-terminal inhibitors, GA and 17-DMAG showed no significant change in FN levels. One possible explanation as to why the effects of NOV on FN are different to those of GA, might be because NOV (and the other C-terminal Hsp90 inhibitors) do not induce a stress response (Butler et al., 2016; Eskew et al., 2011; Shelton et al., 2009). GA is known to induce a HSR (Bagatell et al., 2000; Sittler et al., 2001) and whilst it may also cause some FN turnover, this is likely to be masked by the induction of FN expression. To support this, studies in our group have showed that GA increased total FN mRNA levels in an HSF-1 dependent manner, whilst NOV treatment had no significant effect on FN mRNA (Dhanani, Samson, & Edkins, 2017; Boel MSc Thesis, 2016) confirming that expression of FN is not altered by NOV. Another possible explanation for the differences observed may be related to the significantly lower levels of ATP in the extracellular space. Since N-terminal Hsp90 inhibitors function by blocking the ATP binding site, it is possible that eHsp90 can function independently of ATP in this space and thus inhibitors targeting the ATPase domain of Hsp90 are less effective than ones which function by inhibiting Hsp90 dimerisation (Calderwood, 2017; Wong & Jay, 2016). In this study we also showed that NOV induced a dose dependent loss of MMP activity. Considering FN and MMP-

2 are extracellular clients of Hsp90 (Eustace et al., 2004; Hunter et al., 2014) and we observe a loss of both these proteins it is possible that the response we observe upon C-terminal Hps90 inhibition is specific to extracellular clients. To the best of our knowledge, no evidence for the degradation of extracellular clients by C-terminal specific Hsp90 inhibition has been previously reported.

3.2.2 NOV-induced LRP1-mediated FN loss is more likely due to increased turnover rather than FN assembly defects

Coupled to the loss of total FN protein levels, NOV treatment increased the colocalisation of LRP1 and FN intracellularly (Boel et al., 2018). We showed previously that blocking LRP1 using a commercial monoclonal LRP1 blocking antibody caused a loss in FN matrix similar to that observed for NOV treatment (Boel et al., 2018). This indicates that NOV may inhibit LRP1 function and might suggest a possible role for LRP1 in FN fibrillogenesis and/or stabilization of FN fibril assembly, in addition to the previously described role for LRP1 in FN endocytosis and catabolism (Boel et al., 2018; Salicioni et al., 2002). FN matrix polymerization regulates the stability of FN matrix fibrils, and inhibitors of FN polymerization have been shown to diminish the amount of FN accumulating in the extracellular matrix (Altrock et al., 2014). Therefore, events that slow polymerization of FN into fibrils (such as reduced integrins, a reduced source of FN, or increased proteolysis) will increase FN endocytosis (Singh, Carraher, & Schwarzbauer, 2010). The α5β1 integrins, are the main integrins responsible for matrix assembly, and have also been shown to be involved in FN endocytosis (Shi & Sottile, 2008; Sottile & Chandler, 2005). We might then expect that increased FN internalisation might be directly related to levels of these integrins, however our data did not show a change in the levels of β1 integrin subunit upon NOV treatment. It is possible that other FN binding integrins (e.g. αVβ3, αVβ1, α4β1) not tested for here may be responsible for the internalisation of FN (Huttenlocher & Horwitz, 2011). Whilst the total amount of integrin was unchanged it is still possible that surface expression levels of integrin might change. We would need to perform flow cytometry analysis to determine whether cell surface levels of β1 integrin were altered in response to NOV as described by Shi & Sottile (2011). Studies have shown that LRP1 regulates cell surface levels of β1 integrin whereby LRP1 expression promotes maturation of β1 integrin precursor and was associated with an increase in β1 integrin at the cell surface (Salicioni et al., 2004), therefore, since LRP1 levels were unchanged by NOV this would

suggests that cell surface β1 integrin levels in our study were not altered. It is also possible that a change in the activation state of these integrins might contribute to the observed FN response. A very recent study exploited a FRET analysis to determine the extent of activation of α5β1 integrin dimers expressed on the surface of leukocytes by measuring the conformational changes from an inactive bent state to an active extended state (Sambrano et al., 2018). An alternative option would be to use the SNA KA51 antibody, which recognises the active form of α5 integrin (Clark et al., 2012). Finally, we did not observe a reduction in the source of FN by demonstrating that FN mRNA levels were unchanged in response to NOV (Dhanani et al., 2017). It is possible that a reduction in the polymerization of FN into an insoluble matrix might be responsible for the observed FN response, thus, treatment of cells with the peptide, pUR4 which binds to and blocks polymerization of FN (Tomasini-Johansson et al., 2001) would allow for us to address the possibility of reduced FN polymerization in response to NOV as a contribution to the reduced total FN protein levels. Whilst our data do not support a role for reduced FN synthesis and export from cells as has been shown in prostate cancer explants for the Hsp90 inhibitor AUY922, another important consideration may be to investigate an integrin-independent mechanism of FN secretion (Armstrong et al., 2018). Most of the literature focuses on integrin-mediated binding of soluble FN and clustering of integrins at the cell surface to mediate FN polymerization, however, evidence of FN in exosomes (Sung et al., 2015; Welton et al., 2016) suggests that perhaps an alternative mechanism of cellular release of FN and other matrix-related factors by exocytic vesicles may play a bigger role than previously thought. Considering extracellular Hsp90 are thought to arise by release from exosomes (McCready et al., 2010) it is possible that Hsp90 may associate with soluble FN intracellularly and assist in its export from the cell. To test this, we would need to determine whether LRP1, FN and Hsp90 colocalised in exosomes and whether NOV perturbed this interaction and/or release of these exosomes from cells.

Extracellular degradation by MMPs, plasmin and other proteases are one of the principal molecular mechanisms believed to be involved in the turnover of matrix proteins. FN is a substrate for many proteases, including MMPs (Kenny et al., 2008; Stellas et al., 2010). Given this, we might then expect that loss of FN be attributed to increased processing and be directly linked to increased MMP activity. However, we showed that MMPs are not required for LRP1-mediated FN turnover in response to NOV as we did not observe an increase in MMP

activity, in fact, activity of MMPs were dose dependently decreased in response to NOV. This might be explained by the fact that MMP2, MMP3 and MMP9 are also clients of extracellular Hsp90 (Correia et al., 2013; Eustace et al., 2004; Stellas et al., 2010), or, together with our data on the FN response, might suggest that C-terminal Hsp90 inhibition is more effective at inhibiting extracellular clients. To confirm this, we would need to test whether a cell-impermeable N-terminal inhibitor, such as DMAG-N-oxide, was able to induce the same response observed here. Additionally, NOV alone caused turnover of FN, and the MMP inhibitor Prinomastat failed to recapitulate the NOV response, and Prinomastat failed to recover FN following NOV treatment, which taken together further suggest that MMP inhibition is not a requirement. However, the possible synergism between Prinomastat and NOV is interesting and could be explored further.

In support of our data, a role for Hsp90 inhibition in regulating ECM components was also demonstrated by Armstrong and colleagues. Using RNA-seq analysis, a second generation N-terminal Hsp90 inhibitor, AUY922, was shown to selectively alter cellular pathways involved in the actin cytoskeleton and extracellular matrix in patient derived explants (PDE) from prostate cancer (PCa) (Armstrong et al., 2018). They showed increased expression of total FN and FN in the cytosol of AUY922 treated PCa cell lines and that FN secretion was markedly reduced by AUY922, the consequences of which were a marked reduction in cell invasion. Comparatively, in our study, we showed no significant change in FN levels with either GA or 17-DMAG. AUY922 binds Hsp90α and Hsp90β with affinities of 4.5 and 3.2 nmol/l respectively whilst 17-DMAG binds Hsp90α and Hsp90β with affinities of 5.8 nmol/l and 4.8 nmol/l respectively. Since the binding affinities of these two inhibitors are very similar it is unlikely that this would contribute to the differences in FN response. Instead, a more likely explanation for differences are due to the toxicity and specificity of the different inhibitors or the duration of treatment with AUY922, together with the differences in the biological systems. Each of these N-terminal inhibitors are known to induce the HSR, and AUY922 treatments demonstrated increased Hsp70 levels so it could be that AUY922 produces a greater HSR which is why they were able to see a marked induction of FN compared to GA or 17-DMAG treatments, although we would need to verify this by testing for the induction of Hsps in our study. Furthermore, the observation that AUY922 altered signalling pathways involved in the cytoskeleton and ECM was performed on tumour PDE tissues (Armstrong et

al., 2018). This is a very different, complex model system compared to the cell lines we used in our study but it might still be interesting to address whether NOV reduces FN secretion by altered intracellular trafficking of FN containing vesicles along microtubules. These data may in fact support an alternative mechanism for NOV.

3.2.3 RIP of LRP1 does not directly affect FN turnover

An alternative mechanism of FN regulation might be by altering levels of LRP1 itself. Since roles for LRP1 in endocytosis and catabolism of FN have been described (Boel et al., 2018; Salicioni et al., 2002), with the possibility of an extended role in fibrillogenesis proposed by us, it is possible that loss of LRP1 levels may directly affect FN turnover. We showed that LRP1 levels were unchanged in response to NOV but that there was a concomitant increase in a smaller LRP1 fragment (LRP1-58). LRP1 is one of the several membrane spanning proteins known to undergo regulated intramembrane proteolysis (RIP), a process in which sequential proteolysis of a transmembrane protein ultimately leads to release of its intracellular domain (ICD). This process allows for cells to respond to extracellular signals or regulate their surface levels. During RIP, LRP1 is cleaved by various enzymes into smaller fragments of different size (Figure 3). Several studies have demonstrated a role for these shed LRP1 fragments to modulate cell signalling by translocation to the nucleus where it interacts with various transcription modulators (Kinoshita et al., 2003; May et al., 2002; Polavarapu et al., 2008; Zurhove et al., 2008). An example of such a study by Zurhove and colleagues demonstrated that LRP-ICD interacts with and represses a subset of LPS-inducible genes (p65, NFkB and IRF-3) by facilitating their export from the nucleus thereby limiting the inflammatory response (Zurhove et al., 2008). We speculated that perhaps NOV induced RIP of LRP1 (as supported by the increased LRP1-58 fragments isolated in cytosolic fractions) might result in translocation of LRP1-ICD fragments to the nucleus where it could regulate genes involved in FN turnover. However, we did not observe the presence of ICD fragments in the nuclei isolated from NOV-treated MEF-1 cells. An interesting observation from this study however was the presence of increased levels of FN in NOV treated nuclear fractions. Considering that ECM proteins contain secretory signal peptides, how ECM proteins end up in the cytoplasm or nucleus is still unclear, but it is suspected to occur either by escape from the endo/lysosomal degradation pathway or by alternative splicing of mRNA that results in omission of the secretory signal peptide (Hellewell & Adams, 2015). An example of such an

ECM protein is the adipocyte enhancer binding protein 1 which due to alternative splicing, exists both in the nucleus where it acts as a transcription repressor, and in the ECM (Hellewell & Adams, 2015). Several ECM proteins have been shown to localise to the nucleus by possessing a nuclear localisation sequence (NLS) (Liang et al., 1997; Rucci et al., 2009). Some examples of such ECM proteins include biglycan and prolargin of the small leucine rich proteoglycan (SLRP) family, decorin and osteopontin (Hellewell & Adams, 2015). No NLSs were predicted in FN using a variety of online NLS mapper platforms. We also have not observed the nuclear localisation of FN in any of our confocal analyses with NOV treated cells, so we suspect that the presence of FN in the nucleus here may be a technicality of its insoluble nature being fractionated in nuclear fractions. Interestingly, increased FN in nuclear fractions upon treatment with the Hsp90 inhibitor, AUY922, was proposed in a similar nuclear fractionation assay (Armstrong et al., 2018). Whether this was also due to technical issues was not addressed by the authors. To confirm these results, we would need to perform an alternative nuclear/cytoplasmic fractionation assay which relies on factors other than insolubility to isolate these fractions. Increased cytosolic FN fractions in response to NOV is not unexpected. Considering NOV causes internalisation of extracellular FN matrix, we might anticipate an increase in intracellular levels of FN as supported by the internalisation of FN by NOV previously.

Whilst the presence of LRP1-ICD was not detected, the increased proteolytic processing of LRP1 into its 58 kDa fragment might still contribute to the observed FN turnover. We hypothesized that LRP1 cleavage by MMP activity at the plasma membrane would show less LRP1 shedding in the presence of the MMP inhibitor, Prinomastat. Indeed, LRP1 cleavage into its 58 kDa fragment was prevented in the presence of Prinomastat. However, the fact that NOV results in LRP1 processing even though MMP activity is reduced in these treatments suggests that MMPs are not essential for RIP. Considering MMPs process FN and inhibition of MMPs lead to accumulation of FN, an important consideration is the many interactions and perturbations observed in the case of a broad spectrum MMP inhibitor like Prinomastat (Butler & Overall, 2007) which render it difficult to definitively ascribe the FN induced effects to the altered processing of any one substrate, in this case; LRP1. Further downstream of the LRP1 proteolytic pathway is γ-secretase which cleaves the 25 kDa fragment into the ICD. Inhibition of γ-secretase by DAPT was used to examine whether γ-secretase-dependent

processing of LRP1 plays a role in regulating FN turnover. DAPT has been shown to cause an accumulation of the LRP1 25 kDa fragment and significantly inhibit LRP1-ICD (12 kDa) production (Derocq et al., 2012; May et al., 2002). In our study, we could not detect the 25 kDa and 12 kDa LRP1 fragments, which might be because the recognition site of the LRP1 antibody used here does not bind to the regions generated by cleavage of these enzymes or that levels generated by these enzymes are too low for detection. DAPT alone increased FN levels initially followed by a loss, whilst co-treatment with NOV attenuated FN levels. γ-secretase is a protease complex of four integral membrane proteins, with presenilin-1 (PS1) as the apparent catalytic component. By demonstrating an accumulation of FN in PS1 deficient cells and a corresponding loss of FN upon reintroduction of PS1 into these cells, PS1 has been shown to regulate fibronectin levels in endothelial cells by modulating the constitutive turnover of the fibronectin matrix (Gasperi, Sosa, & Elder, 2012). Therefore, we might expect that inhibition of PS1 by the inhibitory activity of DAPT might cause an accumulation of FN, which is what we observed in our study upon DAPT treatment, although this was not as significant as the FN accumulation in Prino treatments. The fact that we are seeing similar responses with two different inhibitors of LRP1 processing, and that neither of these are able to block the NOV phenotype suggests that RIP of LRP1 is not necessary for FN turnover. It might also suggest that γ-secretase may play a previously unrecognised role in FN degradation albeit to a lesser extent than MMPs. To better demonstrate the possibility of a regulatory mechanism via LRP1 fragments we designed various truncations of LRP1 (LRP1-58, LRP1-25 and LRP1-ICD) to determine whether overexpression of either fragments would be able to induce FN responses similar to NOV (data not shown). Transfections of these various construct however were unsuccessful and require further optimization. In addition to this, introduction of a non-cleavable LRP1 mutant into the PEA-13 line would also be another interesting addition to these sets of experiments to determine whether cleavage of LRP1 is necessary for the observed FN response.

3.2.4 eHsp90-LRP1 downstream signalling pathways and complex formation may regulate FN turnover

Roles for eHsp90-LRP1 cross-membrane signalling have previously been reported, whereby binding of extracellular Hsp90 to LRP1 induced the activation of downstream signalling pathways (Gopal et al., 2011). Some of these downstream eHsp90-LRP1 pathways directly

regulate cell migration, such as the activation of mTOR, ERK and Akt phosphorylation which have been shown to promote EMT and cell migration (Hance et al., 2014; Tsen et al., 2013). Some of these downstream targets also play a role in regulating FN matrix dynamics. The activation of NFkB and Akt pathways by eHsp90-LRP1 was shown to induce FN expression (Chen et al., 2013; Qin et al., 2015; You et al., 2017). In LRP1-expressing and deficient cells, we observed a significant NOV-induced increase in the levels of phosphorylated Akt suggesting an activation of this pathway, however this did not translate into an induction of FN expression, at either the protein or mRNA level. Levels of phosphorylated ERK were reduced in NOV-treatments. Interestingly, these responses were conserved in both LRP1 -expressing and -deficient cells suggesting that the difference in activation of these signalling proteins is not via LRP1 or an eHsp90-LRP1 induced signalling cascade. A study by Dong and coworkers demonstrated that inhibition of eHsp90α with the monoclonal antibody 1G6-D7 attenuated FN synthesis and deposition in lung fibrosis through inhibition of ERK signalling. They showed that inhibition of eHsp90α caused significant downregulation of pERK but not pAkt and that this was mediated by disrupted eHsp90-LRP1 signalling (Dong et al., 2018). In another study, Loureirin B used to inhibit scar formation, down regulated pERK which was associated with a reduction in COL1 and FN (He et al., 2015). This highlights an important role for the activation of the ERK pathway in regulating FN synthesis and deposition. Binding of extracellular FN to integrins and induction of ADAMs at the cell surface led to an activation of ERK, p38 and Akt (Matsuo et al., 2006). Therefore, whilst this does not explain the different responses of pERK and pAkt levels in our study, it does suggest that perhaps NOV-induced loss of extracellular FN might cause inactivation of some of these pathways (which we do see for pERK). Perhaps then, a role for FN in regulating levels of pAkt and pERK rather than the other way around should be considered.

Impaired interaction of FN and Hsp90 with the LRP1 receptor upon NOV treatment might be an alternative mechanism of FN regulation. In Hsp90 IPs, we demonstrated an association of LRP1 and FN with extracellular Hsp90 which was disrupted upon NOV treatment. We isolated extracellular matrix and/or membrane associated fractions from NOV treated lysates which contained reduced FN levels. Studies from Wei Li's group have provided direct evidence of cross-membrane signalling by eHsp90 via interaction with LRP1. They showed that eHsp90α promotes skin cell migration and accelerates wound closure by binding to subdomain II of the

LRP1 ectodomain and activating the NPVY motif in the LRP1 cytoplasmic tail to activate downstream Akt kinases (Tsen et al., 2013). Interestingly, their data also showed that none of the NPXY motifs was involved in eHsp90α signaling to activate the ERK1/2 pathway. It might be worthwhile determining whether NOV induces phosphorylation of the NPVY and NPXY motifs on LRP1 ICD. Loss of FN in response to treatment with mLRPab (Boel et al., 2018) might also support a role for complex formation at the cell surface in that mLRPab binding to LRP1 receptor might block FN and Hsp90 interaction with LRP1. LRP1 IPs of the same fractions revealed reduced Hsp90 and increased FN levels. It is unclear why these two IPs may be isolating different levels of FN but it may be due in part to isolation of different complexes in the different IPs. Either way, our data demonstrate that NOV is perturbing the interaction of these proteins at the cell surface and isolating different pools of FN which might explain the observed FN response upon NOV treatments. To validate the changes in the Hsp90-LRP1-FN complexes upon NOV treatment, we could perform a bimolecular fluorescence complementation (BiFC) assay as described by Shyu and coworkers. This is based on FRET and would involve fusing an LRP1-containing plasmid to half of a Venus YFP fluorophore and the other half to FN to determine whether a FRET signal is obtained to an Hsp90 fused YFP plasmid (Shyu et al., 2006).

Another experiment would be to identify the specific interaction site of FN on LRP1. Using various recombinant LRP1 constructs (Mikhailenko et al., 2001). We plan as part of future studies to perform solid phase binding assays to determine the interaction sites between these proteins. Using surface plasmon resonance (SPR) studies we will further be able to identify how stable the interactions are in the presence of NOV by acquiring detailed information on the kinetics of this interaction and whether these proteins compete for binding on LRP1.

From this study, we were unable to identify the underlying mechanism of LRP1 mediated FN turnover. Given that we observed no significant impact of integrins, MMPs or LRP1 processing on FN turnover and considering the changes in cell surface Hsp90-LRP1-FN protein complexes and phosphorylated protein levels of key downstream signalling pathways it is likely that an altered eHsp90-LRP1 signalling cascade is responsible for the NOV-induced FN turnover and will be the focus of future studies.

Chapter 4: **ANALYSIS OF THE BIOLOGICAL CONSEQUENCES ASSOCIATED WITH NOV-INDUCED FN TURNOVER**

4.1 Introduction

Cell-derived matrices (CDMs) are three-dimensional structures generated by cells grown at high density *in vitro* for extended periods of time. The resulting matrix scaffolds represent a physiologically relevant in vivo-like matrix environment which provides a useful system to study matrix composition and organisation (Castello-Cros & Cukierman, 2009). In addition to the biochemical, structural and mechanical features of the ECM, the matrix is also a major storage compartment for growth factors, cytokines and various extracellular proteins that may affect behaviour of surrounding cells such as influencing cell adhesiveness and migratory abilities. Here we generated CDMs from Hs578T breast cancer cells using a protocol adapted from Castello-Cros & Cukierman (2009). We generated CDMs using Hs578T cells as these produce high levels of endogenous FN ECM and are an amenable in vitro model to study matrix deposition by a cancer cell line. It is postulated that cells are directly affected by the composition, three-dimensionality and rigidity of their substratum and that the matrix microenvironment may induce differentiation of certain cell types which can lead to diseased states (Amatangelo et al., 2005). This study contributes to the understanding of how Hsp90 inhibition may alter tumour derived matrices and the consequences which this has on neighbouring cell behaviour. This will have an impact not only on tumour progression but also in wound healing, inflammation and fibrosis. The in vitro systems such as those described in this study could facilitate the possibility of conducting more examinations of events that could assist in developing stroma targeted therapeutic drugs in the future. In particular, the aims of this study were:

1. To determine the morphological changes in thickness, composition and organisation of matrices from untreated and treated (NOV and eHsp90β) CDMs.

2. To determine some of the functional consequences such as changes in proliferative, adhesive and migratory abilities of cells replated onto various treated CDMs.

4.1.1 Adhesive, migratory and proliferative abilities of cells on CDMs is affected by NOV

We wanted to assess whether replating either normal or cancer cells onto extracted CDMs would have physiological effects on the cells' ability to adhere, grow or migrate. We performed a crystal violet adhesion assay to assess the morphological changes in cell shape upon adhering to the various matrices. Cells were seeded into wells of a 24 well plate containing prepared CDMs (or no CDM) and allowed to adhere and spread over 4 hours. Cells were fixed and stained for crystal violet and images taken using an inverted light microscope. Figure 17 shows panels for CDMs alone (CDM), replating of Hs578T (+ Hs578T) and MEF-1 (+MEF-1) cells. We observed that the crystal violet stain which typically binds DNA, also stained the matrices (Figure 17). Therefore, to quantify the number of cells attached to the CDMs we subtracted the staining of the CDM alone from the staining of the CDM + cells CDMs (Figure 18A). We observed significantly more MEF-1 and Hs578T cells adhered to NOV treated CDMs (at 50 μM and 500 μM NOV) compared to untreated CDMs (Figure 18A). Additionally, we looked at changes in the cell shape and morphology of the adhered cells determined by using a cell-index function by dividing the cell length by the cell width across multiple cells per image (Figure 18B). Cell index (CI) values closer to 1 represent round cells, while values greater than 1 represent more elongated cells. MEF-1 cells had significantly higher cell index values on 500 μM NOV treated CDMs (CI= 2.9) compared to UNT CDMs (CI = 1.9) and compared to cells adhered to no CDM (CI = 1.9) (Figure 18B). This increase in cell index suggests MEF-1 cells on these NOV-treated matrices are more elliptical and less spread compared to MEF-1 cells on UNT matrices which are rounder and more spread. Similarly, we observed higher cell indexes of Hs578T cells on 500 μM NOV treated CDMs (CI = 2.1) versus UNT CDMs (CI = 1.2). No significant differences were observed in cell adhesiveness between the different Hsp90β treated matrices.

Together, these data suggest that cells are more adherent to NOV treated CDMs and exhibited more elongated cell shapes on these matrices. We also noted that MEF-1 cells were

generally more elongated than Hs578T cells as was evident by the almost two-fold greater cell indexes.

Changes in matrix stiffness as well as transition between 2D and 3D matrix contacts influence cell proliferation profoundly. Thus, tumour progression involves not only genetic alterations of cancer cells but also changes in the tumour microenvironment. To investigate this, we compared the ability of CDMs generated from cancer cells to influence cancer cell and normal cell proliferation. Here, we replated MEF-1 and Hs578T cells onto Hs578T-derived CDMs and allowed them to grow for 48, 72 and 96 hours. At each of these time points, an MTT assay was performed to determine the number of active, proliferating cells on each of the matrices (Figure 19). There did not appear to be any difference in the proliferation of Hs578T cells seeded onto any of the matrices (Figure 19A), however we did observe changes in proliferation of the MEF-1 cells. In general, these cells appeared to have a reduced ability to grow on each of the treated Hs578T CDMs when compared to the untreated CDMs (red line) (Figure 19B). Specifically, we found both 200 µM NOV and 5 ng/ml Hsp90β treated matrices to significantly reduce the proliferation of MEF-1 cells on these CDMs (Figure 19B).

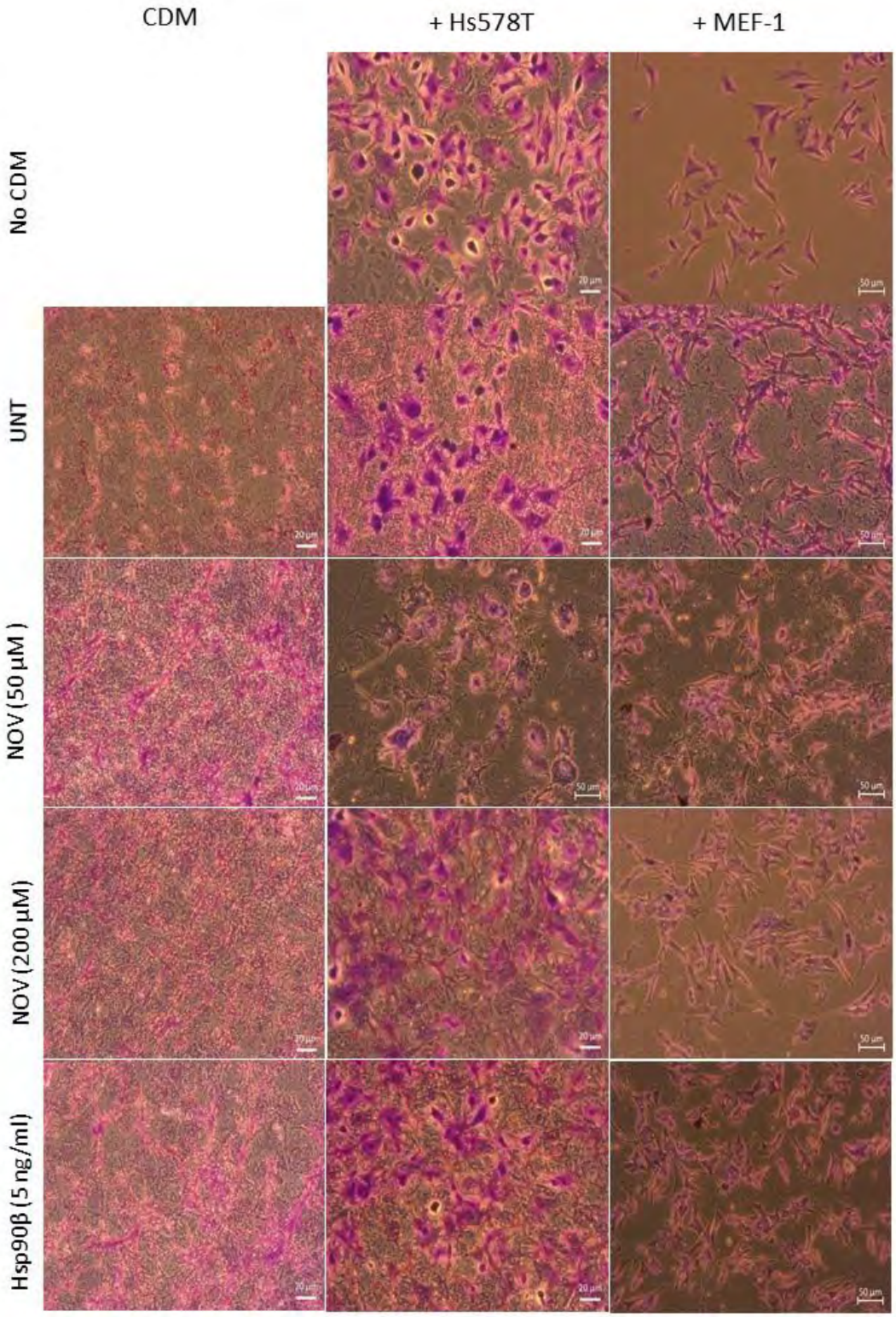

Figure 17: Adhesion of MEF-1 and Hs578T cells as determined by a crystal violet stain

Hs578T and MEF-1 cells were seeded into wells of a 24-well plate containing previously prepared CDMs, or no CDM, and allowed to adhere for 4 hours before fixing and staining with crystal violet as described in Methods. The first panel shows CDMs lacking replated cells stained by crystal violet. The middle and last panel shows Hs578T and MEF-1 cells adhered to CDMs respectively. Images were captured using the Zeiss Inverted light microscope with the 20x objective. Images are representative of triplicate independent experiments.

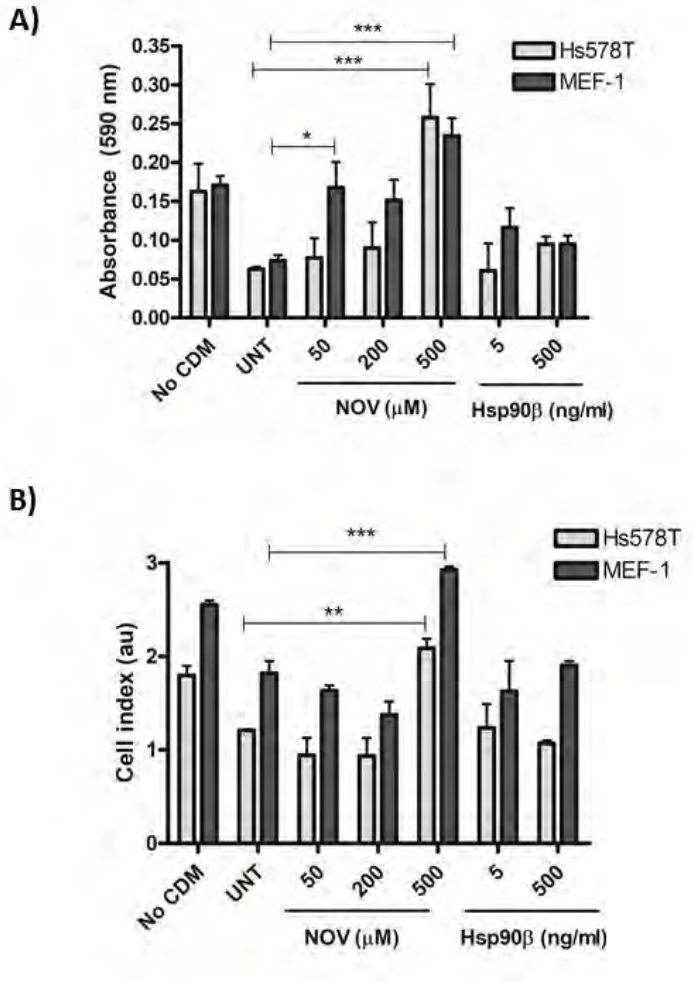

Figure 18: Quantification of adhesion and cell morphology on CDMs in response to NOV and Hsp90β

MEF-1 and Hs578T cells were seeded on to Hs578T CDMs as described previously and after 4 hours **A)** adhesion was measured by solubilizing crystal violet stain and reading absorbance at 590 nm. Measurements were quantified in ImageJ and statistical significance determined using a two-way ANOVA and Bonferroni's Multiple comparison post-tests (*p<0.5; ***p<0.001). **B)** Cell index measurements were quantified using ImageJ and statistical significance was determined in GraphPad Prism 4 with a two-way ANOVA and Bonferroni's Multiple comparison post-tests (**p<0.01; ***p<0.001). Data are averages (±SD) of triplicate independent experiments.

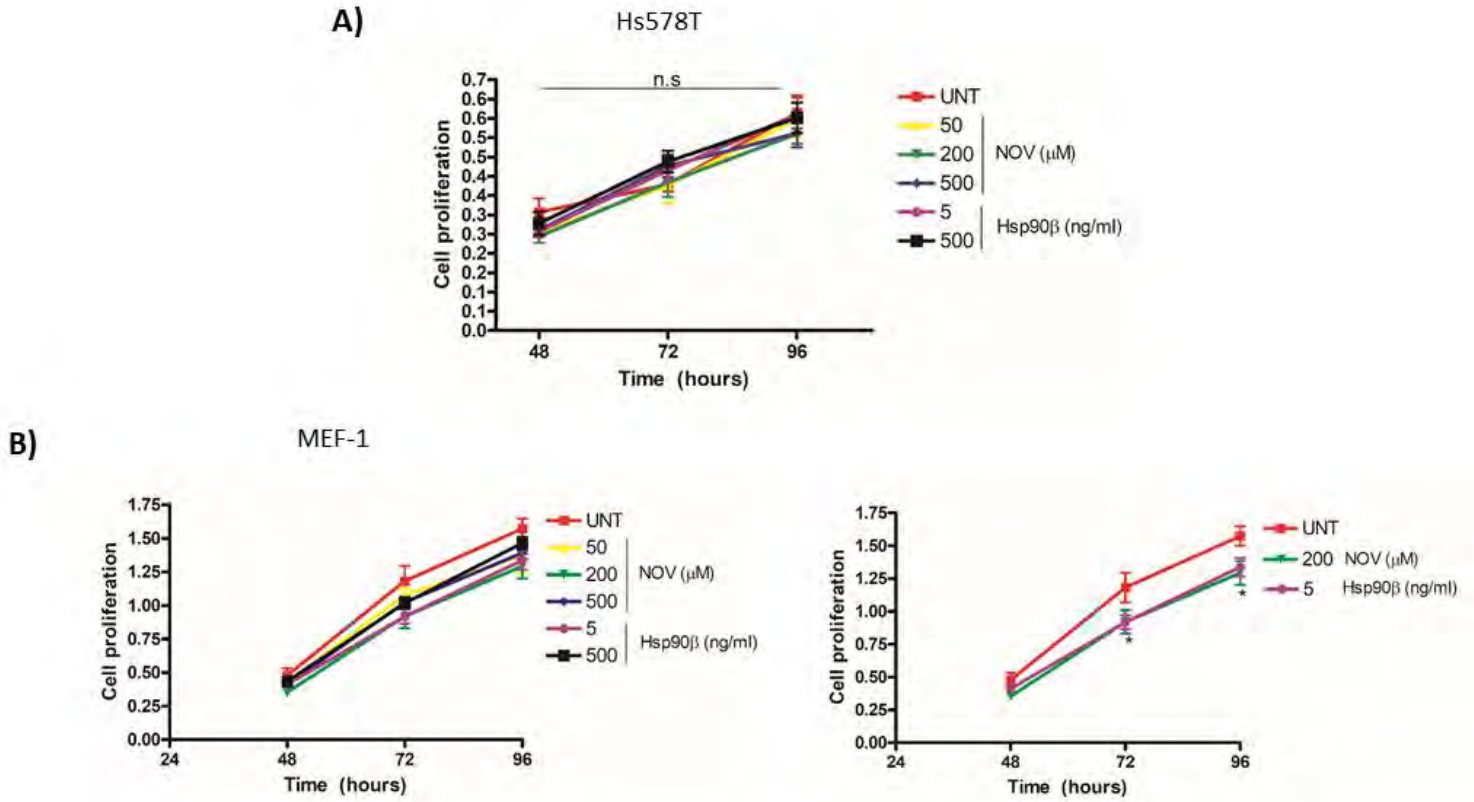

Figure 19: MEF-1 cells are significantly less proliferative on treated CDMs versus untreated CDMs

MTT assays were performed to compare **A)** Hs578T and **B)** MEF-1 cell proliferation (as measured by absorbance at 450 nm) on untreated (UNT) and treated CDMs (NOV and Hsp90β). Equal numbers of cells were seeded (in triplicate per time point) into wells of a 24-well plate containing CDMs and processed for MTT assay at 48, 72 and 96 hours. One-way ANOVA and Bonferroni's Multiple comparison post-tests were performed to determine statistical significance (*p<0.5). Significance of MEF-1 cell proliferation is shown in the graph to the right in **B.**

To assess the migratory capacity of cells on untreated and treated CDMs, we employed a technique that would maintain the composition and integrity of the CDMs. Here, we used a spheroid cell migration assay. For this, we generated spheroids of MEF-1 and Hs578T cells and after allowing drops to adhere to the CDM (~4 hours), images were taken of the adhered spheroids (t= 0 hours) and again after migration (t= 20 hours) (Figure 20). To determine the extent of migration outward from the spheroid, we used the Analyse spheroid cell migration plugin in ImageJ (Baecker, 2017). Representative images of MEF-1 cell migration on plastic (no CDM) and CDMs are shown in Figure 20A. The last panel shows the output image generated from the plugin, which measures the area in red of cells migrated outward from the spheroid. Quantification of the migratory capacity was determined by subtracting the area in red measured at (t= 20 hours) from the area in red at (t= 0 hours). Visual analysis of the images shows that MEF-1 cells are more migratory when no CDM is present (as is evidenced by the larger area in red) compared to the untreated and 200 μM NOV treated CDMs (smaller area in red) (Figure 20A). This was consistent for Hs578T cells. We showed that migration of MEF-1 cells was significantly reduced on 50 μM NOV treated CDMs but increased on 500 μM NOV treated CDMs compared to untreated CDMs (Figure 20B). Comparatively, migration of Hs578T cells was unaffected by treated CDMs (Figure 20C). These data collectively demonstrate that MEF-1 cells generate a more noticeable and significant physiological response compared to the Hs578T cells suggesting an ability of normal cells to be more greatly affected in terms of their growth and migration on a cancer cell line derived matrix. Lastly, these data also show that inhibition of Hsp90 produces matrices which affect the ability of cells to adhere (Figure 18), grow (Figure 19) and migrate (Figure 20).

To investigate different modes of migration and possible changes in cell morphologies upon NOV treatment, we performed a migration assay using 4-well chamber inserts into which cells were seeded to create a confluent monolayer. Cells were left untreated or treated with NOV for 16 hours before removal of the chamber inserts (t=0) and replacement of media lacking any inhibitors. Cells were allowed to migrate outward and imaged after 12 hours (t=12) to determine their migratory capacity away from the monolayer following pre-treatment of the Hsp90 inhibitor (Figure 21A). We observed NOV-treated cells to migrate collectively as a group of cells from the original cell mass whilst untreated cells, which appeared to migrate as individual cells, broke away from the cell monolayer (Figure 21A). Magnified images of NOV-

treated cells at the border of the cell mass show the presence of interconnected cells via long projections which maintain their connection to the cell mass of the insert chamber. Comparatively, untreated cells appear more detached from the surrounding cells and cell mass (Figure 21B). Quantification of this migration was determined by measuring the distance from the right hand side border of the cell monolayer to the furthest migrated cells. Significant loss in migration was observed in cells that had been pre-treated with NOV. These data support the wound healing data at this concentration and also demonstrate that cells are still viable after NOV treatment and capable of migration, albeit at a reduced rate.

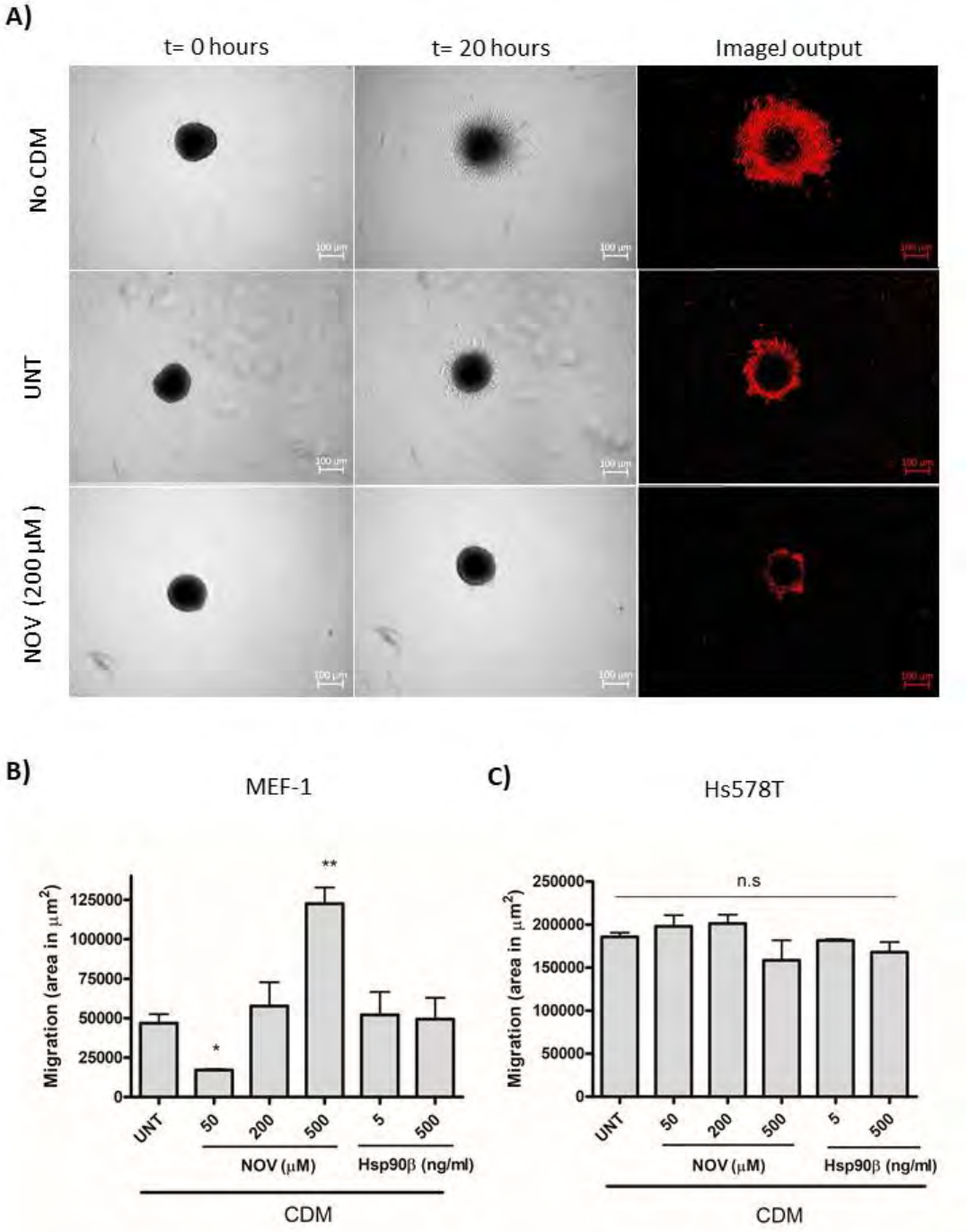

Figure 20: Migration of MEF-1 and Hs578T cells is reduced on CDMs

A) Representative images were taken of MEF-1 spheroids adhered to untreated (UNT), 200 µM NOV treated CDMs, or no CDM, (t= 0 hours) and after migration (t= 20 hours) using a Zeiss Primovert inverted light microscope with the 4x objective lens. Scale bars are 100 µm. Panel on the far right is a graphical representation of the output image generated from the ImageJ plugin which quantifies the area migrated (in red) by the cells from the spheroid. Quantification of **B)** MEF-1 and **C)** Hs578T cell migration was determined using ImageJ by subtracting the area of cells migrated at t=20 hours from the area migrated at t=0 hours. Graphs shown represent the average migration distance from technical replicates in triplicate independent samples. Statistical significance was determined in GraphPad Prism 4 using an unpaired Student's t-test. Statistics are indicated on the graphs as such: *p<0.5, **p<0.01, n.s not significant for comparison to untreated (UNT) CDMs. Data are representative or averages (±SD) of triplicate independent studies.

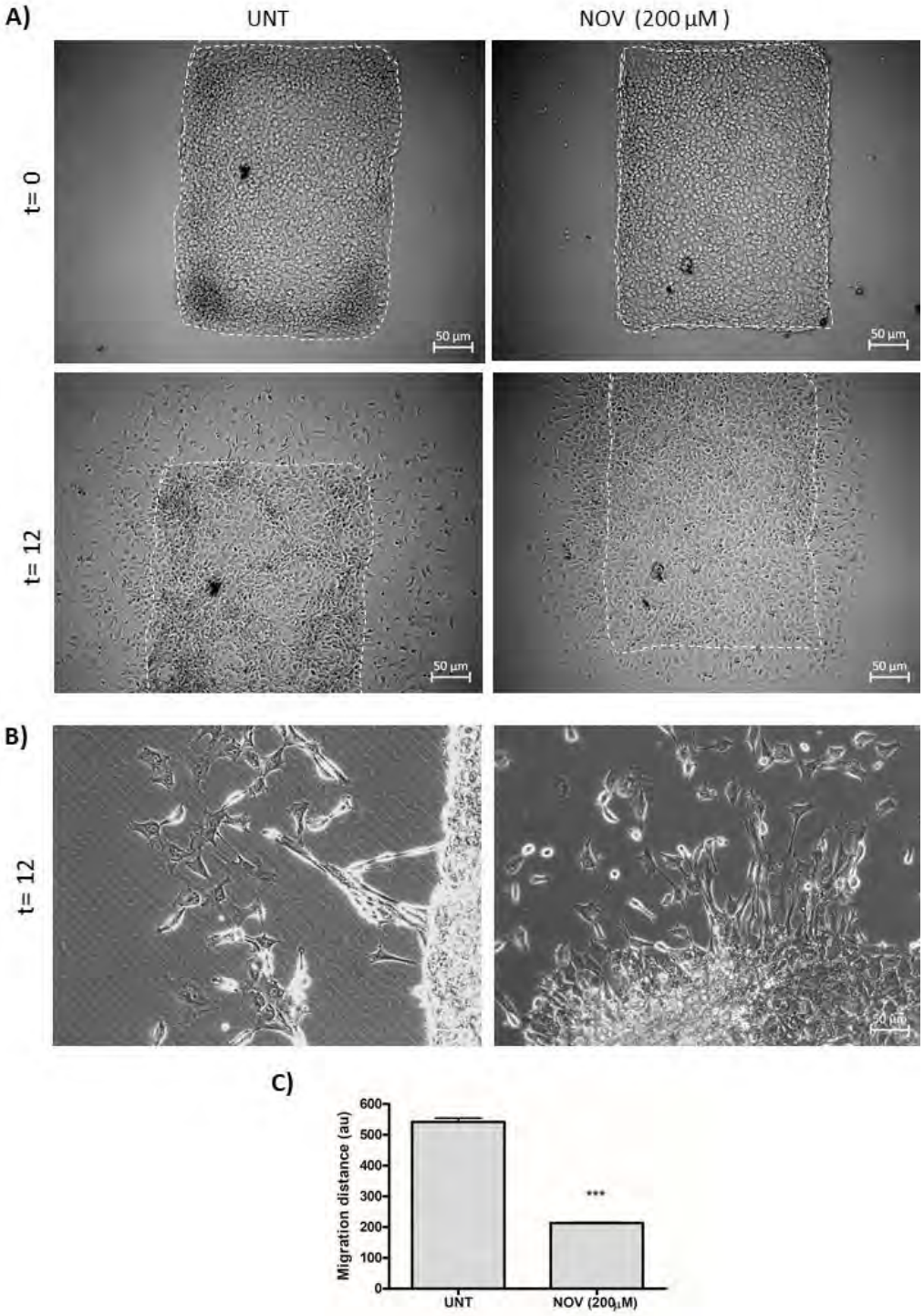

Figure 21: Pre-treatment with NOV hinders the ability of Hs578T cells to migrate

A) Hs578T cells were seeded into a 4-well chamber and allowed to create a confluent monolayer. Cells were left untreated (UNT) or treated with novobiocin (NOV 200 µM) for 16 hours. Images were taken of the confluent cell monolayer upon removal of the chambers (t=0) and again after 12 hours migration using a Zeiss Primovert inverted light microscope with camera using the 5x objective. White dotted lines demarcate the edges of the insert chamber which contained the confluent cell mass taken at t=0 in each image. **B)** Magnified images of cells after migrating for 12 hours using the 20x objective. Images are representative of a triplicate study. **C)** Average distances migrated outward from the cell border at t=12 were measured using ImageJ. Statistical analysis was performed using unpaired two-tailed t-tests in GraphPad Prism 4. Statistics are indicated on the graph as such: ***= p< 0.001.

One of the limitations of a wound healing assay is that creating wounds destroys the underlying matrix therefore, in this analysis we focus on the ability of cells to migrate into wounds independent of an underlying CDM. Therefore, this analysis identified changes at a cellular level compared to matrix-induced changes in migration. We performed wound healing assays in MEF-1, Hs578T and PEA-13 cells treated with Hsp90 inhibitors (GA and NOV) (Figure 22) and exogenous Hsp90β (Figure 23). Treatment with NOV at low concentrations (i.e. 50 μM) caused a significant increase in migration in both MEF-1 and Hs578T cells (Figure 22A and B) followed by a dose-dependent decrease. This observation mimicked trends observed for total FN levels (Figure 6) and the presence of DOC-insoluble FN matrix levels in response to NOV (Boel et al., 2018). No increase in migration was observed in the PEA-13 cells, although they did show a dose-dependent decrease in cell migration with increasing NOV concentration. This suggested that the reduced migration phenotype in response to NOV was not linked to LRP1 expression. Treatment with the N-terminal Hsp90 inhibitor, GA, caused only a dose-dependent loss in migration in both MEF-1 and PEA-13 cells (Figure 22C). In cases where cells are treated with Hsp90β we use a human recombinant endotoxin-free source of Hsp90β. Although we treated mouse cell lines with human Hsp90β, we confirmed using a protein BLAST that mouse Hsp90 has 99% sequence identity to the human isoform. We tested what effect exogenous Hsp90β (which has previously been shown to stabilize and enhance the extracellular FN matrix (Boel et al., 2018) would have on migration of cells. Addition of Hsp90β to MEF-1 cells appeared to cause an increase in migration (Figure 23A) whilst Hsp90β had no significant effect on migration of PEA-13 cells (Figure 23A).

In order to assess whether enhanced migration could be linked to increased concentrations of FN we seeded cells onto pre-coated plates with increasing concentrations of purified FN (0 – 1000 μg/ml) and monitored the migration response of these cells following wound denudation. Interestingly we observed an increase in migration in both MEF-1 and PEA-13 cells with increasing FN concentration although the increase observed in the MEF-1 cells was much greater (Figure 23B). These data would suggest that FN concentration directly translates into an increased ability of cells to migrate (irrespective of LRP1 expression) and by extension would suggest that loss in FN matrix (as seen with NOV treatment) should reduce migration.

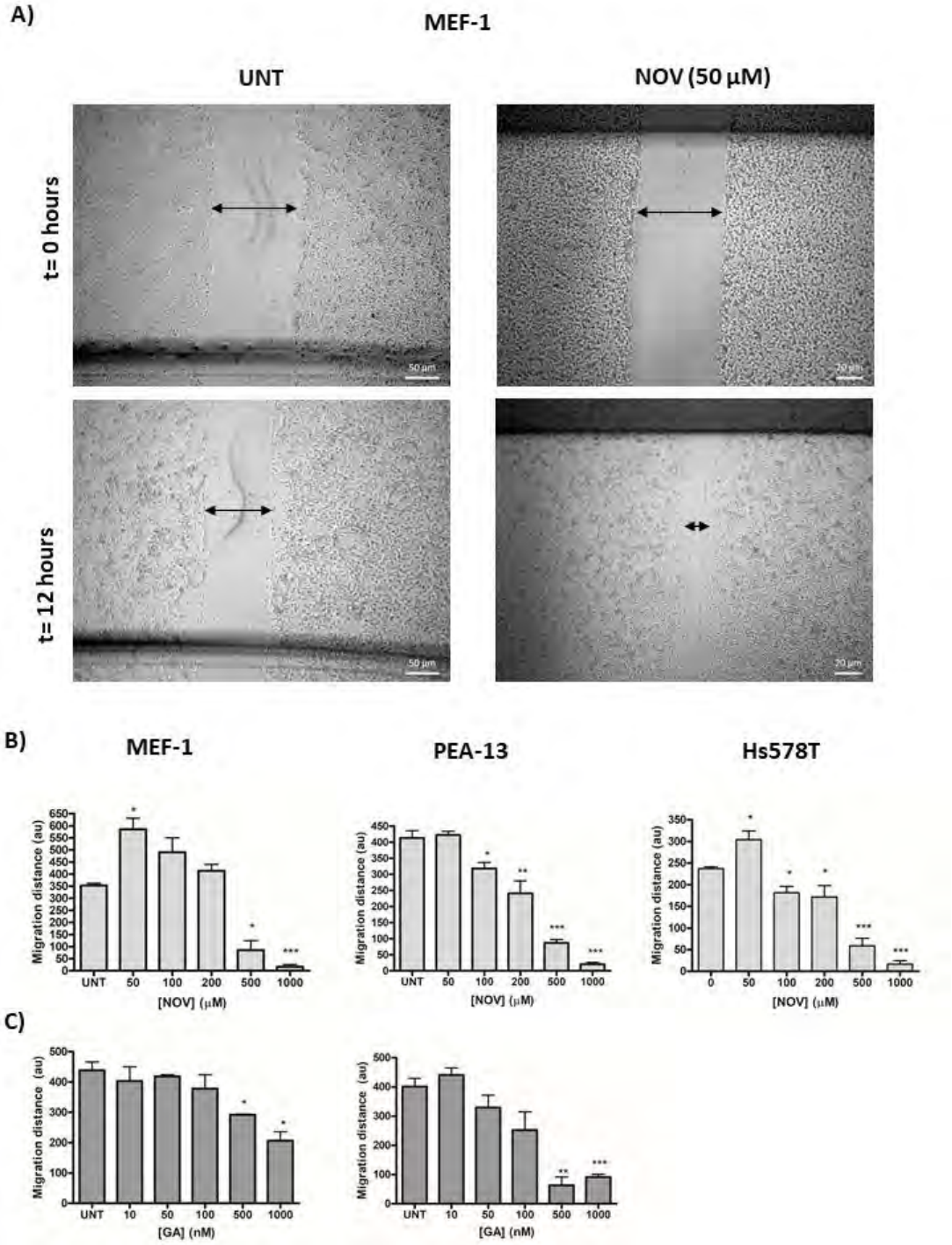

Figure 22: Effect of NOV and GA treatment on cell migration

A) Representative image of linear wounds created in MEF-1 cells during the wound healing assay with NOV treatment. Black arrows indicate wound closure. Wounds were made in confluent MEF-1, PEA-13 and Hs578T cell monolayers followed by treatment in media with **B)** NOV or **C)** GA at varying concentrations. The width of the wound was measured at each time point using ImageJ with the difference in the width at 0 and 12 hrs presented as the migration distance. Statistical analysis was performed using unpaired two-tailed t-tests in GraphPad Prism 4 and are indicated on the graph as such: *= $p<0.05$, **= $p<0.01$, ***= $p< 0.001$. Images are representative of averages (±SD) of triplicate independent experiments.

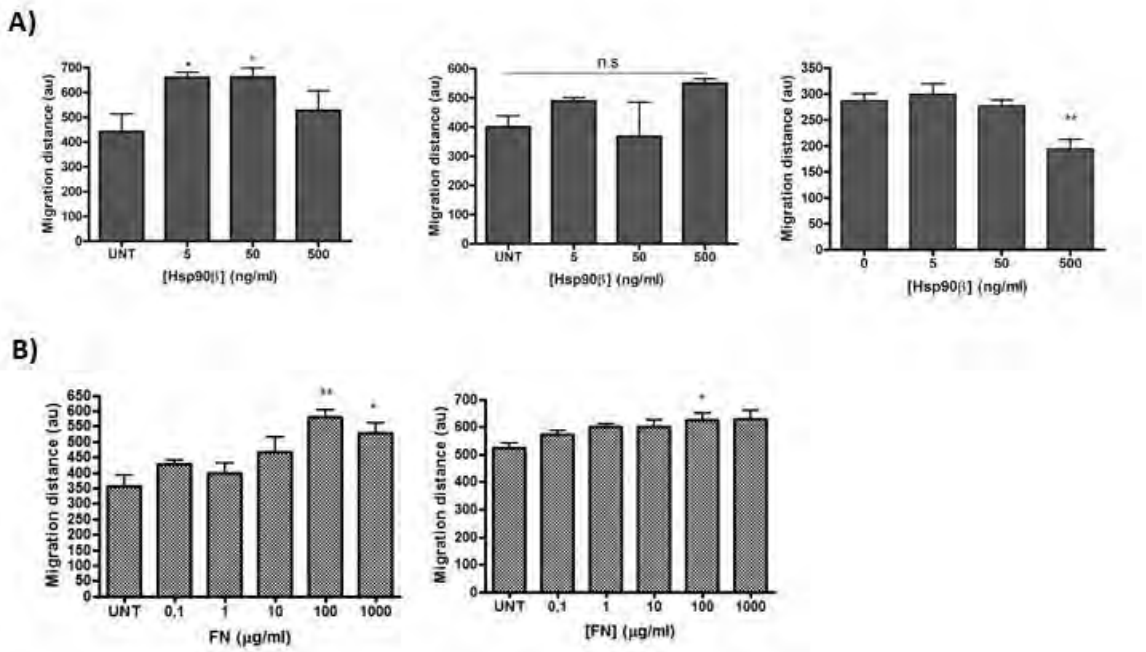

Figure 23: Effect of exogenous Hsp90β and fibronectin concentration on cell migration

A) Linear wounds were created in confluent MEF-1, PEA-13 and Hs578T cell monolayers followed by treatment in media with exogenous Hsp90β at varying concentrations. Images were captured at time 0 hrs and 12 hrs post treatment and analysed in ImageJ. Average distances migrated were measured using ImageJ. Statistical analysis was performed using unpaired two-tailed t-tests in GraphPad Prism 4**. B)** MEF-1 (left) and PEA-13 (right) cells were seeded on to plates precoated with increasing concentrations of FN (0.1 – 1000 μg/ml) and distances migrated quantitated. Data are representative of triplicate independent experiments. Statistical analysis was performed using unpaired two-tailed t-tests in GraphPad Prism 4. Statistics are indicated on the graph as such: *= $p<0.05$, **= $p<0.01$, ***= $p< 0.001$; n.s not significant. Images are representative or averages (±SD) of triplicate independent experiments.

4.1.2 Investigating whether cell migration responses are determined by matrix-associated FN

We compared levels of extracellular and intracellular FN using a DOC assay (Brenner et al., 2000) to isolate the soluble and insoluble fractions of FN which putatively represents the intracellular and extracellular (matrix associated) pools of FN, respectively. We previously showed that NOV induced an increase in insoluble FN at low NOV concentrations (i.e. 50 µM) followed by a dose dependent loss, specific to LRP1-expressing cells (Boel et al., 2018). Here we showed that treatment with Hsp90β has different effects on extracellular FN in each of the cell lines tested (Figure 24). We first validated the study by demonstrating that our assay was fractionating insoluble and soluble fractions by showing an enrichment of the cytosolic marker, GAPDH in the soluble fractions but not the insoluble fractions (Figure 24A). The insoluble (matrix-associated) FN levels increased in Hs578T cells whilst soluble FN levels appeared to decrease. This was different for the LRP1 expressing MEF-1 cells where we observed reduced insoluble FN levels upon Hsp90β treatment with a concomitant increase in soluble FN levels (Figure 24B). This suggests that there is a relationship between insoluble and soluble FN levels, whereby decreased soluble FN levels translate into increased insoluble levels and vice versa. Interestingly, soluble FN levels were increased in PEA-13 cells upon Hsp90β treatment whilst insoluble FN appeared to be unchanged or slightly increased. Whether these differences could be due to a normal versus cancer response is not known but the data do suggest that Hsp90 may play a role in regulating the matrix formation.

Taken together with the migration data the fact that we observed increased migration of MEF-1 cells in exogenous Hsp90β treatments despite the loss in insoluble/matrix FN (Figure 24B) suggests that FN concentration is not solely responsible for migration capacity and that other factors related to the matrix structure and/or composition must play a role.

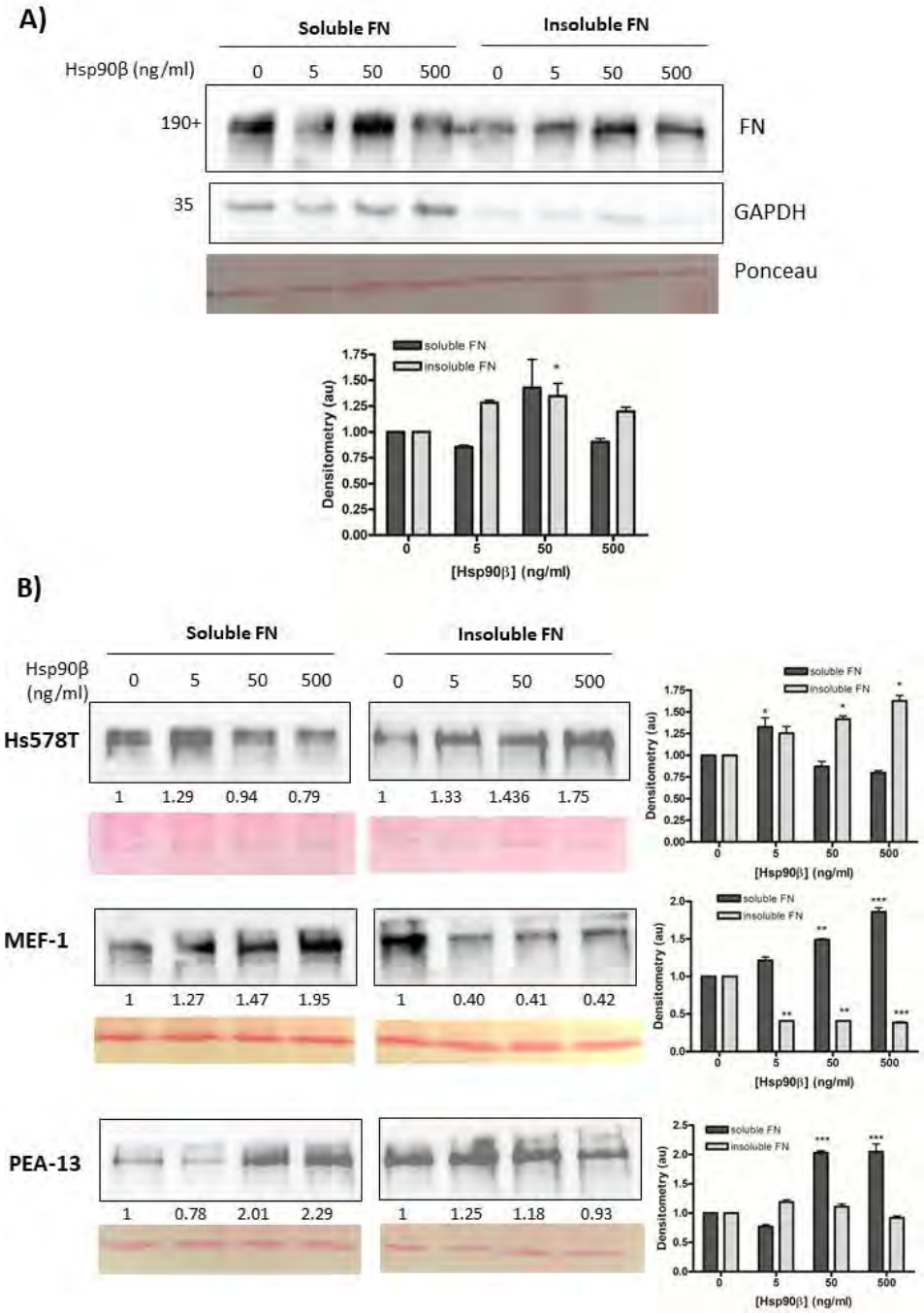

Figure 24: Levels of matrix-associated insoluble FN are differentially affected by Hsp90β

To test the effect of Hsp90β on soluble and insoluble levels of fibronectin, **A)** Hs578T cells were treated with increasing doses of purified endotoxin free human Hsp90β for 16 hours at 37˚C. Equivalent numbers of cells were harvested and the soluble and insoluble FN fractions separated using the DOC assay. Levels of FN and GAPDH were detected by immunoblotting with rabbit anti-human FN and mouse anti-GAPDH antibodies respectively. Ponceau indicates equal total protein loading in each treatment and GAPDH indicates enriched intracellular fractions isolated during DOC assay in soluble FN isolates versus insoluble FN. **B)** Hs578T, MEF-1 (wild type) and PEA-13 (LRP1-deficient) cells were treated as in A). Ponceau stains and densitometry values of the band intensities as determined in ImageJ are indicated below each lane. Densitometry values of the band intensities normalized to Ponceau stains as determined in ImageJ are indicated in bar graphs presented alongside. Statistical significance was determined compared to the untreated control by a two-tailed t-test in GraphPad Prism 4 (*$p < 0.05$, **$p < 0.01$, ***$p < 0.001$). Determining the maturation state of differentially treated CDMs

An increasing type I collagen (COL1) to FN ratio is indicative of a mature 3D matrix state in vitro (Amatangelo et al., 2005). The maturation state of matrices was determined by calculating the ratio of COL1 to FN in each of the CDMs. Here we harvested and solubilised CDMs and performed a western blot analysis to quantify levels of various proteins in each of the CDMs. Western analysis demonstrated that cells which remained undecellularized and thereby served as a control (C) were positive for the presence of intracellular proteins including Hsp90, LRP1 and GAPDH (Figure 25A). Decellularized matrices lacked the presence of these intracellular proteins confirming successful removal of cellular components from matrices. We compared total levels of FN and COL1 in each of the matrices after normalising the levels to the Ponceau stain (Figure 25A). Here we observed a significant increase in FN levels in 50 µM NOV and 5 ng/ml Hsp90β treated matrices. Relative to untreated matrices, COL1 levels were decreased at 500 µM NOV treated matrices and both Hsp90β treated matrices (Figure 25B).

To quantify levels of FN and COL1 in these CDMs we performed a solid phase binding assay whereby solubilised CDMs were coated onto the wells of a high-binding 96 well ELISA plate and incubated with anti-FN and anti-COL1 antibodies. We observed FN levels to have a similar trend to that observed in western analysis. That is, FN levels increased in 50 µM NOV and both 5 and 500 ng/ml Hsp90β treated matrices (Figure 25C). Levels of FN were reduced in 500 µM NOV matrices similar to observations in the western blot. Comparatively COL1 levels showed no statistically significant differences (Figure 25C) even though we observed changes at the protein level in the western analysis. We also tested for levels of Hsp90 and LRP1 in each of the CDMs and observed no significantly detectable levels of either of these proteins (data not shown) which further confirms successful removal of cellular components during generation of CDMs.

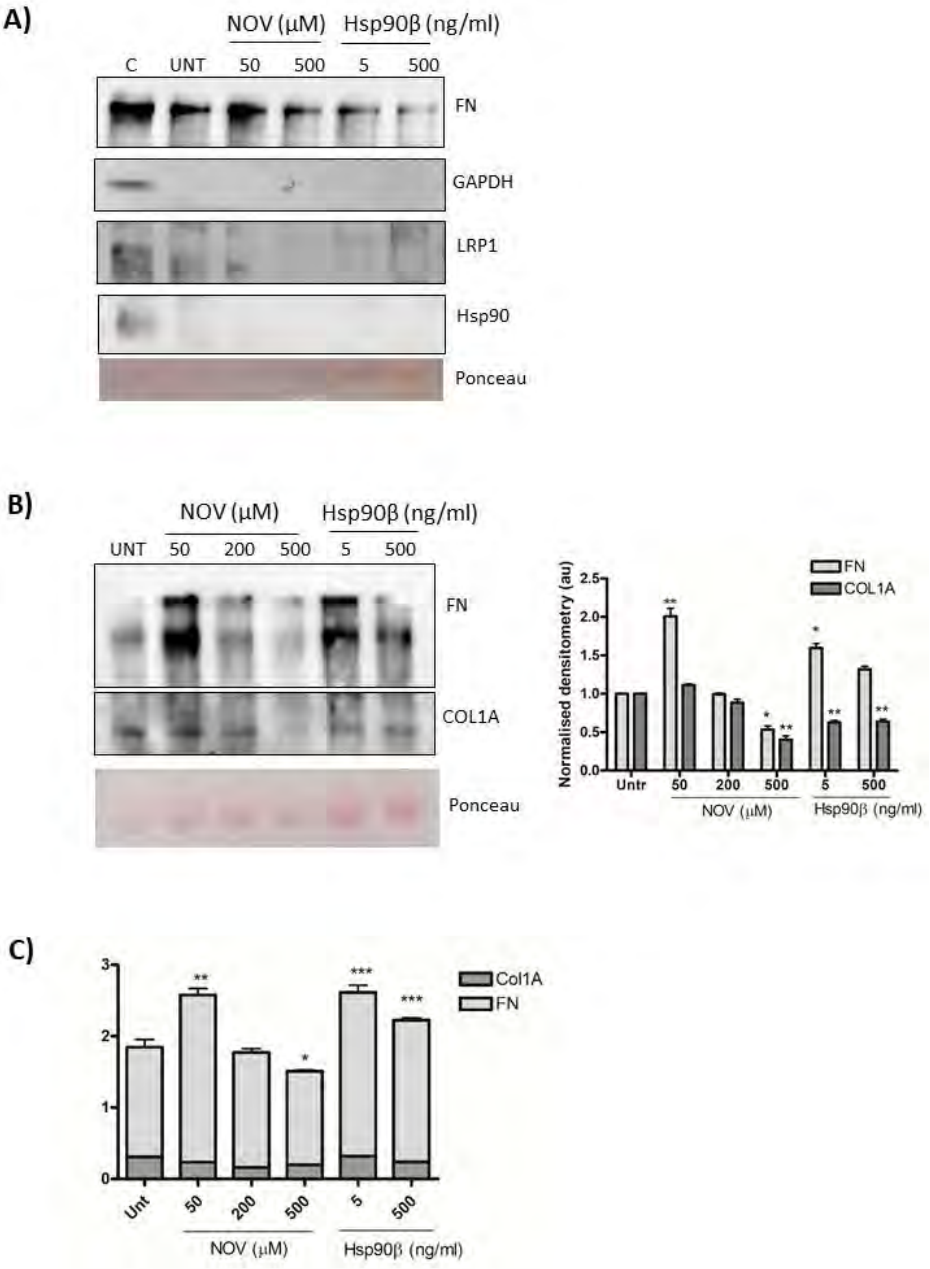

Figure 25: Quantification of levels of FN and COL1A in CDMs

Hs578T cells were cultured for 6 days and treated with either NOV or Hsp90β or left untreated (UNT) for 24 hours prior to decellularization. **A)** CDMs were solubilized and equal total protein was resolved on a 10% SDS gel and probed for FN, LRP1, Hsp90 and GAPDH using rabbit anti-FN, rabbit anti-LRP1, mouse anti-Hsp90 and rabbit anti-GAPDH primary antibodies respectively. A control sample (C) which was undecellularized was included as a positive control to confirm the lack of intracellular markers in decellularized samples. Ponceau was used to demonstrate equal total protein loading. **B)** Equal total protein of CDMs was resolved on an 8% SDS gel and probed for FN and COL1A using mouse anti-FN and rabbit anti-COL1A primary antibodies respectively. Alongside is the densitometry normalized to the Ponceau stain. Statistical analysis was determined in GraphPad Prism 4 using a One-Way ANOVA with Bonferroni's post-tests (*p<0.5, **p<0.01). **C)** Solid phase binding of CDMs adhered to high binding 96 well ELISA plates were used to quantify levels of FN and COL1. Statistical analysis was determined using a Two-way ANOVA with Bonferroni's Multiple Comparison post-tests (*p<0.5, **p<0.01, ***p<0.001). Images are representative or averages (±SD) of triplicate independent experiments.

CDMs were prepared on glass coverslips, stained for FN and COL1 and analyzed by confocal microscopy (Figure 26). Coverslips were mounted using a non-hardening aqueous mounting medium to maintain the integrity and 3-dimensionality of the matrices. Colocalisation was measured in ImageJ using the Intensity Correlation Analysis (ICA) plugin (Li et al., 2004). The degree of colocalisation between the red and green channels representing COL1 and FN respectively is represented as a Pearson's correlation coefficient (Rr) in merged images (Figure 26) where -1 values represents total exclusion, 0 represents random overlap and +1 represents a perfect positive correlation (Morgan, Humphries, & Bass, 2007). We showed here that there was reduced colocalisation between FN and COL1 in 50 μM NOV (Rr = 0.52) and 500 μM NOV treated matrices (Rr = 0.46) compared to untreated matrices (Rr = 0.66) Interestingly, the highest colocalisation was observed in the 5 and 500 ng/ml Hsp90β treated CDMs with Rr values of 0. 81 and 0.71 respectively (Figure 26).

Quantification of the staining intensities for each of the channels was determined using ImageJ. No change in FN intensities was observed in the CDMs whereas COL1 intensities appeared to be significantly decreased in NOV treated CDMs (Figure 27). We demonstrated that all the treated matrices, that is, both NOV and Hsp90β treated CDMs were significantly less mature than untreated matrices (Figure 27). Unextracted Hs578T matrices were prepared on glass coverslips and processed for immunofluorescent staining of FN and COL1 as was done for the extracted CDMs. Colocalisation of FN and COL1 in unextracted CDM cultures (Figure 28) showed a similar degree of colocalisation in each of the different treatments suggesting that the decellularization process did not alter the colocalisation.

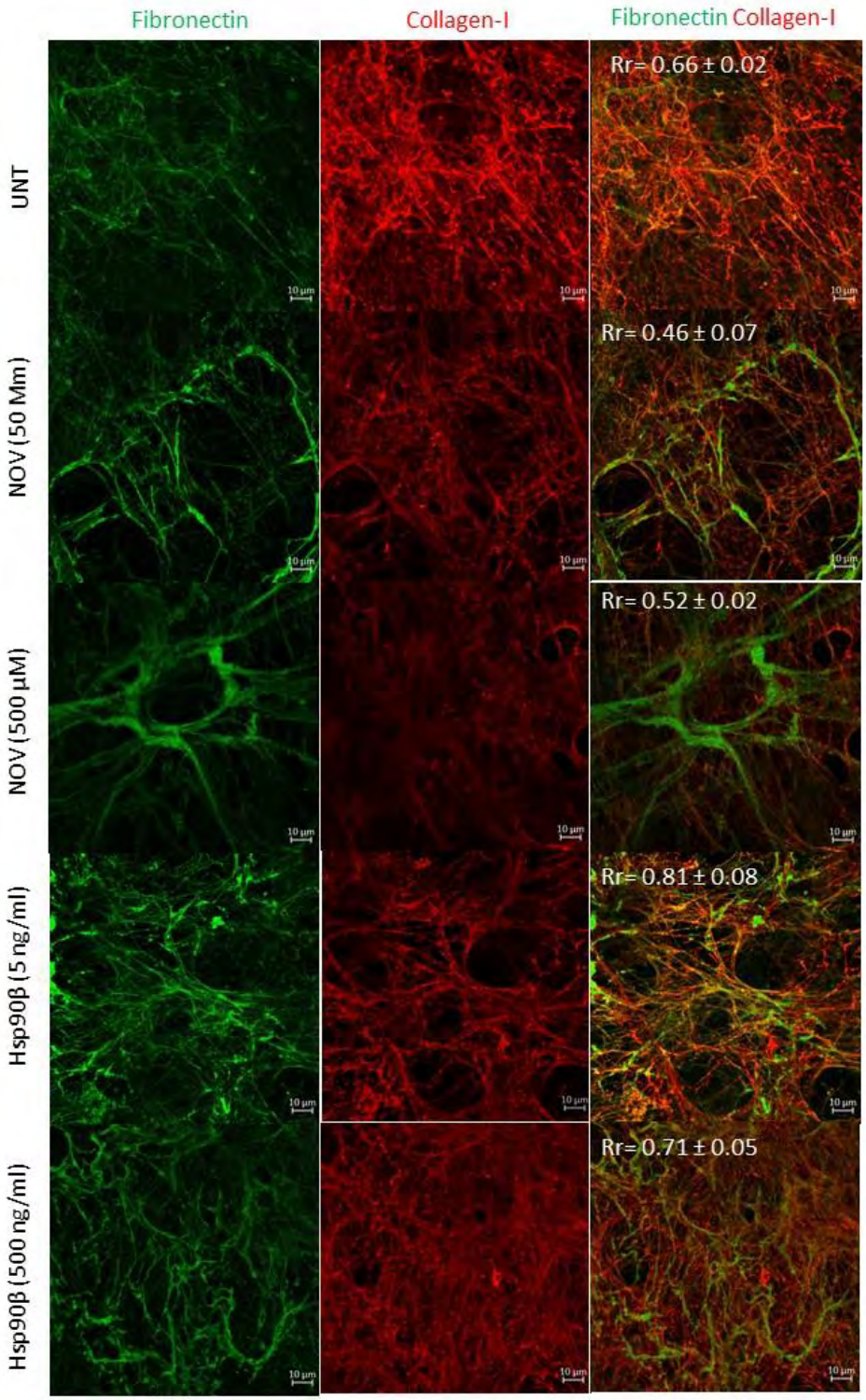

Figure 26: Colocalisation of FN and COL1A is reduced in NOV-treated CDMs

Glass coverslips of Hs578T derived CDMs were fixed with 4% paraformaldehyde and incubated with mouse anti-FN (green) and rabbit anti-COL1A (red) primary antibodies followed by donkey anti-mouse Alexa Fluor-488 and donkey anti-rabbit Alexa Fluor-555 respectively. Coverslips were mounted onto glass slides using VectorShield non-hardening mounting medium. Images were captured using the 63x objective on the Zeiss LSM 780 laser scanning confocal microscope and analysed using ZenBlue software (Zeiss, Germany). Colocalisation analysis was determined using ImageJ and Pearson's correlation coefficients (Rr) are indicated in white in the merged panels. Data are representative of triplicate independent studies. Scale bars represent 10 µm.

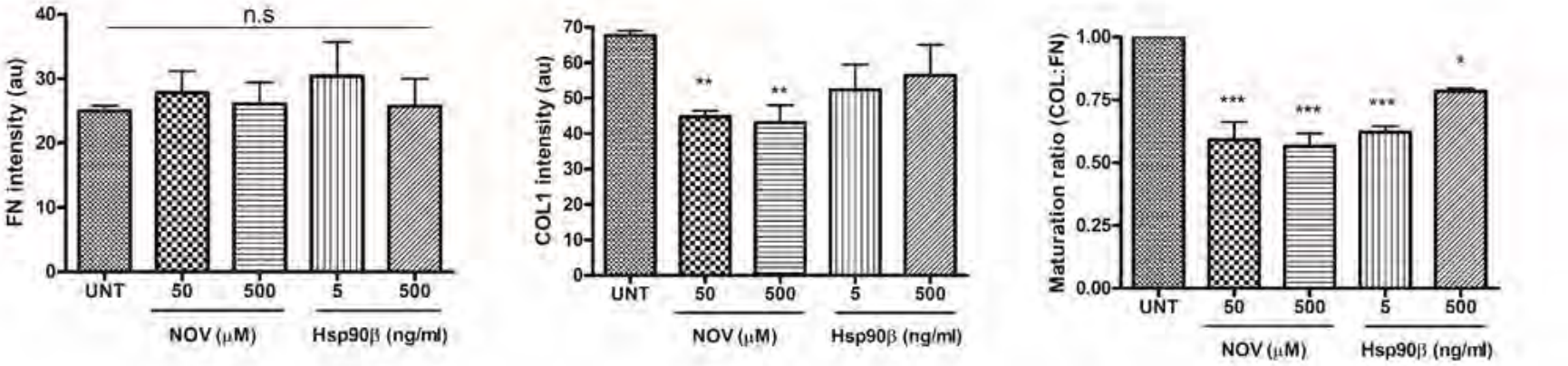

Figure 27: NOV and Hsp90β treated cell derived matrices are less mature than untreated CDMs

Graphs representing the quantification of intensity of FN fibres and COL1 fibres using ImageJ. Matrix maturation ratio of CDMs was determined in by the ratio of COL1 and FN staining. Statistical significance was determined using GraphPad Prism 4 with a one-way ANOVA and Bonferroni's Multiple Comparison post-tests (*p<0.5, **p<0.01, ***p<0.001, n.s. not significant). Graphs are averages (±SD) of triplicate independent experiments.

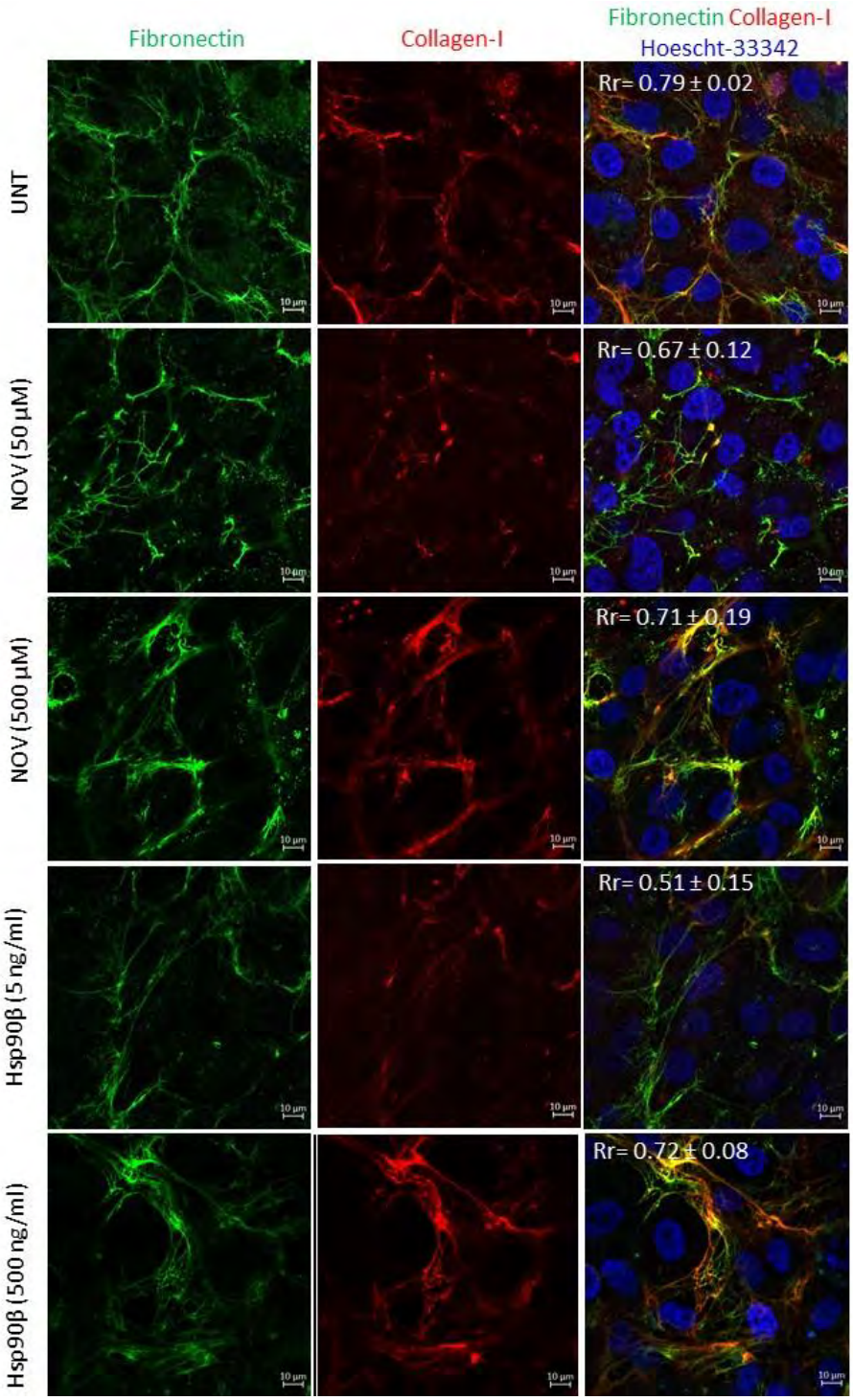

Figure 28: Colocalisation of FN and COL1 is similar in extracted and unextracted Hs578T CDMs

Glass coverslips of unextracted Hs578T 3D cultures were fixed with 4% paraformaldehyde and incubated with mouse anti-FN (green) and rabbit anti-COL1A (red) primary antibodies followed by donkey anti-mouse Alexa Fluor-488 and donkey anti-rabbit Alexa Fluor-555 respectively. Nuclei were stained with Hoechst-33342 (blue). Coverslips were mounted onto glass slides using VectorShield non-hardening mounting medium. Images were captured using the 63x objective on the Zeiss LSM 780 laser scanning confocal microscope and analysed using ZenBlue software (Zeiss, Germany). Colocalisation analysis was determined using ImageJ and Pearson's correlation coefficients (Rr) are indicated in white in the merged panels. Data are representative of triplicate studies. Scale bars represent 10 µm.

4.1.3 NOV induces structural changes in thickness and three-dimensionality of ECM and FN

We next compared the average thickness of matrices from unextracted (Figure 29) and extracted (Figure30) 3D cultures by capturing z-slices from the bottom to the top of surfaces in each sample using the z-function in ZenBlack software. Representative images of untreated (UNT) and 50 µM NOV treated CDMs are shown (Figure 29A). White lines through the image indicate the locations at which orthogonal views through the z-stack of CDMs are shown below (Figure 29B). Visual inspection of these views showed that untreated matrices are much thicker than NOV treated CDMs. Furthermore, the nuclei in NOV treated matrices appear flattened whilst nuclei in untreated CDMs are more 3-dimensional and interspersed within the matrix.

Acquired z-slices were overlaid to create a 3D maximum intensity projection image of the z-stacks (Figure 29C). Images shown contain both FN (green) and nuclei (blue) channels. 3D views of the untreated CDMs showed matrices that were thicker and more three-dimensional compared to the NOV treated matrices (Figure 29C). The FN channel alone was subjected to depth coding in the 3D projection viewer in ZenBlue to generate a colour coded heat map representing varying depths of the matrix. Again, untreated CDMs appeared denser, with a greater variation of colours in the matrix indicating increased depth and greater three-dimensionality compared to the NOV treated sample (Figure 29D).

The same analysis was performed on extracted 3D cultures (Figure 30A). Orthogonal views of slices through the z-stack of untreated CDMs demonstrate a thicker and more continuous pattern of FN staining compared to NOV treated CDMs (Figure 30B). 3D projections of the z-stacks also showed similar trends in the thickness of matrices between untreated and NOV treated samples to those in the unextracted cultures. Treated matrices also have noticeable gaps where no FN is present whereas gaps in the untreated CDMs still appear to have underlying FN (e.g. position Y=63 in UNT). Even though the z-plane shows a scale of 14 µm for both CDM samples, the untreated CDMs are visually thicker than the NOV treated matrices. We also noted that extracted 3D cultures were thinner compared to the unextracted cultures which is likely as a result of some loss of the matrix during the cell extraction process or that some of the staining in the unextracted samples represent soluble and/or intracellular FN.

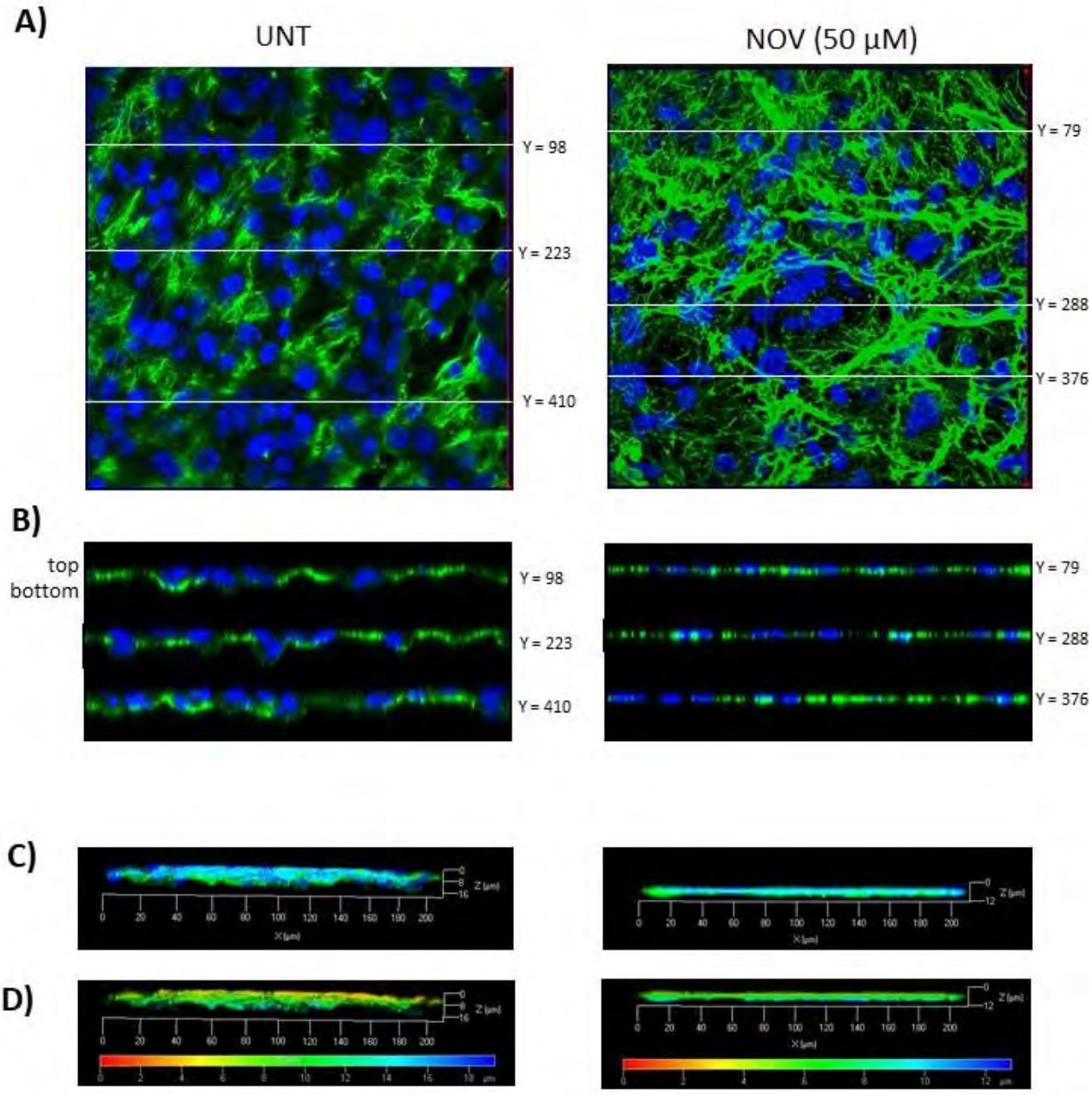

Figure 29: Untreated matrices are thicker and more three-dimensional compared to NOV treated matrices in unextracted CDM cultures

A) Unextracted Hs578T 3D cultures were fixed with 4% paraformaldehyde and incubated with mouse anti-FN (green) primary antibodies followed by donkey anti-mouse Alexa Fluor-488. Nuclei were stained with Hoechst-33342 (blue). Coverslips were mounted onto glass slides using VectorShield non-hardening mounting medium. Images were captured using the 40x objective on the Zeiss LSM 780 laser scanning confocal microscope and analysed using ZenBlue software (Zeiss, Germany). Data are representative of images obtained from triplicate studies with similar results. **B)** Orthogonal views of the 3D matrix at different slices through the Y plane (as indicated by the white lines) to generate XZ projections of the z-stack. **C)** 3-dimensional z-stack of confocal images (FN in green and nuclei in blue) of CDMs. **D)** Depth coding of 3-dimensional z-stack projections. Scale bar shown below is colour coded to indicate depths of matrices in µm.

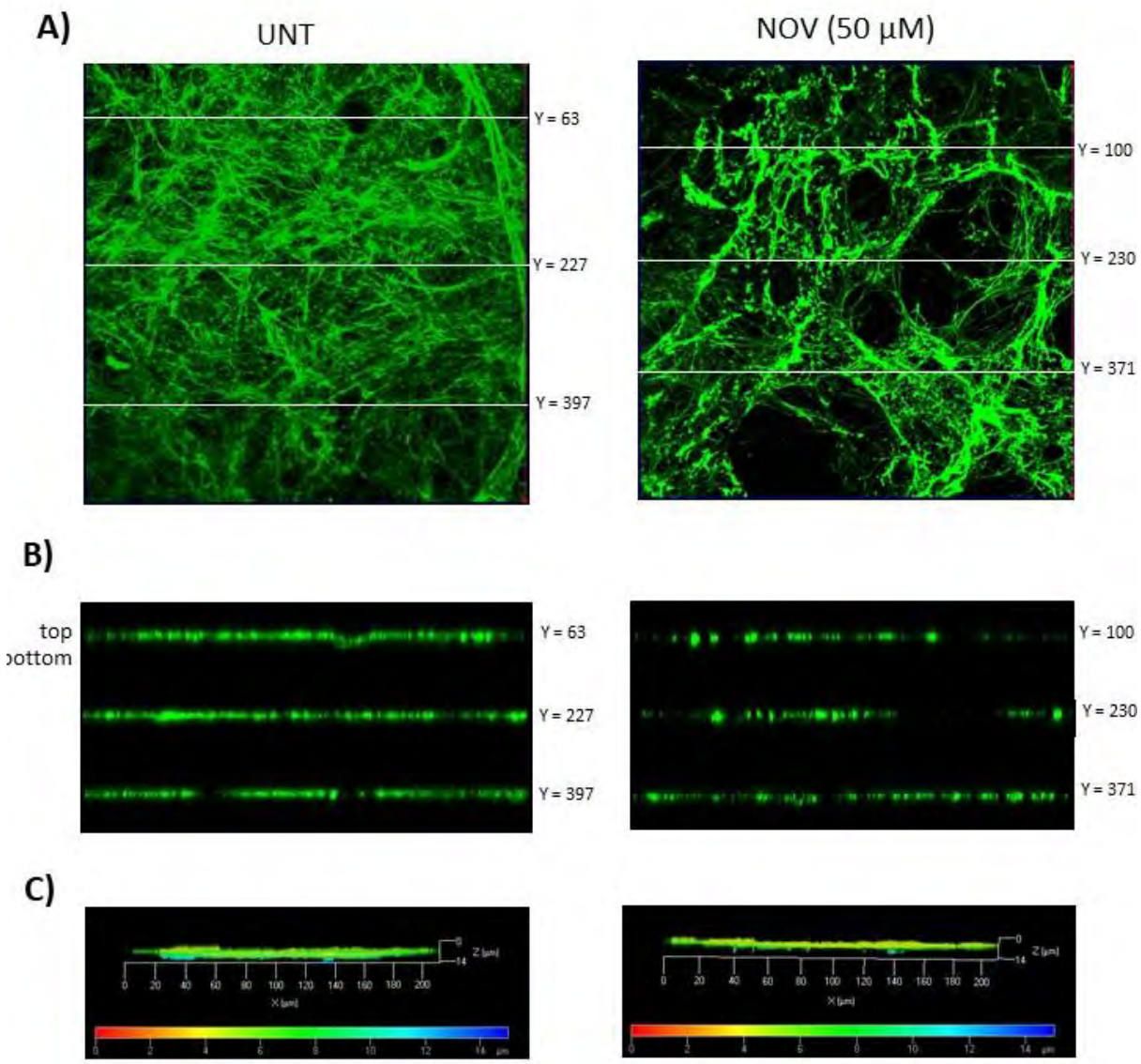

Figure 30: Untreated matrices are thicker compared to NOV treated matrices in extracted CDM cultures

A) Extracted Hs578T CDMs were fixed with 4% paraformaldehyde and incubated with mouse anti-FN (green) primary antibodies followed by donkey anti-mouse Alexa Fluor-488. Coverslips were mounted onto glass slides using VectorShield non-hardening mounting medium. Images were captured using the 40x objective on the Zeiss LSM 780 laser scanning confocal microscope and analysed using ZenBlue software (Zeiss, Germany). Data are representative of images obtained from triplicate studies with similar results. **B)** Orthogonal views of the 3D matrix through various slices of the Y plane (as indicated by the white lines) to generate XZ projections of the z-stack. **C)** Depth coding of 3-dimensional z-stack projections of CDMs. Scale bar shown below is colour coded to indicate depths of matrices in µm

We next analysed the ECM structure using electron microscopy. Representative scanning electron microscopy (SEM) images demonstrate profound differences between untreated (UNT) and treated CDMs (Figure 31). The undecellularized image shows the presence of three cells (large white grey ovals) in images taken at x2.5K magnification (Figure 31) thus indicating that image frames represent a matrix isolated from approximately two to four cells. We quantified the visual differences by subjecting SEM images to the BoneJ plugin (Figure 31, lower panel) which computes thickness of individual fibres by aligning spheres of different coloured intensities along fibres (Doube et al., 2010). Here black indicates absence of fibrils and white indicates the highest degree of thickness. Since this analysis does not discriminate between constituents of the ECM, this represents a global observation of the phenotypic changes that occur in the ECM response to treatment. We observed thicker rope-like ECM structures present in NOV treatments whilst untreated CDMs were thinner and more mesh-like. Hsp90β treatment appeared to produce more densely packed fibrils which were thicker than untreated CDMs but different to that of NOV-treated CDMs. Hs578T matrices grown on glass coverslips, which were left untreated (UNT) or treated with NOV (50 μM or 500 μM) or Hsp90β (5 ng/ml or 500 ng/ml) for 24 hours before cell extraction, were stained for FN (Figure 32). Absence of nuclei in cell-derived matrices confirmed successful decellularization when compared to the control images of undecellularized matrices (undecell) (Figure 32A). Immunofluorescence staining for FN showed that CDMs following NOV treatment were less dense with more spaces between fibres compared to untreated CDMs. Furthermore, NOV treatments appeared to change the morphology of the FN matrix to form thicker, rope-like fibres, with a branching morphogenesis phenotype (Figure 32A). Treatment with Hsp90β also had a noticeable impact on the morphology of the FN matrix, creating thicker, but shorter and more condensed fibrils. Quantification of fibre thickness and spacing was determined using the BoneJ plugin for ImageJ as done for SEM images (Figure 32A, lower panel). Quantification of fibre thickness computed by the plugin revealed NOV and Hsp90β treatments produced thicker FN fibrils with NOV being the highest compared to untreated CDMs (Figure 32B). A similar trend was observed for spacing measurements whereby NOV and Hsp90β treatments had significantly more gaps between their fibres compared to untreated CDMs (Figure 32C).

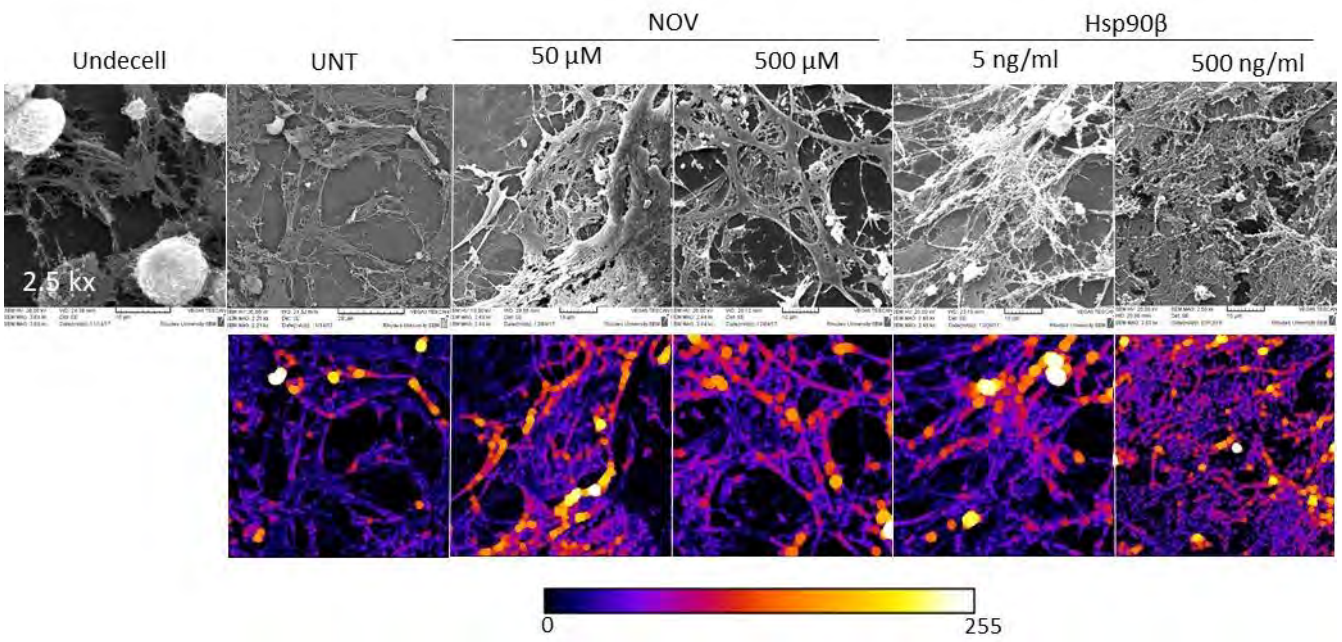

Figure 31: Scanning electron microscopy reveals thicker ECM structures in NOV and Hsp90β treated matrices

Hs578T cells were cultured on glass coverslips for 6 days and treated with varying concentrations of NOV or Hsp90β or left untreated (UNT) for 24 hours prior to decellularization. Coverslips were process for scanning electron microscopy (SEM) analysis as described in Methods. Images of undecellularized (Undecell) and decellularized matrices were taken at 2500x magnifications using the Vega Tescan SEM. Images are representative of triplicate independent experiments. Lower panel of SEM images represented through the BoneJ plugin to calculate fibre thickness where pseudocoloured spheres fit along fibres represent intensity maps of fibre thickness, with an intensity color bar scale (0-255 intensity tone values) shown below.

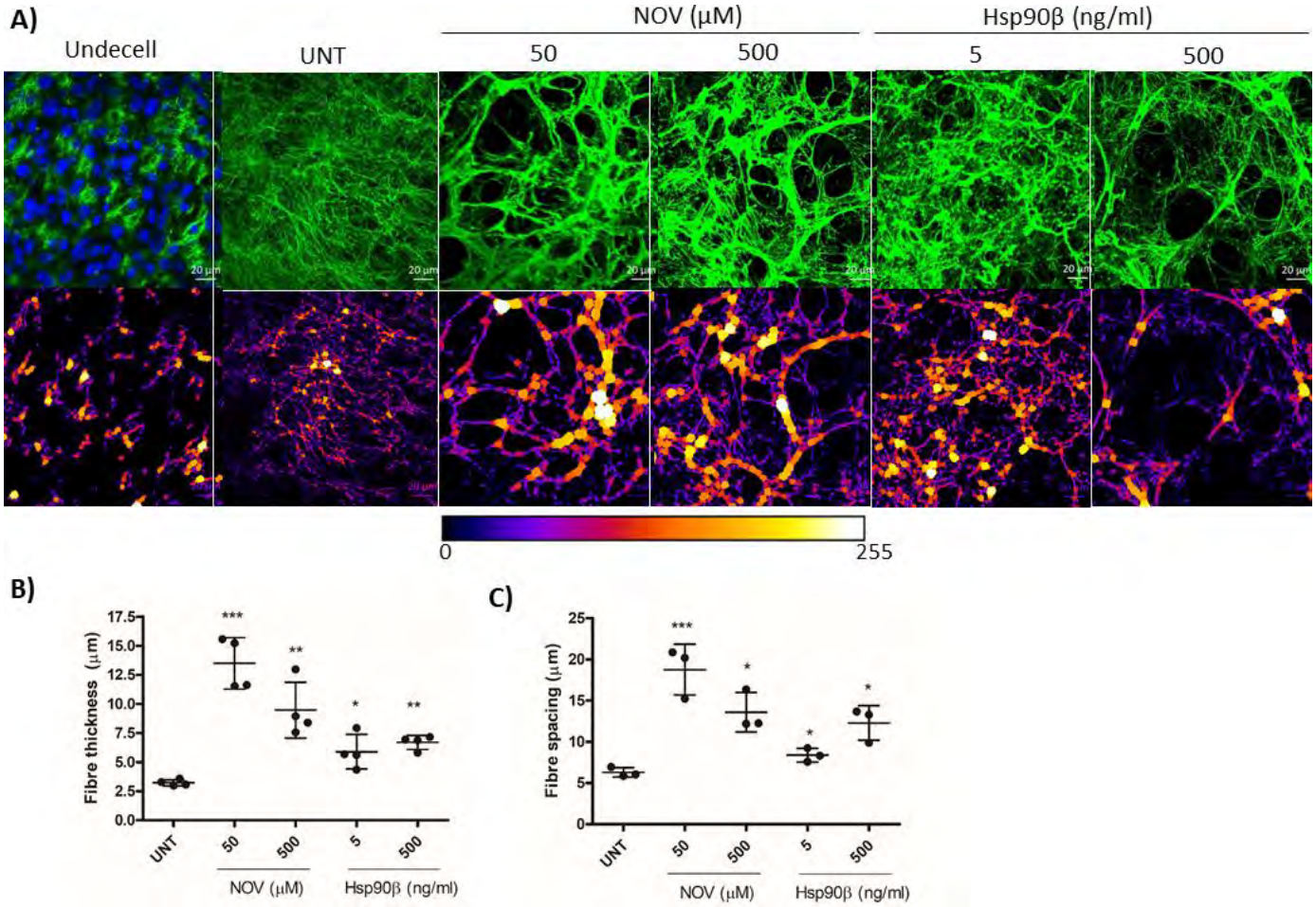

Figure 32: Confocal microscopy analysis of NOV and Hsp90β reveals altered extracellular FN matrix morphology in Hs578T cells

Hs578T cells were cultured for 6 days and treated with either NOV or Hsp90β for 24 hours prior to decellularization. **A)** Confocal microscopy of decellularized matrices stained using mouse anti-FN (green) primary antibody followed by donkey anti-mouse Alexa Fluor-488. Nuclei were stained with Hoechst-33342 (blue). Images were captured using the 40x oil objective of the Zeiss LSM 780 Meta laser scanning confocal microscope and analysed using Zen Blue software. Scale bars represent 20 µm. Images are representative of triplicate independent experiments. Lower panel of confocal images represented through the BoneJ plugin to calculate fibre thickness where pseudocoloured spheres fit along fibres represent intensity maps of fibre thickness, with an intensity color bar scale (0-255 intensity tone values) shown below. **B)** Quantification of fibre thickness represented as mean thickness and **C)** gaps between fibres represented as mean spacing taken from triplicate independent images. Statistical significance comparing to the untreated CDM was determined using GraphPad Prism 4 with an unpaired Student's t-test (*= p<0.5, **= p< 0.1, ***p= <0.001)

SEM images taken at higher magnifications (x10K) (Figure 33A) showed more detailed changes in the morphology and organisation of these CDMs. To estimate the orientation of matrices we used OrientationJ, which is an ImageJ plugin which evaluates orientation and isotropic properties (coherency and energy) of pixels in an image to generate a hue-saturation-brightness (HSB) colour coded map which shows the angles of the oriented structures in the image (Franco-Barraza et al., 2017; Rezakhaniha et al., 2012). Representative images of CDMs (Figure 33B) shows visual outputs from the OrientationJ software. OrientationJ also computes numerical outputs of the fibres to generate a Gaussian distribution curve representation of the orientation distributions (Figure 33C). The x-axis corresponds to degree angle distributions and the y-axis indicates the number of fibres distributed for each given angle/orientation. We observed similarly disordered ECM fibres in UNT, NOV and Hsp90β treated CDMs, although NOV and Hsp90β CDMs appeared oriented slightly skewed to the right of 0 ° (that is, containing more fibres oriented in the positive direction). Untreated CDMs had a mode angle of -30°, whilst NOV and Hsp90β CDM had mode angles of 4° and 8° respectively (Figure 33C).

The morphological differences observed in CDM architecture generated by both NOV and Hsp90β treatments suggested differential patterning and arrangement of ECM proteins. Representative images of FN stained CDMs from confocal microscopy shows visual outputs from the OrientationJ software (Figure 34A). Gaussian distribution curves of the orientations of FN matrices showed untreated matrices to have a mode angle of about -18° whereas NOV and Hsp90β treated matrices had mode angles of -50° and -30° respectively (Figure 34B). The untreated matrices contained more similarly oriented fibres compared to the treated matrices which is evident by the predominantly green and cyan colour coded fibres (Figure 34A) and orientation evenly distributed around 0°. Taken together, these data suggest changes in the ECM three-dimensionality, orientation distribution and fibre thickness upon treatment with NOV or Hsp90β.

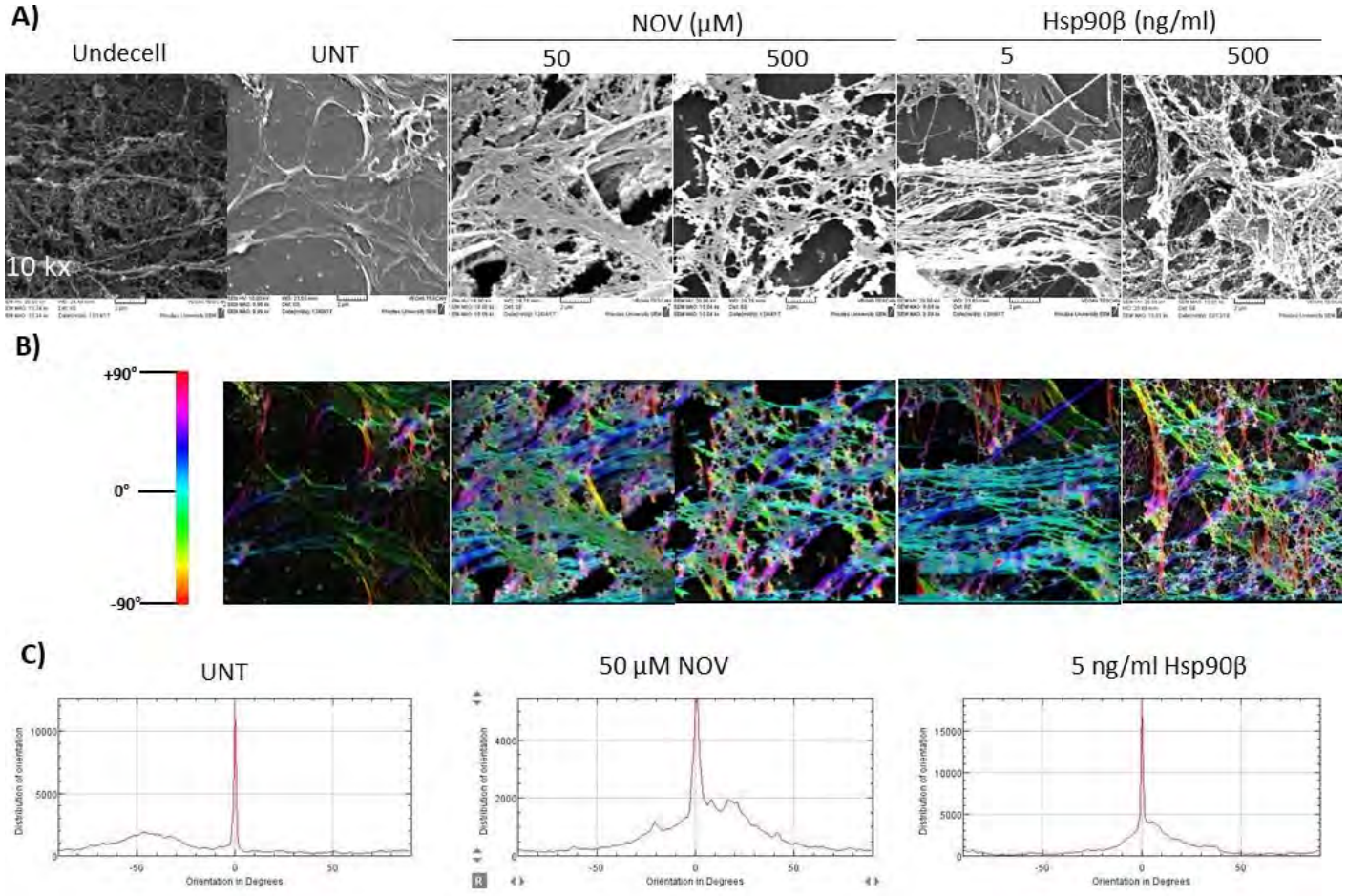

Figure 33: Scanning electron microscopy of Hs578T-derived CDMs reveals disordered orientation of ECMs

Hs578T extracted CDMs were prepared as described previously. **A)** SEM images taken at 10 000x magnification of the extracted and unextracted (undecell) Hs578T CDMs. **B)** Images of extracted CDMs were analyzed using the OrientationJ plugin in ImageJ to measure fibre angle distributions in each of the CDM images. The images were to create a binary image output that identifies individual fibres by presenting them as pseudo-colored objects (see Materials and Methods for details). Colour-coded scale bar to the left represents the angles revealed by the software. **C)** Histograms of orientations constitute numeral outputs from B where graphs display the orientation in degrees along the x-axis and distribution of fibres along the y-axis B). Data are representative of triplicate independent experiments.

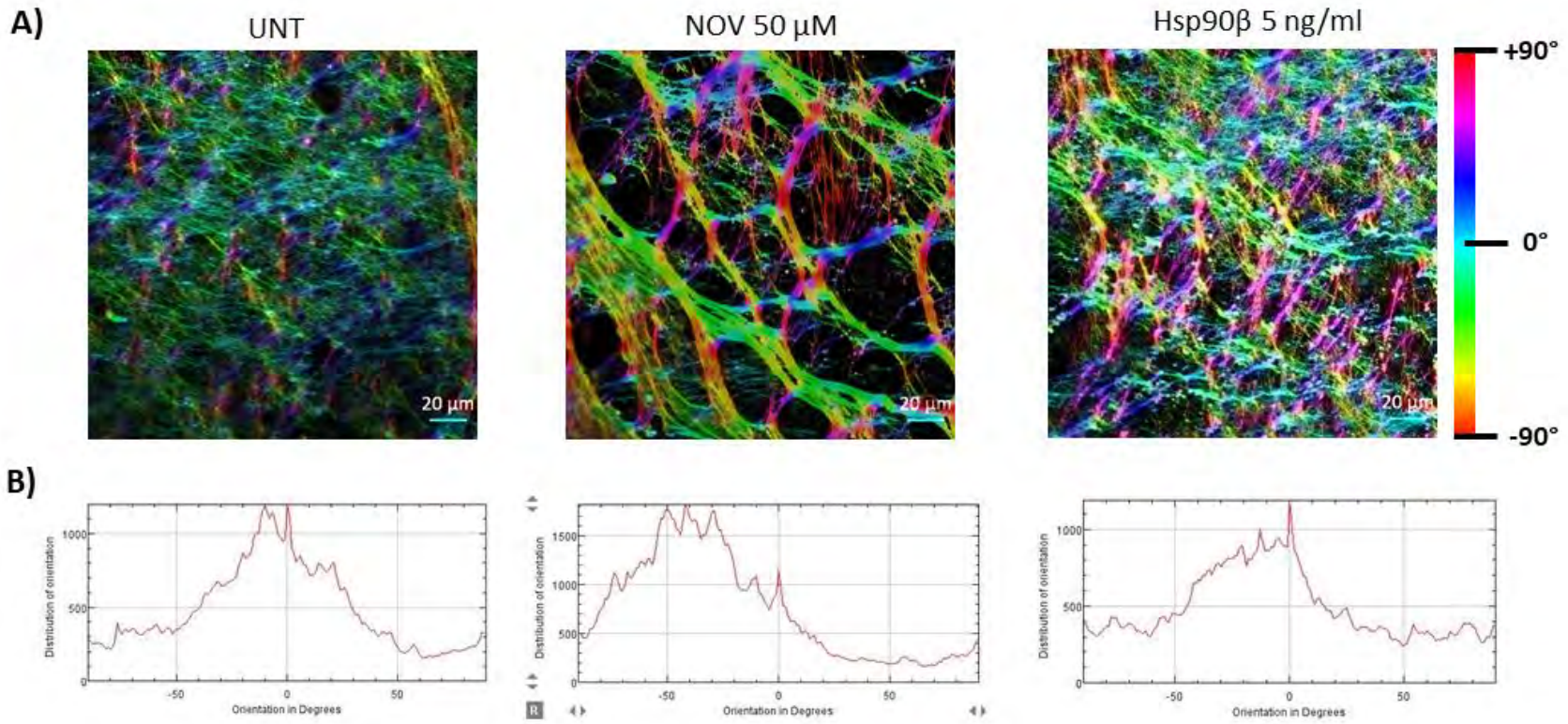

Figure 34: NOV and Hsp90β treated FN matrices contain more disordered fibrils

A) Images of extracted CDMs were analyzed using the OrientationJ plugin in ImageJ to measure fibre angle distributions in each of the CDM images. The plugin generates output images which identifies individual fibres by presenting them as pseudo-colored objects (see Materials and Methods for details). Coloured scale bars to the right represent the angles revealed by the software. **(B)** Histograms of fibre orientations constitute numeral outputs from A). Data are representative of triplicate independent experiments.

4.2 Discussion

We have evidence which demonstrates an increased ability of LRP1-expressing cells to migrate at certain concentrations of NOV (Boel MSc thesis, 2016), suggesting putative physiological consequences associated with FN remodelling due to Hsp90 inhibition. In this study we use cell derived matrices (CDMs), which cells naturally encounter in vivo (Tello et al., 2016) and consist of a heterogeneous mixture of proteins, proteoglycans and growth factors similar to the native stromal environment. This provides a more accurate in vitro model for studying cell-ECM interactions (Yamada & Cukierman, 2007). CDMs also provide a more complex, physiological alternative to purified 3D matrix protein scaffolds, such as polymerized type I collagen or fibrin gels or basement membrane extracts (BME or matrigels). CDMs are naturally produced extracellular matrices by cells cultured at a high density in vitro for a period of 4-12 days (Yamada & Cukierman, 2007). After removal of the cells that produced the matrix, an assembled 3D matrix scaffold is left behind which closely mimics a native stromal environment (Hakkinen et al., 2011). When used as a substrate for other cells, these matrices allow for the characterization of cell behaviour and function, which differs drastically from that observed on 2D substrate surfaces. Importantly, CDMs are able to mimic in vivo situations which regulates cell growth, migration and differentiation to name a few (Cukierman, 2002; Tello et al., 2016). Here we characterize CDMs harvested from human breast cancer epithelial cells (Hs578T) and observe the responses of normal fibroblasts (MEF-1) and tumourigenic cells (Hs578T) on these CDMs. NOV treatments reduced the thickness and three-dimensionality of matrices and created thicker FN fibrils which allowed for increased migration on these matrices. NOV treated matrices contained more spaces between fibrils which allowed for enhanced adhesion but reduced spreading of cells. Both NOV and Hsp90β CDMs reduced proliferation of MEF-1 cells but not Hs578T cells. Untreated CDMs were more mature, generally thicker and more three-dimensional although individual fibrils were thin and mesh-like with fewer spaces in between which translated into an increased ability of cells to spread and proliferate on these matrices. The use of human cancer-derived cells as the source of CDMs is significant because it allows for the behavioral study of various cell types (both normal and tumorigenic origin) in the setting of a typical cancer matrix. Additional experiments will be important to consider whether the above cell responses are similar in CDMs derived from other cancer cell lines.

4.2.1 Increased cell adhesion but reduced cell spreading was observed on NOV-treated CDMs

Using simple geometric calculations to judge cell circularity we observed that most of the treated CDMs (with the exception of 500 µM NOV CDM) significantly pressured MEF-1 and Hs578T cells to form a more circular shape indicating increased cell spreading, rather than the elliptical shape conferred by cells on plastic (i.e. no CDM). This is inconsistent with data from Hakkinen and colleagues where they demonstrated that human fibroblasts were more spread on 2D matrices or glass substrates compared to 3D matrices (Hakkinen et al., 2011). It is possible that these differences may arise from the automated method used to calculate cell length, width and total cell spread area by Hakkinen and colleagues compared to the manual measurements used in our study. Between the treated CDMs, we found that a greater number of cells adhered to 500 µM NOV-treated CDMs compared to untreated CDMs. This was consistent in both MEF-1 and Hs578T cells. These cells also exhibited a more spindle-like morphology on these matrices. Cells can typically adhere to CDMs after as little as 10 minutes of seeding (Cukierman, 2002), therefore, since we observed changes in cell shape after 4 hours it is likely that the cell morphologies observed in our study are representative of a more migratory phenotype. This might suggest then that cells cultured on CDMs which presented rounder, more spread morphologies were less migratory compared to the more spindle shaped cells which were more migratory (i.e. on 500 µM NOV CDMs). This would be consistent with the spindle shaped morphology and increased migration of MEF-1 cells observed on 500 µM NOV CDMs.

4.2.2 Cell migration was significantly altered on Hsp90 or NOV-treated CDMs

Changes in cell morphology can induce drastic alterations in cells' capabilities to proliferate and migrate, as has been reported previously (Pasqualato et al., 2013). Using a metabolism-based MTT assay, we observed that proliferation of normal cells, but not tumourigenic cells was attenuated on some treated CDMs (200 µM NOV and 5 ng/ml Hsp90β CDMs being most significant). It is interestingly that we should observe similar responses on both Hsp90β (5 ng/ml) and NOV (200 µM) CDMs because this would mean that both addition of Hsp90β and inhibition of Hsp90 may induce similar biological consequences. We and other authors have previously reported that levels of extracellular Hsp90 in breast, colon and brain cancer cell lines range from approximately 5 – 20 ng/ml per 10^6 cells (Gopal et al. 2011, de la Mare,

Jurgens et al. 2017). Therefore, the concentration of Hsp90 used here (5 ng/ml) at which reduced proliferation was observed represents a physiologically relevant concentration close to that which has been detected endogenously in cell lines. A study by Kaukonen and colleagues (2017) showed that cancer cell proliferation was reduced on a normal fibroblast matrix, and that this growth inhibition was maintained in these cells following detachment from the matrix and replating on plastic, suggesting that the CDM has the potential to revert malignant cell proliferation. They went on to do a whole-genome transcriptome analysis of cells harvested from CDMs and showed that exposure of cells to CDM induced changes in epigenetic modifiers, thereby suppressing cancer cell growth in a sustained manner (Kaukonen et al., 2017). Our study would benefit from a detailed microarray analysis to determine expression changes in genes of cells seeded onto different CDMs.

We used several approaches to evaluate the cellular migration responses to Hsp90 inhibition. Migration is known to be involved in many physiological and pathological processes, such as development, immune, surveillance, and cancer metastasis (Friedl & Gilmour, 2009). Treatment of cells with exogenous Hsp90β increased insoluble FN in Hs578T cells but decreased insoluble FN in MEF-1 cells. Interestingly, we observed increased migration in MEF-1 cells despite their loss in insoluble FN levels and reduced migration in Hs578T cells despite their increase in insoluble FN levels. This would suggest an indirect relationship between levels of insoluble FN and migration capacity. The wound healing data evaluating the effects of the different Hsp90 inhibitors on a cell's ability to migrate revealed a trend similar to that observed for total levels of FN in the western analyses. The migratory capacity appears to be sensitive to Hsp90 inhibitor concentrations. That is, at low NOV concentrations, we observed an increase in cell migration in LRP1 expressing cells, and at higher NOV concentrations, there was a dose dependent decrease in cell migration which could be linked to the increase in FN and then reduction in FN at these concentrations. Interestingly, these responses were conserved between a cancer and non-cancer cell line model suggesting possible implications of Hsp90 inhibition in cancer development and normal cell physiological functions. To determine whether this response was as a direct result of Hsp90 inhibition or due to changes in total FN levels we demonstrated that GA (which we showed previously was unable to alter FN levels) was unable to induce migration in cells like that observed for NOV treatment. Whether these migratory responses were directly related to the amount of FN was tested.

LRP1-expressing and LRP1-deficient cells exhibited a dose-dependent increase in cell migration on FN substrate. However, it is important to note that FN in solution does not form fibrils (Singh et al., 2010) and thus, the increased migration we observe for both MEF-1 and PEA-13 cells is likely unrelated to an enhanced FN matrix and we would require a better assay to determine the contribution of an extracellular matrix to the migratory capacity of cells. We used a 4 well insert to measure modes of migration similar to that described for a cell scattering assay (De Rooij, Kerstens et al., 2005). Here we were able to assess the dispersion of compact colonies of cells in NOV treatments. We noted that cells which remained untreated, detached from neighbouring cells and migrated outward in a "scatter" phenomenon. This type of migration is often described as amoeboid or mesenchymal (Kunwar et al., 2006). Comparatively, the mode of migration exhibited by NOV-treated cells was more collective and distances migrated were not as far as untreated cells. This type of migration is characteristic of epithelial cancer cell migration and involves clusters of cells connected by adherens junctions migrating as a sheet (Kunwar et al., 2006).

Cells interact with ECM through adhesions and a large repertoire of receptors capable of binding to the ECM (Morgan et al., 2007). They provide a physical link to the ECM and allow cells to transduce signals emanating from the ECM by adapting their behaviour to the properties of this complex microenvironment (Tello et al., 2016). An interesting addition would have been to assess the presence of focal adhesions in these CDMs. Studies by Cukierman and colleagues demonstrated a dependence of cells in the 3D matrix for α5 integrins for cell attachment, migration and proliferation on CDMs. They demonstrated that a function blocking monoclonal antibody specific for the α5 subunit blocked all enhanced cellular responses to CDMs (Cukierman et al., 2001).

The importance of studying these physiological changes is demonstrated in studies by Amatangelo and colleagues (2005). They showed that tumour-associated CDM was able to promote desmoplastic differentiation of normal fibroblasts and trigger invasive behavior of breast cancer cells, indicating that these matrices contain the necessary physical and molecular cues to induce transformation events observed in vivo during stromatogenesis. To address possible transformation events in cells, we attempted to reseed cells on Hs578T-derived CDMs and probe for levels of typical EMT markers such as vimentin and E-cadherin but these experiments were unsuccessful. This might be worthwhile optimizing in the future

in order to assess whether treated CDMs can alter EMT markers of replated cells which could induce a more migratory phenotype.

Collectively these migration data demonstrate that low and high NOV concentrations may cause different migratory responses in cells and that NOV affects the mode of migration of cells from a mesenchymal to epithelial-like. In the spheroid migration assay, Hs578T cells demonstrated no significant changes in the migration on either NOV or Hsp90β treated Hs578T-derived matrices. MEF-1 cells, however, were significantly more migratory on the Hs578T-derived CDMs treated with higher NOV concentrations (500 µM) compared to untreated CDMs, and significantly less migratory on 50 µM NOV CDMs. The fact that we observe increased migration at 500 µM NOV in spite of the reduced proliferation of these cells on treated CDMs suggests that there must be a structural or morphological change in the ECM that allows for these differences in migratory capacities at two different concentrations of NOV.

4.2.3 Structural changes in the ECM may account for physiological responses of cells on CDMs

Cell migration and invasion on CDMs is regulated by the molecular composition of the matrix as well as topographical cues provided by the physical organisation of the ECM. In particular, ECM FN fibrils have the capacity to stimulate a variety of cellular activities, including cell spreading, growth, migration, and contractility (Hocking & Chang, 2003; Hocking et al., 2000; Sottile et al., 2000). The specific contribution of the matrix itself has not been addressed in detail. Increased levels of FN have been associated with increased invasion and metastatic capability in some cancers, (Akiyama et al., 1995; Ioachim et al., 2002; Zheng et al., 2007), while on the other hand, high levels of FN expression have been found to correlate with reduced cell proliferation, migratory capacity, and are associated with a more favorable prognosis in breast cancer patients (Bae et al., 2013; Lochter & Bissell, 1995; Swiatoniowski et al., 2005). This demonstrates that expression of FN alone is not a true determination of cancer outcome and prognosis but rather involves factors related to the maturity, organisation and structure of the matrix. Here we showed that the differences observed in migration were not dependent on FN concentration. Immunoblotting and SPB analyses of solubilised CDMs demonstrated an increase in total FN levels from 50 µM NOV treated CDMs

which did not translate into an enhanced ability of cells on these matrices to migrate. Rather, we observed increased migration on matrices which produced significantly less FN. However, since these represent two different populations of cell derived matrix (i.e. one which is solubilised versus another which maintains its three-dimensionality) it is impossible to make any causal relationship between the two. Instead, a more likely explanation for the differences in migration of MEF-1 cells at two different NOV concentrations are morphological changes in these CDMs.

4.2.4 NOV treatment reduces the maturity of matrices

During tumor progression, the stromal microenvironment changes to produce a more progressive and permissive scaffold. Cells within the tumor-associated stroma produce an organized fibrotic ECM rich in FN and type I collagen and such an ECM is associated with poor prognosis and increased cancer progression (Amatangelo et al., 2005). In order to determine the maturity of an ECM we compared the thickness of matrices produced and ratios of type I collagen to fibronectin. Confocal microscopy images of FN in extracted matrices show that untreated ECMs appear exactly like a “normal” or “primed” ECM with thinner fibrils similar to that observed for primary ovarian fibroblasts (Quiros et al., 2008). Normal primary fibroblast cultures were not capable of overcoming growth inhibition by contact and produced thin CDMs of only 9 µm thick (Amatangelo et al., 2005). In our study, Hs578T derived CDMs generated from NOV treatments were thinner, less dense and flatter (thickness measured ~10 µm), with fewer cell layers and large gaps between fibrils. The individual fibres appeared thicker but underdeveloped and there was a reduced mesh-like network perhaps suggesting the loss of branching between fibres. Comparatively, untreated unextracted cultures were able to form significantly thicker and more 3D matrices that averaged between 12 µm and 17 µm. This would suggest any number of things including possible defects in branching causing fibres to clump together generating a flatter and less 3D matrix, or that NOV treatment alters the ability of overcoming growth inhibition by contact and renders cells growth inhibited with a reduced ability to make multilayers in culture (Amatangelo et al., 2005).

Type I collagen to FN ratios serve as a good determinant of the maturity of a matrix because this relies on the fact that assembly of an initial FN network is often a prerequisite for the deposition of collagen (Amatangelo et al., 2005; Singh et al., 2010; Sottile & Hocking, 2002).

FN and type I collagen fibres are often found together in tissues and the reported colocalization of both FN and procollagen within the cell further demonstrates a likely synergistic relationship between these two ECM proteins (Ledger, Uchida, & Tanzer, 1980; Wang et al., 2016). Reduced levels of collagen in NOV-treated CDMs coupled to a reduced colocalisation with FN suggests that deposition of FN in these cells were insufficient to generate a robust collagen matrix consequently producing underdeveloped, immature matrices. We showed that each of the treated CDMs were less mature than untreated CDMs suggesting an effect of treatment (whether it be Hsp90 inhibition of exogenous Hsp90 addition) that alters ECM stability. Whilst many groups have shown that collagen fibrils do not accumulate in the absence of FN matrix (Dallas et al., 2005; Mcdonald, Kelley, & Broekelmann, 1984; Sottile & Hocking, 2002) some reports, however have indicated that collagen contributes to and enhances FN assembly (Dzamba et al., 1993). An important consideration when comparing COL1 levels is that addition of ascorbic acid to culture media increases the collagen content in CDMs (Soucy & Romer, 2009) but since we treat all our CDMs in the same way we can assume this to be inconsequential to our comparative analyses.

Taken together, both the reduced matrix maturation and reduced three-dimensionality or density of NOV and Hsp90β treated CDMs may account for the reduced proliferative ability of cells on these matrices. Although 50 µM and 500 µM NOV treatments produced similarly immature matrices, we observed differences in migration of MEF-1 cells on these CDMs which suggests that factors other than the matrix maturity and FN levels contribute to migratory ability. Rather, the ability of MEF-1 cells to migrate more on the 500 µM NOV CDMs and less on the 50 µM NOV CDMs (compared to UNT) is likely related to the structure of the matrix fibrils and possible interaction of cells within gaps of the 3D matrix.

4.2.5 NOV and Hsp90β result in changes to FN fibre thickness and orientation

FN fibres are highly elastic and comprise multiple molecular conformations, from compact and relaxed to extended and unfolded (Wang et al., 2016). This increase in conformational flexibility may account for the significant changes in thickness of FN fibrils compared to collagen fibrils observed in treated matrices. Robinson and colleagues showed that pancreatic stellate cells (PSCs) were able to remodel the ECM by showing a significant increase in collagen fibre thickness (Robinson et al., 2016). They suggest that the increase of collagen

fibre thickness may be a result of the increased remodelling on the thinner collagen fibrils (Kadler et al., 1996; Robinson et al., 2016). Remodelling may lead to more fibrils being drawn into collagen fibres leading to an increase in fibre thickness due to the packaging of a greater number of fibrils. They also add that the bundling of more collagen into fibres may also account for the observed increasing in spacing between fibres. In NOV treated CDMs we observed significantly thicker rope-like fibrils and increased spacing, potentially indicative of bundles of fibrils and increased packaging of FN, as observed by Robinson and colleagues which might suggest increased remodelling. These points of bundled FN fibres may also represent branching points containing local focal adhesion clusters for the formation of new fibrils. Inhibition of FN assembly or synthesis blocks branching (Schwarzbauer & DeSimone, 2011) which might explain why NOV treatment induced bundling of fibres but does not explain why Hsp90β treatment also results in a similar phenotype. Our data might also suggest fewer crosslinking and consequently a less stiff matrix but this would need to be tested by atomic force microscopy measurements. Very little is known about the structure of bundled fibrils and mechanism of formation but studies by Früh et al., (2015) have demonstrated that thicker fibres show random bundling of protofibrils. They use stochastic optical reconstruction microscopy to demonstrate that formation of thick FN fibres is mediated by FN type III_{1-2} and FN type III_{4-5} domains which mediate lateral bundling of protofibrils forming a compact structure with dimerisation capacity leading to the formation of thick fibril structures. Studies have shown spreading of fibroblasts to be slower on fibres due to cells overcoming the effect of high curvature of the fiber and in this way the structure of fibres may directly influence rates of cell adhesion (Wòjciak-Stothard et al., 1997). Therefore, although in NOV treated CDMs we observed an increase in cell adhesion (likely due to the increased availability of gaps between fibrils) we observed a concomitant reduction in cell spreading on these matrices which might be explained by the NOV-induced thickening and rope-like phenotype of FN fibres which retards a cell's ability to spread once adhered.

The orientation of FN fibres plays a large role in migration and directionality of movement of cells. A few studies have identified factors that can lead to ECM alignment, including the serine proteinase fibroblast activation protein (Lee et al., 2011), however the exact mechanism of how cells organise the matrix remains largely unclear. Recently, Erdogan et al., (2017) presented a new mechanism by which fibroblasts might organise the FN matrix. They

propose that cancer associated fibroblasts (CAFs) align the FN matrix by increasing nonmuscle myosin II and platelet-derived growth factor receptor α (PDGFR)-mediated contractility which are transduced to FN through α5β1 integrin. The aligned FN fibre orientation guides cancer cells to migrate directionally and upon blockade of α5β1 using an RGD peptide they found that CAFs produced a disordered, mesh-like fibre organisation in the CDMs (Erdogan et al., 2017). In our study, it would appear that fibres align and become thicker with treatment losing their web-like structure which might suggest a move towards forming fibres in the same direction rather than at right angles to each other. Whether this change in organisation upon treatment is caused by the above mentioned factors would need to be determined by immunofluorescence staining of PDGFR and integrins and contractility assays as described by the authors.

The increased migratory phenotype of MEF-1 cells observed on 500 µM NOV CDMs may be explained by increased spacing between fibrils which creates more gaps into which cells can invade and therefore more closely resembles the highly migratory phenotype of cells observed on no CDM (plastic) controls. On the other hand, it is difficult to explain how 500 µM NOV treated CDMs with similarly thick fibres and spacing have an opposite migratory response. Further studies to characterise velocity and directionality of cell migration using live time lapse analyses (Kaukonen et al., 2017) would be interesting to determine how individual cells orient themselves in the matrix, along fibrils and how quickly they migrate on treated CDMs. From these data, it is unclear whether maturation state of the ECM or structural changes in individual fibres contributes to the observed cell physiological consequences but it is likely that a combination of the two may be responsible. As a first step, it might be worthwhile performing quantitative mass spectrometry analysis on the treated CDMs to get a global analysis of changes in ECM constituents of these matrices as a means to investigate what may account for the observed responses in this study.

An interesting study by Bellaye and colleagues demonstrated that fibrotic rat lung slices which are stiffer and produce excessive ECM compared to normal lungs, secrete larger amounts of Hsp90α driven by the increased stiffness and mechanical stretch of the fibrotic ECM. They further showed that circulating Hsp90α levels correlated with increased collagen deposition in an animal model of lung fibrosis and also correlated with disease severity in patients with IPF (Bellaye et al., 2018). We did not observe increased collagen deposition in Hsp90β treated

CDMs suggesting that circulating levels of Hsp90 alone are insufficient to accumulate collagen levels. Given this, we might anticipate that NOV would reduce levels of active Hsp90 and thereby reduce stiffness of matrices whilst eHsp90β treatment might increase stiffness of matrices. However, in our case Hsp90β treatments unexpectedly often recapitulated the effects of NOV treatments. It would therefore be interesting to perform measurements of stiffness, elasticity and stretch on our NOV treated CDMs as has been described in studies by Tello and colleagues (2016) using atomic force microscopy (AFM).

Chapter 5: **FINAL CONCLUSIONS**

Whilst we could not isolate any single underlying mechanism for the NOV-induced FN turnover, we have determined that the LRP1-mediated loss of FN is more likely due to increased turnover rather than assembly defects. We suspect that a large contributor is likely to be the disruption of Hsp90:LRP1:FN protein complexes at the cell surface by NOV which alters downstream eHsp90-LRP1 signalling cascades to reduce FN deposition (or increase endocytosis) that may involve the activation of Akt and/or deactivation of ERK pathways. An important consideration is the role which eHsp90 plays in the extracellular space. Several studies have suggested that eHsp90 still acts as a chaperone outside cells, in which eHsp90 binds and maintains its extracellular client proteins in their active forms, whilst others have argued that eHsp90 no longer functions as a chaperone but instead acts as a cytokine by activating downstream signalling to execute its function. Our studies would suggest a role for eHsp90 in both maintaining FN stability in the extracellular space as a chaperone and functioning as a cytokine via LRP1.

Most often in the study of cancer, FN is examined as a marker of the mesenchymal phenotype associated with EMT and is studied primarily in the context of fibroblastic stroma in the tumour microenvironment. Much less is known about the potential roles that FN may play in normal and malignant epithelium. This is the first study to examine the effects of Hsp90 and Hsp90 inhibition on Hs578T breast cancer cell-derived matrix and the physiological consequences of cells replated on these matrices. We demonstrate that Hs578T cancer cell derived ECM can directly alter cell morphology, cell proliferation and migration properties of MEF-1 cell lines. Importantly, the identification that addition of Hsp90β and inhibition of Hsp90 with NOV induce similar biological consequences means that treatment of cancer with Hsp90 inhibitors may need to be carefully considered. Further investigation into the physiological consequences associated with Hsp90 inhibition and FN turnover is required in order to better understand mechanisms of tumour progression and better inform drug design strategies.

As advances are made in our knowledge of FN nanostructure, assembly (e.g. fibrillogenesis, orientation of fibres, remodelling), mechanics (e.g. stiffness, tension) and mechanisms of structure-function relationships during tumour progression, the development of therapeutic strategies and diagnostic tools will continue to improve to mitigate tumourigenesis. Our results have implications in contexts where diseases are characterised by increased FN deposition by unknown mechanisms (such as fibrosis) and diseases in which Hsp90 inhibition is considered a druggable target (such as cancer). Considering NOV is also used to treat bacterial infections an important consideration will be to assess the side effects induced by regular treatment with NOV and how this may impact on FN turnover and consequent cancer progression in the long term. Thus, the fact that certain Hsp90 inhibitors, which are intended for clinical use, cause deregulation of FN via a receptor that is ubiquitously expressed, means that these inhibitors may induce unintended ECM remodelling in a range of cell types which could ultimately culminate in disease. Whilst we acknowledge that FN is a major component of the ECM, there are other matrix proteins, such as, collagen, laminin and vitronectin which may allow for migration when FN is lost. Also, since we observed some functional responses to be similar in both a normal and tumourigenic cell lines, this demonstrates that the role of the ECM is more complex than originally thought and it remains inconclusive as to whether Hsp90 inhibition, particularly with NOV, may be beneficial or detrimental to metastases of tumours. Moreover, a greater understanding of the NOV-induced changes in both tumourigenic and non-tumourigenic cells may have therapeutic importance in determining whether interventions should be done through inhibiting FN/eHsp90 itself, LRP1 or intracellular signaling in response to ECM turnover.

Chapter 6: **REFERENCES**

Adams, J. C., & Lawler, J. (2011). The Thrombospondins. In *Cold Spring Harbor Perspectives in Biology* (Vol. 3). https://doi.org/10.1101/cshperspect.a009712

Akerfelt, M., Morimoto, R. I., & Sistonen, L. (2010). Heat shock factors: integrators of cell stress, development and lifespan. *Nat Rev Mol Cell Biol*, *11*(8), 545–555. https://doi.org/10.1038/nrm2938.Heat

Akiyama, S. K., Olden, K., & Yamada, K. M. (1995). Fibronectin and integrins in invasion and metastasis. *Cancer and Metastasis Reviews*, *14*(3), 173–189. https://doi.org/10.1007/BF00690290

Alexander, L. D., Sellers, R. P., Davis, M. R., Ardi, V. C., Victoria, A., Vasko, R. C., & Mcalpine, S. R. (2009). Evaluation of Di-Sansalvamide A derivatives: Synthesis, structure-activity relationship, and mechanism of action. *Journal of Medicinal Chemistry*, *52*(24), 7927–7930. https://doi.org/10.1021/jm901566c.Evaluation

Allan, R. K., Mok, D., Ward, B. K., & Ratajczak, T. (2006). Modulation of Chaperone Function and Cochaperone Interaction by Novobiocin in the C-terminal Domain of Hsp90. *Journal of Biological Chemistry*, *281*(11), 7161–7171. https://doi.org/10.1074/jbc.M512406200

Althoff, K., Müllberg, J., Aasland, D., Voltz, N., Kallen, K., Grötzinger, J., & Rose-John, S. (2001). Recognition sequences and structural elements contribute to shedding susceptibility of membrane proteins. *The Biochemical Journal*, *353*(Pt 3), 663–72. Retrieved from http://www.pubmedcentral.nih.gov/articlerender.fcgi?artid=1221613&tool=pmcentrez&rendertype=abstract

Altieri, D. C. (2006). Targeted therapy by disabling crossroad signaling networks: the survivin paradigm. *Molecular Cancer Therapeutics*, *5*(3), 478–82. https://doi.org/10.1158/1535-7163.MCT-05-0436

Altrock, E., Sens, C., Wuerfel, C., Vasel, M., Kawelke, N., Dooley, S., … Nakchbandi, I. A. (2014). Inhibition of fibronectin deposition improves experimental liver fibrosis. *Journal of Hepatology*, *62*(3), 625–633. https://doi.org/10.1016/j.jhep.2014.06.010

Amatangelo, M. D., Bassi, D. E., Klein-Szanto, A. J. P., & Cukierman, E. (2005). Stroma-derived three-dimensional matrices are necessary and sufficient to promote desmoplastic differentiation of normal fibroblasts. *American Journal of Pathology*, *167*(2), 475–488. https://doi.org/10.1016/S0002-9440(10)62991-4

Anckar, J., & Sistonen, L. (2011). Regulation of HSF1 Function in the Heat Stress Response : Implications in Aging and Disease. *Annual Review of Biochemistry*, *80*, 1089–1115. https://doi.org/10.1146/annurev-biochem-060809-095203

Annamalai, B., Liu, X., Gopal, U., & Isaacs, J. (2009). Hsp90 is an essential regulator of EphA2 receptor stability and signaling: Implications for cancer cell migration and metastasis. *Mol Cancer Res*, *7*(7), 1012–1032. https://doi.org/10.1016/j.neuroimage.2013.08.045.The

Arap, M. A., Lahdenranta, J., Mintz, P. J., Hajitou, A., Sarkis, A. S., Arap, W., & Pasqualini, R. (2004). Cell surface expression of the stress response chaperone GRP78 enables tumor targeting by circulating ligands. *Cancer Cell*, *6*(3), 275–284. https://doi.org/10.1016/j.ccr.2004.08.018

Armstrong, H. K., Gilli, J. L., Johnson, I. R. D., Nassar, Z. D., Moldovan, M., Levrie, C., … Butler, L. M. (2018). Dysregulated fibronectin trafficking by Hsp90 inhibition restricts prostate cancer cell invasion. *Scientific Reports*, *8*(2090), 1–14. https://doi.org/10.1038/s41598-018-19871-4

Au, D. T., Arai, A. L., Fondrie, W. E., Muratoglu, S. C., & Strickland, D. K. (2018). Role of the LDL receptor-related protein 1 in regulating protease activity and signaling pathways in the vasculature. *Current Drug Targets*, *19*(11), 1276–1288. https://doi.org/10.2174/1389450119666180511162048

Bae, Y. K., Kim, A., Kim, M. K., Choi, J. E., Kang, S. H., & Lee, S. J. (2013). Fibronectin expression in carcinoma cells correlates with tumor aggressiveness and poor clinical outcome in patients with invasive breast cancer. *Human Pathology*, *44*(10), 2028–37. https://doi.org/10.1016/j.humpath.2013.03.006

Baecker, V. (2017). New FIJI Toolsets for Bioimage Analysis. In *Journée Biocampus Montpellier 2017*. https://doi.org/10.13140/RG.2.2.15064.60167

Bagatell, R., Paine-Murrieta, G. D., Taylor, C. W., Pulcini, E. J., Akinaga, S., Benjamin, I. J., & Whitesell, L. (2000). Induction of a heat shock factor 1-dependent stress response alters the cytotoxic activity of Hsp90-binding agents. *Clinical Cancer Research*, *6*(8), 3312–3318.

Bao, R., Lai, C. J., Qu, H., Wang, D., Yin, L., Zifcak, B., … Qian, C. (2009). CUDC-305, a novel synthetic HSP90 inhibitor with unique pharmacologic properties for cancer therapy. *Clinical Cancer Research*, *15*(12), 4046–4057. https://doi.org/10.1158/1078-0432.CCR-09-0152

Barrott, J. J., Hughes, P. F., Osada, T., Yang, X.-Y., Hartman, Z. C., Loiselle, D. R., … Haystead, T. a. (2013). Optical and radioiodinated tethered hsp90 inhibitors reveal selective internalization of ectopic hsp90 in malignant breast tumor cells. *Chemistry & Biology*, *20*(9), 1187–97. https://doi.org/10.1016/j.chembiol.2013.08.004

Bartl, M. M., Luckenbach, T., Bergner, O., Ullrich, O., & Koch-Brandt, C. (2001). Multiple receptors mediate apoJ-dependent clearance of cellular debris into nonprofessional phagocytes. *Experimental Cell Research*, *271*(1), 130–41. https://doi.org/10.1006/excr.2001.5358

Basford, J. E., Moore, Z. W. Q., Zhou, L., Herz, J., & Hui, D. Y. (2010). NIH Public Access, *29*(11), 1772–1778. https://doi.org/10.1161/ATVBAHA.109.194357.Smooth

Basu, S., Binder, R. J., Ramalingam, T., & Srivastava, P. K. (2001). CD91 is a common receptor for heat shock proteins gp96, hsp90, hsp70, and calreticulin. *Immunity*, *14*(3), 303–13. Retrieved from http://www.ncbi.nlm.nih.gov/pubmed/11290339

Bellahcène, A., Castronovo, V., Ogbureke, K. U. E., Fisher, L. W., & Fedarko, N. S. (2008). Small integrin-binding ligand N-linked glycoproteins (SIBLINGs): multifunctional

proteins in cancer. *Nature Reviews. Cancer*, *8*(3), 212–26. https://doi.org/10.1038/nrc2345

Bellaye, P. S., Shimbori, C., Yanagihara, T., Carlson, D. A., Hughes, P., Upagupta, C., … Kolb, M. (2018). Synergistic role of HSP90α and HSP90β to promote myofibroblast persistence in lung fibrosis. *European Respiratory Journal*, *51*(2). https://doi.org/10.1183/13993003.00386-2017

Belofsky, G. N., Jensen, P. R., & Fenical, W. (1999). Sansalvamide: A new cytotoxic cyclic depsipeptide produced by a marine fungus of the genus Fusarium. *Tetrahedron Letters*, *40*(15), 2913–2916. https://doi.org/10.1016/S0040-4039(99)00393-7

Binder, R. J., & Srivastava, P. K. (2018). *Heat Shock Proteins in the Immune System*. (R. J. Binder & P. K. Srivastava, Eds.). Springer Nature.

Blagosklonny, M. V, Toretsky, J., Boheniii, S., Neckers, L., & by Keith Yamamoto, C. (1996). Mutant conformation of p53 translated in vitro or in vivo requires functional HSP90. *Cell Biology*, *93*(August), 8379–8383. https://doi.org/10.1073/pnas.93.16.8379

Boel, N., Hunter, M. C., & Edkins, A. L. (2018). LRP1 is required for novobiocin-mediated fibronectin turnover. *Scientific Reports*, *8*(1), 11438. https://doi.org/10.1038/s41598-018-29531-2

Boel, N. M., & Edkins, A. L. (2018). Regulation of the Extracellular Matrix by Heat Shock Proteins and Molecular Chaperones. In R. J. Binder & P. K. Srivastava (Eds.), *Heat Shock Proteins in the Immune System* (pp. 97–121). Springer Nature.

Bonnans, C., Chou, J., & Werb, Z. (2014). Remodelling the extracellular matrix in development and disease. *Nature Reviews Molecular Cell Biology*, *15*(12), 786–801. https://doi.org/10.1038/nrm3904

Bornstein, P., & Sage, E. H. (2002). Matricellular proteins: extracellular modulators of cell function. *Current Opinion in Cell Biology*, *14*(5), 608–16. Retrieved from http://www.ncbi.nlm.nih.gov/pubmed/12231357

Boucher, P., & Herz, J. (2011). Signaling through LRP1: Protection from atherosclerosis and beyond. *Biochemical Pharmacology*, *81*(1), 1–5. https://doi.org/10.1016/j.bcp.2010.09.018

Bourdoulous, S., Orend, G., Mackenna, D. A., & Pasqualini, R. (1998). Fibronectin Matrix Regulates Activation of RHO and CDC42 GTPases and Cell Cycle Progression. *Journal of Cell Biology*, *143*(1), 267–276.

Bradshaw, A. D. (2012). Diverse biological functions of the SPARC family of proteins. *International Journal of Cell Biology*, *44*(3), 480–488. https://doi.org/10.1016/j.biocel.2011.12.021.Diverse

Brekken, R. a, & Sage, E. H. (2000). SPARC, a matricellular protein: at the crossroads of cell-matrix communication. *Matrix Biology*, *19*, 816–827.

Brenner, K. A., Corbett, S. A., & Schwarzbauer, J. E. (2000). Regulation of fibronectin matrix assembly by activated Ras in transformed cells. *Oncogene*, *19*, 3156–3163. https://doi.org/10.1038/sj.onc.1203626

Bretscher, M. S. (1989). Endocytosis and recycling of the fibronectin receptor in CHO cells. *EMBO Journal*, *8*(5), 1341–8. https://doi.org/10.1021/cb5008713

Bridgewater, R. E., Norman, J. C., & Caswell, P. T. (2012). Integrin trafficking at a glance. *Journal of Cell Science*, *125*(Pt 16), 3695–701. https://doi.org/10.1242/jcs.095810

Bu, G., & Marzolo, M. P. (2001). Role of RAP in the Biogenesis of Lipoprotein Receptors. *Trends Cardiovascular Medicine*, *10*(4), 148–155. https://doi.org/10.1016/S1050-1738(00)00045-1

Burlison, J. A., Avila, C., Vielhauer, G., Lubbers, D. J., Holzbeierlein, J., & Blagg, B. S. J. (2008). Development of novobiocin analogues that manifest anti-proliferative activity against several cancer cell lines. *Journal of Organic Chemistry*, *73*(6), 2130–2137. https://doi.org/10.1021/jo702191a

Burlison, J. A., Neckers, L., Smith, A. B., Maxwell, A., & Blagg, B. S. J. (2006). Novobiocin : Redesigning a DNA Gyrase Inhibitor for Selective Inhibition of Hsp90. *Journal of American Chemical Society*, *128*(7), 15529–15536.

Bussenius, J., Blazey, C. M., Aay, N., Anand, N. K., Arcalas, A., Baik, T., … Rice, K. D. (2012). Discovery of XL888: A novel tropane-derived small molecule inhibitor of HSP90. *Bioorganic and Medicinal Chemistry Letters*, *22*(17), 5396–5404. https://doi.org/10.1016/j.bmcl.2012.07.052

Butler, G. S., & Overall, C. M. (2007). Proteomic validation of protease drug targets: pharmacoproteomics of matrix metalloproteinase inhibitor drugs using isotope-coded affinity tag labelling and tandem mass spectrometry. *Current Pharmaceutical Design*, *13*(3), 263–270. https://doi.org/10.2174/138161207779313524

Butler, L. M., Ferraldeschi, R., Armstrong, H. K., & Centenera, M. M. (2016). Maximizing the Therapeutic Potential of Hsp90 Inhibitors. *Mol Cancer Res*, *13*(11), 1445–1451. https://doi.org/10.1158/1541-7786.MCR-15-0234

Caccavari, F., Valdembri, D., Sandri, C., Bussolino, F., & Serini, G. (2010). Integrin signaling and lung cancer. *Cell Adhesion and Migration*, *4*(1), 124–129. https://doi.org/10.4161/cam.4.1.10976

Caldas-lopes, E., Cerchietti, L., Ahn, J. H., Clement, C. C., Robles, A. I., Rodina, A., … Chiosis, G. (2009). Hsp90 inhibitor PU-H71, a multimodal inhibitor of malignancy, induces complete responses in triple-negative breast cancer models. *PNAS*, *106*(20), 8368–8373.

Calderwood, S. K. (2017). Heat shock proteins and cancer: intracellular chaperones or extracellular signalling ligands? *Philosphical Transcations Royal Society B*, *373*. https://doi.org/10.1098/rstb.2016.0524

Calderwood, S. K., Gong, J., Murshid, A., Eden, W. Van, Wheeler, R. T., Wang, X., & Calderwood, S. K. (2016). Extracellular HSPs: The Complicated Roles of Extracellular HSPs in Immunity, *7*(April). https://doi.org/10.3389/fimmu.2016.00159

Calderwood, S. K., Khaleque, M. A., Sawyer, D. B., & Ciocca, D. R. (2006). Heat shock proteins in cancer: Chaperones of tumorigenesis. *Trends in Biochemical Sciences*, *31*(3), 164–172. https://doi.org/10.1016/j.tibs.2006.01.006

Cam, J. a, Zerbinatti, C. V, Li, Y., & Bu, G. (2005). Rapid endocytosis of the low density lipoprotein receptor-related protein modulates cell surface distribution and processing of the beta-amyloid precursor protein. *The Journal of Biological Chemistry*, *280*(15), 15464–70. https://doi.org/10.1074/jbc.M500613200

Cao, X., & Sudhof, T. C. (2001). A transcriptively active complex of APP with Fe65 and histone acetyltransferase Tip60 (vol 293, pg 115, 2001). *Science*, *293*(5534), 1436.

Castello-Cros, R., & Cukierman, E. (2009). Stromagenesis during tumorigenesis: characterization of tumor-associated fibroblasts and stroma-derived 3D matrices. *Methods in Molecular Biology*, *522*, 275–305. https://doi.org/10.1007/978-1-59745-413-1

Castelló-Cros, R., Khan, D. R., Simons, J., Valianou, M., & Cukierman, E. (2009). Staged stromal extracellular 3D matrices differentially regulate breast cancer cell responses through PI3K and beta1-integrins. *BMC Cancer*, *9*, 1–19. https://doi.org/10.1186/1471-2407-9-94

Chadli, A., Felts, S. J., Wang, Q., Sullivan, W. P., Botuyan, M. V., Fauq, A., … Mer, G. (2010). Celastrol inhibits Hsp90 chaperoning of steroid receptors by inducing fibrillization of the co-chaperone p23. *Journal of Biological Chemistry*, *285*(6), 4224–4231. https://doi.org/10.1074/jbc.M109.081018

Chang, H. C., Nathan, D. F., & Lindquist, S. (1997). In vivo analysis of the Hsp90 cochaperone Sti1 (p60). *Molecular and Cellular Biology*, *17*(1), 318–325. https://doi.org/10.1128/MCB.17.1.318

Chaudhuri, T. K., & Paul, S. (2006). Protein-misfolding diseases and chaperone-based therapeutic approaches. *The FEBS Journal*, *273*(7), 1331–49. https://doi.org/10.1111/j.1742-4658.2006.05181.x

Chen, C., Chen, Y., Dai, K., Chen, P., Riley, D. J., & Lee, W. (1996). A New Member of the hsp90 Family of Molecular Chaperones Interacts with the Retinoblastoma Protein during Mitosis and after Heat Shock. *Molecular and Cell Biology*, *16*(9), 4691–4699.

Chen, J.-S., Hsu, Y.-M., Chen, C.-C., Chen, L.-L., Lee, C.-C., & Huang, T.-S. (2010). Secreted heat shock protein 90alpha induces colorectal cancer cell invasion through CD91/LRP-1 and NF-kappaB-mediated integrin alphaV expression. *The Journal of Biological Chemistry*, *285*(33), 25458–66. https://doi.org/10.1074/jbc.M110.139345

Chen, W., Chen, C., Chen, L., Lee, C., & Huang, T. (2013). Secreted Heat Shock Protein 90alpha (HSP90a) Induces Nuclear Factor-k B-mediated TCF12 Protein Expression to Down-regulate E-cadherin and to Enhance Colorectal Cancer Cell Migration and Invasion *. *Journal of Biological Chemistry*, *288*(13), 9001–9010. https://doi.org/10.1074/jbc.M112.437897

Cheng, C.-F., Fan, J., Fedesco, M., Guan, S., Li, Y., Bandyopadhyay, B., … Li, W. (2008). Transforming growth factor alpha (TGFalpha)-stimulated secretion of HSP90alpha: using the receptor LRP-1/CD91 to promote human skin cell migration against a TGFbeta-rich environment during wound healing. *Molecular and Cellular Biology*, *28*(10), 3344–58. https://doi.org/10.1128/MCB.01287-07

Chiosis, G., Lucas, B., Shtil, A., Huezo, H., & Rosen, N. (2002). Development of a purine-scaffold novel class of Hsp90 binders that inhibit the proliferation of cancer cells and induce the degradation of Her2 tyrosine kinase. *Bioorganic & Medicinal Chemistry*, *10*(11), 3555–64. Retrieved from http://www.ncbi.nlm.nih.gov/pubmed/12213470

Chiosis, G., Timaul, M. N., Lucas, B., Munster, P. N., Zheng, F. F., Sepp-Lorenzino, L., & Rosen, N. (2001). A small molecule designed to bind to the adenine nucleotide pocket of Hsp90 causes Her2 degradation and the growth arrest and differentiation of breast cancer cells. *Chemistry and Biology*, *8*(3), 289–299. https://doi.org/10.1016/S1074-5521(01)00015-1

Chlenski, A., Guerrero, L. J., Salwen, H. R., Yang, Q., Tian, Y., la Madrid, A., … Cohn, S. L. (2011). Secreted protein acidic and rich in cysteine is a matrix scavenger chaperone. *PLoS ONE*, *6*(9). https://doi.org/10.1371/journal.pone.0023880

Clark, K., Pankov, R., Travis, M. A., Askari, J. A., Mould, A. P., Craig, S. E., … Humphries, M. J. (2012). Europe PMC Funders Group A Specific α 5 β 1 Integrin Conformation Promotes Directional Integrin Translocation and Fibronectin Matrix Formation. *J Cell Sci*, *118*(Pt 2), 291–300. https://doi.org/10.1242/jcs.01623.A

Condeelis, J., & Segall, J. E. (2003). Intravital imaging of cell movement in tumours. *Nature Reviews Cancer*, *3*(12), 921–930. https://doi.org/10.1038/nrc1231

Correia, A. L., Mori, H., Chen, E. I., Schmitt, F. C., & Bissell, M. J. (2013). The hemopexin domain of MMP3 is responsible for mammary epithelial invasion and morphogenesis through extracellular interaction with HSP90β. *Genes and Development*, *27*(7), 805–817. https://doi.org/10.1101/gad.211383.112

Cox, T. R., & Erler, J. T. (2011). Remodeling and homeostasis of the extracellular matrix: implications for fibrotic diseases and cancer. *Disease Models & Mechanisms*, *4*(2), 165–78. https://doi.org/10.1242/dmm.004077

Crowe, L. B., Hughes, P. F., Alcorta, D. A., Osada, T., Smith, A. P., Totzke, J., … Haystead, T. A. J. (2017). A Fluorescent Hsp90 Probe Demonstrates the Unique Association between Extracellular Hsp90 and Malignancy in Vivo. *ACS Chemical Biology*, *12*(4), 1047–1055. https://doi.org/10.1021/acschembio.7b00006

Csermely, P., Schnaider, T., Soti, C., Prohászka, Z., & Nardai, G. (1998). The 90-kDa Molecular Chaperone Family: Structure, function, and clinical applications. A comprehensive review. *Pharmacology & Therapeutics*, *79*(2), 129–168. https://doi.org/10.1016/S0163-7258(98)00013-8

Cukierman, E. (2002). Preparation of Extracellular Matrices Produced by Cultured Fibroblasts. *Current Protocols in Cell Biology*, 1–15.

Cukierman, E., Pankov, R., Stevens, D. R., Yamada, K. M., Adhesions, C., & Yamada, K. M. (2001). Taking Cell-Matrix Adhesions to the Third Dimension. *Science*, *294*(5547), 1708–1712. https://doi.org/10.1126/science.1064829

Daley, W. P., Peters, S. B., & Larsen, M. (2008). Extracellular matrix dynamics in development and regenerative medicine. *Journal of Cell Science*, *121*(Pt 3), 255–264. https://doi.org/10.1242/jcs.006064

Dallas, S. L., Sivakumar, P., Jones, C. J. P., Chen, Q., Peters, D. M., Mosher, D. F., … Kielty, C. M. (2005). Fibronectin regulates latent transforming growth factor-β (TGFβ) by controlling matrix assembly of latent TGFβ-binding protein-1. *Journal of Biological Chemistry*, *280*(19), 18871–18880. https://doi.org/10.1074/jbc.M410762200

Das, F., Ghosh-Choudhury, N., Dey, N., Bera, A., Mariappan, M. M., Kasinath, B. S., & Choudhury, G. G. (2014). High glucose forces a positive feedback loop connecting Akt kinase and Foxo1 transcription factor to activate mTORC1 kinase for mesangial cell hypertrophy and matrix protein expression. *Journal of Biological Chemistry*, *289*(47), 32703–32716. https://doi.org/10.1074/jbc.M114.605196

de Bock, C., Lin, Z., Mekkawy, H. ., Byrne, A. ., & Wang, Y. (2010). Interaction between urokinase receptor and heat shock protein MRJ enhances cell adhesion. *International Journal of Oncology*, *36*, 1155–1163. https://doi.org/10.3892/ijo

De Rooij, J., Kerstens, A., Danuser, G., Schwartz, M. A., & Waterman-Storer, C. M. (2005). Integrin-dependent actomyosin contraction regulates epithelial cell scattering. *Journal of Cell Biology*, *171*(1), 153–164. https://doi.org/10.1016/j.ceramint.2016.08.140

Deboer, C., Meulman, P. A., Wnuk, R. J., & Peterson, D. H. (1970). Geldanamycin, a new antibiotic. *The Journal of Antibiotics*, (9), 442–447. https://doi.org/10.7164/antibiotics.23.442

Derocq, D., Prébois, C., Beaujouin, M., Laurent-Matha, V., Pattingre, S., Smith, G. K., & Liaudet-Coopman, E. (2012). Cathepsin D is partly endocytosed by the LRP1 receptor and inhibits LRP1-regulated intramembrane proteolysis. *Oncogene*, *31*(26), 3202–12. https://doi.org/10.1038/onc.2011.501

Dhanani, K. C. H., Samson, W. J., & Edkins, A. L. (2017). Fibronectin is a stress responsive gene regulated by HSF1 in response to geldanamycin. *Scientific Reports*, *7*(1), 17617. https://doi.org/10.1038/s41598-017-18061-y

Ding, Y., Xian, X., Holland, W. L., Tsai, S., & Herz, J. (2016). EBioMedicine Low-Density Lipoprotein Receptor-Related Protein-1 Protects Against Hepatic Insulin Resistance and Hepatic Steatosis. *EBIOM*, *7*, 135–145. https://doi.org/10.1016/j.ebiom.2016.04.002

Domogatskaya, A., Rodin, S., & Tryggvason, K. (2012). Functional Diversity of Laminins. *Annual Review of Cell and Developmental Biology*, *28*(1), 523–553. https://doi.org/10.1146/annurev-cellbio-101011-155750

Dong, H., Luo, L., Zou, M., Huang, C., Wan, X., Hu, Y., … Cai, S. (2018). Blockade of extracellular heat shock protein 90 ␣by 1G6-D7 attenuates pulmonary fibrosis through inhibiting ERK signaling. *Am J Physiol Lung Cell Mol Physiol*, *313*, 1006–1015. https://doi.org/10.1152/ajplung.00489.2016

Donnelly, A., & Blagg, B. S. J. (2008). Novobiocin and Additional Inhibitors of the Hsp90 C-Terminal Nucleotide-binding Pocket. *Curr Med Chem*, *15*(26), 2702–2717.

Donnelly, A., Mays, J. R., Burlison, J. A., Nelson, J. T., Vielhauer, G., Holzbeierlein, J., & Blagg, B. S. J. (2008). The design, synthesis, and evaluation of coumarin ring derivatives of the novobiocin scaffold that exhibit antiproliferative activity. *Journal of Organic Chemistry*, *73*(22), 8901–8920. https://doi.org/10.1021/jo801312r

Doube, M., K, M., Arganda-carreras, I., Cordelières, F. P., Dougherty, R. P., Jackson, J. S., … Shefelbine, S. J. (2010). BoneJ : Free and extensible bone image analysis in ImageJ, *47*, 1076–1079. https://doi.org/10.1016/j.bone.2010.08.023

Dzamba, B. J., Wu, H., Jaenisch, R., & Peters, D. M. (1993). Fibronectin binding site in type I collagen regulates fibronectin fibril formation. *Journal of Cell Biology*, *121*(5), 1165–1172. https://doi.org/10.1083/jcb.121.5.1165

Eccles, S. A., Massey, A., Raynaud, F. I., Sharp, S. Y., Box, G., Valenti, M., … Workman, P. (2008). NVP-AUY922: A novel heat shock protein 90 inhibitor active against xenograft tumor growth, angiogenesis, and metastasis. *Cancer Research*, *68*(8), 2850–2860. https://doi.org/10.1158/0008-5472.CAN-07-5256

Edenberg, J. . (1980). Novobiocin inhibition of simian virus 40 DNA replication. *Nature*, *286*, 529–531.

Edkins, A. L. (2016). Hsp90 co-chaperones as drug targets in cancer : current perspectives. In *Heat Shock Protein Inhibitors* (pp. 21–54). Springer Nature. https://doi.org/10.1007/7355_2015_99

Egeblad, M., Rasch, M. G., & Weaver, V. M. (2010). Dynamic interplay between the collagen scaffold and tumor evolution. *Current Opinion in Cell Biology*, *22*(5), 697–706. https://doi.org/10.1016/j.ceb.2010.08.015

Egeblad, M., & Werb, Z. (2002). New functions for the matrix metalloproteinases in cancer progression. *Nature Reviews Cancer*, *2*(3), 161–174. https://doi.org/10.1038/nrc745

El Hamidieh, A., Grammatikakis, N., & Patsavoudi, E. (2012). Cell surface Cdc37 participates in extracellular HSP90 mediated cancer cell invasion. *PLoS ONE*, *7*(8). https://doi.org/10.1371/journal.pone.0042722

Erdogan, B., Ao, M., White, L. M., Means, A. L., Brewer, B. M., Yang, L., … Webb, D. J. (2017). Cancer-associated fibroblasts promote directional cancer cell migration by aligning fibronectin. *Journal of Cell Biology*, *216*(11), 3799–3816. https://doi.org/10.1083/jcb.201704053

Erickson, H. P. (2002). Stretching fibronectin. *Journal of Muscle Research and Cell Motility*, *23*(5–6), 575–80. Retrieved from http://www.ncbi.nlm.nih.gov/pubmed/12785106

Eskew, J. D., Sadikot, T., Morales, P., Duren, A., Dunwiddie, I., Swink, M., … Vielhauer, G. A. (2011). Development and characterization of a novel C-terminal inhibitor of Hsp90 in androgen dependent and independent prostate cancer cells. *BMC Cancer*, *11*(1), 468. https://doi.org/10.1186/1471-2407-11-468

Etique, N., Verzeaux, L., Dedieu, S., & Emonard, H. (2013). LRP-1 : A Checkpoint for the Extracellular Matrix Proteolysis. *BioMed Research International*, 1–7.

Eustace, B. K., & Jay, D. G. (2004). Extracellular Roles for the Molecular Chaperone, Hsp90. *Cell Cycle*, *3*(9), 1098–1100.

Eustace, B. K., Sakurai, T., Stewart, J. K., Yimlamai, D., Unger, C., Zehetmeier, C., … Jay, D. G. (2004). Functional proteomic screens reveal an essential extracellular role for hsp90 alpha in cancer cell invasiveness. *Nature Cell Biology*, *6*(6), 507–14.

https://doi.org/10.1038/ncb1131

Felts, S. J., Owen, B. A. L., Trepel, J., Donner, D. B., Toft, D. O., & Nguyen, P. (2000). The hsp90-related Protein TRAP1 Is a Mitochondrial Protein with Distinct Functional Properties. *The Journal of Biological Chemistry*, *275*, 3305–3312. https://doi.org/10.1074/jbc.275.5.3305

Fonović, M., & Turk, B. (2014). Cysteine cathepsins and extracellular matrix degradation. *Biochimica et Biophysica Acta*, *1840*(8), 2560–70. https://doi.org/10.1016/j.bbagen.2014.03.017

Forsyth, C. B., Pulai, J., & Loeser, R. F. (2002). Fibronectin fragments and blocking antibodies to alpha2beta1 and alpha5beta1 integrins stimulate mitogen-activated protein kinase signaling and increase collagenase 3 (matrix metalloproteinase 13) production by human articular chondrocytes. *Arthritis and Rheumatism*, *46*(9), 2368–2376. https://doi.org/10.1002/art.10502

Franco-Barraza, J., Francescone, R., Luong, T., Shah, N., Madhani, R., Cukierman, G., … Cukierman, E. (2017). Matrix-regulated integrin αvβ5 maintains α5β1-dependent desmoplastic traits prognostic of neoplastic recurrence. *ELife*, *6*, 1–46. https://doi.org/10.7554/eLife.20600

Frantz, C., Stewart, K. M., & Weaver, V. M. (2010). The extracellular matrix at a glance The Extracellular Matrix at a Glance. *Journal of Cell Science*, *2010*, 4195–4200. https://doi.org/10.1242/jcs.023820

Friedl, P., & Gilmour, D. (2009). Collective cell migration in morphogenesis, regeneration and cancer. *Nature Reviews. Molecular Cell Biology*, *10*(7), 445–57. https://doi.org/10.1038/nrm2720

Früh, S. M., Schoen, I., Ries, J., & Vogel, V. (2015). Molecular architecture of native fibronectin fibrils. *Nature Communications*, *6*. https://doi.org/10.1038/ncomms8275

Fulda, S., Gorman, A. M., Hori, O., & Samali, A. (2010). Cellular stress responses: cell survival and cell death. *International Journal of Cell Biology*, *2010*, 214074. https://doi.org/10.1155/2010/214074

Galante, L. L., & Schwarzbauer, J. E. (2007). Requirements for sulfate transport and the diastrophic dysplasia sulfate transporter in fibronectin matrix assembly. *The Journal of Cell Biology*, *179*(5), 999–1009. https://doi.org/10.1083/jcb.200707150

Garrido, C., Gurbuxani, S., Ravagnan, L., & Kroemer, G. (2001). Heat shock proteins: endogenous modulators of apoptotic cell death. *Biochemical and Biophysical Research Communications*, *286*(3), 433–442. https://doi.org/10.1006/bbrc.2001.5427

Gasperi, R. De, Sosa, M. A. G., & Elder, G. A. (2012). Presenilin-1 regulates the constitutive turnover of the fibronectin matrix in endothelial cells. *BMC Biochemistry*, *13*(28), 1–20. https://doi.org/10.1186/1471-2091-13-28

Gaultier, A., Arandjelovic, S., Li, X., Janes, J., Dragojlovic, N., Zhou, G. P., … Campana, W. M. (2008). A shed form of LDL receptor – related protein – 1 regulates peripheral nerve injury and neuropathic pain in rodents. *Journal of Clinical Investigation*, *118*(1), 161–172. https://doi.org/10.1172/JCI32371.In

Gaultier, A., Hollister, M., Reynolds, I., Hsieh, E., & Gonias, S. L. (2010). LRP1 regulates remodeling of the extracellular matrix by fibroblasts. *Matrix Biology : Journal of the International Society for Matrix Biology*, *29*(1), 22–30. https://doi.org/10.1016/j.matbio.2009.08.003

Gaultier, A., Salicioni, A. M., Arandjelovic, S., & Gonias, S. L. (2006). Regulation of the composition of the extracellular matrix by low density lipoprotein receptor-related protein-1: Activities based on regulation of mRNA expression. *Journal of Biological Chemistry*, *281*(11), 7332–7340. https://doi.org/10.1074/jbc.M511857200

Ghosh, S., Shinogle, H. E., Garg, G., Vielhauer, G. A., Holzbeierlein, M., Dobrowsky, R. T., & Blagg, B. S. J. (2015). Hsp90 C ‐ Terminal Inhibitors Exhibit Antimigratory Activity by Disrupting the Hsp90 α /Aha1 Complex in PC3-MM2 Cells.

González-Ramos, M., Calleros, L., López-Ongil, S., Raoch, V., Griera, M., Rodríguez-Puyol, M., … Rodríguez-Puyol, D. (2013). HSP70 increases extracellular matrix production by human vascular smooth muscle through TGF-β1 up-regulation. *The International Journal of Biochemistry & Cell Biology*, *45*(2), 232–42. https://doi.org/10.1016/j.biocel.2012.10.001

Gopal, U., Bohonowych, J. E., Lema-tome, C., Liu, A., Garrett-, E., Wang, B., & Isaacs, J. S. (2011). A Novel Extracellular Hsp90 Mediated Co-Receptor Function for LRP1 Regulates EphA2 Dependent Glioblastoma Cell Invasion. *PLoS ONE*, *6*(3), 1–14. https://doi.org/10.1371/journal.pone.0017649

Gorovoy, M., Gaultier, A., Campana, W. M., & Firestein, G. S. (2010). Inflammatory mediators promote production of shed LRP1 / CD91 , which regulates cell signaling and cytokine expression by macrophages. *Journal of Leukocyte Biology*, *88*(October), 769–778. https://doi.org/10.1189/jlb.0410220

Grad, I., Cederroth, C. R., Walicki, J., Grey, C., Barluenga, S., Winssinger, N., … Picard, D. (2010). The molecular chaperone hsp90a is required for meiotic progression of spermatocytes beyond pachytene in the mouse. *PLoS ONE*, *5*(12), 1–11. https://doi.org/10.1371/journal.pone.0015770

Grammatikakis, N., Vultur, A., Ramana, C. V, Siganou, A., Schweinfest, C. W., Watson, D. K., & Raptis, L. (2002). The Role of Hsp90N , a New Member of the Hsp90 Family , in Signal Transduction and Neoplastic Transformation. *The Journal of Biological Chemistry*, *277*, 8312–8320. https://doi.org/10.1074/jbc.M109200200

Grenert, J. P., Sullivan, W. P., Fadden, P., Haystead, T. a, Clark, J., Mimnaugh, E., … Toft, D. O. (1997). The amino-terminal domain of heat shock protein 90 (hsp90) that binds geldanamycin is an ATP/ADP switch domain that regulates hsp90 conformation. *The Journal of Biological Chemistry*, *272*(38), 23843–23850. Retrieved from http://www.ncbi.nlm.nih.gov/pubmed/9295332

Gutman, a, Yamada, K. M., & Kornblihtt, a. (1986). Human fibronectin is synthesized as a pre-propolypeptide. *FEBS Letters*, *207*(1), 145–148. Retrieved from http://www.sciencedirect.com/science/article/pii/0014579386800291

Guttman, M., Betts, G. N., Barnes, H., Ghassemian, M., Geer, P. Van Der, & Komives, E. A. (2009). Interactions of the NPXY microdomains of the LDL Receptor-Related Protein 1.

Proteomics, *9*(22), 5016–5028. https://doi.org/10.1002/pmic.200900457.Interactions

Haas, T. L. (2005). Endothelial cell regulation of matrix metalloproteinases. *Canadian Journal of Physiology and Pharmacology*, *83*(1), 1–7. https://doi.org/10.1139/y04-120

Haggerty, T. J., Dunn, I. S., Rose, L. B., Newton, E. E., Pandolfi, F., & Kurnick, J. T. (2014). Heat Shock Protein-90 Inhibitors Enhance Antigen Expression on Melanomas and Increase T Cell Recognition of Tumor Cells. *PLoS ONE*, *9*(12), 1–23. https://doi.org/10.1371/journal.pone.0114506

Hakkinen, K. M., Harunaga, J. S., Doyle, A. D., & Yamada, K. M. (2011). Direct Comparisons of the Morphology, Migration, Cell Adhesions, and Actin Cytoskeleton of Fibroblasts in Four Different Three-Dimensional Extracellular Matrices. *Tissue Engineering Part A*, *17*(5–6), 713–724. https://doi.org/10.1089/ten.tea.2010.0273

Hall, A. J., Seearala, S., Rice, N., Kopel, L., Halaweish, F., & Blagg, B. S. J. (2015). Cucurbitacin D Is a Disruptor of the HSP90 Chaperone Machinery. *J Nat Prod*, *78*(4), 873–879. https://doi.org/10.1016/j.trsl.2014.08.005.The

Halper, J., & Kjaer, M. (2014). Basic Components of Connective Tissues and Extracellular Matrix: Elastin, Fibrillin, Fibulins, Fibrinogen, Fibronectin, Laminin, Tenascins and Thrombospondins. In J. Halper (Ed.), *Progress in Heritable Soft Connective Tissue Diseases* (Vol. 802). Springer. https://doi.org/10.1007/978-94-007-7893-1

Hance, M. W., Dole, K., Gopal, U., Bohonowych, J. E., Jezierska-drutel, A., Neumann, C. A., … Isaacs, J. S. (2012). Secreted Hsp90 Is a Novel Regulator of the Epithelial to Mesenchymal Transition (EMT) in Prostate Cancer. *The Journal of Biological Chemistry*, *287*(45), 37732–37744. https://doi.org/10.1074/jbc.M112.389015

Hance, M. W., Nolan, K. D., & Isaacs, J. S. (2014). The Double-Edged Sword: Conserved Functions of Extracellular Hsp90 in Wound Healing and Cancer. *Cancers*, *6*, 1065–1097. https://doi.org/10.3390/cancers6021065

Hartl, F. U., & Hayer-Hartl, M. (2002). Molecular Chaperones in the Cytosol: from Nascent Chain to Folded Protein. *Science*, *295*, 1852–1858. https://doi.org/10.1126/science.1068408

Hartl, U., Bracher, A., & Hayer-hartl, M. (2011). Molecular chaperones in protein folding and proteostasis. *Nature*, *475*. https://doi.org/10.1038/nature10317

He, T., Bai, X., Yang, L., Fan, L., Li, Y., Su, L., & Gao, J. (2015). Loureirin B Inhibits Hypertrophic Scar Formation via Inhibition of the TGF- β 1- ERK / JNK Pathway, (127), 666–676. https://doi.org/10.1159/000430385

Hegmans, J. P. J. J., Bard, M. P. L., Hemmes, A., Luider, T. M., Kleijmeer, M. J., Prins, J.-B., … Lambrecht, B. N. (2004). Proteomic analysis of exosomes secreted by human mesothelioma cells. *The American Journal of Pathology*, *164*(5), 1807–1815. https://doi.org/10.1016/S0002-9440(10)63739-X

Hellewell, A. L., & Adams, J. C. (2015). Insider trading: Extracellular matrix proteins and their non-canonical intracellular roles. *BioEssays*, 77–88. https://doi.org/10.1002/bies.201500103

Hendrick, J., & Hartl, U. (1993). Molecular chaperone functions of heat-shock proteins. *Annual Review of Biochemistry, 62*(1), 349–384. https://doi.org/10.1146/annurev.bi.62.070193.002025

Herz, J., Goldstein, L., Stricklandn, K., & Brown, S. (1991). 39-kDa Protein Modulates Binding of Ligands to Low Density Lipoprotein Receptor-related Protein/α2-Macroglobulin Receptor*. *Journal of Biological Chemistry*, *266*(31), 21232–21236. Retrieved from http://www.jbc.org/content/266/31/21232

Herz, J., & Strickland, D. K. (2001). LRP: a multifunctional scavenger and signaling receptor. *J.Clin.Invest*, *108*(6), 779–784. https://doi.org/10.1172/JCI200113992.

Hocking, D. C., & Chang, C. H. (2003). Fibronectin matrix polymerization regulates small airway epithelial cell migration. *American Journal of Physiology-Lung Cellular and Molecular Physiology*, *285*(1), L169–L179. https://doi.org/10.1152/ajplung.00371.2002

Hocking, D. C., Sottile, J., & Langenbach, K. J. (2000). Stimulation of integrin-mediated cell contractility by fibronectin. *Journal of Biological Chemistry*, *275*(14), 10673–10682. https://doi.org/10.1074/jbc.275.14.10673

Horibe, T., Kohno, M., Haramoto, M., Ohara, K., & Kawakami, K. (2011). Designed hybrid TPR peptide targeting Hsp90 as a novel anticancer agent. *Journal of Translational Medicine*, *9*(1), 8. https://doi.org/10.1186/1479-5876-9-8

Hu, Q. D., Ang, B. T., Karsak, M., Hu, W. P., Cui, X. Y., Duka, T., … Xiao, Z. C. (2003). F3/contactin acts as a functional ligand for notch during oligodendrocyte maturation. *Cell*, *115*(2), 163–175. https://doi.org/10.1016/S0092-8674(03)00810-9

Hu, Y., & Mivechi, N. F. (2003). HSF-1 interacts with Ral-binding protein 1 in a stress-responsive, multiprotein complex with HSP90 in vivo. *Journal of Biological Chemistry*, *278*(19), 17299–17306. https://doi.org/10.1074/jbc.M300788200

Huang, G., & Greenspan, D. S. (2012). ECM roles in the function of metabolic tissues. *Trends in Endocrinology and Metabolism: TEM*, *23*(1), 16–22. https://doi.org/10.1016/j.tem.2011.09.006

Hunter, M. C., O'Hagan, K. L., Kenyon, A., Dhanani, K. C. H., Prinsloo, E., & Edkins, A. L. (2014). Hsp90 Binds Directly to Fibronectin (FN) and Inhibition Reduces the Extracellular Fibronectin Matrix in Breast Cancer Cells. *PLoS ONE*, *9*(1), e86842. https://doi.org/10.1371/journal.pone.0086842

Hussy, P., Maass, G., Tummler, B., Grosse, F., & Schomburg, U. (1986). Effect of 4-quinolones and novobiocin on calf thymus DNA polymerase α primase complex, topoisomerases I and II, and growth of mammalian lymphoblasts. *Antimicrobial Agents and Chemotherapy*, *29*(6), 1073–1078. https://doi.org/10.1128/AAC.29.6.1073

Huttenlocher, A., & Horwitz, A. R. (2011). Integrins in Cell Migration. In R. O. Hynes & K. M. Yamada (Eds.), *Additional Perspectives on Extracellular Matrix Biology* (pp. 1–16). Cold Spring Harb Perspect Biol. https://doi.org/10.1101/cshperspect.a005074

Hynes, R. O. (2009). The extracellular matrix: not just pretty fibrils. *Science*, *326*(5957), 1216–1219. https://doi.org/10.1126/science.1176009

Hynes, R. O., & Naba, A. (2012). Overview of the matrisome--an inventory of extracellular matrix constituents and functions. *Cold Spring Harbor Perspectives in Biology*, *4*(1), a004903. https://doi.org/10.1101/cshperspect.a004903

Iadonato, S. P., Bu, G., Maksymovitch, E., & Schwartz, A. (1993). Interaction of a 39 kDa protein with the low-density-lipoprotein-receptor-related protein (LRP) on rat hepatoma cells. *The Biochemical Journal*, *296*, 867–75. Retrieved from http://www.pubmedcentral.nih.gov/articlerender.fcgi?artid=1137774&tool=pmcentrez&rendertype=abstract

Infante, J. R., Weiss, G. J., Jones, S., Tibes, R., Bauer, T. M., Bendell, J. C., … Ramanathan, R. K. (2014). Phase i dose-escalation studies of SNX-5422, an orally bioavailable heat shock protein 90 inhibitor, in patients with refractory solid tumours. *European Journal of Cancer*, *50*(17), 2897–2904. https://doi.org/10.1016/j.ejca.2014.07.017

Ioachim, E., Charchanti, a, Briasoulis, E., Karavasilis, V., Tsanou, H., Arvanitis, D. ., … Pavlidis, N. (2002). Immunohistochemical expression of extracellular matrix components tenascin, fibronectin, collagen type IV and laminin in breast cancer: their prognostic value and role in tumour invasion and progression. *European Journal of Cancer*, *38*(18), 2362–2370. https://doi.org/10.1016/S0959-8049(02)00210-1

Jakob, U., Gaestel, M., Engel, K., & Buchner, J. (1993). Small heat shock proteins are molecular chaperones. *The Journal of Biological Chemistry*, *268*(3), 1517–1520.

Jayaprakash, P., Dong, H., Zou, M., Bhatia, A., O'Brien, K., Chen, M., … Li, W. (2015). Hsp90 and Hsp90 together operate a hypoxia and nutrient paucity stress-response mechanism during wound healing. *Journal of Cell Science*, *128*(8), 1475–1480. https://doi.org/10.1242/jcs.166363

Kadler, K. E., Holmes, D. F., Trotter, J. A., & Chapman, J. A. (1996). Collagen fibril formation. *Journal of Biochemistry*, *316*(Pt 1), 1–11.

Kamal, A., Thao, L., Sensintaffar, J., Zhang, L., Boehm, M. F., Fritz, L. C., & Burrows, F. J. (2003). A high-affinity conformation of Hsp90 confers tumour selectivity on Hsp90 inhibitors. *Nature*, *425*(6956), 407–10. https://doi.org/10.1038/nature01913

Kaukonen, R., Jacquemet, G., Hamidi, H., & Ivaska, J. (2017). Cell-derived matrices for studying cell proliferation and directional migration in a complex 3D microenvironment. *Nature Protocols*, *12*(11), 2376–2390. https://doi.org/10.1038/nprot.2017.107

KcKeown-Longo, P. J., & Mosher, D. F. (1985). Interaction of the 70,000-mol-wt amino-terminal fragment of fibronectin with the matrix-assembly receptor of fibroblasts. *Journal of Cell Biology*, *100*(2), 364–374. https://doi.org/10.1083/jcb.100.2.364

Kenny, H. A., Kaur, S., Coussens, L. M., & Lengyel, E. (2008). The initial steps of ovarian cancer cell metastasis are mediated by MMP-2 cleavage of vitronectin and fibronectin. *Journal of Clinical Investigation*, *118*(4), 1367–1379. https://doi.org/10.1172/JCI33775.degrade

Khalil, A. a, Kabapy, N. F., Deraz, S. F., & Smith, C. (2011). Heat shock proteins in oncology: diagnostic biomarkers or therapeutic targets? *Biochimica et Biophysica Acta*, *1816*(2),

89–104. https://doi.org/10.1016/j.bbcan.2011.05.001

Khandelwal, A., Kent, C. N., Balch, M., Peng, S., Mishra, S. J., Deng, J., … Blagg, B. S. J. (2018). Structure-guided design of an Hsp90β N-terminal isoform-selective inhibitor. *Nature Communications*, *9*(1), 1–7. https://doi.org/10.1038/s41467-017-02013-1

Kijima, T., Prince, T. L., Tigue, M. L., Yim, K. H., Schwartz, H., Beebe, K., … Neckers, L. (2018). HSP90 inhibitors disrupt a transient HSP90-HSF1 interaction and identify a noncanonical model of HSP90-mediated HSF1 regulation. *Scientific Reports*, *8*(1), 1–13. https://doi.org/10.1038/s41598-018-25404-w

Kim, Y., Hipp, M. S., Bracher, A., Hayer-Hartl, M., & Hartl, F. U. (2013). *Molecular chaperone functions in protein folding and proteostasis. Annual review of biochemistry* (Vol. 82). https://doi.org/10.1146/annurev-biochem-060208-092442

Kim, Y. S., Jung, D. H., Kim, N. H., Lee, Y. M., & Kim, J. S. (2007). Effect of magnolol on TGF-β1 and fibronectin expression in human retinal pigment epithelial cells under diabetic conditions. *European Journal of Pharmacology*, *562*(1–2), 12–19. https://doi.org/10.1016/j.ejphar.2007.01.048

Kimura, E., Kanzaki, T., Tahara, K., Hayashi, H., Hashimoto, S., Suzuki, A., … Sawada, T. (2014). Identification of citrullinated cellular fibronectin in synovial fluid from patients with rheumatoid arthritis. *Modern Rheumatology*, *24*(5), 766–769. https://doi.org/10.3109/14397595.2013.879413

Kinoshita, A., Shah, T., Tangredi, M. M., Strickland, D. K., & Hyman, B. T. (2003). The Intracellular Domain of the Low Density Lipoprotein Receptor-related Protein Modulates Transactivation Mediated by Amyloid Precursor Protein and Fe65 *. *The Journal of Biological Chemistry*, *278*(42), 41182–41188. https://doi.org/10.1074/jbc.M306403200

Koay, Y. C., McConnell, J. R., Wang, Y., Kim, S. J., Buckton, L. K., Mansour, F., & McAlpine, S. R. (2014). Chemically accessible hsp90 inhibitor that does not induce a heat shock response. *ACS Medicinal Chemistry Letters*, *5*(7), 771–776. https://doi.org/10.1021/ml500114p

Kounnas, M. Z., Moir, R. D., Rebeck, G. W., Bush, a I., Argraves, W. S., Tanzi, R. E., … Strickland, D. K. (1995). LDL receptor-related protein, a multifunctional ApoE receptor, binds secreted beta-amyloid precursor protein and mediates its degradation. *Cell*, *82*(2), 331–40. Retrieved from http://www.ncbi.nlm.nih.gov/pubmed/7543026

Kumazaki, T., Mitsui, Y., Hamada, K., Sumida, H., & Nishiyama, M. (1999). Detection of alternative splicing of fibronectin mRNA in a single cell. *Journal of Cell Science*, *112 (Pt 1*, 1449–53. Retrieved from http://www.ncbi.nlm.nih.gov/pubmed/10212139

Kummar, S., Gutierrax, E. ., Gardner, R. ., Chen, X., Figg, D. ., Zajac-kaye, M., … Murgo, J. . (2011). Phase I Trial of 17-Dimethylaminoethylamino-17- Demethoxygeldanamycin (17-DMAG), a Heat Shock Protein Inhibitor, Administered Twice Weekly in Patients with Advanced Malignancies. *European Journal of Cancer*, *46*(2), 1–15. https://doi.org/10.1016/j.ejca.2009.10.026.Phase

Kunwar, P. S., Siekhaus, D. E., & Lehmann, R. (2006). In Vivo Migration: A Germ Cell

Perspective. *Annual Review of Cell and Developmental Biology*, *22*(1), 237–265. https://doi.org/10.1146/annurev.cellbio.22.010305.103337

Labat-Robert, J. (2002). Fibronectin in malignancy. Effect of aging. *Biophotonics International*, *12*, 187–195. https://doi.org/10.1016/S1044

Laemmli, U. K. (1970). Cleavage of structural proteins during the assembly of the head of bacteriophage T4. *Nature*, *227*(5259), 680–685. https://doi.org/10.1038/227680a0

Lane, T. F., & Sage, E. H. (1994). The biology of SPARC, a protein that modulates cell-matrix interactions. *The FASEB Journal : Official Publication of the Federation of American Societies for Experimental Biology*, *8*(2), 163–173.

Lauwers, E., Wang, Y. C., Gallardo, R., Van der Kant, R., Michiels, E., Swerts, J., … Verstreken, P. (2018). Hsp90 Mediates Membrane Deformation and Exosome Release. *Molecular Cell*, *71*(5), 689–702.e9. https://doi.org/10.1016/j.molcel.2018.07.016

Leavesley, D. I., Kashyap, A. S., Croll, T., Sivaramakrishnan, M., Shokoohmand, A., Hollier, B. G., & Upton, Z. (2013). Vitronectin--master controller or micromanager? *IUBMB Life*, *65*(10), 807–18. https://doi.org/10.1002/iub.1203

Ledger, P. W., Uchida, N., & Tanzer, M. L. (1980). Immunocytochemical localization of procollagen and fibronectin in human fibroblasts: Effects of the monovalent lonophore, monensin. *Journal of Cell Biology*, *87*(3), 663–671. https://doi.org/10.1083/jcb.87.3.663

Lee, H. O., Mullins, S. R., Franco-Barraza, J., Valianou, M., Cukierman, E., & Cheng, J. D. (2011). FAP-overexpressing fibroblasts produce an extracellular matrix that enhances invasive velocity and directionality of pancreatic cancer cells. *BMC Cancer*, *11*(1), 245. https://doi.org/10.1186/1471-2407-11-245

Lee, T.-H., McKleroy, W., Khalifeh-Soltani, A., Sakuma, S., Lazarev, S., Riento, K., … Atabai, K. (2014). Functional genomic screen identifies novel mediators of collagen uptake. *Molecular Biology of the Cell*, *25*(5), 583–93. https://doi.org/10.1091/mbc.E13-07-0382

Lei, H., Romeo, G., & Kazlauskas, A. (2004). Heat Shock Protein 90α-Dependent Translocation of Annexin II to the Surface of Endothelial Cells Modulates Plasmin Activity in the Diabetic Rat Aorta. *Circulation Research*, *94*(7), 902–909. https://doi.org/10.1161/01.RES.0000124979.46214.E3

Lemańska-Perek, A., Leszek, J., Krzyanowska-Goląb, D., Radzik, J., & Kątnik-Prastowska, M. I. (2009). Molecular status of plasma fibronectin as an additional biomarker for assessment of alzheimer's dementia risk. *Dementia and Geriatric Cognitive Disorders*, *28*(4), 338–342. https://doi.org/10.1159/000252764

Lemmon, C. a, Ohashi, T., & Erickson, H. P. (2011). Probing the folded state of fibronectin type III domains in stretched fibrils by measuring buried cysteine accessibility. *The Journal of Biological Chemistry*, *286*(30), 26375–82. https://doi.org/10.1074/jbc.M111.240028

Lepelletier, F. X., Mann, D. M. A., Robinson, A. C., Pinteaux, E., & Boutin, H. (2017). Early changes in extracellular matrix in Alzheimer's disease. *Neuropathology and Applied Neurobiology*, *43*(2), 167–182. https://doi.org/10.1111/nan.12295

Li, J., & Buchner, J. (2013). Structure, function and regulation of the hsp90 machinery. *Biomedical Journal*, *36*(3), 106–17. https://doi.org/10.4103/2319-4170.113230

Li, J., Soroka, J., & Buchner, J. (2012). The Hsp90 chaperone machinery: Conformational dynamics and regulation by co-chaperones. *Biochimica et Biophysica Acta - Molecular Cell Research*, *1823*(3), 624–635. https://doi.org/10.1016/j.bbamcr.2011.09.003

Li, Q., Lau, A., Morris, T. J., Guo, L., Fordyce, C. B., & Stanley, E. F. (2004). A syntaxin 1, Galpha(o), and N-type calcium channel complex at a presynaptic nerve terminal: analysis by quantitative immunocolocalization. *The Journal of Neuroscience : The Official Journal of the Society for Neuroscience*, *24*(16), 4070–81. https://doi.org/10.1523/JNEUROSCI.0346-04.2004

Li, W., Li, Y., Guan, S., Fan, J., Cheng, C.-F., Bright, A. M., … Woodley, D. T. (2007). Extracellular heat shock protein-90alpha: linking hypoxia to skin cell motility and wound healing. *The EMBO Journal*, *26*(5), 1221–1233. https://doi.org/10.1038/sj.emboj.7601727

Li, W., Sahu, D., & Tsen, F. (2011). Secreted heat shock protein-90 (Hsp90) in wound healing and cancer. *Biochimica et Biophysica Acta (BBA)*, *1823*(3), 730–41. https://doi.org/10.1016/j.bbamcr.2011.09.009

Li, W., Tsen, F., Sahu, D., Bhatia, A., Chen, M., Multhoff, G., & Woodley, D. T. (2013). Extracellular Hsp90 (eHsp90) as the Actual Target in Clinical Trials: Intentionally or Unintentionally. *Int Rev Cell Mol Biol*, *303*, 203–235. https://doi.org/10.1016/B978-0-12-407697-6.00005-2.Extracellular

Li, Y., & C. Reynolds, R. (2012). LRP1: A Tumor and Metastasis Promoter or Suppressor? *Biochemistry & Pharmacology: Open Access*, *01*(05), 1–2. https://doi.org/10.4172/2167-0501.1000e121

Li, Z., Zhang, L., Zhao, Y., Li, H., Xiao, H., Fu, R., … Li, Z. (2013). Cell-surface GRP78 facilitates colorectal cancer cell migration and invasion. *The International Journal of Biochemistry & Cell Biology*, *45*(5), 987–94. https://doi.org/10.1016/j.biocel.2013.02.002

Liang, Y., Häring, M., Roughley, P. J., Margolis, R. K., & Margolis, R. U. (1997). Glypican and Biglycan in the Nuclei of Neurons and Glioma Cells: Presence of Functional Nuclear Localization Signals and Dynamic Changes in Glypican During the Cell Cycle, *139*(4), 851–864.

Lillis, A. P., Duyn, L. B. Van, Murphy-Ullrich, J. E., & Strickland, D. K. (2008). The low density lipoprotain receptor-related protein 1: Unique tissue-specifici functions revealed by selective gene knockout studies. *Physiol Rev*, *88*(3), 887–918. https://doi.org/10.1152/physrev.00033.2007.The

Lin, Q. C., & Bissell, M. J. (1993). Multi-faceted regulation of of cell differentiation by extracellular matrix. *The FASEB Journal*, *7*, 737–743.

Lin, Y., Peng, N., Zhuang, H., Zhang, D., Wang, Y., & Hua, Z. C. (2014). Heat shock proteins HSP70 and MRJ cooperatively regulate cell adhesion and migration through urokinase receptor. *BMC Cancer*, *14*, 639. https://doi.org/10.1186/1471-2407-14-639

Liu, B., Dai, J., Zheng, H., Stoilova, D., Sun, S., & Li, Z. (2003). Cell surface expression of an

endoplasmic reticulum resident heat shock protein gp96 triggers MyD88-dependent systemic autoimmune diseases. *Proceedings of the National Academy of Sciences of the United States of America*, *100*(26), 15824–9. https://doi.org/10.1073/pnas.2635458100

Liu, C. X., Ranganathan, S., Robinson, S., & Strickland, D. K. (2007). Gamma-secretase-mediated release of the low density lipoprotein receptor-related protein 1B intracellular domain suppresses anchorage- independent growth of neuroglioma cells. *Journal of Biological Chemistry*, *282*(10), 7504–7511. https://doi.org/10.1074/jbc.M608088200

Lochter, A., & Bissell, M. J. (1995). Involvement of extracellular matrix constituents in breast cancer. *Cancer Biology*, *6*, 165–173.

Lu, P., Takai, K., Weaver, V. M., & Werb, Z. (2011). Extracellular matrix degradation and remodeling in development and disease. *Cold Spring Harb Perspect Biol*, *3*(12). https://doi.org/10.1101/cshperspect.a005058

Lu, P., Weaver, V. M., & Werb, Z. (2012). The extracellular matrix: A dynamic niche in cancer progression. *Journal of Cell Biology*, *196*(4), 395–406. https://doi.org/10.1083/jcb.201102147

Lundgren, K., Zhang, H., Brekken, J., Huser, N., Powell, R. E., Timple, N., … Burrows, F. J. (2009). BIIB021, an orally available, fully synthetic small-molecule inhibitor of the heat shock protein Hsp90. *Molecular Cancer Therapeutics*, *8*(4), 921–929. https://doi.org/10.1158/1535-7163.MCT-08-0758

Mao, H., Lockyer, P., Townley-tilson, W. H. D., Xie, L., & Pi, X. (2015). LRP1 Regulates Retinal Angiogenesis by Inhibiting PARP-1 Activity and Endothelial Cell Proliferation. *Arteriosclerosis, Thrombosis, and Vascular Biology*, *36*(2), 350–360. https://doi.org/10.1161/ATVBAHA.115.306713

Marambaud, P., Shioi, J., Serban, G., Georgakopoulos, A., Sarner, S., Nagy, V., … Robakis, N. K. (2002). A presenilin-1/gamma-secretase cleavage releases the E-cadherin intracellular domain and regulates disassembly of adherens junctions. *EMBO Journal*, *21*(8), 1948–1956. https://doi.org/10.1093/emboj/21.8.1948

Marambaud, P., Wen, P. H., Dutt, A., Shioi, J., Takashima, A., Siman, R., & Robakis, N. K. (2003). A CBP binding transcriptional repressor produced by the PS1/ e-cleavage of N-Cadherin is inhibited by PS1 FAD mutations. *Cell*, *114*(5), 635–645. https://doi.org/10.1016/j.cell.2003.08.008

Marcu, M. G., Schulte, T. W., & Neckers, L. (2000). Novobiocin and related coumarins and depletion of heat shock protein 90-dependent signaling proteins. *Journal of the National Cancer Institute*, *92*(3), 242–8. Retrieved from http://www.ncbi.nlm.nih.gov/pubmed/10655441

Martinek, N., Shahab, J., Sodek, J., & Ringuette, M. (2007). Is an Evolutionarily Conserved Collagen Chaperone ? *J Dent Res*, *86*(4), 296–305.

Matsuo, M., Sakurai, H., Ueno, Y., Ohtani, O., & Saiki, I. (2006). Activation of MEK / ERK and PI3K / Akt pathways by fibronectin requires integrin α v-mediated ADAM activity in hepatocellular carcinoma : A novel functional target for gefitinib, *97*(2), 155–162.

https://doi.org/10.1111/j.1349-7006.2006.00152.x

May, P., Reddy, Y. K., & Herz, J. (2002). Proteolytic processing of low density lipoprotein receptor-related protein mediates regulated release of its intracellular domain. *The Journal of Biological Chemistry*, *277*(21), 18736–43. https://doi.org/10.1074/jbc.M201979200

May, P., Rohlmann, A., Bock, H. H., Zurhove, K., Marth, J. D., Schomburg, E. D., … Herz, J. (2004). Neuronal LRP1 Functionally Associates with Postsynaptic Proteins and Is Required for Normal Motor Function in Mice, *24*(20), 8872–8883. https://doi.org/10.1128/MCB.24.20.8872

Mayer, M., Nikolay, R., & Bukau, B. (2002). Aha , Another Regulator for Hsp90 Chaperones. *Molecular Cell*, *10*, 1255–1256.

Mayer, M. P., & Bukau, B. (2005). Hsp70 chaperones: Cellular functions and molecular mechanism. *Cellular and Molecular Life Sciences*, *62*(6), 670–684. https://doi.org/10.1007/s00018-004-4464-6

McCarthy, J. B., & Furcht, L. T. (1984). Laminin and Fibronectin Promote the Haptotactic Migration of B16 Mouse Melanoma Cells In Vitro. *Journal of Cell Biology*, *98*, 1474–1480.

McConnell, J. R., Alexander, L. A., & Mcalpine, S. R. (2015). A heat shock protein 90 inhibitor that modulates the immunophilins and regulates hormone receptors without inducing the heat shock response. *Bioorg Med Chem Lett*, *24*(2), 661–666. https://doi.org/10.1016/j.bmcl.2013.11.059.A

McCready, J., Sims, J. D., Chan, D., & Jay, D. G. (2010). Secretion of extracellular hsp90α via exosomes increases cancer cell motility : a role for plasminogen activation. *BMC Cancer*, *10*(294), 1–10. Retrieved from http://www.biomedcentral.com/1471-2407/10/294%0APage

McCready, J., Wong, D. S., Burlison, J. a, Ying, W., & Jay, D. G. (2014). An Impermeant Ganetespib Analog Inhibits Extracellular Hsp90-Mediated Cancer Cell Migration that Involves Lysyl Oxidase 2-like Protein. *Cancers*, *6*(2), 1031–46. https://doi.org/10.3390/cancers6021031

Mcdonald, J. A., Kelley, D. G., & Broekelmann, T. J. (1984). Role of Fibronectin in Collagen Deposition : Fab ' to the Gelatin-binding Domain of Fibronectin Inhibits Both Fibronectin and Collagen Organization in Fibroblast Extracellular Matrix Isolation of Procollagens and Collagen for Absorption of Antisera. *Journal of Cell Biology*, *92*(29), 485–492.

McKeown-Longo, P. J., & Mosher, D. F. (1985). Interaction of the 70,000-mol-wt amino-terminal fragment of fibronectin with the matrix-assembly receptor of fibroblasts. *The Journal of Cell Biology*, *100*(2), 364–74. Retrieved from http://www.pubmedcentral.nih.gov/articlerender.fcgi?artid=2113439&tool=pmcentrez&rendertype=abstract

Mikhailenko, I., Battey, F. D., Migliorini, M., Ruiz, J. F., Argraves, K., Moayeri, M., & Strickland, D. K. (2001). Recognition of alpha 2-macroglobulin by the low density

lipoprotein receptor-related protein requires the cooperation of two ligand binding cluster regions. *The Journal of Biological Chemistry*, *276*(42), 39484–91. https://doi.org/10.1074/jbc.M104382200

Morgan, M. R., Humphries, M. J., & Bass, M. D. (2007). Synergistic control of cell adhesion by integrins and syndecans, *8*(december). https://doi.org/10.1038/nrm2289

Mosher, D. F., Fogerty, F. J., Chernousov, M. a, & Barry, E. L. (1991). Assembly of fibronectin into extracellular matrix. *Annals of the New York Academy of Sciences*, *614*(V), 167–80. Retrieved from http://www.ncbi.nlm.nih.gov/pubmed/1673833

Mouw, J. K., Ou, G., & Weaver, V. M. (2014). Extracellular matrix assembly: a multiscale deconstruction. *Nature Reviews. Molecular Cell Biology*, *15*(12), 771–785. https://doi.org/10.1038/nrm3902

Nagai, N., Hosokawa, M., Itohara, S., Adachi, E., Matsushita, T., Hosokawa, N., & Nagata, K. (2000). Embryonic lethality of molecular chaperone Hsp47 knockout mice is associated with defects in collagen biosynthesis. *Journal of Cell Biology*, *150*(6), 1499–1505. https://doi.org/10.1083/jcb.150.6.1499

Nagaraju, G. P., Long, T.-E., Park, W., Landry, J. C., Taliaferro-Smith, L., Farris, A. B., … El-Rayes, B. F. (2014). Heat shock protein 90 promotes epithelial to mesenchymal transition, invasion, and migration in colorectal cancer. *Molecular Carcinogenesis*, *1158*(April), 1–12. https://doi.org/10.1002/mc.22185

Nakajima, C., Haffner, P., Goerke, S. M., Zurhove, K., Adelmann, G., Frotscher, M., … May, P. (2014). The lipoprotein receptor LRP1 modulates sphingosine-1- phosphate signaling and is essential for vascular development, 4513–4525. https://doi.org/10.1242/dev.109124

Narayanan, K., Ramachandran, A., Hao, J., He, G., Park, K. W., Cho, M., & George, A. (2003). Dual functional roles of dentin matrix protein 1. Implications in biomineralization and gene transcription by activation of intracellular Ca2+ store. *Journal of Biological Chemistry*, *278*(19), 17500–17508. https://doi.org/10.1074/jbc.M212700200

Neckers, L., Blagg, B., Haystead, T., Trepel, J. B., Whitesell, L., & Picard, D. (2018). Methods to validate Hsp90 inhibitor specificity , to identify off-target effects , and to rethink approaches for further clinical development. *Cell Stress and Chaperones*. https://doi.org/10.1007/s12192-018-0877-2

Nemoto, T., & Sato, N. (1998). Oligomeric forms of the 90-kDa heat shock protein. *The Biochemical Journal*, *330 (Pt 2*, 989–95. Retrieved from http://www.pubmedcentral.nih.gov/articlerender.fcgi?artid=1219235&tool=pmcentrez&rendertype=abstract

Obermann, W. M. J., Sondermann, H., Russo, A. A., Pavletich, N. P., & Hartl, F. U. (1998). In Vivo Function of Hsp90 Is Dependent on ATP Binding and ATP Hydrolysis, *143*(4), 901–910.

Obermoeller-McCormick, L. M., Li, Y., Osaka, H., Fitzgerald, D. J., Schwartz, A. L., & Bu, G. (2000). Dissection of receptor folding and ligand-binding property with functional minireceptors of LDL receptor-related protein. *Journal of Cell Science*, *114*, 899–908.

Ohashi, T., & Erickson, H. P. (2009). Revisiting the mystery of fibronectin multimers: the fibronectin matrix is composed of fibronectin dimers cross-linked by non-covalent bonds. *Matrix Biology : Journal of the International Society for Matrix Biology*, *28*(3), 170–5. https://doi.org/10.1016/j.matbio.2009.03.002

Ohkubo, S., Kodama, Y., Muraoka, H., Hitotsumachi, H., Yoshimura, C., Kitade, M., … Yonekura, K. (2015). TAS-116, a Highly Selective Inhibitor of Heat Shock Protein 90 and , Demonstrates Potent Antitumor Activity and Minimal Ocular Toxicity in Preclinical Models. *Molecular Cancer Therapeutics*, *14*(1), 14–22. https://doi.org/10.1158/1535-7163.MCT-14-0219

Oskarsson, T., Acharyya, S., Zhang, X. H.-F., Vanharanta, S., Tavazoie, S. F., Morris, P. G., … Massagué, J. (2011). Breast cancer cells produce tenascin C as a metastatic niche component to colonize the lungs. *Nature Medicine*, *17*(7), 867–74. https://doi.org/10.1038/nm.2379

Panaretou, B., Siligardi, G., Meyer, P., Maloney, A., Sullivan, J. K., Singh, S., … Prodromou, C. (2002). Activation of the ATPase activity of Hsp90 by the stress-regulated cochaperone Aha1. *Molecular Cell*, *10*(6), 1307–1318. https://doi.org/10.1016/S1097-2765(02)00785-2

Pasqualato, A., Lei, V., Cucina, A., Dinicola, S., D'Anselmi, F., Proietti, S., … Bizzarri, M. (2013). Shape in migration: Quantitative image analysis of migrating chemoresistant HCT-8 colon cancer cells. *Cell Adhesion and Migration*, *7*(5), 450–459. https://doi.org/10.4161/cam.26765

Patwardhan, C. A., Fauq, A., Peterson, L. B., Miller, C., Blagg, B. S. J., & Chadli, A. (2013). Gedunin inactivates the co-chaperone p23 protein causing cancer cell death by apoptosis. *Journal of Biological Chemistry*, *288*(10), 7313–7325. https://doi.org/10.1074/jbc.M112.427328

Pearl, L. H. (2005). Hsp90 and Cdc37 - A chaperone cancer conspiracy. *Current Opinion in Genetics and Development*, *15*(1), 55–61. https://doi.org/10.1016/j.gde.2004.12.011

Pepin, K., Momose, F., Ishida, N., & Nagata, K. (2000). Molecular Cloning of Horse Hsp90 cDNA and Its Comparative Analysis with Other Vertebrate Hsp90 Sequences. *J.Vet. Med. Sci.*, *63*(2), 115–124.

Perdew, G. H., & Whitelaw, M. L. (1991). Evidence that the 90-kDa heat shock protein (HSP90) exists in cytosol in heteromeric complexes containing HSP70 and three other proteins with Mr of 63,000, 56,000, and 50,000. *Journal of Biological Chemistry*, *266*(11), 6708–6713.

Pickup, M. W., Mouw, J. K., & Weaver, V. M. (2014). The extracellular matrix modulates the hallmarks of cancer. *EMBO Reports*, *15*(12), 1243–53. https://doi.org/10.15252/embr.201439246

Pimienta, G., Herbert, M. ., & Regan, L. (2011). A compound that inhibits the HOP-Hsp90 complex formation and has unique killing effects in breast cancer cell lines. *Molecular Pharmeceutics*, *8*, 2252–2261. https://doi.org/10.1021/mp200346y

Piper, P. W., & Millson, S. H. (2011). Mechanisms of Resistance to Hsp90 Inhibitor Drugs: A

Complex Mosaic Emerges. *Pharmaceuticals*, *4*, 1400–1422. https://doi.org/10.3390/ph4111400

Polavarapu, R., An, J., Zhang, C., & Yepes, M. (2008). Regulated Intramembrane Proteolysis of the Low-Density Lipoprotein Receptor-Related Protein Mediates Ischemic Cell Death. *The American Journal of Pathology*, *172*(5), 1355–1362. https://doi.org/10.2353/ajpath.2008.070975

Pratt, B. (1998). The hsp90-based Chaperone System : Involvement in Signal Transduction from a variety of hormone and growth factor receptors. *Society for Experimental Biology and Medicin*, *217*.

Preissner, K.T. and Reuning, U. (2011). Vitronectin in vascular context: facets of a multitalented matricellular protein. In *Seminars in thrombosis and hemostasis* (pp. 408–424).

Prodromou, C., Roe, S. M., Brien, R. O., Ladbury, J. E., Piper, P. W., & Pearl, L. H. (1997). Identification and Structural Characterization of the ATP / ADP-Binding Site in the Hsp90 Molecular Chaperone. *Cell*, *90*, 65–75.

Qin, D., Zhang, G.-M., Xu, X., & Wang, L.-Y. (2015). The PI3K/Akt signaling pathway mediates the high glucose-induced expression of extracellular matrix molecules in human retinal pigment epithelial cells. *Journal of Diabetes Research*, *2015*, 1–11. https://doi.org/10.1155/2015/920280

Quinn, K. A., Pye, V. J., Dai, Y., Chesterman, C. N., Owensby, D. A., & Al, Q. E. T. (1999). Characterization of the Soluble Form of the Low Density Lipoprotein Receptor-Related Protein (LRP). *Experimental Cell Research*, *251*, 433–441.

Quiros, R. M., Valianou, M., Kwon, Y., Brown, K. M., Godwin, A. K., & Cukierman, E. (2008). Ovarian normal and tumor-associated fibroblasts retain in vivo stromal charactersistics in a 3D matrix-dependent manner. *Gynecol Oncol*, *110*(1), 99–109. https://doi.org/10.1016/j.ygyno.2008.03.006.Ovarian

Ravindran, S., Gao, Q., Ramachandran, A., Blond, S., Predescu, A. ., & George, A. (2011). Stress chaperone Grp78 functions in mineralized matrix formation. *Journal of Biological Chemistry*, *286*(11), 8729–8739.

Reyes-del Valle, J., Chavez-Salinas, S., Medina, F., & del Ange, R. (2005). Heat Shock Protein 90 and Heat Shock Protein 70 Are Components of Dengue Virus Receptor Complex in Human Cells. *Journal of Virology*, *79*(8), 4557–4567. https://doi.org/10.1128/JVI.79.8.4557

Rezakhaniha, R., Agianniotis, A., Schrauwen, J. T. C., Griffa, A., Sage, D., Bouten, C. V. C., … Stergiopulos, N. (2012). Experimental investigation of collagen waviness and orientation in the arterial adventitia using confocal laser scanning microscopy. *Biomechanics and Modeling in Mechanobiology*, *11*(3–4), 461–473. https://doi.org/10.1007/s10237-011-0325-z

Richter, K., & Buchner, J. (2011). Closing in on the Hsp90 chaperone-client relationship. *Structure*, *19*(4), 445–446. https://doi.org/10.1016/j.str.2011.03.007

Ritossa, F. (1962). A new puffing pattern induced by temperature shock and DNP in

drosophila. *Experientia*, *18*(12), 571–573. https://doi.org/10.1007/BF02172188

Robinson, B. K., Cortes, E., Rice, A. J., Sarper, M., & del Río Hernández, A. (2016). Quantitative analysis of 3D extracellular matrix remodelling by pancreatic stellate cells. *Biology Open*, *5*(6), 875–882. https://doi.org/10.1242/bio.017632

Rodina, A., Wang, T., Yan, P., Gomes, E. D., Dunphy, M. P. S., Pillarsetty, N., … Chiosis, G. (2016). The epichaperome is an integrated chaperome network that facilitates tumour survival. *Nature*, *538*(7625), 397–401. https://doi.org/10.1038/nature19807

Roe, S. M., Prodromou, C., O'Brien, R., Ladbury, J. E., Piper, P. W., & Pearl, L. H. (1999). Structural Basis for Inhibition of the Hsp90 Molecular Chaperone by the Antitumor Antibiotics Radicicol and Geldanamycin. *J. Med. Chem.*, *42*(2), 260–266. https://doi.org/10.1021/jm980403y

Röhl, A., Rohrberg, J., & Buchner, J. (2013). The chaperone Hsp90: changing partners for demanding clients. *Trends in Biochemical Sciences*, *38*(5), 253–62. https://doi.org/10.1016/j.tibs.2013.02.003

Rozanov, D. V., Hahn-Dantona, E., Strickland, D. K., & Strongin, A. Y. (2004). The Low Density Lipoprotein Receptor-related Protein LRP Is Regulated by Membrane Type-1 Matrix Metalloproteinase (MT1-MMP) Proteolysis in Malignant Cells. *Journal of Biological Chemistry*, *279*(6), 4260–4268. https://doi.org/10.1074/jbc.M311569200

Rozario, T., & DeSimone, D. W. (2010). The extracellular matrix in development and morphogenesis: a dynamic view. *Developmental Biology*, *341*(1), 126–40. https://doi.org/10.1016/j.ydbio.2009.10.026

Rucci, N., Rufo, A., Alamanou, M., Capulli, M., Fattore, A. Del, Åhrman, E., … Teti, A. (2009). The glycosaminoglycan-binding domain of PRELP acts as a cell type–specific NF- B inhibitor that impairs osteoclastogenesis, *187*(5), 669–683. https://doi.org/10.1083/jcb.200906014

Ruckova, E. V. A., Muller, P., & Nenutil, R. (2012). Alterations of the Hsp70/Hsp90 chaperone and the HOP/CHIP co-chaperone system in cancer. *Celluar and Molecular Biology Letters*, *17*, 446–458. https://doi.org/10.2478/s11658-012-0021-8

Rukosuev, V. S., Nanaev, A. K., & Milovanov, A. P. (1990). Participation of collagen types I, III, IV, V, and fibronectin in the formation of villi fibrosis in human term placenta. *Acta Histochemica*, *89*(1), 11–16. https://doi.org/10.1016/S0065-1281(11)80308-9

Salicioni, A. M., Gaultier, A., Brownlee, C., Cheezum, M. K., & Gonias, S. L. (2004). Low Density Lipoprotein Receptor-related Protein-1 Promotes 1 Integrin Maturation and Transport to the Cell Surface. *The Journal of Biological Chemistry*, *279*(11), 10005–10012. https://doi.org/10.1074/jbc.M306625200

Salicioni, A. M., Mizelle, K. S., Loukinova, E., Mikhailenko, I., Strickland, D. K., & Gonias, S. L. (2002). The low density lipoprotein receptor-related protein mediates fibronectin catabolism and inhibits fibronectin accumulation on cell surfaces. *Journal of Biological Chemistry*, *277*(18), 16160–16166. https://doi.org/10.1074/jbc.M201401200

Salicioni, A. M., Mizelle, K. S., Mikhailenko, I., Dudley, K., Gonias, S. L., Loukinova, E., & Strickland, D. K. (2002). The Low Density Lipoprotein Receptor-related Protein

Mediates Fibronectin Catabolism and Inhibits Fibronectin Accumulation on Cell Surfaces The Low Density Lipoprotein Receptor-related Protein Mediates Fibronectin. *The Journal of Biological Chemistry*, *277*(18), 16160–16166. https://doi.org/10.1074/jbc.M201401200

Sambrano, J., Sklar, L. A., Houston, J. P., Sambrano, J., Chigaev, A., Nichani, K. S., … Sklar, L. A. (2018). Evaluating integrin activation with time-resolved flow cytometry. *Journal of Biomedical Optics*, *23*(07), 1. https://doi.org/10.1117/1.JBO.23.7.075004

Sato, N., Yamamoto, T., Sekine, Y., Yumioka, T., Junicho, A., Fuse, H., & Matsuda, T. (2003). Interaction between STAT3 and Hsp90. *Biochemical and Biophysical Research Communications*, *300*(4), 847–852.

Sato, S., Fujita, N., & Tsuruo, T. (2000). Modulation of Akt kinase activity by binding to Hsp90. *Proceedings of the National Academy of Sciences*, *97*(20), 10832–10837. https://doi.org/10.1073/pnas.170276797

Schwarzbauer, J. E. (1991). Fibronectin: from gene to protein. *Current Opinion in Cell Biology*, *3*(5), 786–91. Retrieved from http://www.ncbi.nlm.nih.gov/pubmed/1931080

Schwarzbauer, J. E., & DeSimone, D. W. (2011). Fibronectins, their fibrillogenesis, and in vivo functions. *Cold Spring Harbor Perspectives in Biology*, *3*(7), 1–19. https://doi.org/10.1101/cshperspect.a005041

Schwarzbauer, J. E., & Sechler, J. L. (1999). Fibronectin fibrillogenesis: a paradigm for extracellular matrix assembly. *Current Opinion in Cell Biology*, *11*(5), 622–627. Retrieved from http://www.ncbi.nlm.nih.gov/pubmed/10508649

Schweinfest, C. W., Graber, M. W., Henderson, K. W., Papas, T. S., Baron, P. L., & Watson, D. K. (1998). Cloning and sequence analysis of Hsp89 αN, a new member of the Hsp90 gene family. *Biochimica et Biophysica Acta*, 18–24.

Setati, M. M., Prinsloo, E., Longshaw, V. M., Murray, P. A., Edgar, D. H., & Blatch, G. L. (2010). Leukemia Inhibitory Factor Promotes Hsp90 Association with STAT3 in Mouse Embryonic Stem Cells, *62*(January), 61–66. https://doi.org/10.1002/iub.283

Shelton, S. N., Shawgo, M. E., Matthews, S. B., Lu, Y., Donnelly, A. C., Szabla, K., … Robertson, J. D. (2009). KU135 , a Novel Novobiocin-Derived C-Terminal Inhibitor of the 90-kDa Heat Shock Protein , Exerts Potent Antiproliferative Effects in Human Leukemic Cells, *76*(6), 1314–1322. https://doi.org/10.1124/mol.109.058545.associated

Shi, F., & Sottile, J. (2008). Caveolin-1-dependent beta1 integrin endocytosis is a critical regulator of fibronectin turnover. *Journal of Cell Science*, *121*(Pt 14), 2360–2371. https://doi.org/10.1242/jcs.014977

Shi, F., & Sottile, J. (2011). MT1-MMP regulates the turnover and endocytosis of extracellular matrix fibronectin. *Journal of Cell Science*, *124*(23), 4039–4050. https://doi.org/10.1242/jcs.087858

Shimamura, T., Perera, S. A., Foley, K. P., Sang, J., Rodig, S. J., Inoue, T., … Shapiro, G. I. (2012). Ganetespib (STA-9090), a nongeldanamycin HSP90 inhibitor, has potent antitumor activity in in vitro and in vivo models of non-small cell lung cancer. *Clinical Cancer Research*, *18*(18), 4973–4985. https://doi.org/10.1158/1078-0432.CCR-11-2967

Shin, B. K., Wang, H., Yim, A. M., Le Naour, F., Brichory, F., Jang, J. H., … Hanash, S. M. (2003). Global profiling of the cell surface proteome of cancer cells uncovers an abundance of proteins with chaperone function. *Journal of Biological Chemistry*, *278*(9), 7607–7616. https://doi.org/10.1074/jbc.M210455200

Shyu, Y. J., Liu, H., Deng, X., & Hu, C. (2006). Identification of new fluorescent protein fragments for bimolecular fluorescence complementation analysis under physiological conditions. *BioTechniques*, *40*, 61–66. https://doi.org/10.2144/000112036

Sidera, K., El Hamidieh, A., Mamalaki, A., & Patsavoudi, E. (2011). The 4C5 cell-impermeable anti-HSP90 antibody with anti-cancer activity, is composed of a single light chain dimer. *PloS One*, *6*(9), e23906. https://doi.org/10.1371/journal.pone.0023906

Sidera, K., Gaitanou, M., Stellas, D., Matsas, R., & Patsavoudi, E. (2008). A critical role for HSP90 in cancer cell invasion involves interaction with the extracellular domain of HER-2. *The Journal of Biological Chemistry*, *283*(4), 2031–41. https://doi.org/10.1074/jbc.M701803200

Sidera, K., & Patsavoudi, E. (2014). HSP90 inhibitors: current development and potential in cancer therapy. *Recent Patents on Anti-Cancer Drug Discovery*, *9*(1), 1–20. Retrieved from http://www.ncbi.nlm.nih.gov/pubmed/23312026

Sidera, K., Samiotaki, M., Yfanti, E., Panayotou, G., & Patsavoudi, E. (2004). Involvement of cell surface HSP90 in cell migration reveals a novel role in the developing nervous system. *Journal of Biological Chemistry*, *279*(44), 45379–45388. https://doi.org/10.1074/jbc.M405486200

Silverstein, A. M., Grammatikakis, N., Cochran, B. H., Chinkers, M., & Pratt, W. B. (1998). p50(cdc37) binds directly to the catalytic domain of Raf as well as to a site on hsp90 that is topologically adjacent to the tetratricopeptide repeat binding site. *Journal of Biological Chemistry*, *273*(32), 20090–20095. https://doi.org/10.1074/jbc.273.32.20090

Sims, J. D., McCready, J., & Jay, D. G. (2011). Extracellular heat shock protein (Hsp)70 and Hsp90α assist in matrix metalloproteinase-2 activation and breast cancer cell migration and invasion. *PloS One*, *6*(4), e18848. https://doi.org/10.1371/journal.pone.0018848

Singh, P., Carraher, C., & Schwarzbauer, J. E. (2010). Assembly of fibronectin extracellular matrix. *Annual Review of Cell and Developmental Biology*, *26*, 397–419. https://doi.org/10.1016/S0959-440X(05)80155-1

Sittler, A., Lurz, R., Lueder, G., Priller, J., Lehrach, H., Hayer-Hartl, M. K., … Wanker, E. E. (2001). Geldanamycin activates a heat shock response and inhibits huntingtin aggregation in a cell culture model of Huntington's disease. *Human Molecular Genetics*, *10*(12), 1307–1315. https://doi.org/10.1093/hmg/10.12.1307

Sodek, J., Ganss, B., & McKee, D. . (2000). Osteopontin. *Crit Rev Oral Biol Med*, *1*(3), 279–303.

Solit, D. B., & Chiosis, G. (2008). Development and application of Hsp90 inhibitors. *Drug Discovery Today*, *13*(1–2), 38–43. https://doi.org/10.1016/j.drudis.2007.10.007

Somanath, P. R., Kandel, E. S., Hay, N., & Byzova, T. V. (2007). Akt1 Signaling Regulates Integrin Activation, Matrix Recognition, and Fibronectin Assembly. *Journal of Biological*

Chemistry, *282*(31), 22964–22976. https://doi.org/10.1074/jbc.M700241200

Song, H., Li, Y., Lee, J., Schwartz, A. L., & Bu, G. (2009). Low-Density Lipoprotein Receptor-Related Protein 1 Promotes Cancer Cell Migration and Invasion by Inducing the Expression of Matrix Metalloproteinases 2 and 9. *Cancer Research*, *69*(3), 879–887. https://doi.org/10.1158/0008-5472.CAN-08-3379

Song, X., Wang, X., Zhuo, W., Shi, H., Feng, D., Sun, Y., … Luo, Y. (2010). The regulatory mechanism of extracellular Hsp90{alpha} on matrix metalloproteinase-2 processing and tumor angiogenesis. *The Journal of Biological Chemistry*, *285*(51), 40039–49. https://doi.org/10.1074/jbc.M110.181941

Sottile, J., & Chandler, J. (2005). Fibronectin matrix turnover occurs through a caveolin-1-dependent process. *Molecular Biology of the Cell*, *16*(2), 757–68. https://doi.org/10.1091/mbc.E04-08-0672

Sottile, J., & Hocking, D. C. (2002). Fibronectin Polymerization Regulates the Composition and Stability of Extracellular Matrix Fibrils and Cell-Matrix Adhesions. *Molecular Biology of the Cell*, *13*, 3546–3559. https://doi.org/10.1091/mbc.E02

Sottile, J., Hocking, D. C., & Langenbach, K. J. (2000). Fibronectin polymerization stimulates cell growth by RGD-dependent and -independent mechanisms. *Journal of Cell Science*, *113 Pt 23*, 4287–99. Retrieved from http://www.ncbi.nlm.nih.gov/pubmed/11069773

Soucy, P. A., & Romer, L. H. (2009). Endothelial cell adhesion, signaling, and morphogenesis in fibroblast-derived matrix. *Matrix Biology*, *28*(5), 273–283. https://doi.org/10.1016/j.matbio.2009.04.005

Spuch, C., Ortolano, S., & Navarro, C. (2012). LRP-1 and LRP-2 receptors function in the membrane neuron . Trafficking mechanisms and proteolytic processing in Alzheimer ' s disease. *Frontiers in Membrane Physiology and Biophysics*, *3*(269), 1–14. https://doi.org/10.3389/fphys.2012.00269

Sreedhar, A. S., & Csermely, P. (2004). Heat shock proteins in the regulation of apoptosis: new strategies in tumor therapy: a comprehensive review. *Pharmacology & Therapeutics*, *101*(3), 227–57. https://doi.org/10.1016/j.pharmthera.2003.11.004

Sreeramulu, S., Gande, S. L., Göbel, M., & Schwalbe, H. (2009). Molecular mechanism of inhibition of the human protein complex Hsp90-Cdc37, a kinome chaperone-cochaperone, by triterpene celastrol. *Angewandte Chemie - International Edition*, *48*(32), 5853–5855. https://doi.org/10.1002/anie.200900929

Steeg, P. S. (2006). Tumor metastasis: mechanistic insights and clinical challenges. *Nature Medicine*, *12*(8), 895–904. https://doi.org/10.1038/nm1469

Stellas, D., El Hamidieh, A., & Patsavoudi, E. (2010). Monoclonal antibody 4C5 prevents activation of MMP2 and MMP9 by disrupting their interaction with extracellular HSP90 and inhibits formation of metastatic breast cancer cell deposits. *BMC Cell Biology*, *11*, 51. https://doi.org/10.1186/1471-2121-11-51

Strickland, K.D., Kounnas, Maria.Z., Argraves, S. (1995). LDL receptor-related for lipoprotein protein : a multiligand catabolism receptor and proteinase. *FASEB Journal*, *9*, 890–898.

Strickland, D. K., Ashcorns, J. D., Williams, S., Burgessq, W. H., Migliorinis, M., & Argravess, W. S. (1990). Sequence Identity between the α2- Macroglobulin Receptor and Low Density Lipoprotein Receptor- related Protein Suggests That This Molecule Is a Multifunctional Receptor*. *Journal of Biological Chemistry*, *265*(29), 17401–17405.

Sung, B. H., Ketova, T., Hoshino, D., Zijlstra, A., & Weaver, A. M. (2015). Directional cell movement through tissues is controlled by exosome secretion. *Nature Communications*, *6*(May), 1–14. https://doi.org/10.1038/ncomms8164

Suzuki, K., Bose, P., Leong-quong, R. Y. Y., Fujita, D. J., & Riabowol, K. (2010). REAP : A two minute cell fractionation method. *BMC Research Notes*, *3*(294), 1–6.

Suzuki, S., & Kulkarni, A. B. (2010). Extracellular heat shock protein HSP90β secreted by MG63 osteosarcoma cells inhibits activation of latent TGF-β1. *Biochemical and Biophysical Research Communications*, *398*(3), 525–531. https://doi.org/10.1016/j.bbrc.2010.06.112

Swiatoniowski, G., Matkowski, R., Suder, E., Bruzewicz, S., Setta, M., & Kornafel, J. A. N. (2005). E-cadherin and Fibronectin Expressions Have No Prognostic Role in Stage II Ductal Breast Cancer. *Anticancer Research*, *25*, 2879–2883.

Taguchi, T., & Razzaque, M. S. (2007). The collagen-specific molecular chaperone HSP47: is there a role in fibrosis? *Trends in Molecular Medicine*, *13*(2), 45–53. https://doi.org/10.1016/j.molmed.2006.12.001

Taipale, M., Krykbaev, I., Koeva, M., Kayatekin, C., Westover, D. ., Karras, G. I., & Lindquist, S. (2012). Quantitative Analysis of Hsp90-Client Interactions Reveals Principles of substrate recognition. *Cell*, *150*(5), 987–1001. https://doi.org/10.1016/j.cell.2012.06.047.Quantitative

Takada, Y., Ye, X., & Simon, S. (2007). The integrins. *Genome Biology*, *8*(5), 215. https://doi.org/10.1186/gb-2007-8-5-215

Tello, M., Spenlé, C., Hemmerlé, J., Mercier, L., Fabre, R., Allio, G., … Goetz, J. G. (2016). Generating and characterizing the mechanical properties of cell-derived matrices using atomic force microscopy. *Methods*, *94*, 85–100. https://doi.org/10.1016/j.ymeth.2015.09.012

Theocharis, A. D., Skandalis, S. S., Gialeli, C., & Karamanos, N. K. (2015). Extracellular matrix structure. *Advanced Drug Delivery Reviews*, 1–23. https://doi.org/10.1016/j.addr.2015.11.001

Tissières, a, Mitchell, H. K., & Tracy, U. M. (1974). Protein synthesis in salivary glands of Drosophila melanogaster: relation to chromosome puffs. *Journal of Molecular Biology*, *84*(3), 389–398. https://doi.org/10.1016/0022-2836(74)90447-1

To, W. S., & Midwood, K. S. (2011). Plasma and cellular fibronectin: distinct and independent functions during tissue repair. *Fibrogenesis & Tissue Repair*, *4*, 1–21. https://doi.org/10.1186/1755-1536-4-21

Tomasini-Johansson, B. R., Kaufman, N. R., Ensenberger, M. G., Ozeri, V., Hanski, E., & Mosher, D. F. (2001). A 49-Residue Peptide from Adhesin F1 of Streptococcus pyogenes Inhibits Fibronectin Matrix Assembly. *Journal of Biological Chemistry*, *276*(26), 23430–

23439. https://doi.org/10.1074/jbc.M103467200

Trepel, J., Mollapour, M., Giaccone, G., & Neckers, L. (2010). Targeting the dynamic HSP90 complex in cancer. *Nature Reviews. Cancer*, *10*(8), 537–49. https://doi.org/10.1038/nrc2887

Triantafilou, M., & Triantafilou, K. (2004). Heat-shock protein 70 and heat-shock protein 90 associate with Toll-like receptor 4 in response to bacterial lipopolysaccharide. *Biochem Soc Trans*, *32*(Pt 4), 636–639. https://doi.org/10.1042/BST0320636

Tsen, F., Bhatia, A., O'Brien, K., Cheng, C.-F., Chen, M., Hay, N., … Li, W. (2013). Extracellular heat shock protein 90 signals through subdomain II and the NPVY motif of LRP-1 receptor to Akt1 and Akt2: a circuit essential for promoting skin cell migration in vitro and wound healing in vivo. *Molecular and Cellular Biology*, *33*(24), 4947–59. https://doi.org/10.1128/MCB.00559-13

Tsutsumi, S., Scroggins, B., Koga, F., Lee, M.-J., Trepel, J., Felts, S., … Neckers, L. (2008). A small molecule cell-impermeant Hsp90 antagonist inhibits tumor cell motility and invasion. *Oncogene*, *27*(17), 2478–2487. https://doi.org/10.1038/sj.onc.1210897

Tukaj, S., Hellberg, L., Ueck, C., Martin, H., Samavedam, U., Zillikens, D., … Kasperkiewicz, M. (2015). Heat shock protein 90 is required for ex vivo neutrophil-driven autoantibody-induced tissue damage in experimental epidermolysis bullosa acquisita. *Experimental Dermatology*, *24*, 471–473. https://doi.org/10.1111/exd.12680

Ullrich, S. J., Robinson, E. A., Law, L. W., Willinghamt, M., & Appella, E. (1986). A mouse tumor-specific transplantation antigen is a heat shock related protein. *Proc Natl Acad. Sci*, *83*, 3121–3125.

Vasko, R. C., Rodriguez, R. A., Cunningham, C. N., Ardi, V. C., Agard, D. A., & McAlpine, S. R. (2010). Mechanistic Studies of Sansalvamide A-Amide: An Allosteric Modulator of Hsp90. *ACS Medicinal Chemistry Letters*, *1*(1), 4–8. https://doi.org/10.1021/ml900003t

Villiger, B., Kelley, D. G., Engleman, W., Kuhn, C., & McDonald, J. a. (1981). Human alveolar macrophage fibronectin: synthesis, secretion, and ultrastructural localization during gelatin-coated latex particle binding. *The Journal of Cell Biology*, *90*(3), 711–20. Retrieved from http://www.pubmedcentral.nih.gov/articlerender.fcgi?artid=2111908&tool=pmcentrez&rendertype=abstract

Von Arnim, C. A. F., Kinoshita, A., Peltan, I. D., Tangredi, M. M., Herl, L., Lee, B. M., … Hyman, B. T. (2005). The low density lipoprotein receptor-related protein (LRP) is a novel beta-secretase (BACE1) substrate. *Journal of Biological Chemistry*, *280*(18), 17777–17785. https://doi.org/10.1074/jbc.M414248200

Voss, A., Thomas, T., & Gruss, P. (2000). Mice lacking HSP90beta fail to develop a placental labyrinth. *Development*, *127*(1), 1–11. Retrieved from file://localhost/Users/tom/Documents/Papers/2000/Voss/Development 2000 Voss.pdf

Waas, E. T., Lomme, R. M. L. M., DeGroot, J., Wobbes, T., & Hendriks, T. (2002). Tissue levels of active matrix metalloproteinase-2 and -9 in colorectal cancer. *British Journal of Cancer*, *86*(12), 1876–1883. https://doi.org/10.1038/sj.bjc.6600366

Wandinger, S. K., Richter, K., & Buchner, J. (2008). The Hsp90 chaperone machinery. *The Journal of Biological Chemistry*, *283*(27), 18473–7. https://doi.org/10.1074/jbc.R800007200

Wang, K., Seo, B. R., Fischbach, C., & Gourdon, D. (2016). Fibronectin Mechanobiology Regulates Tumorigenesis. *Cellular and Molecular Bioengineering*, *9*(1), 1–11. https://doi.org/10.1007/s12195-015-0417-4

Wang, X., Song, X., Zhuo, W., Fu, Y., Shi, H., Liang, Y., … Luo, Y. (2009). The regulatory mechanism of Hsp90alpha secretion and its function in tumor malignancy. *Proceedings of the National Academy of Sciences of the United States of America*, *106*(50), 21288–21293. https://doi.org/10.1073/pnas.0908151106

Wang, Y., Koay, C., & Mcalpine, S. R. (2017). Redefining the Phenotype of Heat Shock Protein 90 (Hsp90) Inhibitors. *Chem. Eur. Journal*, *23*, 2010–2013. https://doi.org/10.1002/chem.201604807

Wang, Y., & McAlpine, S. R. (2015). Combining an Hsp70 inhibitor with either an N- or C-terminal Hsp90 inhibitor produces mechanistically distinct phenotypes. *Organic & Biomolecular Chemistry*, *13*(12), 3691–3698. https://doi.org/10.1039/C5OB00147A

Wegele, H., Müller, L., & Buchner, J. (2004). Hsp70 and Hsp90—a relay team for protein folding. *Reviews of Physiology, Biochemistry and Pharmacology*, (151), 1–44. https://doi.org/10.1007/s10254-003-0021-1

Welton, J. L., Brennan, P., Gurney, M., Webber, J. P., Spary, L. K., Carton, D. G., … Clayton, A. (2016). Proteomics analysis of vesicles isolated from plasma and urine of prostate cancer patients using a multiplex, aptamer-based protein array. *Journal of Extracellular Vesicles*, *5*(1). https://doi.org/10.3402/jev.v5.31209

Whitesell, L., & Lindquist, S. L. (2005). HSP90 AND THE CHAPERONING OF CANCER. *Nature Reviews*, *5*, 761–772. https://doi.org/10.1038/nrc1716

Wierzbicka-Patynowski, I., & Schwarzbauer, J. E. (2003). The ins and outs of fibronectin matrix assembly. *Journal of Cell Science*, *116*(Pt 16), 3269–76. https://doi.org/10.1242/jcs.00670

Williams, S. E., Ashcom, J. D., Argraves, W. S., & Strickland, D. K. (1992). A Novel Mechanism for Controlling the Activity of α2-Macroglobulin Receptor / Low Density Lipoprotein Receptor-related Protein. *Journal of Biological Chemistry*, *267*(13), 9035–9040.

Wòjciak-Stothard, B., Denver, M., Mishra, M., & Brown, R. A. (1997). Adhesion, orientation, and movement of cells cultured on ultrathin fibronectin fibers. *In Vitro Cellular and Developmental Biology - Animal*, *33*(2), 110–117. https://doi.org/10.1007/s11626-997-0031-4

Wong, D. S., & Jay, D. G. (2016). Emerging Roles of Extracellular Hsp90 in Cancer. In *Advances in Cancer Research* (1st ed., Vol. 129, pp. 141–163). Elsevier Inc. https://doi.org/10.1016/bs.acr.2016.01.001

Woodhead, A. J., Angove, H., Carr, M. G., Chessari, G., Congreve, M., Coyle, J. E., … Woolford, A. J. A. (2010). Discovery of (2,4-Dihydroxy-5-isopropylphenyl)-[5-(4-methylpiperazin-1- ylmethyl)-1,3-dihydroisoindol-2-yl]methanone (AT13387), a novel

inhibitor of the molecular chaperone Hsp90 by fragment based drug design. *Journal of Medicinal Chemistry*, *53*(16), 5956–5969. https://doi.org/10.1021/jm100060b

Wozniak, M. A., Modzelewska, K., Kwong, L., & Keely, P. J. (2004). Focal adhesion regulation of cell behavior. *Biochimica et Biophysica Acta*, *1692*, 103–119. https://doi.org/10.1016/j.bbamcr.2004.04.007

Xu, W., Mimnaugh, E. G., Kim, J. S., Trepel, J. B., & Neckers, L. M. (2002). Hsp90, not grp94, regulates the intracellular trafficking and stability of nascent ErbB2. *Cell Stress and Chaperones*, *7*(1), 91–96. https://doi.org/10.1379/1466-1268(2002)007<0091:HNGRTI>2.0.CO;2

Yamada, K. M., & Cukierman, E. (2007). Modeling Tissue Morphogenesis and Cancer in 3D. *Cell*, *130*(4), 601–610. https://doi.org/10.1016/j.cell.2007.08.006

Yin, Z., Henry, E. C., & Gasiewicz, T. A. (2009). (-)-EPIGALLOCATECHIN-3-GALLATE IS A NOVEL HSP90 INHIBITOR. *Biochemistry*, *48*(2), 336–345. https://doi.org/10.1021/bi801637q.

You, D., Jung, S. P., Jeong, Y., Bae, S. Y., & Lee, J. E. (2017). Fibronectin expression is upregulated by PI-3K / Akt activation in tamoxifen-resistant breast cancer cells. *BMB Reports*, *50*(12), 615–620.

Zemskov, E. a, Mikhailenko, I., Strickland, D. K., & Belkin, A. M. (2007). Cell-surface transglutaminase undergoes internalization and lysosomal degradation: an essential role for LRP1. *Journal of Cell Science*, *120*(Pt 18), 3188–99. https://doi.org/10.1242/jcs.010397

Zhang, D., Shao, S., Shuai, H., Ding, Y., Shi, W., Wang, D., & Yu, X. (2013). SDF-1α reduces fibronectin expression in rat mesangial cells induced by TGF-β1 and high glucose through PI3K/Akt pathway. *Experimental Cell Research*, *319*(12), 1796–1803. https://doi.org/10.1016/j.yexcr.2013.03.030

Zhang, T., Hamza, A., Cao, X., Wang, B., Yu, S., Zhan, C.-G., & Sun, D. (2008). A novel Hsp90 inhibitor to disrupt Hsp90/Cdc37 complex against pancreatic cancer cells. *Molecular Cancer Therapeutics*, *7*(1), 162–170. https://doi.org/10.1158/1535-7163.MCT-07-0484

Zhang, T., Li, Y., Yu, Y., Zou, P., Jiang, Y., & Sun, D. (2009). Characterization of celastrol to inhibit Hsp90 and Cdc37 interaction. *Journal of Biological Chemistry*, *284*(51), 35381–35389. https://doi.org/10.1074/jbc.M109.051532

Zhang, X., Chen, C. T., Bhargava, M., & Torzilli, P. A. (2013). A Comparative Study of Fibronectin Cleavage by MMP-1, -3, -13, and -14. *Cartilage*, *3*(3), 267–277. https://doi.org/10.1177/1947603511435273

Zheng, J., Luo, W., & Tanzer, M. L. (1998). Aggrecan Synthesis and Secretion : A paradigm for molecular and cellular coordination of multiglobular protein folding and intracellular trafficking. *Journal of Biological Chemistry*, *273*(21), 12999–13006.

Zheng, Y., Ritzenthaler, J. D., Roman, J., & Han, S. (2007). Nicotine Stimulates Human Lung Cancer Cell Growth by Inducing Fibronectin Expression. *Am J Respir Cell Mol Biol*, *37*, 681–690. https://doi.org/10.1165/rcmb.2007-0051OC

Zhu, J., Xiong, G., Fu, H., Evers, B. M., Zhou, B. P., & Xu, R. (2015). Chaperone Hsp47 drives

malignant growth and invasion by modulating an ECM gene network. *Cancer Research*, *75*(8), 1580–1591. https://doi.org/10.1158/0008-5472.CAN-14-1027

Zhu, J., Xiong, G., Trinkle, C., & Xu, R. (2014). Integrated extracellular matrix signaling in mammary gland development and breast cancer progression. *Histol Histopathol*, *29*(9), 1083–1092. https://doi.org/10.1530/ERC-14-0411.Persistent

Zlokovic, B. V, Martel, C. L., Matsubara, E., McComb, J. G., Zheng, G., McCluskey, R. T., … Ghiso, J. (1996). Glycoprotein 330/megalin: probable role in receptor-mediated transport of apolipoprotein J alone and in a complex with Alzheimer disease amyloid beta at the blood-brain and blood-cerebrospinal fluid barriers. *Proceedings of the National Academy of Sciences of the United States of America*, *93*(9), 4229–4234. https://doi.org/10.1073/pnas.93.9.4229

Zou, M., Bhatia, A., Dong, H., Jayaprakash, P., Guo, J., Sahu, D., … Li, W. (2016). Evolutionarily conserved dual lysine motif determines the non-chaperone function of secreted Hsp90alpha in tumour progression. *Oncogene*, *36*, 2160–2171. https://doi.org/10.1038/onc.2016.375

Zügel, U., & Kaufmann, S. H. (1999). Role of heat shock proteins in protection from and pathogenesis of infectious diseases. *Clinical Microbiology Reviews*, *12*(1), 19–39.

Zurawska, A., Urbanski, J., & Bieganowski, P. (2008). Hsp90n - An accidental product of a fortuitous chromosomal translocation rather than a regular Hsp90 family member of human proteome. *Biochimica et Biophysica Acta*, *1784*(11), 1844–6. https://doi.org/10.1016/j.bbapap.2008.06.013

Zurhove, K., Nakajima, C., Herz, J., Bock, H. H., & May, P. (2008). Gamma-secretase limits the inflammatory response through the processing of LRP1. *Science Signaling*, *1*(47), 1–24. https://doi.org/10.1126/scisignal.1164263

Chapter 7: **APPENDIX**

7.1 Supplementary Information

7.1.1 Determining a working concentration of the MMP inhibitor, Prinomastat

To determine an effective concentration with which to use Prinomastat in combination treatments with NOV, we performed a gelatin zymography assay where adherent cells were treated in serum-free media for 16 hours with increasing concentrations of Prinomastat (Prino). Harvested supernatants were processed according to the zymography assay. No change in levels of MMP activity were observed across a wide range of Prinomastat concentrations (Supplementary Figure 1A). Coomassie stained total protein of a single band at 50 kDa on a separate gelatin gel was used as a loading control to compare levels of MMP activity. This was different to the effect observed with NOV. This led us to believe that the inhibitor may be bound to MMPs in such a way that during development of the assay we lost the inhibitor and the effect could not be observed. We modified our protocol to allow for development of the gel together with inhibitor overnight in developing solution. Resultant bands of clearance showed successful inhibition of MMP activity at 1 nM Prinomastat in both MEF-1 and PEA-13 cells compared to an untreated gel without inhibitor (Supplementary Figure 1).

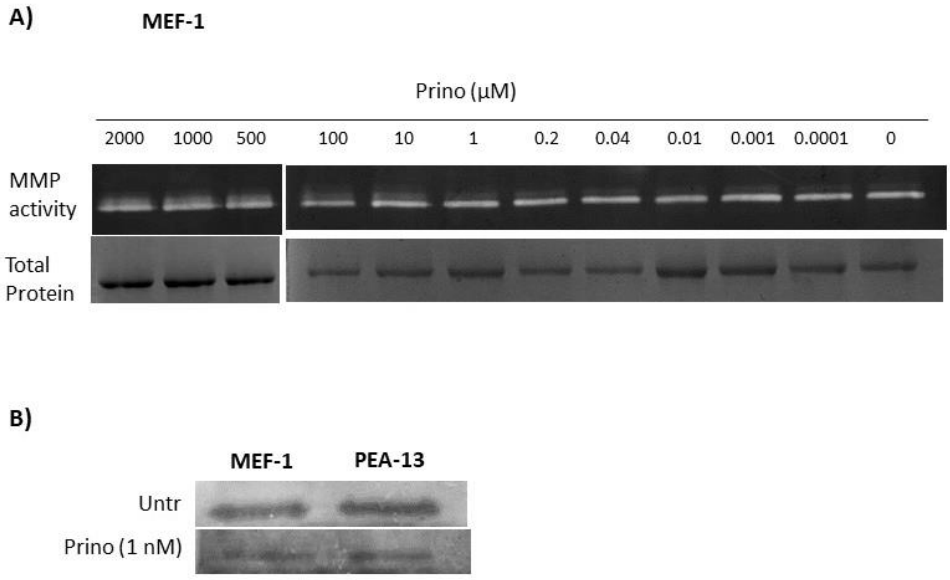

Supplementary Figure 1: Gelatin Zymography of Prinomastat treated MEF-1 and PEA-13 cells

A) Adherent MEF-1 cells were treated in serum free media with increasing concentrations of the MMP inhibitor, Prinomastat (Prino) for 16 hours. The supernatant containing MMPs were harvested and processed according to the zymography assay described previously. Levels of MMP activity are represented by white bands of clearance against a dark background. Coomassie stained total protein was used as a loading control. **B)** Adherent MEF-1 and PEA-13 cells were treated for 16 hours in serum free media lacking inhibitor. Media was harvested the following day and analysed by gelatin zymography.